An Ultra Scale-Down Approach to the Rapid Evaluation of Pleated Membrane Cartridge Filter Performance

A thesis submitted to University College London for the degree of Doctor of Engineering

By

Andrew Ian Brown

Department of Biochemical Engineering
University College London
Torrington Place
London
WC1E 7JE

2011

I, Andrew Ian Brown, confirm that the work presented in this thesis is my own. Where information has been derived from other sources, I confirm that this has been indicated in the thesis.

Signed……..

Date……

Abstract

Pleated membrane cartridge filters are used extensively throughout a typical bioprocess. They are exposed to a range of operating conditions and feedstocks. Discrepancies between the performance of the flat sheet membrane and pleated membrane have previously been identified, although little has been done to fully characterise the effects of pleating. As current scale-up techniques use the flat sheet membrane to predict the performance of the large-scale pleated cartridge, the discrepancy in performance between flat sheet and pleated cartridge leads to inaccuracy in scale-up. This inaccuracy is accounted for by over-sizing of the equipment. In turn this reduces the efficiency of the bioprocess and increases capital costs. At the present time no accurate and reliable scale-up methodology exists that accounts for the effects of pleating.

A systematic investigation into the effect of pleating has been conducted. By varying the key pleat characteristics: pleat height, type and packing density, the impact upon cartridge performance of these characteristics has been determined. Using this knowledge, new scale-down cartridge filters have been developed, fabricated and tested. When faced with both clean water and a pepsin protein solution, performance was within 10% of the large-scale 10” counterpart, whilst operating with a 1000 fold reduction in feed volume. This compares well to flat sheet membrane which showed up to 53% variation in performance to the pleated cartridge filter.

The scale-down cartridge is limited to the degree in which reduction of feedstock can be achieved. So as to reduce feed volume requirements further, a ultra scale-down methodology has been developed that uses experimental models to account for the effect that pleating has upon cartridge performance. When coupled with experimental data derived from flat sheet discs, the scale-up performance improves predictions with flat sheet membrane however discrepancies still exist between the two scales, suggesting that the method is not yet robust.

Based upon the work of this thesis the close performance between the scale-down cartridges and the large-scale cartridges, coupled with the low feed requirement, make the device an excellent method by which rapid scale-up can be achieved during the process development of biopharmaceutical products. However, it is recommended that the ultra scale-down approach is developed further, so as to build a robust method to predict the performance of industrial scale pleated filter cartridges using significantly reduced areas of flat sheet membrane.

Acknowledgements

First and foremost I would like to thank my academic supervisor Professor Gary Lye, my industrial supervisor Dr Peter Levison, and my academic advisor Professor Nigel Titchener-Hooker for their immense support, patience and encouragement throughout the development of this thesis. They have taught me many valuable lessons, applicable not just to this work, but to life as well.

I would like to thank my student, Mr Michael Delahaye for his assistance in conducting investigations into the hydrodynamics within the standard cartridge housing. I thank too the members of the BioChemical Engineering workshop who have also their skill and labour in building me prototypes, rigs and other devices. Their support is gratefully acknowledged. There are many individuals within Pall Europe who have greatly assisted me during this work. Particularly I must acknowledge the support of Dr MayLing Yeow during the early stages of my project and Mr Chris Haslam in the latter stages of the project. My thanks also go to Mr Chris Snowdon and Mr Gareth Pontain for their skill and labour in fabricating the many devices used within this work. Generally I thank all at the R&D centre at Pall Walton Road, who always made me feel most welcome when I visited.

I gratefully acknowledge the financial support of the Engineering and Physical Sciences Research Council (EPSRC) and Pall Europe Ltd. The support of the Innovative Manufacturing Research Centre (IMRC) for Bioprocessing within the Department of Biochemical Engineering at UCL is also acknowledged.

I owe a massive debt of gratitude to my Parents for their continued and unwavering love and support in all.

My final thanks go to Adriana, who I was lucky enough to discover at the beginning and who has been a rock and companion throughout this journey. Long may this continue into the future.

For Adriana……

..... and my Parents

Table of Contents

List of Figures

List of Tables

Nomenclature

Symbols

ΔP	Pressure difference	Pa
A_{eff}	Effective membrane area	m^2
$A_{eff, IA}$	Effective membrane area obtained from image analysis	m^2
$A_{eff, water}$	Effective membrane area obtained from water flux experiments	m^2
A_m	Membrane area	m^2
c_S	mass wet cells per unit volume	kgm^{-3}
C_b	Bulk concentration	kgm^{-3}
D	Diameter of capillary	m
d_C	diameter of cartridge	m
d_d	diameter of disc	m
f'	Fractional amount of deposit	-
FMEA	Failure modes and effects analysis	-
h_P	Height of pleats	m
HV	Hand valve	-
J	Volume flux	$m^3m^{-2}s^{-1}$
J*	Critical flux	$m^3m^{-2}s^{-1}$
J_0	Initial volume flux	$m^3m^{-2}s^{-1}$
k	Permeability of porous material	m^3m^{-2}
K	Kozeny-Carman dimensionless constant	-
K_L	Pressure at which bulk flow begins	Pa
L_c	Length of cartridge	m
L_H	Length of housing	m
P	Pressure	Pa
P_0	Intial pressure	Pa
PES	Polyethersulphone	-
PG	Pressure gauge	-
PI	Pressure indicator	-
PPD	Pleat packing density	-
PVDF	Polyvinylidene fluoride	-
Q	Volume flow-rate	m^3s^{-1}

Q_0	Initial volume flow-rate	m^3s^{-1}
r	Pore radius	m
R'	Cake resistance	mkg^{-1}
R_a	Resistance due to solute adsorption	m^{-1}
R_C	Regenerated cellulose	-
R_{cp}	Resistance due to concentration polarisation	m^{-1}
R_g	Resistance due to gel layer formation	m^{-1}
R_m	Intrinsic membrane resistance	m^{-1}
R_O	Reverse osmosis	-
R_p	Resistance due to pore-blocking	m^{-1}
R_{p0}	Resistance of a single cake deposit	m^{-1}
RPN	Risk priority number	-
R_{tot}	Sum of resistances to flow through porous media	m^{-1}
S	Surface area of spherical particles per unit volume	m^3m^{-2}
t	time	s
t_{20}	Time for permeate volume flow rate to drop below $Q/Q_0 = 0.2$	s
TMP	transmembrane pressure difference	Pa
t_P	Pore blockage time	s
USD	Ultra scale-down	-
V	Volume	m^3
V_{cum}	Cumulative volume collected	m^3
V_{max}	Maximum filterable volume	m^3
x	Pore length	m

Greek letters

μ	Viscosity	Pas
ε	Porosity	-
τ	Tortuosity factor	-
α_c	Specific cake resistance	mkg^{-1}
α	Pore blockage parameter	m^2kg^{-1}
β	Pore constriction parameter	-
θ	Angle between pleats	°
θ_w	Wetting angle	°
γ	surface tension	Nm^{-1}

1 Introduction

1.1 Manufacture of Biopharmaceuticals

Since the first production of recombinant human insulin in 1982 (Pavlou et al., 2004), the manufacture of recombinant proteins has become an important route for provision of new therapies to combat human diseases. These biopharmaceutical drugs are typically large complex molecules that are dependant upon shape and structure to retain therapeutic activity (Buckland, 2005; Kee et al., 2008).

Classical chemical syntheses could not generate these complex molecules, so new production methods were required. As microorganisms naturally produce proteins, a method was generated to use a genetically engineered host cell system to mass produce therapeutic proteins (Cohen et al., 1973). These host cell systems can now be: microbial, funghi, mammalian, insect, or plant cells. The production of the bioproduct within the microorganism is carried out in a fermenter, where the environmental conditions are altered so as to activate expression of the bioproduct and maximise production. Once expressed, the bioproduct requires isolation and purification. An example flowsheet for a bioprocess to achieve production of a recombinant protein is shown in Figure 1-1. Unless the bioproduct has been secreted from the microorganism into the culture broth (Option B), then after fermentation the cells will need to be harvested and then ruptured (Option A), so that the product can be released. The cell debris is removed through a sequence of clarification steps. Option A typically involves the use of centrifugation, where as Option B will involve the use of tangential flow filtration (Parnham et al., 1996; van Reis et al., 1991). After clarification the product is purified through a number of process steps, until it attains a purity greater than 99.9% (Asenjo et al., 2008). After a sterile filtration step the concentrated product solution is sent for formulation and filling

.

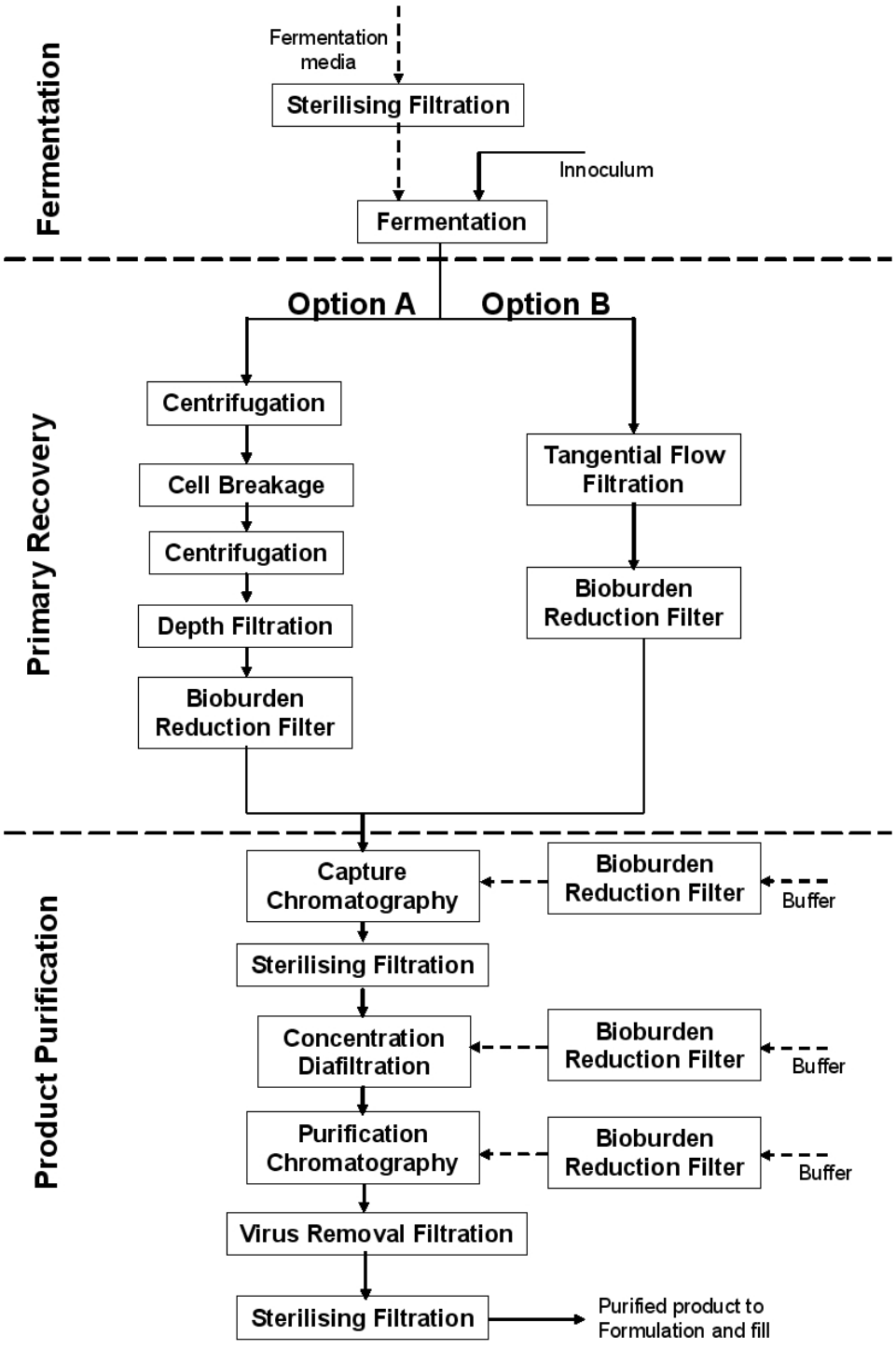

Figure 1-1: Example bioprocess flowsheet for production, recovery and purification of a bioproduct expressed in a cell culture. Bold solid arrows represent the flow of the bioproduct through the process. Generally there are two main options available for the primary recovery stage, selection of which depends upon whether the product is produced intra-cellularly (Option A) or extra-cellularly (Option B).

It can be seen from Figure 1-1 that filtration plays a key role both within the main bioprocess sequence and in related operations. Of particular note is the number of bioburder reduction, sterilising filtration and viral filtration steps used. All of these steps will use pleated membrane cartridge filters during the operation. It can also be seen that the bioprocess contains many individual unit operations. If each step had a yield of 80% then the overall yield of the bioprocess after 9 steps would be less than 15%. Thus the correct design and optimisation of each step in the bioprocess is essential. If knowledge for the design of each operation can be derived at an early stage in development using small-scale equipment, then this will improve the chances of developing a robust and high yielding process by the time the bioproduct is brought through clinical trials to market.

1.2 Filtration Principles

Filtration is a separation technique widely used within the bioprocess industry (Zydney, 2009). It is capable of separating a wide range of materials, depending upon the type of filter medium used. Membranes are used to separate entities with a small diameter, such as micro-organisms, colloidal molecules, proteins etc. Membrane filtration works largely on a size exclusion principle. There is a range of membrane techniques, and these are primarily defined by the size range of the pores and thus the components that they can prevent from passing through their structure. Table 1-1 gives a summary of key properties linked to the five types of filtration typically used within bioprocesses.

Microfiltration operates within the range of 0.1µm to 5µm, with ultrafiltration operating within the range of 0.002µm to 0.1µm (Mulder, 1997). Both types of filtration are pressure driven processes, requiring a pressure difference to be applied across the membrane. Ultrafiltration membranes have smaller pores, and thus require higher pressure differences. This accounts for the higher pressure drop and osmotic resistance of the membrane. Viral filtration is a specialist form of ultrafiltration that targets a log reduction in virus concentration (Dileo et al.,

1993). As such, the pore size range is narrow and comes in a 20nm or 50nm format. Nanofiltration and reverse osmosis are used primarily to purify water.

Ultrafiltration and microfiltration have two main modes of operation. Normal flow (also known as dead end flow) applies the solution to be filtered at a direction normal to the membrane surface. Tangential flow filtration (also known as cross flow filtration) applies the solution to be filtered across the surface of the membrane. Each of these modes of operation will have common factors that will affect their operation, such as viscosity, temperature and transmembrane pressure difference. However, other factors have specific significance for cross-flow filtration, such as cross flow rate and shear rate.

The various configurations in which membranes can be fabricated are summarised in Table 1-2. Typically, pleated cartridges are used where high flow is required and the concentration of fouling material is low. Flat plate membranes are typically favoured over hollow fibre units, as flat plate membranes are easy to replace should one fail. If a hollow fibre fails, then the entire unit will require replacing. Vibrating or rotating membranes are used where the concentration of fouling material is very high. By rotating the membrane disc, an increased shear force is generated at the surface of the membrane which reduces fouling (Jaffrin, 2008). This higher shear force is at the expense of membrane packing density, which leads to units that can only process small volumes of feed. In practice these systems are widely used during the manufacture of antibiotics (Postlethwaite et al., 2004). Membrane chromatography was initially explored a number of years ago without any substantial commercial success (van Reis et al., 2001), however new preparations of adsorptive membranes have shown higher capture efficiency and higher productivity than column chromatography (Zeng et al., 1999).

Table 1-1: Key characteristics of various filtration types used within bioprocesses.

Filtration Type	Application within Bioprocess[I]		Typical Fabrication Material[II]	Pore Size		Typical Operating Pressure[III] (bar)
	Retained Particles	Particles that pass through membrane		nm	MWCO (Da)	
Microfiltration	Intact cells Cell debris	Small colloids Viruses Proteins Salts	PES PVDF	100 – 5000[III]	500,000+[II]	0.1 – 2.0[III]
Viruses	Viruses	Proteins Buffers	PVDF	20 – 50	-	1 – 2
Ultrafiltration	Proteins	Amino acids Antifoam Buffers	PES RC	2 – 100[III]	2000 – 500,000[III]	1.0 – 5.0[III]
Nanofiltration	Divalent ions Amino acids Antibiotics	Salts Water	Proprietary	0.7 – 70[III]	300 – 10,000[III]	5.0 – 20[III]
Reverse Osmosis	Amino acids Sugars Salts	Water	Proprietary	0.1 – 1.0[III]	10 – 500[III]	10 - 100[III]

[I] Based on (van Reis et al., 2007)
[II] Abbreviations: PES = Polyethersulphone, PVDF = Polyvinylidenefluoride, RC = regenerated cellulose.
[III] Based on (Mulder, 1997)

Table 1-2: Advantages and limitations of various membrane configurations available.

Configuration	Normal Operational Mode	Membrane Packing Density (m^2m^{-3})	Advantages	Limitations
Pleated membrane cartridge	Normal Flow	710	High flux. High membrane packing density. Disposable. Low pumping costs.	Low capacity with fouling feed. Difficult to clean.
Flat plate	Cross flow	300[I]	Process fouling feed. Easy to clean Moderate membrane packing density. Moderate shear.	Moderate pumping costs. Non-disposable.
Hollow fibre	Cross flow	1200[I]	Very high membrane packing density. Low pumping costs. High shear.	Difficult to clean. Moderate capacity with fouling feed.
Spiral bound	Cross flow	600[I]	Low pumping costs. High membrane packing density. Low pumping costs. Low shear.	Low capacity with fouling feed. Difficult to clean. Difficult to fabricate
Rotating / vibrating	Cross flow (Enhanced)	10[I]	Process highly fouling feed. Easy to clean. High shear.	Very low membrane packing density. Non-disposable.
Membrane chromatography	Normal Flow	-	Disposable. High flux. Adsorptive binding.	Difficult to clean. Low capacity with fouling feed. Moderate pumping costs.

[I] Based on (Zeman et al., 1996)

1.2.1 Transport Through Porous Membranes for Pressure Driven Processes

For transport through a porous membrane a potential difference is required across the membrane. The potential difference causes a driving force through the membrane, and can arise from differences in either: pressure, concentration, temperature or electrical potential (Mulder, 1997). Only pressure driven processes will be considered here as they represent the bulk of the membrane operations seen in bioprocesses.

1.2.2 Theory for Non Pore-Blocking Solutions

For non pore-blocking (clean) solutions the empirical relationship describing fluid flow through a porous media was first defined as follows (Darcy, 1856):

$$J = -\frac{k}{\mu}\Delta P \tag{1-1}$$

where J is the rate of flow through a surface element of unit area, k is the permeability of the porous media, μ is the fluid viscosity and $\triangle P$ is the pressure gradient.

For laminar convective flow through a porous structure both the Hagen-Poiseuille and the Kozeny-Carman equations can be applied for pores represented by straight capillaries and nodular structures respectively (Mulder, 1997). These expressions help define the permeability of the porous media in terms of the geometry of the pores. The Hagen-Poiseulle equation is:

$$J = -\frac{\varepsilon r^2}{8\mu\tau}\frac{\Delta P}{\Delta x} \tag{1-2}$$

where r is the pore radius, ε is the porosity, τ is the tortuosity factor and μ is the fluid dynamic viscosity and x is the pore length. The Kozeny-Carman equation is represented as:

$$J = -\frac{\varepsilon^3}{K\mu S^2}\frac{\Delta P}{\Delta x} \tag{1-3}$$

where K is the dimensionless constant which depends upon the pore geometry and S is the surface area of the spherical particles per unit volume.

1.2.3 Theory for Pore-Blocking Solutions

1.2.3.1 Flux Decline

During a pressure driven membrane process the flux through a membrane can change over time. Flux decline can be caused by many factors, such as: concentration polarisation, adsorption, gel layer formation and plugging of the pores (Zeman et al., 1996). The effects that cause flux decline can be lumped into various resistances that can be incorporated into Equation (1-1):

$$J = \frac{\Delta P}{\mu R_{tot}} \tag{1-4}$$

where R_{tot} is defined as:

$$R_{tot} = R_P + R_a + R_m + R_g + R_{CP} \tag{1-5}$$

where R_P is the resistance due to pore-blocking, R_a is the resistance due to solute adsorption within the pores, R_m is the intrinsic membrane resistance, R_g is the resistance due to gel layer formation and R_{CP} is the resistance due to concentration polarisation. Pore blocking and adsorption cause fouling of the membrane and will be discussed in Section 1.2.3.2. The gel layer resistance is due to the concentration of accumulated solids becoming high enough that a gel layer forms which in turn exerts a resistance to flow that is independent of osmotic pressure (Zaidi et al., 2005).

Concentration polarisation is defined as the reversible build-up of dissolved or suspended solute in the solution phase near the membrane-solution interface due to a balance between the convective drag toward and through the membrane (resulting from the permeation flux) and back-transport away from the membrane (Belfort et al., 1994). It most often occurs in microfiltration with colloids and particles which have low diffusion coefficients, and causes a reduction in permeate flux by increasing the osmotic pressure at the upstream face of the membrane, leading to a decrease in the transmembrane pressure difference. The effects of concentration polarisation are typically lower than for fouling as illustrated in Figure 1-2. The effects of flux decline can be reduced through a number of techniques (Belfort et al., 1994). These techniques are summarised in Table 1-3.

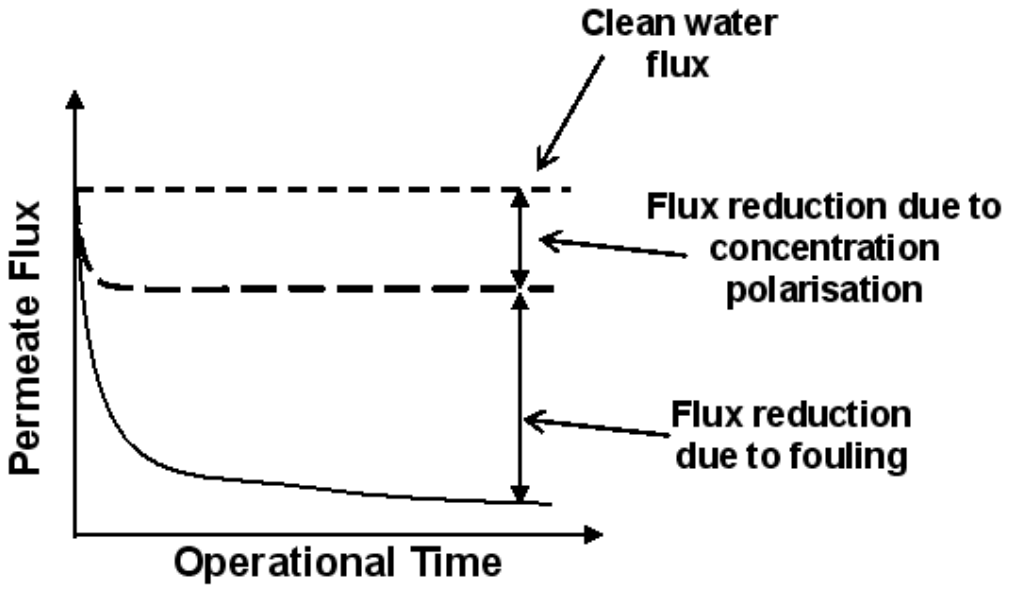

Figure 1-2: Illustration of the relative effects of fouling and concentration polarisation upon flux decline.

Table 1-3: Typical methods for the reduction of fouling and concentration polarisation, and hence flux decline.

Method	Examples
Hydrodynamic	Chemical. e.g. heterogeneous chemical modification; adsorption of hydrophilic polymers Physical. e.g. irradiation; low temperature plasma activation
Instabilities	Turbulent flow Inserts
Vortices	Rough surface Pulsation Couette flow (Taylor vortices) Flow in a curved channel (Dean vortices)

1.2.3.2 Membrane Fouling

For blocking solutions, which cause the porous media to foul, the rate of flow through the membrane will decrease over time. Where a cake forms on the surface of the membrane, this fouling can be described by a cake resistance (Foley, 2006):

$$J = \frac{\Delta P}{\mu\left(R_m + \alpha_C m\right)} \tag{1-6}$$

Where m is given by $c_s V_s / A_m$ and:

$$\alpha_C = \frac{\left(\Delta P / \mu J\right) - R_m}{c_s V_s / A_m} \tag{1-7}$$

Where α_C is the specific cake resistance, c_s is mass wet cells per unit volume of suspension, V_s is the suspension volume, and A_m is the membrane area.

There are many instances where cakes can form upon membrane surfaces, e.g. the filtration of microbial fermentation broths. For this case, the membrane cake resistance is seen to be dependent on many additional factors, especially the harvest time of the cells (Okamoto et al., 2001).

In practice, fouling is often due to more than one mechanism than just the resistance of the cake. Flux decline data are typically analysed using one of the classical filtration models (Hermia, 1982). These are: standard pore blockage, intermediate pore blockage, pore constriction and cake filtration. A schematic representation of the four flux decline models is given in Figure 1-3. The governing equations for the flux decline models have been collected and summarised in their linear forms by van Reis and Zydney (van Reis et al., 2007). The linearised forms can be used to identify the decline regime from experimental data. Further details are given in Table 1-4.

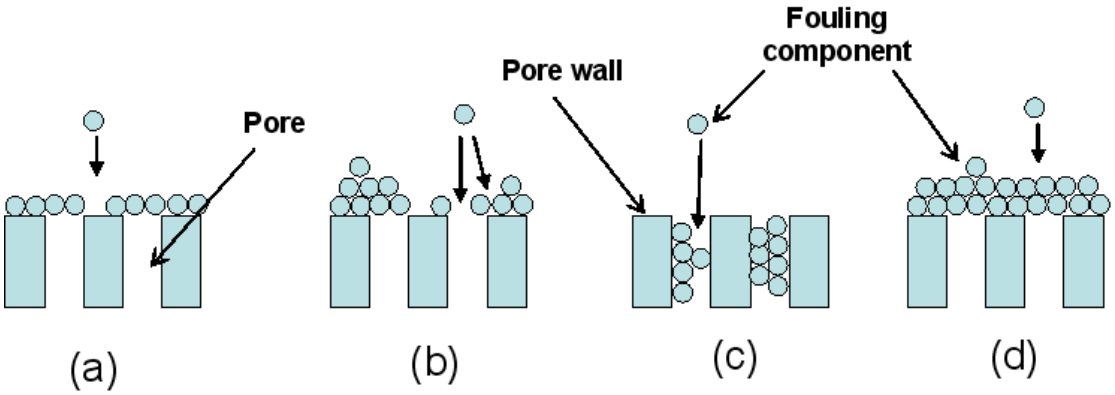

Figure 1-3: Schematic representation of flux decline models described in Table 1-4. (a) pore blockage, (b) intermediate blockage, (c) pore constriction, (d) cake filtration.

Table 1-4: Governing equations for flux decline models (assuming constant pressure)

Flux decline model	Definition[I]	Flow rate[II]	Linearised form
Pore blockage (complete blocking)	Each particle arriving to the membrane participates in blocking some pore(s) with no superposition of particles	$\frac{Q}{Q_0} = e^{(-\beta \cdot t)}$	$\ln(Q) = a \cdot t + b$
Intermediate blockage	Each particle can settle on other particles previously arrived and already blocking some pores or it can also directly block some membrane area.	$\frac{Q}{Q_0} = (1 + \beta \cdot t)^{-1}$	$\frac{1}{Q} = a \cdot t + b$
Pore constriction (standard blocking)	Each particle arriving at to the membrane is deposited onto the internal pore wall leading to a decrease in pore volume.	$\frac{Q}{Q_0} = (1 + \beta \cdot t)^{-2}$	$\frac{t}{V} = a \cdot t + b$
Cake filtration	Each particle locates on others already arrived and already blocking some pores. There is no room for directly obstructing the membrane area.	$\frac{Q}{Q_0} = (1 + \beta \cdot t)^{-1/2}$	$\frac{t}{V} = a \cdot V + b$

[I] Definitions based on (Bowen et al., 1995).
[II] Where: Q is the filtrate flow rate, Q_0 is the Initial filtrate flow rate, t is the time, V is the cumulative filtrate volume.

Whilst the flux decline models given in Table 1-4 have been used as stand alone models, in real operation it is likely that there will be a transition in fouling behaviour from initial flux decline associated with pore constriction and/or pore blockage followed by cake filtration (van Reis et al., 2007). An attempt has been made to use the flux models as successive steps to describe the fouling of the membrane (Bowen et al., 1995). Taking this approach further, a model has been developed to combine the two mechanisms of pore blockage and cake filtration for membranes with non-interconnected pores (Ho et al., 2000):

$$\frac{Q}{Q_0} = \left[\exp\left(-\frac{\alpha \Delta P C_b}{\mu R_m} t \right) + \frac{R_m}{R_m + R_P} \left(1 - \exp\left(-\frac{\alpha \Delta P C_b}{\mu R_m} t \right) \right) \right] \quad (1\text{-}8)$$

Where α is a pore blockage parameter, C_b is the bulk concentration of fouling component, R_m is the membrane resistance and R_P is the resistance of the cake. R_P is defined as:

$$R_P = \left[\left(R_m + R_{P0} \right) \sqrt{1 + \frac{2 f' R' \Delta P C_b}{\mu \left(R_m + R_{P0} \right)^2} t} \right] - R_m \quad (1\text{-}9)$$

Where R_{P0} is the Resistance of a single cake deposit, f' is the fractional amount of deposit that leads to cake growth, R' is the specific cake resistance.

The first term in Equation 1-8 is equivalent to the classical pore blockage model. At longer filtration times the volumetric flow is dominated by the second term and is thus proportional to the ratio of the membrane resistance to the total resistance. For Equations 1-8 and 1-9 the parameters α; f'R'; and R_{P0} require evaluation from experimental data.

This model has been tested primarily with a bovine serum albumin (BSA) feedstock and shows good agreement with the experimental data (Ho et al., 2000). It has also been tested with a range of other protein solutions (Palacio et al., 2002; Palacio et al., 2003). The two-mechanism model has been extended to account for asymmetric membranes consisting of a top layer of non-interconnected pores and a sub-layer of highly interconnected pores (Ho et al., 2001). It has also been applied to membranes containing highly interconnected pores (Zydney et al., 2003). Thus a combined model exists to describe either the flow of liquid through the structure of symmetric or through asymmetric membranes with differing pore connectivity.

A three-mechanism model has recently been developed (Duclos-Orsello et al., 2006) to include three of the decline models given in Table 1-4. These are: pore blockage, pore constriction and cake filtration. This model was developed with

the assumption that fluid flow through the pores can be described by Hagen-Poiseuille flow and is given below:

$$\frac{Q}{Q_0} = \frac{1}{\left(1+\beta Q_o C_b t\right)^2}\exp\left(-\frac{\alpha C_b J_0 t}{1+\beta Q_o C_b t}\right) + \ldots$$
$$\ldots + \int_0^t \frac{\left(\alpha C_b J_0 \Big/ \left(1+\beta Q_0 C_b t_p\right)^2\right)\exp\left(-\left(\alpha C_b J_0 t_P \Big/ \left(1+\beta Q_0 C_b t_p\right)\right)\right)}{\sqrt{\left[\left(R_{P0}\Big/R_m\right)+\left(1+\beta Q_0 C_b t_P\right)^2\right]^2 + 2\left(f' R' \Delta P C_b \Big/ \mu R_m^2\right)\left(t-t_P\right)}} dt_P \qquad (1\text{-}10)$$

Where t_P is the pore blockage time, β is the pore constriction parameter, and J_0 is the initial flux. Whilst the three-mechanism model may offer the ability to calculate the relative influence of each of the fouling mechanisms, the actual practical use is limited in industrial situations due to the complexity of the model.

As there is a trade-off between the physical detail and the numerical complexity of the theoretical model, five combined models have been derived that require the fitting of only two parameters (Bolton et al., 2006a). These combined models had a reduced model fit error when compared against the stand alone flux decline models for the filtration of a BSA solution and also for a human plasma ImmunoglobulinG (IgG) solution. This approach was taken further with the incorporation of flow rate through the pore on the rate of adsorptive particle deposition onto the pore (Bolton et al., 2006b). A good fit to experimental data for a human IgG solution was reported. Importantly, by incorporating flow rate into the combined model, the model more closely represents the operation of membrane units at large-scale, which are typically run under a constant flow regime, as opposed to a constant pressure regime.

1.2.3.3 Reversible Membrane Fouling

Experiments supporting the existence of a critical filtered volume (CFV) have been presented for the normal-flow filtration of colloids (Bessiere et al., 2005). CFV is defined as the filtered volume below which there is no irreversible

fouling on the membrane surface. However, to reverse the membrane fouling the filtration operation must be halted to rinse the surface of the membrane. This approach may hold value where the cost of the membranes is high. However for processes where the cost of membranes is relatively low and where by cleaning would be a time-consuming exercise (such as sterile filtration in bioprocesses) there is probably limited application for the technique.

1.2.4 Solute Interactions

All materials dispersed in aqueous media acquire a surface charge (Bowen, 1993). This can lead to solute-solute and solute-membrane interactions. Solute-solute interactions can lead to formation of aggregates, which in turn can lead to fouling. Solute-membrane interactions can lead to adsorption to the membrane of the solute, which over time can also lead to membrane fouling. These interactions have been considered for protein (BSA) filtration with ultrafiltration membranes (Bowen et al., 1996) and enzyme (alcohol dehydrogenase) filtration with microfiltration membranes (Bowen et al., 1992) and the filtration of silica particles through ultrafiltration membranes (Bowen et al., 2003). A model based upon a monte carlo simulation technique, has been derived for the simulation of colloidal normal flow membrane filtration (Chen et al., 2005). It incorporates hydrodynamic effects with inter-particle interactions. Whilst exhibiting promise for the simulation of every force and particle displacement, the model requires testing with a diverse range of feedstocks.

1.2.5 Cross-Flow Considerations

The focus of this thesis will be on normal flow membrane filtration, therefore only a brief discussion of cross-flow transport effects will be presented here.

1.2.5.1 Critical Flux Concept

A critical flux concept has been derived for microfiltration (Field et al., 1995), stating that at start-up there exists a flux below which a decline of flux with time

does not occur. Above it fouling is observed. The classical filtration laws given in Table 1-4 were modified to incorporate cross-flow removal mechanisms. It was demonstrated that provided certain terms took finite values, fluxes should exist at which there is no observed decline of flux with time. The general form of the critical flux model is:

$$-\frac{dJ}{dt}J^{n-2} = k\left(J - J^{*}\right) \tag{1-11}$$

Where J is the flux, k is a constant, and J^* is the critical flux. n takes values of: 0 for cake filtration, 2 for complete blocking and 1 for intermediate blocking.

1.2.5.2 Aggregate Transport Model

A methodology, called the aggregate transport model has been developed, which can predict the pressure-independent permeate flux and yield of target species for the cross-flow microfiltration of poly-disperse solutions (Baruah et al., 2003a). The model involves a number of steps, which ultimately leads to the generation of predicted permeate flux and yield as a function of wall shear rate for the pressure-independent regime. The model has been tested with a transgenic goat milk feed for the recovery of a human IgG fusion protein (Baruah et al., 2003b). Despite milk being an extremely complicated poly-disperse suspension, good agreement between the model and experimental data was reported. This technique was taken a step further to optimize an existing transgenic goat milk process (Baruah et al., 2004). In this case the recovery of IgG was increased from 1% to 95% for the crossflow microfiltration step. The model also works well for predicting the separation of BSA from haemoglobin (Hb), and BSA from IgG (Baruah et al., 2005), and integrates into a two-step membrane process for the recovery of heterologous IgG from transgenic goats milk (Baruah et al., 2006). However, to date no independent review of the model has been published.

1.3 Applications of Normal Flow Filtration

Normal flow filtration is used in the biopharmaceutical industry in two key areas: sterile filtration; and viral filtration. Sterile filtration is a microfiltration process that removes bacteria from a process stream. Viral filtration acts to significantly reduce the concentration of viruses in a process stream. Of the configurations discussed in Section 1.2, normal flow membrane filters for industrial applications are primarily fabricated as pleated cartridges.

1.3.1 Sterile Filtration

Sterile filtration is used in processes where bacteria and other microbial contaminants require removal from a process stream, but where the product is labile and sensitive to high temperatures or gamma irradiation (Griffiths et al., 2000). Sterile filtration is conducted at ambient temperatures, and has widespread use within the pharmaceutical industry. Pall Corporation sells the Supor® membrane in 25.4cm 10" cartridges (other cartridge sizes are also available), whilst Millipore markets the Durapore® membrane. The key properties of these membranes are given in Table 1-5.

The ASTM F 838-83 code, is one of the first standard test methods for determining bacterial retention (Madsen, 2006), and has since been re-designated as ASTM F 838-05 (ASTM, 2005). The sterile filters of Pall and Millipore are still tested to meet this standard. The standard deals with the bacterial retention characteristics of membrane filters using *Brevundimonas diminuta* as the challenge organism. When grown in a nutritionally-limiting growth medium the size of *B. diminuta* is small enough at 0.5 μm that it represents a rigorous challenge to the retention ability of the membrane. For a filter to meet the standard, it must completely retain the *B. Diminuta* organism at a challenge concentration of 1×10^7 colony forming units (cfu) per cm^2 of membrane area (Waterhouse et al., 1995).

Table 1-5: Properties of membrane filters used in sterile filtration of biopharmaceuticals.

Manufacturing company	Pall Corporation	Millipore
Product name	Supor® EKV	Durapore®
Membrane material	Polyethersulfone	Polyvinylidene fluoride
Wettability	Hydrophilic	Hydrophilic
Pore size (µm)	0.22	0.45 or 0.22
Cartridge length (inch)	10	10
Area per cartridge (m^2)	0.72	0.55
Max. forward flow (ml/min)	17[I]	NS
Bubble point (psig)	NS	18[II]

[I] Water used to wet membrane
[II] Mixture of 60/40% IPA/water used to wet membrane
NS: not stated

There also exist some 0.22 µm filters that are not validated to achieve full sterility. These so called bioburden reduction filters come in the same pleated format as sterile filters and are used primarily for the reduction of microbial cells and the protection of chromatography columns further down the bioprocess sequence (Figure 1-1).

Typical feedstocks faced by sterile/bioburden reduction filters are given in Table 1-6. High concentration protein solutions have been seen to foul sterile filters, although the formation of fouling components is complicated. This will be discussed further in the Section 1.3.2.

Table 1-6: Characteristics of typical feedstocks filtered using sterile/bioburden reduction filters.

Feed Type	Typical Composition	Type (Fouling / Non-fouling)	Position Within Bioprocess Train
Buffer Solution	Varying viscosity. Range of composition depending upon position within bioprocess train.	Non-fouling	Buffer feed to fermenter. Before buffer lines to chromatography columns. Buffer lines to cross-flow filtration step.
Fermentation Broth	Low concentration of microbial cells, lysate.	Fouling	After centrifugation and depth filtration steps.
Protein Solution	High concentration of protein.	Fouling	Before chromatography columns. At the end of the bioprocess train before formulation.

1.3.2 BSA as a Fouling Feedstock

BSA has been used by many groups as a fouling feedstock for the study of membranes of varying pore size (Ahrer et al., 2006; Chan et al., 2004; Girones et al., 2006; Guell et al., 1996; Kelly et al., 1993; Kelly et al., 1997; Manttari et al., 2006; Meireles et al., 1991; Mourouzidis-Mourouzis et al., 2006; Nakamura et al., 2006; Tracey et al., 1994; Wang, 2005). Generally these groups have experienced varying degrees of fouling dependent upon the source of BSA, operating conditions and membrane type.

1.3.2.1 BSA Source

There are several methods by which BSA is purified from bovine serum. A cold ethanol or heat shock method can be used for the initial fractionation. This can then be combined with an additional purification step such as charcoal filtration, recrystallization, alkylation or dialysis (Kelly et al., 1993). The method of purification affects the rate of flux decline when a BSA solution (Kelly et al., 1993). These authors found that a cold ethanol/ charcoal filtration purification

methodology lead to the fastest rate of flux decline using a 0.16µm pore size polyethersulfone membrane.

1.3.2.2 Fouling Mechanism

The size of a BSA at 66kDa is not notionally large enough to foul a microfiltration membrane with pore size in the range of 0.1-0.5µm. Instead it is thought that BSA solutions contain a low concentration of polymeric BSA aggregates, which have a size large enough to foul microfilters. These aggregates act as nucleation sites, to which native BSA attaches, thus enhancing fouling. Thus the mechanism takes place in stages: deposition of BSA aggregates via convective flow, followed by chemical attachment of native BSA to nucleation sites. It is believed that this chemical attachment takes place via disulfide linkages (Kelly et al., 1993) and is enhanced if the protein contains a free thiol group (Kelly et al., 1994; Kelly et al., 1997; Kim et al., 1993; Liu et al., 1991).

1.3.2.3 Other Protein Types

One group (Kelly et al., 1997) has compared the fouling of microfiltration membranes with different proteins as well as BSA. Using discs of 0.22µm PVDF membrane, they saw that pepsin, ovalbumin and β-lactoglobulin showed similar flux decline to that of BSA. Despite having no free thiol groups pepsin had a greater rate of flux decline than BSA, whilst ovalbumin and β-lactoglobulin showed the greatest rate of flux decline.

1.3.2.4 Effects of Agitation

Two groups (Guell et al., 1996; Kelly et al., 1995), have presented data that shows that stirring increases the aggregation of BSA, leading to a greater rate of flux decline.

1.3.3 Viral Filtration

Viral filtration utilises ultrafiltration membranes, operated in a normal flow configuration, to remove viruses from a product stream. During the manufacture of biotherapeutics derived from mammalian cells and human cells there is a risk of contamination by virus or virus-like type A and type C particles (Dileo et al., 1993). These must be removed during the down stream processing operation. Pall Corporation produce the Ultipor® membrane, whilst Millipore market the Viresolve® membrane. The key properties of the membrane are given in Table 1-7. The standard test organism for viral filtration is the murine Leukaemia virus (Aranha-Creado et al., 1998). This virus, with a size range of 80-120nm, offers a good model for A or C retrovirus type molecules. The forward flow test is another means by which the integrity of the filter can be assessed, and is commonly used by manufacturers of filters (Dowd, 2009).

The membrane is used to remove all manner of viruses from a solution, whilst allowing the target protein to pass through the membrane. Generally when validating the membrane, target proteins are not used, thus the log removal of the virus by the membrane is the key measured parameter. However some examples do exist where Human Serum Albumin (HSA) has been used as the target protein (Dileo et al., 1993).

Table 1-7: Key properties of virus removal filters

Company	Pall Corporation	Millipore
Product name	Ultipor®	Viresolve®
Membrane material of construction	Modified Polyvinylidene fluoride	Polyethersulfone
Wettability	Hydrophilic	Hydrophilic
Pore size (nm)	20 or 50	Unknown
Cartridge length (inch)	10	10
Area per cartridge (m^2)	1 (20nm) 1.6 (50nm)	0.48

Instead of using an actual virus to test the system, a biological or non-biological surrogate can be used. The mechanism through which the membrane retains the virus defines the important physical properties that the surrogate must contain.

The retention of viruses is dependent upon two factors (Oshima et al., 1998): size exclusion of the virus and adsorption of the virus to the membrane structure. Size exclusion is considered to be the most significant mechanism through which retention is achieved. If surrogates are to be used instead of the actual virus, then the size and conformation of the surrogate is important. Bacteriophages are viruses that propagate within bacteria. Some, such as PR772, can be produced using *E. Coli* as the host bacterium. This makes them much easier to generate and isolate than human viruses such as influenza or polio that require mammalian cells. As such, bacteriophages are often used as biological surrogates to mammalian viruses. Two such bacteriophages are Φ6 and PP7, which have sizes of 75nm and 25nm respectively (Aranha-Creado et al., 1999). Some bacteriophages have been labelled with a fluorescent dye, so as to aid in their detection and quantification (Gitis et al., 2002).

Whilst viral filters have some use within bioprocesses, the frequent and varied application of sterile filters make them a relevant and interesting system to work with.

1.4 Fabrication of Pleated Membrane Cartridges

Membrane media can be manufactured by a number of methods, the choice of which depends upon the porous structure required. Phase inversion is the most important technique for commercial membrane production (Reif, 2006). Interfacial polymerisation is used for many microfiltration and ultrafiltration membranes to apply a coating to the surface of the membrane (Reif, 2006). This

surface modification of the membrane creates composite membranes with enhanced properties. The membrane media is fabricated as a flat sheet, which is provided in large rolls. As has been discussed previously in Section 1.2, the pleating of the flat sheet membrane and packing of the pleats into a cartridge configuration provides a method by which large membrane areas can be inserted into a unit that has a smaller footprint than if flat sheet membrane was used (Jornitz, 2006).

An overview of the manufacturing process for the production of pleated membrane cartridges is given in Figure 1-4. This five-step manufacturing procedure is not an automated process, but can be carried out at scale to produce large numbers of cartridges during an operating run. The manufacturing procedure begins with feeding membrane media into the pleating machine (Step 1). The membrane media is placed in-between drainage material, which acts to protect the material and encourage drainage to and from the membrane surface by keeping the membrane pleats apart. The drainage material can be woven, or non-woven. The pleating machine has a tooth above and below the membrane material which act 180° out of phase with each other, so that one is fully inserted into the membrane material the other is fully retracted. The teeth are heated to a high temperature so that the pleated shape becomes set and the membrane material does not return to a flat sheet format. The pleating machine can be fully configured so that the pleat height, rate of pleat production, type of pleat and pleat setting temperature can be adjusted. Increasing the rate of pleat production may lead to irregularities in the pleat structure and depends upon the physical strength of the membrane. The two pleat types produced by Pall Corporation are shown in Figure 1-5. The fan pleat is the standard type of pleat used by most membrane manufacturers. The Ultipleat® is unique to Pall Corporation, and allows for a greater membrane area to be packed into the cartridge (van Reis et al., 2007).

The pleating machine can make either pleat type, however separate tooling is required and this must be set up on the machine before production can begin.

Once the pleated pack has been produced a section is removed with the correct pack length to provide a suitable pleat packing once inserted into the cartridge format.

Step two takes the loose pack of pleats and seals the two ends of the pack together. This produces a cylindrical pleated pack. The two ends are joined using a heat sealing technique. The selection of the correct sealing temperature is important, as to cool or to hot will lead to a poor seal that will leak. In Step 3 the cylindrical pleat pack is trimmed so that the length of the pleat is correct for the required cartridge length. In Figure 1-4 two examples are illustrated representing a 25.4cm (10") or 2.54 cm (1") cartridge length.

Once the pleat pack is trimmed to the suitable lengths it is packed into the annulus between an inner and outer cage (Step 4). The inner and outer cages have holes machined out of their structure to allow for fluid flow (this is not shown in Figure 1-4). The inner core acts as a physical support for the pleated pack to sit upon and thus confers mechanical strength (Jornitz, 2006).

The final step (Step 5) is to fit adaptors onto the ends of the cartridge. This is illustrated in Figure 1-4 where the pleated cartridge is shown without the inner and outer cores. These adaptors are attached by heat sealing at high temperature, and provide the final sealing step. The adaptor at the base of the cartridge is referred to as a 'code 7' design (van Reis et al., 2007) and has two grooves in which 'o' rings are placed to form a seal and two tabs to lock the cartridge into the housing. Once the adaptors are attached, the cartridges are allowed to cool before undergoing a leak test. The standard methodology for the leak test is the reverse bubble test, which will be discussed in Section 1.5.

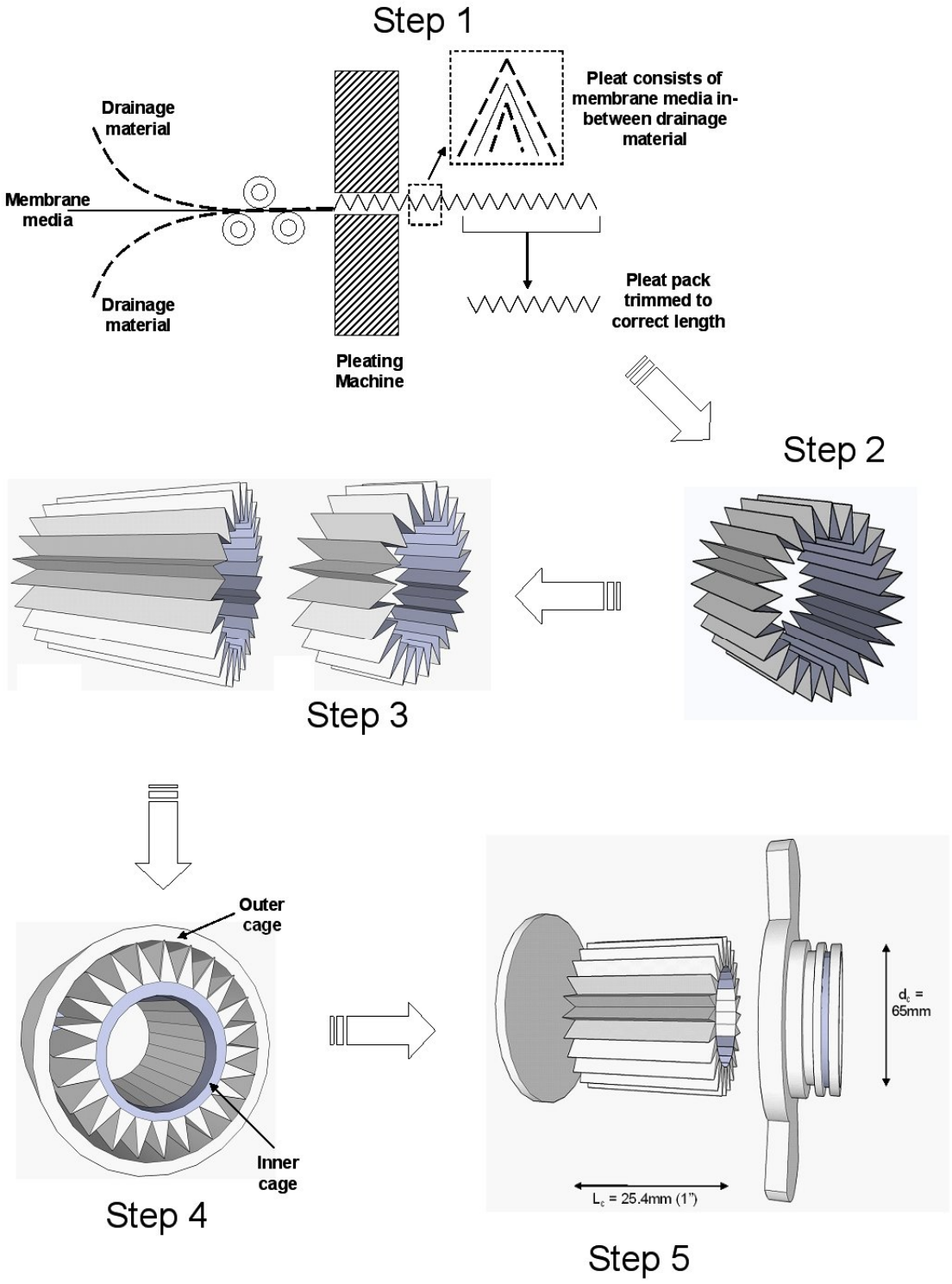

Figure 1-4: Overview of manufacturing process to produce pleated membrane cartridges.

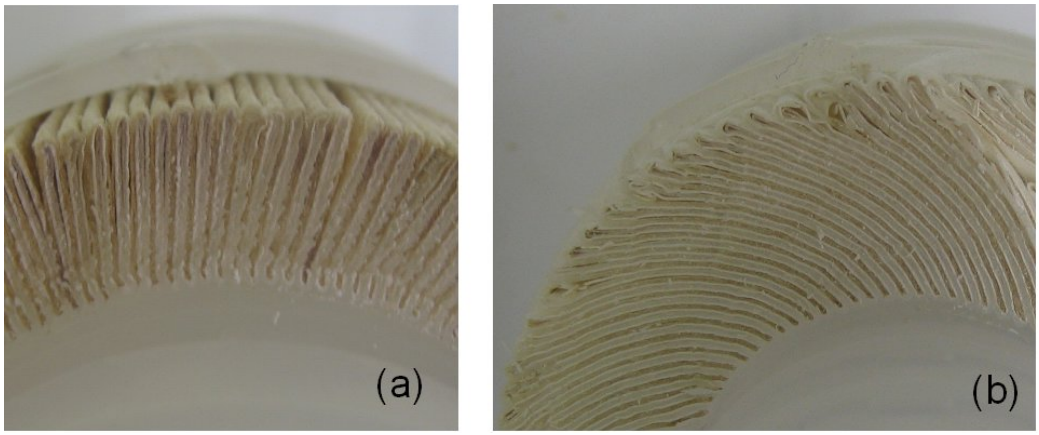

Figure 1-5: Photographs of different pleat types. (a) Photograph of a cross-section of a 10" EAV cartridge with Fan pleat configuration. (b) Photograph of a cross-section of 10" UEAV membrane pleats with a Ultipleat® pleat configuration.

1.4.1 Design Characteristics

The design characteristics of pleated membrane cartridges have been well described (Jornitz, 2006; van Reis et al., 2007). There are three main design characteristics that can be altered during manufacture: pleat height; pleat type (see Figure 1-5); and pleat packing density. Pleat height represents the depth of each pleat and is represented by h_p in Figure 1-6. The pleat packing density is a measure of the number of pleats packed into a given cartridge volume. Increasing the pleat packing density, decreases the angle, θ, between each pleat, and the space between each pleat. This may lead to pleat crowding (Waghode et al., 2007; Wakeman et al., 2005) where the pleats are no longer acting in isolation, a factor that may affect filtration behaviour.

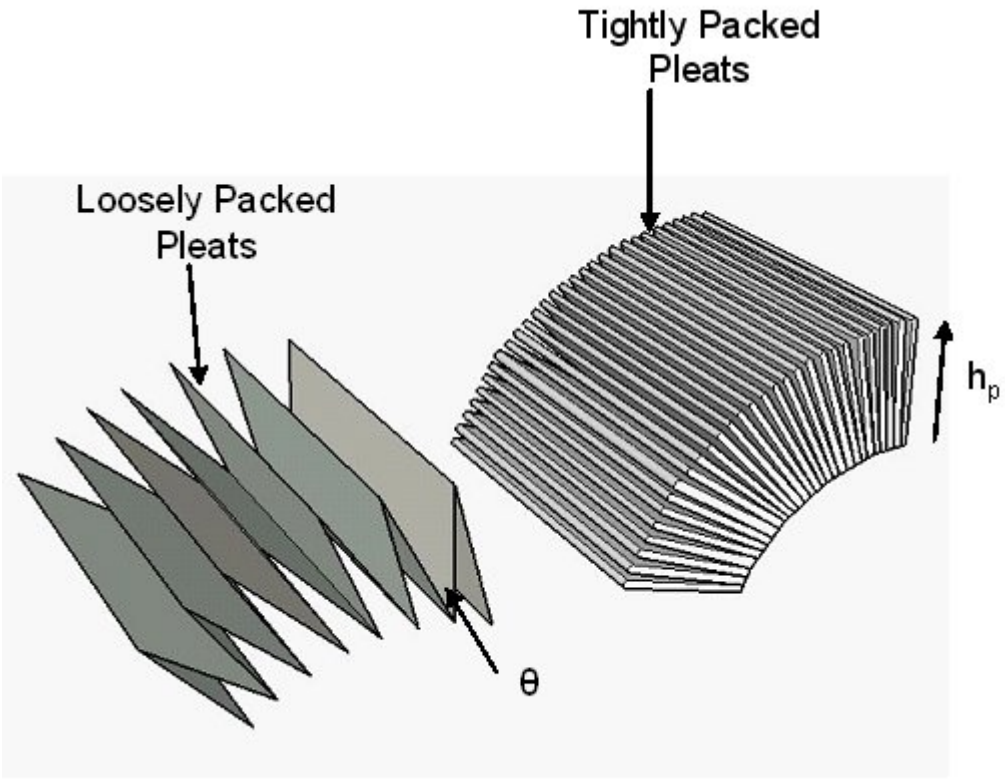

Figure 1-6: Characteristics of pleated membranes. Examples are shown for loosely and tightly packed membrane packs. Increasing the tightness of packing leads to a higher pleat packing density.

1.5 Performance Characterisation of Normal Flow Filtration Devices

The factors that generally affect normal flow filtration process performance are (Ireland et al., 2004):

- The feedstock: components and concentration, presence of aggregates, pH, temperature, viscosity, ionic strength, cake resistance.
- Operating conditions: pressure difference; mode of operation (constant pressure or constant flow); feed flow rate.
- Membrane properties: membrane area; flow distribution; resistances to flow; porosity; diameter of pores.

Generally the following outputs require optimisation:

- Flux of material through the membrane
- Capacity of the membrane
- Product transmission or retention performance
- Performance of the membrane: removal rating (100%) for sterile filtration; reduction rating (6 Log titer) for viral filtration

Clearly there are a large number of variables and this makes the optimisation of filtration step difficult. There are also many ways in which process steps upstream of the membrane filtration step can influence the performance of the membrane operation. The membrane filtration step can also have a significant effect on units downstream of the filter unit. Thus a system that accurately and rapidly assesses the performance of the microfiltration step would be of value. This will be discussed further in Section 1.7.

The flux and capacity of the cartridge can be identified using theory outlined in Sections 1.2.1. A calculation of product transmission will typically require an assay to be conducted that quantifies the concentration of the product in feed and permeate streams. Examples of suitable total protein assays are: the Bradford assay (Bradford, 1976) and the Lowry assay (Lowry et al., 1951). Alternatively HPLC can be used, which can be particularly useful for identifying multiple components of the product. During a normal-flow filtration experiment samples from the feed and permeate are taken and then processed with the chosen assay. For most microfiltration operations high product (protein) transmission would be expected.

The ability of the membrane to remove microbial organisms and viruses (where applicable) can be quantified using invasive and non-invasive tests. These are described in more detail in the Section 1.5.1 and Section 1.5.2 respectively.

1.5.1 Invasive Integrity Testing

It has previously been mentioned in Section 1.3.1 that *B. diminuta* is used to test the integrity of cartridges, due to the small size of the micro-organism. The challenged membrane must retain no less than 1×10^7 colony forming units per cm^2 of available membrane area (Waterhouse et al., 1995) at a maximum test filter differential pressure of 206 kPa and a flow rate of 2 to 4 $Lmin^{-1}cm^{-2}$ (Madsen, 2006). An apparatus for conducting such a test is illustrated in Figure 1-7. A flat sheet disc is placed downstream of the test cartridge. The permeate from the disc and the disc itself are used to identify whether the cartridge passes the test. Incubation of the disc and the permeate on agar can take 7-14 days to yield a result (Waterhouse et al., 1995). An alternative method that uses bioluminescent and fluorescent strains of *B. diminuta* has been proposed (Griffiths et al., 2000), although this method still requires 24 hours to generate a result. The length of time required to conduct the test, coupled to the invasive nature of the test, which renders the cartridge unusable after completion of the test has lead to the generation of non-invasive tests. These are outlined in the Section 1.5.2.

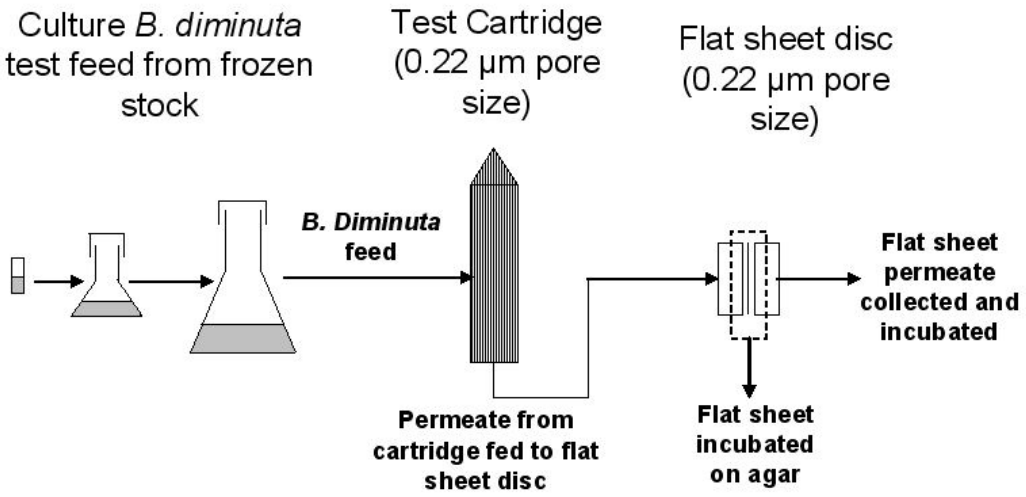

Figure 1-7: Illustration of method for *B. diminuta* integrity test.

1.5.2 Non-Invasive Integrity Testing

It is common industrial practice to integrity test the membranes before and after each batch so as to ensure that the pore size of the membrane is small enough that the membrane will fully retain the microbial challenge. The *B. Diminuta* retention challenge is an invasive test that requires the membrane to be cleaned after the test has taken place. Alternatively non-invasive tests such as the bubble point or the forward flow test are used instead. The bubble point test is designed to determine the pressure at which a continuous stream of bubbles is observed downstream of a wetted filter under gas pressure. Figure 1-8 shows a rig that can be used to quantify the bubble point when using flat sheet discs of membrane. The same type of rig set-up can also be used when identifying the bubble point of pleated membrane cartridges. The membrane is fully immersed in water so that it becomes fully wetted, before being placed within a membrane holder. A gas is applied to the feed side, and as the pressure differential increases the gas dissolves into the water. When the pressure differential reaches the bubble point it is great enough that the air forces trapped water out of the pore, and a steady flow of air travels through the membrane pores. Thus the bubble point is reached and the air travels through the membrane by a mechanism of bulk transport.

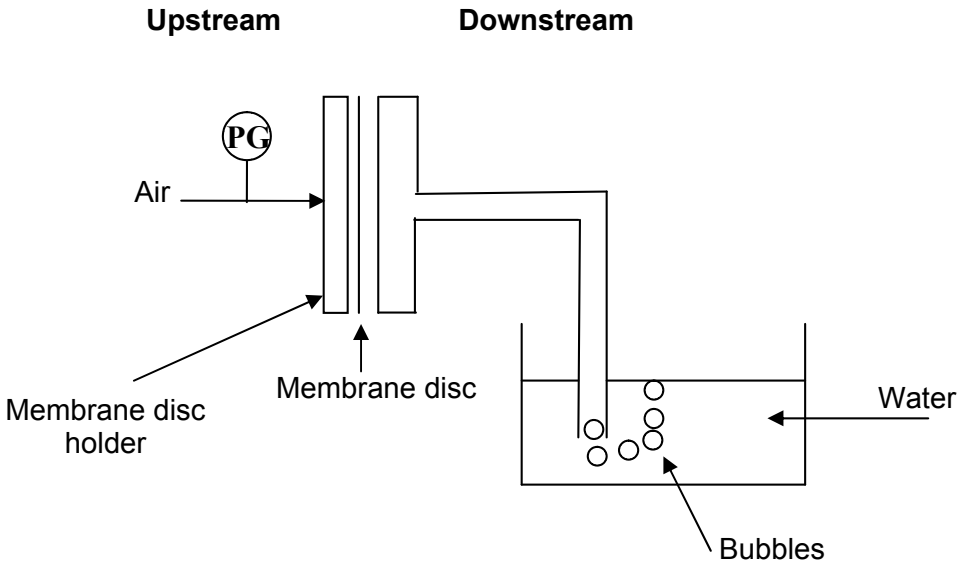

Figure 1-8: Rig for quantifying bubble point using small diameter discs of membrane. PG = pressure gauge.

The bubble point can be used to measure the maximum pore size through the use of the Cantor equation (Meltzer et al., 1998), which is expressed as follows and is derived from the balance of forces in a capillary:

$$D = \frac{4\gamma \cos\theta_W}{\Delta P} \tag{1-12}$$

where ΔP is the pressure differential across the filter; D is the diameter of the capillary; θ_W is the wetting angle between the fluid and the surface of the filter; γ is the surface tension between the liquid and the solid interface material. It has also been demonstrated that for fluids that wet porous materials well the contact angle θ_W is zero. Hence Equation 1-12 reduces to Equation 1-13. However, Equation 1-13 is only valid when the units of ΔP and D are psi and μm respectively.

$$\mathrm{D} = \frac{30}{\Delta \mathrm{P}} \tag{1-13}$$

It is common for membrane manufacturers to quote typical bubble point values for their filters in terms of pressure. They also supply bubble points for all of their membranes that are sold to customers. Thus the customer can use the bubble point to ensure that their filter is correctly installed, and that after each batch it still has the same ability to retain bacteria. If the bubble point was to decrease then the pore size will increase, and thus the membrane filter may no longer have a pore size small enough to fully retain bacteria.

The forward flow test is based upon similar principles, but measurements are taken whilst the pores are still fully wetted. Figure 1-9 shows how gas flow downstream of the filter will change as the differential pressure across the membrane increases.

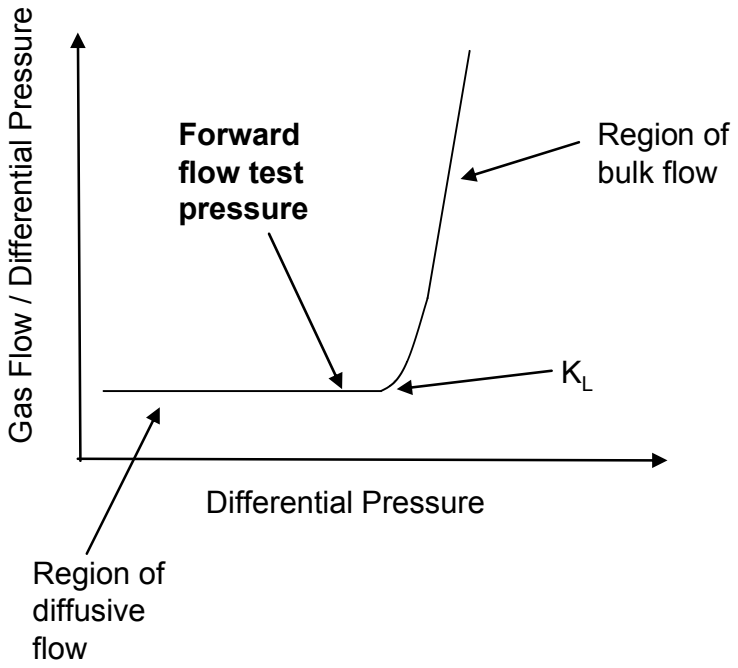

Figure 1-9: Downstream gas flow regimes for membrane with fully wetted pores

The forward flow test works by measuring the gas flow rate downstream of the wetted membrane for a given test pressure. This test pressure should be below the K_L value, which marks the transition between diffusional and bulk flow. If the integrity of the membrane remains the same after each time it is used, then the gas flow rate measured at this test pressure should remain the same. It is standard for manufacturers to quote a maximum allowable forward flow test, which is achieved just before the K_L value is reached. Due to the low gas flow-rates that will be seen downstream of the filter during diffusive flow, the forward flow test is only applied to large scale cartridges, where the surface area of membrane in the cartridge is high.

1.5.3 Leak Testing

A quick methodology to test whether a membrane is perforated or a cartridge contains a leak is to carry out a reverse bubble test. An illustration of the typical experimental set-up is given in Figure 1-10. In this test the cartridge is soaked in a solvent (e.g. IPA/water mix) before having a bung inserted into the permeate hole at the base of the cartridge. An air line passes through the bung and into the permeate side of the cartridge. The wet cartridge is submerged in a vessel containing the solvent used for wetting. Air is applied to the permeate side of the cartridge and the cartridge is observed to see if a steady stream of air bubbles escaping from the feed side of the cartridge, which would indicate a leak. Particular attention is paid to the adaptors welded onto the cartridge, and the pleated membrane side seal.

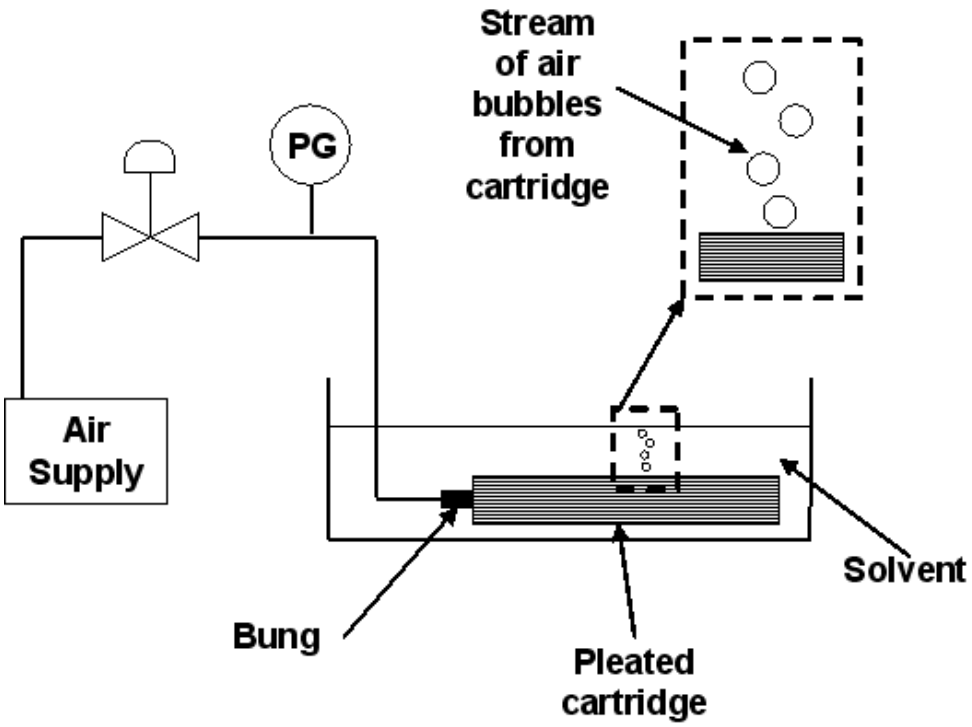

Figure 1-10: Illustration of equipment set-up required for leak testing of a pleated cartridge using the reverse bubble test method. PG represents a pressure gauge.

1.6 Effect of Membrane Pleating on Cartridge Performance

In most applications the filter will be exposed to large volumes of process fluid containing a relatively low concentration of suspended solids (Figure 1-1). Due to the large process volumes it is common practice to strive for the highest membrane area per unit volume of cartridge to minimise the footprint of the overall unit. One option to achieve this is by pleating of the flat sheet membrane and packing a high density of pleats around a central core (Jornitz, 2006).

Pleated geometries are frequently used in the manufacture of air filters, which are used in a number of secondary operations within a typical bioprocess sequence. The filter medium is contained in either a pleated panel or a cylindrical cartridge configuration. A number of studies (Baleo et al., 2000; Caesar et al., 2002; Chen et al., 2008; Chen et al., 1995; Lucke et al., 1996; Subrenat et al., 2003; Tronville et al., 2003) have investigated pleating effects in air filter design. These typically seek to reduce the overall pressure drop by optimising the pleat count per unit length. It has been reported that pleat height also impacts upon overall pressure drop (Chen et al., 1995). More recent studies (Nassehi et al., 2005; Waghode et al., 2007; Wakeman et al., 2005) have produced models utilising computational fluid dynamics to explore the influence that pleat design has on air filter performance. These include compression of the medium, pleat deformation and pleat crowding at high pleat packing densities. When simulations were run incorporating medium compression and area loss, there was good agreement with experimental data. Examination of the data presented suggested that of the two factors incorporated into the model, area loss appeared to have the greatest impact on performance (Waghode et al., 2007; Wakeman et al., 2005). Air filters are similar in basic design to those used in the biopharmaceutical industry, but as noted above are generally optimised so as to reduce the pressure drop across the pleat. The cartridges used in the biopharmaceutical industry are optimised to maximise the filtration area and to handle high viscosity, liquid feeds. Whilst findings generated for air filters may well bear on the characteristics of their biopharmaceutical counterparts these key differences must be borne in mind.

For 0.45 μm PVDF membrane filter cartridges used with liquid feeds, pleating has also been associated with a drop in cartridge performance when compared with flat sheet membranes (Chandler et al., 2004). Several researchers (Giglia et al., 2007; Gollan et al., 1985) have considered the effect of the permeability of the drainage material upon cartridge performance. Golan and Parekh (Gollan et al., 1985) developed permeability models to account for the different process feeds that a cartridge may be required to filter. A drainage permeability term to account for the compressibility of the drainage material was introduced. This varied across the length of the pleat, but no experimental data was presented for model validation. Giglia and Yavorsky (Giglia et al., 2007) built upon this work and compared the performance of a range of sterile cartridges consisting of different pore sizes and membrane materials. A discrepancy in membrane permeability was observed between flat sheet discs and 10" cartridges. Discrepancies have also been reported in two further un-related studies (Chandler et al., 2004; Rajniak et al., 2008).

In summary, there has been little work conducted to fully characterise pleated cartridges. This is especially the case for pleated cartridge filters used for the filtration of liquid feedstocks. This has lead to a problem for those involved in bioprocess design, whereby discrepancies between the performance of flat sheet and pleated membrane have been noticed, but no solution is given (Chandler et al., 2004; Rajniak et al., 2008).

1.7 Scale-Down and Ultra Scale-down

Scale-up involves using small-scale equipment to predict the performance of large-scale process equipment (Pampel et al., 2008). In order to conduct scale-up studies a scale-down device is required that mimics the larger unit whilst maintaining the main geometric parameters constant between scales. Such studies are utilised when feedstock is scarce or expensive, as a means to design or optimise the large-scale equipment. In an ideal scale-up the performance of the large-scale equipment would be exactly mimicked by the small-scale.

Typically this does not happen and scaling factors must be utilised to account for uncertainty in the performance prediction (Anderson et al., 2009). This leads to over-sizing of equipment and process inefficiencies. It also shows limitations in the understanding of the process if these factors must be incorporated. Scale-down beyond a given size range is often difficult to achieve due to the geometrical complexities of the large-scale industrial equipment, and as such a new approach has been developed, called Ultra Scale-down (USD), which aims to seek out key effects and parameters that dominate when scale changes are made (Titchener-Hooker et al., 2008). This approach has been developed primarily for centrifugation and is discussed in greater detail in Section 1.7.5.

In normal flow membrane cartridge filtration most small-scale data is obtained using small flat sheet discs of the membrane, which are typically 47mm in diameter (Badmington et al., 1995). The membrane disc is of the same material as the membrane contained within the cartridge. As has been discussed in Section 1.6 there have been discrepancies reported between the performance of the flat sheet disc and the pleated cartridge. This would affect the ability to scale-up reliably from flat sheet data. As yet, no scale-down device or methodology has been developed to account for the differences between flat sheet and pleated membranes. The standard protocols for use with the flat sheet discs are presented in the following section.

1.7.1 Scaling with Flat Sheet Discs

Flat sheet discs are not geometrically similar to large-scale pleated cartridges, and on this basis can be considered an Ultra Scale-down method of achieving scale-up. Flat sheet disc experiments are operated at constant pressure, provided by a gas supply. Depending upon the feedstock used a variety of parameters can be obtained. For clean solutions the membrane resistance used in Equation 1-1 can be obtained by measuring the permeate flow-rate over a range of trans-membrane pressures. For fouling feedstocks the cake resistance can be evaluated by measuring the mass of cake built up upon the membrane surface and combining with flux decline data (Foley, 2006). For feedstocks that cause

standard blocking of the membrane pores the V_{max} test protocol is used, which allows for the prediction of maximum volume filtered through the membrane before the permeate flow drops to zero (Badmington et al., 1995). V_{max} is defined by:

$$\frac{t}{V} = \frac{t}{V_{max}} + \frac{1}{Q_0} \tag{1-14}$$

Where: Q_0 is the initial flow rate at start of filtration.

Thus V_{max} can be obtained by plotting t/V_{cum} against t, where t is the operational time and V_{cum} is the cumulative volume collected. V_{max} is the gradient of the straight line that is yielded. Normalising V_{max} for the membrane area of the disc provides a parameter to design the size of a cartridge (in terms of membrane area) required to process a given volume of feedstock.

However, as has previously been noted in Section 1.6, the performance prediction from a flat sheet disc does not generally scale well to the large-scale pleated cartridge (Chandler et al., 2004; Rajniak et al., 2008).

1.7.2 High Throughput Membrane Evaluation

Recently a number of studies have shown that high throughput screening of normal flow filtration can be achieved using small areas of membrane discs (0.28 cm^{-2}) (Chandler et al., 2004; Jackson et al., 2006). The membrane discs in these cases are housed in wells, and each filter plate contains 96 wells. The 96 well arrangement allows multiple experiments to be conducted at any one time. Whilst at this scale variation in the porosity of the membrane was reported to be an issue and this can affect the ability to characterise the performance of the membrane. However the method provides a useful scoping approach for the enhancement of larger scale trials.

1.7.3 P_{max} Test

For feedstocks where a constant flow regime is used during the filter operation a concept called P_{max} can be used (van Reis et al., 2007). This method is primarily used for the evaluation of the capacity of depth filters (Tarrach et al., 2003; Wang et al., 2006; Yavorsky et al., 2003). The approach works by monitoring the build-up of pressure on the feed side as fouling occurs. The governing equations for the flux decline models discussed in Section 1.2 are given in Table 1-8. It has also been reported that if fouling is due entirely to pore constriction then (van Reis et al., 2007):

$$\frac{P}{P_0} = \left(1 - \frac{V}{V_{\max}}\right)^{-2} \tag{1-15}$$

This approach has not previously been reported as being used for the prediction of performance for normal flow microfiltration cartridges, but could be used for systems where the concentration of fouling components is low. For systems such as these large volumes of feedstock would be required to conduct the equivalent V_{max} test.

Table 1-8: Governing equations for flux decline models.

Flux Decline Model	Governing Equation	
	Pressure[1]	Linearised Form[1]
Pore blockage (complete blocking)	$\frac{P}{P_0} = (1 - \beta \cdot t)^{-1/2}$	$\frac{1}{P^2} = a - b \cdot V$
Intermediate blockage	$\frac{P}{P_0} = (1 - \beta \cdot t)^{-1}$	$\frac{1}{P} = a - b \cdot V$
Pore constriction (standard blocking)	$\frac{P}{P_0} = (1 - \beta \cdot t)^{-2}$	$\frac{1}{P^{1/2}} = a - b \cdot V$
Cake filtration	$\frac{P}{P_0} = 1 + \beta \cdot t$	$P = a + b \cdot V$

[1] Taken from (van Reis et al., 2007).

1.7.4 Scale-down through reduction of effective area

Scale-down is often achieved through a process of miniaturisation, however, for a disc stack centrifuge an alternative approach has been taken to modify an existing piece of equipment to achieve a lower feed requirement (Mannweiler et al., 1992). The reduction in scale is achieved by blanking off areas of the disc stack centrifuge with solid aluminium discs, which in effect reduces the number of active discs available for the separation of the feed material leading to a reduction in separation capacity. The study reported that up to a 10-fold reduction in separation capacity was achieved. Despite the reduction in separation capacity the recovery of a dilute suspension of polyvinylacetate particles was seen to be similar for the blanked off centrifuge when compared to the centrifuge in its un-blanked standard setup. However, the work also highlighted the importance of careful positioning of the active discs, as performance was seen to vary depending on whether the active discs were positioned at the top or bottom of the centrifuge.

This study was taken further (Maybury et al., 1998) by examining the effect that scaling down in stages had upon both the hold-up volume within the disc stack centrifuge and the separation capacity. The study showed that the maximum scale-down gave a reduction in separation capacity of 76% and a reduction in bowl volume (and hence feed volume requirement) of 70%. Once again, it was seen that despite the reduction in scale of separation capacity and hold-up volume the grade efficiency curves, a measure of the separation performance, produced by the scale-down variants closely follow the curves for the full stack machine.

Whilst the two studies described above were conducted for a centrifuge system, they present an interesting strategy of achieving scale-down as key parameters of the system are held constant (in this case bowl diameter and disc shape). This is contrary to miniaturisation of the device whereby scale-down takes place in all dimensions.

1.7.5 Ultra Scale-Down

Another scale-down strategy that differs significantly from typical scale-down techniques has been presented as an ultra scale-down (USD) methodology (Titchener-Hooker et al., 2008) The USD approach has been developed to improve the ability to predict the performance of large-scale biopharmaceutical unit operations from small-scale experiments (Dunnill et al., 2003). This is achieved by generating data for key engineering parameters around which the scale-up can take place. Ultra scale-down studies are conducted using equipment that does not have geometrical similarity to the large-scale target. For downstream processing equipment that is geometrically complex, this often means that USD studies can be conducted with vastly reduced feed volume requirements (Tustian et al., 2007). Ultra scale-down techniques have been developed primarily for centrifugation (Berrill et al., 2008; Boulding et al., 2002; Hutchinson et al., 2008; Levy et al., 1999; Neal et al., 2003; Pampel et al., 2008; Tustian et al., 2007; Zhang et al., 2007), but have also been extended to candle filters (Reynolds et al., 2003). Further details of various USD studies reported to date are contained in Table 1-9. To date there have been no published studies that use a USD methodology and apply it to normal flow membrane cartridge filters, or any other filter beyond that of a Nutsche filter.

Table 1-9: Key aspects of Ultra Scale-Down studies conducted to date by various researchers.

Unit Operation(s)	Process material	USD Technique / Device	Scale	Findings of Study	Reference
Precipitation, disk-stack centrifuge	Precipitated casein isolation from milk	Rotating disk shear device and lab centrifuge	15ml per experiments	Systematic approach used to generate critical process parameters. From these parameters a process model was produced to predict performance of 1000-fold larger pilot-scale process	(Pampel et al., 2008)
Disk-stack centrifuge	*S. cerevisiae* and *E. coli* studied at concentrations greater than 10% (wet cell weight)	Use of rotating disk shear device followed by dilution of sheared material before lab-scale centrifugation. Mathematical correction applied to clarification results to mimic original feed	250ml per experiment	Improvements were seen in clarification performance over traditional USD protocols.	(Tustian et al., 2007)
Centrifugal pump, mono pump, disc-stack centrifuge	Supercoiled circular plasmid DNA	Rotating disk shear device using elongational strain rate as the engineering scale-up parameter	20ml per experiment	Shear causes degradation of SC plasmid DNA. First order equation was observed to apply for the elongational strain rate. Good agreement seen between USD scale predictions and large-scale equipment.	(Zhang et al., 2007)
Flocculation, disk-stack centrifuge	Heat lysed high concentration *E. coli* cells exposed to flocculating agent.	High speed rotating disk device used to generate low shear and high shear material. Lab-scale centrifuge.	20ml per experiment, 100ml for full characterisation	Introduction of sheared material lead to closer match of pilot-scale clarification compared to material that had not been exposed to shear. High shear reduced the particle size of the solids.	(Berrill et al., 2008)

Precipitation, disc-stack centrifuge	Recovery of serum based immunoglobulins.	Rotating disk device, lab centrifuge. A time-integrated fluid stress used as the scaling factor	Undefined but 'ml' level.	Difference of ±10% between large-scale and USD results. This variation was within the limits of the biological assays used.	(Neal et al., 2003)
Disk-stack centrifuge	Recovery of monoclonal antibodies from a mammalian cell culture broth.	Pre-treatment of centrifuge feed in rotating disk device coupled with lab-scale test tube centrifuge.	20ml per rotating disk experiment. 10ml per lab centrifuge experiment.	Shear lead to reduction in particle size, which in turn lead to a reduction in clarification efficiency. 70% reduction in industrial scale flow-rate attributed to shear effects.	(Hutchinson et al., 2008)
Filtering basket centrifuge	Recovery of an antibody fragment from a fungal broth.	USD filtering centrifuge coupled with critical regime analysis and computational fluid dynamics to match energy dissipation rate between scales.	35ml per experiment	Good prediction of recovery of antibody fragment at same energy dissipation rate between USD device and pilot-plant basket centrifuge.	(Boulding et al., 2002)
Candle filter	Human plasma fraction IV	Nutsche filter modified to become a rotating vertical leaf filter. Iterative calculation of the initial cake resistance made.	Unknown	Continuous operation lead to improved prediction of performance characteristics compared with a batch operated Nutsche filter. This was particularly seen during the initial high flow rate period of filtration.	(Reynolds et al., 2003)

1.7.5.1 Commercial Application of USD

At present bioprocess development will take place in pilot plant trials, using existing equipment and process set-ups. This approach can only take place at late stage drug development after successful studies in animals have lead to filing with regulatory bodies and initiation of Phase I clinical trials (Titchener-Hooker et al., 2008). This leaves little time for process development and optimisation, before the process is locked for regulatory submission. Carrying out process development using pilot-scale equipment is expensive, with large volumes of feedstock required. The advantage of the USD approach described above is that it allows for changes in how process development is integrated into the overall drug development process (Dunnill et al., 2003). As small volumes of feedstock are required then this allows process development to take place at an earlier stage (see Figure 1-11). When coupled with whole bioprocessing modelling (Pampel et al., 2008), a good understanding of the operation of the process is derived, so that pilot plant trials are operated as confirmatory batches, not development batches. USD trials can take place soon after the drug discovery stage has completed and as soon as animal studies give favourable signs for the effectiveness of the drug. At this stage, the volume of process feed to use for process development will be low. Thus the advantage of carrying out process development using low feed requirements is significant.

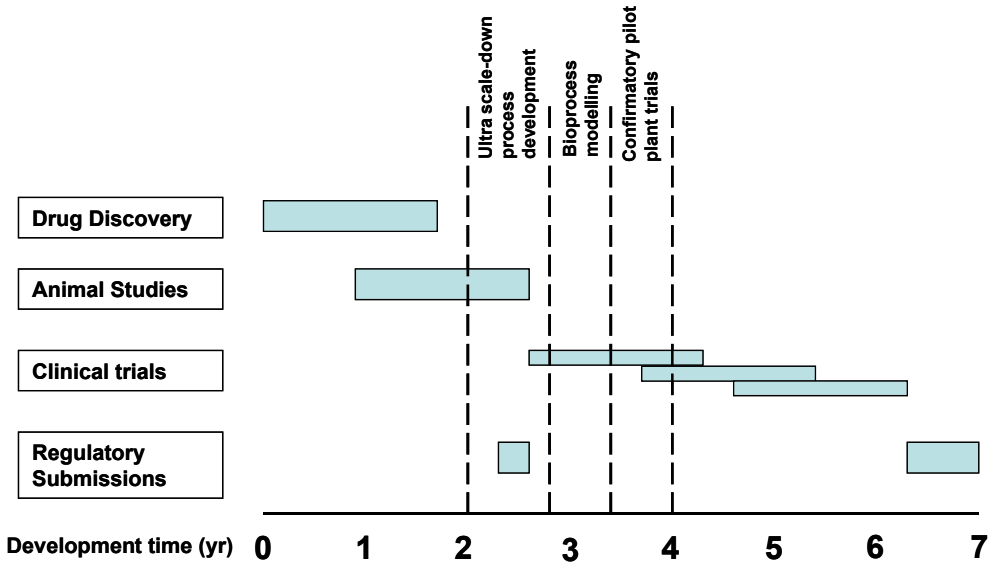

Figure 1-11: Typical timeline for biopharmaceutical drug development (Adapted from (Nealon, 2006). USD allows for process development to take place at an early stage during drug development. This is compared with current practice, which would involve pilot plant trials using existing equipment from year 3 to year 4.

1.8 Aims and Objectives of Thesis

As described in Section 1.1, pleated membrane cartridges are used extensively throughout a typical bioprocess. They operate with a variety of conditions and feedstocks (Section 1.3). Discrepancies between performance of the flat sheet and pleated membranes have been identified (Section 1.6), although little has been done to fully characterise the effects of pleating, particularly for the liquid feeds common in biopharmaceutical applications.

Current scale-up techniques use small flat sheet membrane discs to predict the performance of the large-scale pleated cartridge (Section 1.7). The discrepancy in membrane performance leads to inaccuracies in scale-up, which is overcome in a practical sense by over-sizing of the large-scale equipment. In turn this reduces the efficiency of the bioprocess and increases capital costs. No accurate and reliable scale-up methodology currently exists that accounts for the effects of membrane pleating.

Reducing the active area for separation (as was seen in Section 1.7.4 for centrifugation) by blocking off parts of a pleated cartridge, may offer a means by which a scale-down cartridge device can be produced which will retain the key characteristics of a pleat. Such a device could then be compared against the standard scale-down methodology of using small discs of the flat sheet membrane so as to evaluate whether a better performance prediction can be achieved.

A radically different approach to performing scale-down experiments, through a USD approach, was discussed in Section 1.7.5. Whilst USD techniques have been successfully developed to mimic the performance of centrifuges and other process equipment (see Table 1-9), it has not been applied to pleated cartridge filters. Taking the USD approach of focussing on key engineering parameters and using models to modify experimental data, it may also be possible to adapt experimental data gathered using small discs of flat sheet membrane to improve the performance prediction relative to a large-scale cartridge. This in turn offers the benefits highlighted in Figure 1-11, whereby bioprocess development can take place at an earlier point in the drug development cycle, reducing the amount of pilot scale work required to develop the process. This in turn reduces the cost of process development and provides more time for developing an optimised process.

The aim of this thesis is to establish scale-down and USD approaches to the rapid design and optimisation of microfiltration processes using pleated membrane cartridges. The approach will be to devise solutions that are readily applicable in industry and hence will be illustrated with a fouling feedstock typical of those found in many biopharmaceutical processes. Figure 1-12 provides an overview of the research approach to be taken. The specific objectives of each chapter are described below:

- The initial objective will be to characterise the basic filtration performance of a commercial 10" UEAV 0.2 μm rated pleated membrane cartridge filter in a standard cartridge hosing. This device is typical of the

format and scale currently used in biopharmaceutical applications. This work is described in Chapter 3, which also covers the development of a realistic fouling protein feedstock for use throughout.

- The next objective will be to systematically investigate the influence of pleat design on the filtration performance of protein solutions, since this information is not currently available in the literature. This work will define which characteristics of the pleat geometry have a significant impact upon filtration performance, and hence which will be the characteristics to maintain in the design of a scale-down cartridge device. This work is described in Chapter 4.

- The following objective will be to design and test the effectiveness of a new scale-down cartridge device to predict the performance of the large-scale cartridge characterised in Chapter 3. This study is described in Chapter 5, for a range of fouling and non-fouling feedstocks. Initial comparisons will also be made to the current standard scale-down technique that utilises flat sheet membrane.

- The final objective will be to develop a new USD methodology based on the insights on pleat geometry in Chapter 4, which improves the predictions made using flat sheet membrane and thus allows for improved performance predictions of the large-scale pleated cartridge to be made using reduced feed volumes. This is described in Chapter 6.

In addition to the above, Chapter 2 describes the experimental methods established in order to ensure the generation of accurate and precise quantitative experimental data. As part of the requirements for the award of an Engineering Doctorate (EngD), Chapter 7 describes the key challenges to commercialisation of the scale-down pleated device and the steps required in technical, commercial and validatory areas to overcome these challenges. Chapter 8 gives a summary of the main findings and conclusions of the study as well as suggestions for future work.

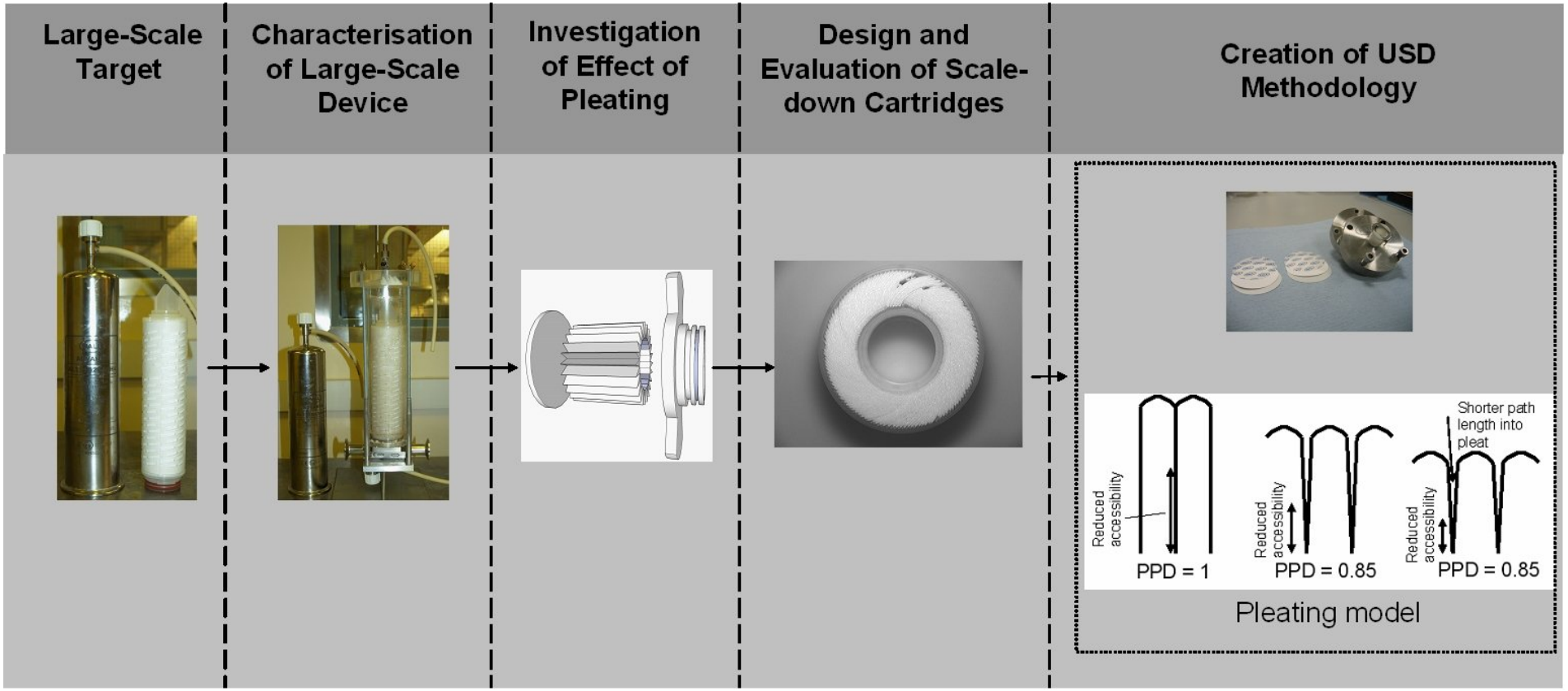

Figure 1-12: Overview of the approach to be taken for the creation of scale-down and USD methods for prediction of large scale pleated membrane cartridge performance.

2 Materials and Methods

2.1 Description of Standard Cartridge and Housing

The standard 10" cartridge type used in this work is shown in Figure 2-1(a). During an operation the cartridge is contained within a stainless steel housing which is also shown in Figure 2-1(a). The housing is attached to a base using a tri-clamp fitting to hold the housing and base together. A rubber o-ring is placed between the housing and base so as to prevent leaks during operation when the housing will be pressurised. The flow of fluid into and out of the housing is illustrated in Figure 2-1(b), which also shows the dimensions of the housing and base.

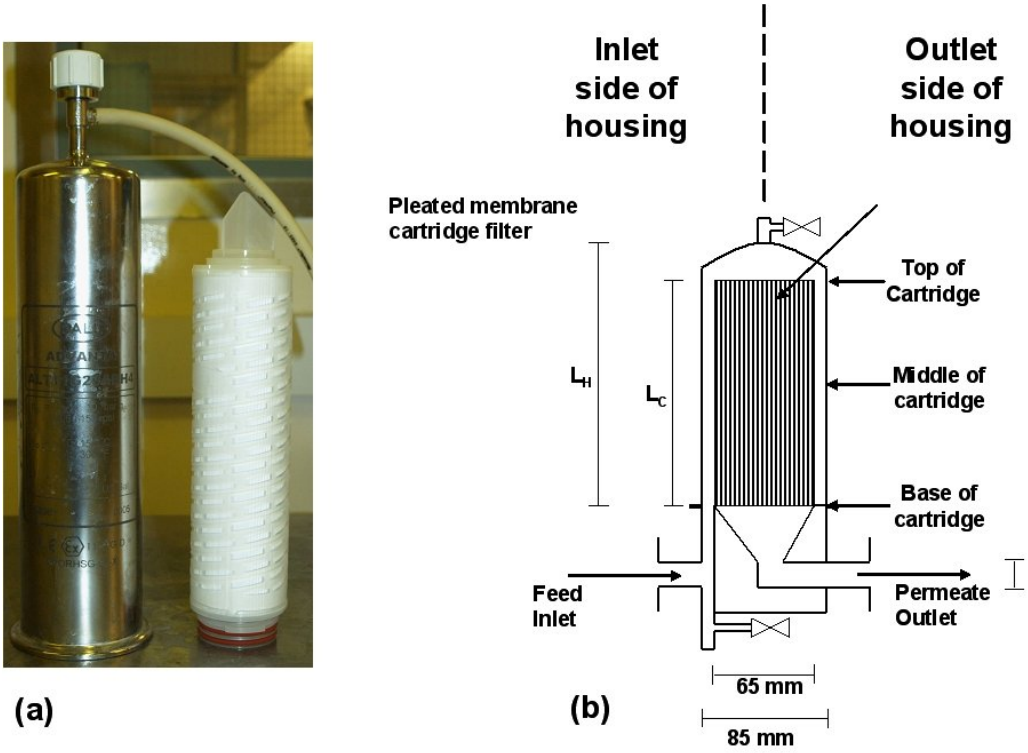

Figure 2-1: Images of standard cartridge and housing. (a) Photograph of a standard 10" pleated membrane cartridge and the standard stainless steel housing in which cartridge is contained when in use. (b) Illustration of standard housing (not to scale), showing dimensions of housing and base L_H = Length of housing and L_C = Length of cartridge. L_H and L_C varied depending upon the type of cartridge used, however the diameter of the base remained constant for all cartridges used, and the dimensions are given.

2.2 Characterisation of Cartridge Housing

To characterise the liquid flow inside the cartridge housing, a transparent housing made from Perspex was fabricated in-house. This had the same internal dimensions as a standard stainless steel housing (Pall Advanta®, Pall Europe Ltd, Portsmouth, UK) and is shown in Figure 2-2. The transparent section was attached to the base of a standard stainless steel housing, with four screw rods used to hold the housing in place whilst under pressure. A rubber 'O' ring was used to seal between the transparent housing and the stainless steel base.

The experimental set-up is shown in Figure 2-3. P- 1, was a diaphragm positive displacement pump (Quattro Flow, M & S Armaturen GmbH, Kürnbach, Germany). P- 2 was a pilot-scale peristaltic pump (605Di, Watson-Marlow Ltd, Cornwall, UK). Pressure indicators used were digital manometers (P2082, Digitron, Torquay, UK). Equipment was connected using Masterflex® PharMed® tubing (Cole-Parmer, London, UK). Tubing had ½" (12.7 mm) inner diameter.

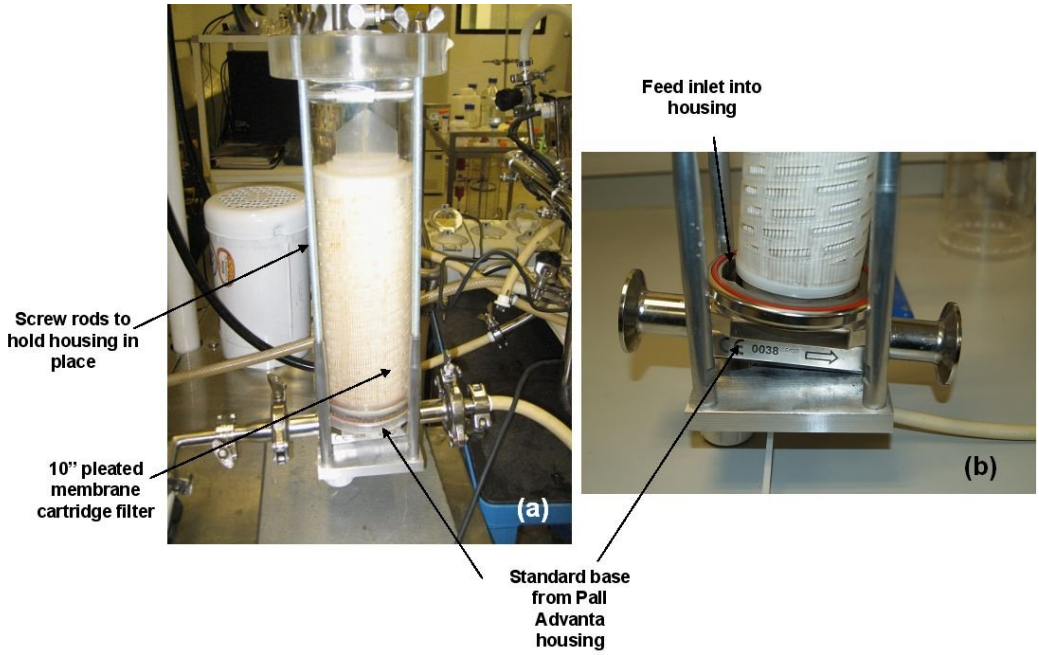

Figure 2-2: Transparent cartridge housing containing 10" pleated membrane cartridge filter.

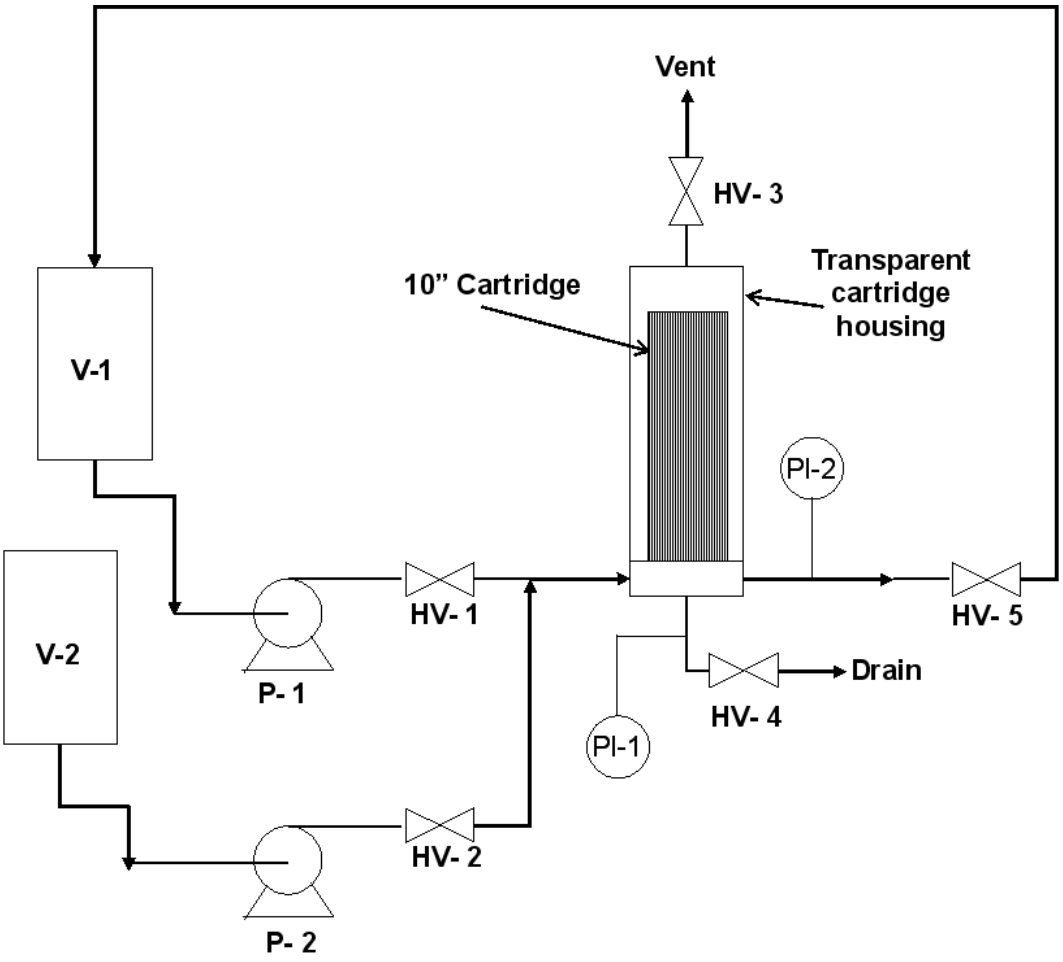

Figure 2-3: Piping and Instrumentation diagram of the experimental set-up used for the observation of the cartridge housing hydrodynamics. V = vessel, HV = hand valves, PI = pressure indicators, P = pump.

2.2.1 Measurements of Axial Mixing

To measure the rate of axial mixing within the 10" housing a 10" pleated membrane cartridge (UEAV, Pall Europe Ltd, Portsmouth, UK) was inserted into the housing base. The transparent housing was secured around it. Vessel 1 was filled with reverse osmosis (RO) water. HV- 1 and HV- 3 were opened before P- 1 was turned on. HV- 2 and HV- 5 were kept closed to allow the cartridge housing to fill with water. When water was seen to exit from the vent line, P- 1 was switched off and HV- 3 closed. HV- 5 was opened and the unit was operated with full recycle back to vessel 1. The pump speed was set to ~9 $Lmin^{-1}$ for 10

minutes to ensure all void spaces within the cartridge were filled and the cartridge was fully wetted. The pump was shut down when the wetting time was completed.

A potassium permanganate solution (Sigma-Aldrich Company Ltd, Gillingham, UK) was prepared to a concentration of 0.1 gL^{-1} and added to V- 2. The coloured permanganate solution allowed easy visualisation of the hydrodynamics within the housing. To image the flows, the flow from P- 1 was set to the required value for the experiment; the flow of P- 2 was set to 0.68 $Lmin^{-1}$. A digital camera (Ixus 55, Canon, Uxbridge, UK) was fixed in place approximately 1 metre from the housing, facing the inlet side (see Figure 2-4). P- 1 was switched on to begin the flow of water through the cartridge. HV- 2 was opened, and P- 2 switched on, so as to pump permanganate into the housing, the camera was switched on and a video recording made. A scale on the inlet side of the housing was used to assess the infiltration of permanganate into the housing. On the outlet side of the housing measurements were made at the base, middle and top of the cartridge, as illustrated in Figure 2-4. These marks represented distances (30 mm, 130 mm, and 220mm from the base of the cartridge respectively). The flowrate of P- 1 was varied for each experiment conducted, each flow rate being repeated three times with video footage acquired for each run.

The video footage was analysed frame by frame using editing software (Windows Movie Maker, Microsoft, Reading, UK). The time taken for the permanganate dye to reach the top of the cartridge (as indicated by the marked scale) was quantified. Actual progress into the housing from the inlet was determined by taking freeze frames of the video footage every 0.23 seconds and comparing the change in dye position relative to the marked scale.

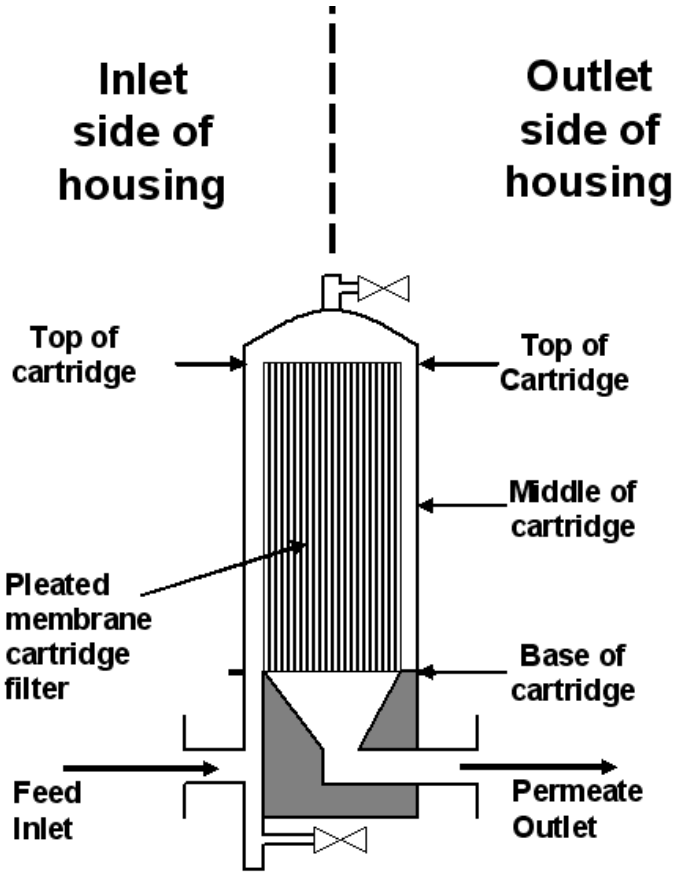

Figure 2-4: Schematic illustration of cartridge housing showing marked positions on each side of the housing that were used to make measurements of mixing times.

2.2.2 Measurements of Radial Mixing

The protocol followed for the measurement of radial mixing within the cartridge housing followed was generally the same as in Section 2.2.1. However the position of the digital camera was changed so that it was fixed in position to face the outlet side of the housing, 180° from the inlet.

The digital camera was fixed in place within 20 cm of each point of measurement in turn. Each experiment was repeated three times. Once again the editing software described in Section 2.2.1 was used to calculate the time at which the dye reached the measurement mark.

2.3 Cartridge Fabrication

2.3.1 Variation of Pleat Packing Density and Pleat Number

In order to investigate the effect that pleat geometry has upon the performance of a filter cartridge, a series of specially fabricated 2.54 cm (1") sections from a 25.4 cm (10") long cartridge (Pall Europe Ltd, Portsmouth, UK) were produced by pleating flat sheet membrane as shown in Figure 2-5. Before pleating a polypropylene drainage support layer, shown in Figure 2-6, was placed above and below the membrane. The pleat height was controlled by the pleat machine and could be set to a range of heights. The pleated pack was cut to the correct pack length to achieve a desired pleat packing density. The ends of the pleated pack were heat sealed together and a perforated polypropylene core inserted inside the cylindrical pleated pack. A perforated polypropylene cage was placed around the outside of it, before adaptors (shown in Figure 2-7) were heat sealed to the top and bottom of the cartridge. The cartridge materials of construction and heat sealing techniques were the same as those used for the commercial production of a 10" cartridge. The 1" cartridges are not available on a commercial basis and were designed to provide a range of pleat geometries between that of 10" cartridges and flat sheet discs (see Figure 2-8). Fully packed 1" and 10" cartridges were defined as having a pleat packing density (PPD) of 1. Two other configurations of 1" cartridges with PPD values of 0.85 and 0.65 were also fabricated. In each case fewer pleats within the 1" cartridge reduced the PPD and increased the distance between each pleat (see Figure 2-7 and Figure 2-8). 25 mm discs of membrane with an effective area of 21.5 mm were punched out of a roll of Supor® EAV membrane for comparison against the 1" cartridges.

The 1" cartridges were also fabricated with two different types and three different heights of pleat. Cartridges fabricated with the Ultipleat® (Figure 2-9) had a pleat height of 24 mm. Cartridges fabricated with the fan pleat (Figure 2-10) had a pleat height of either 15 mm or 10 mm. A 10" long cartridge with h_P = 10 mm and PPD = 1 was also specially fabricated. Standard 10" UEAV cartridges were commercially available, so did not require specialist fabrication.

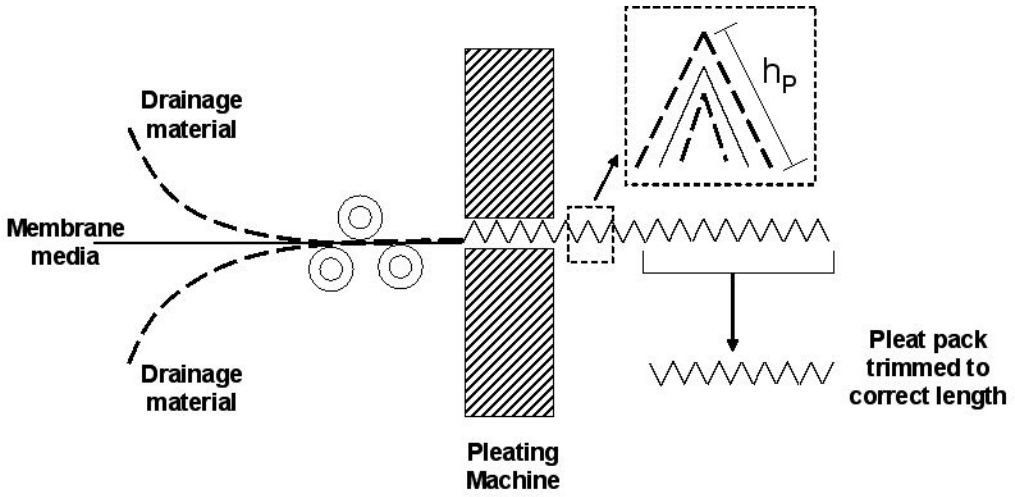

Figure 2-5: Illustration of the method used to pleat flat sheet membrane. h_P = pleat height.

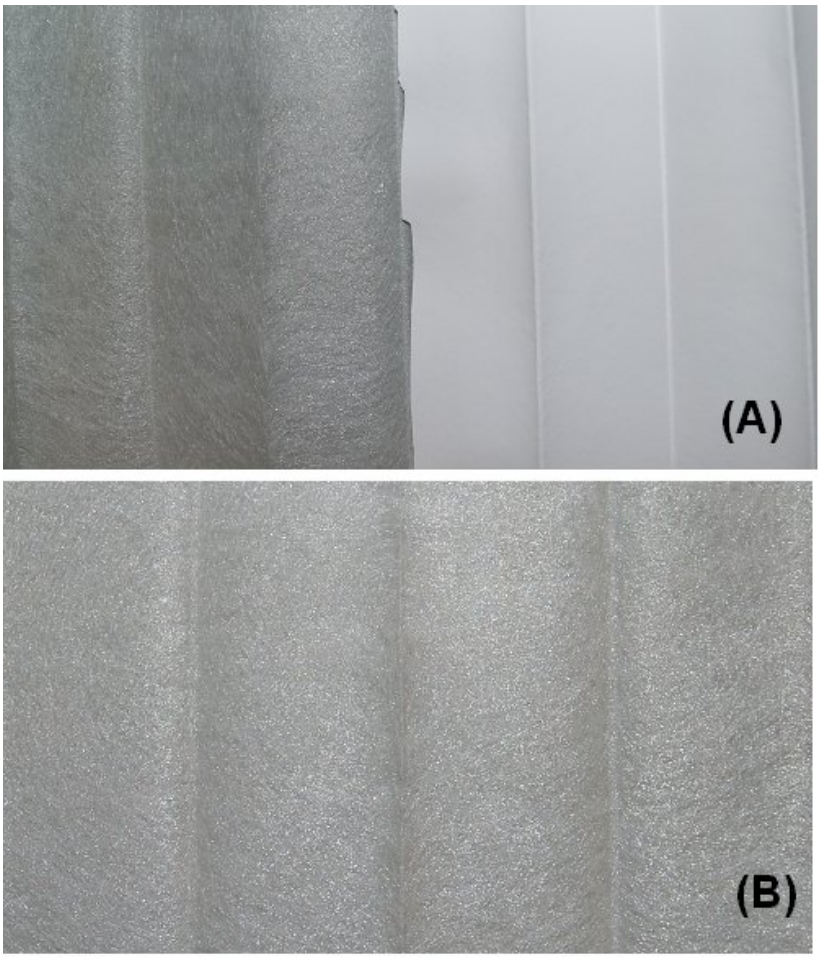

Figure 2-6: Image of polypropylene drainage support material. (A) Photograph of section of drainage material alongside Supor® EAV membrane. (B) Photograph of drainage material illustrating woven nature of the material.

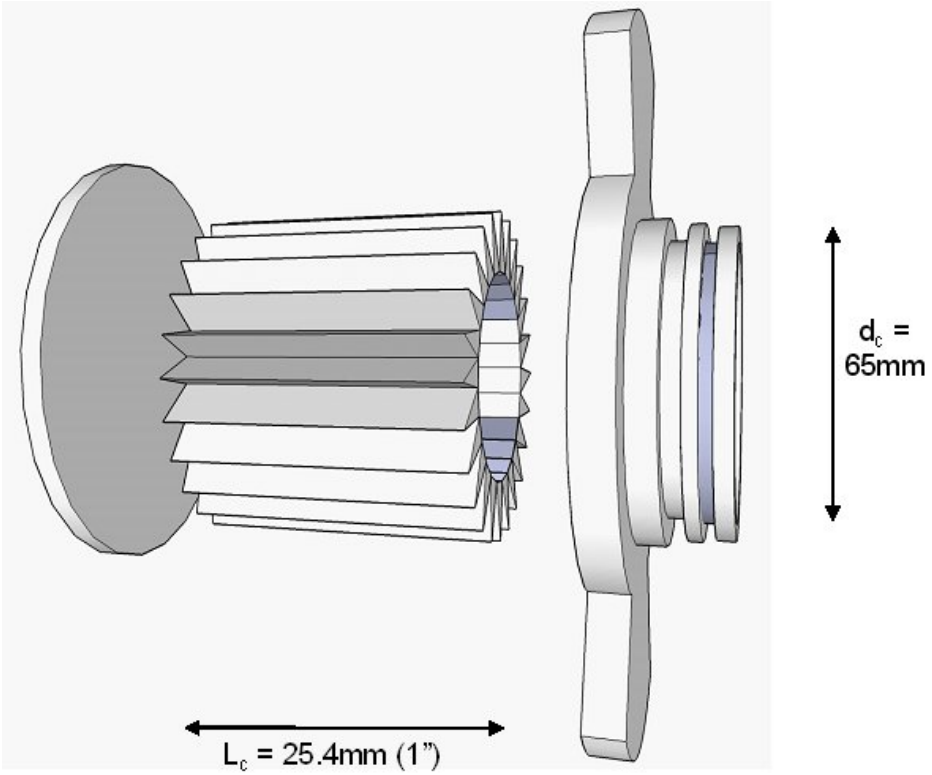

Figure 2-7: Exploded view of a 1" cartridge (without housing), illustrating the way in which the pleated membrane is installed inside the cartridge; in this case a 65% pleated configuration is shown. The illustration does not show the inner and outer perforated cores.

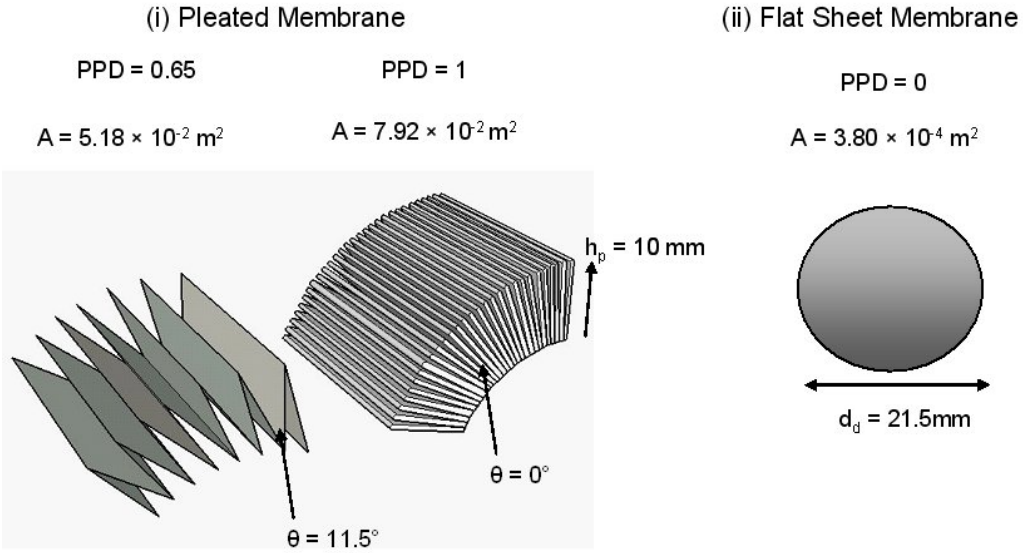

Figure 2-8: Illustration of the different pleat densities and membrane configurations used in this work and the total membrane surface area available per 1" cartridge. PPD = pleat packing density, h_P = pleat height, θ = angle between pleat, d_d = diameter of flat sheet disc, A = membrane area.

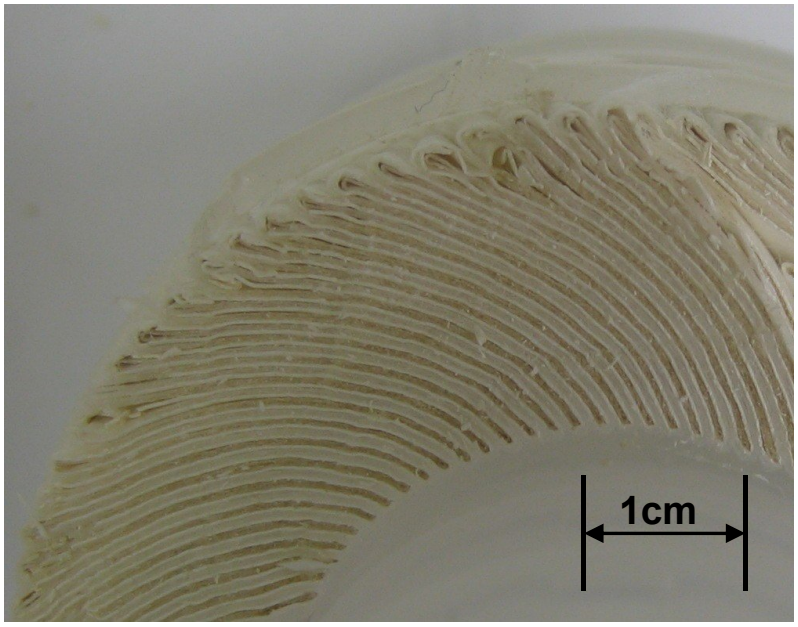

Figure 2-9: Photograph of a cross-section of a 10" UEAV cartridge with an Ultipleat® pleat configuration.

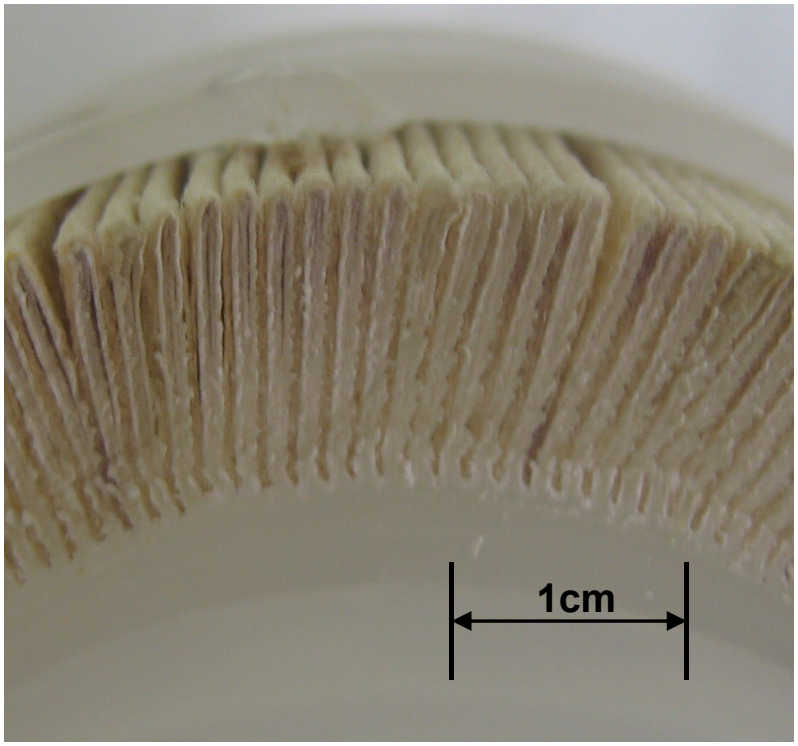

Figure 2-10: Photograph of a cross-section of a 10" EAV cartridge with a fan pleat configuration.

2.3.1.1 Cartridge Nomenclature

The characteristics of the specially fabricated 1" cartridges are given in Table 2-1 alongside those of 10" cartridges fabricated with a fan pleat type and with pleat heights of 15mm or 10mm. In order to simplify representation of each cartridge configuration, the following nomenclature is used to describe each variant: X $Y_{\alpha,\beta}$. X represents the length of the cartridge, Y represents the type of membrane, α represents h_P and β represents PPD. For example: 1" $EAV_{10,\ 0.65}$ is a 1" cartridge formed from an EAV membrane with h_P = 10 mm and PPD = 0.65. The membrane area within this cartridge would be 65% that of a fully packed cartridge (PPD = 1).

Table 2-1: Properties of the various membrane cartridges fabricated for use within this study. All cartridges contained a Supor® EAV 0.22 μm rated membrane.

Nomenclature	**Membrane area (m^2)**	**Pleat type**	**Pleat height, h_p (mm)**	**Pleat packing density (PPD)**	**Angle between pleats, θ (°)**
10" $UEAV_{24,\ 1}$	1.06	Ultipleat®	24	1	~0
10" $EAV_{10,\ 1}$	0.72	Fan	10	1	~0
1" $UEAV_{24,\ 1}$	0.106	Ultipleat®	24	1	~0
1" $EAV_{10,\ 1}$	0.079	Fan	10	1	~0
1" $EAV_{10,\ 0.85}$	0.067	Fan	10	0.85	~6
1" $EAV_{10,\ 0.65}$	0.052	Fan	10	0.65	~12
1" $EAV_{15,\ 1}$	0.090	Fan	15	1	~0
1" $EAV_{15,\ 0.85}$	0.076	Fan	15	0.85	~6
1" $EAV_{15,\ 0.65}$	0.059	Fan	15	0.65	~12

2.3.1.2 Leak Testing

All cartridges were reverse bubble tested after manufacture to assure cartridge integrity. A rubber bung was inserted into the permeate exit at the base of a cartridge to form a tight seal. A 2 L measuring cylinder was 90% filled with a mixture of isopropyl alcohol (IPA) and water (60:40 by volume). The specific gravity was measured with a hydrometer (Les Ateliers Alla, Chemillé, France) to ensure that it was within the range of 0.894 – 0.904. The bunged cartridge was placed into the measuring cylinder and allowed to soak until it was totally submerged and had sunk to the bottom of the tube. The fully wetted cartridge was then taken from the measuring cylinder and the bung removed. A new bung, through which a flexible tube was fed, was placed into the permeate exit of the cartridge. The flexible tube was attached to an air supply via a pressure regulator. The cartridge was submerged within a basin containing the same solvent mixture as used to first wet the cartridge. This set-up is illustrated in Figure 2-11. An air pressure of 10psi was set. Visual inspections were made around the cartridge to identify leaks. Leaks were represented by a steady stream of gas bubbles originating from the cartridge (see Figure 2-11). Special attention was given to the heat seals between the cartridge adaptors and the membrane and the side seal joining the pleated membrane section. Cartridges were passed for filtration studies if no evidence of leaks were observed.

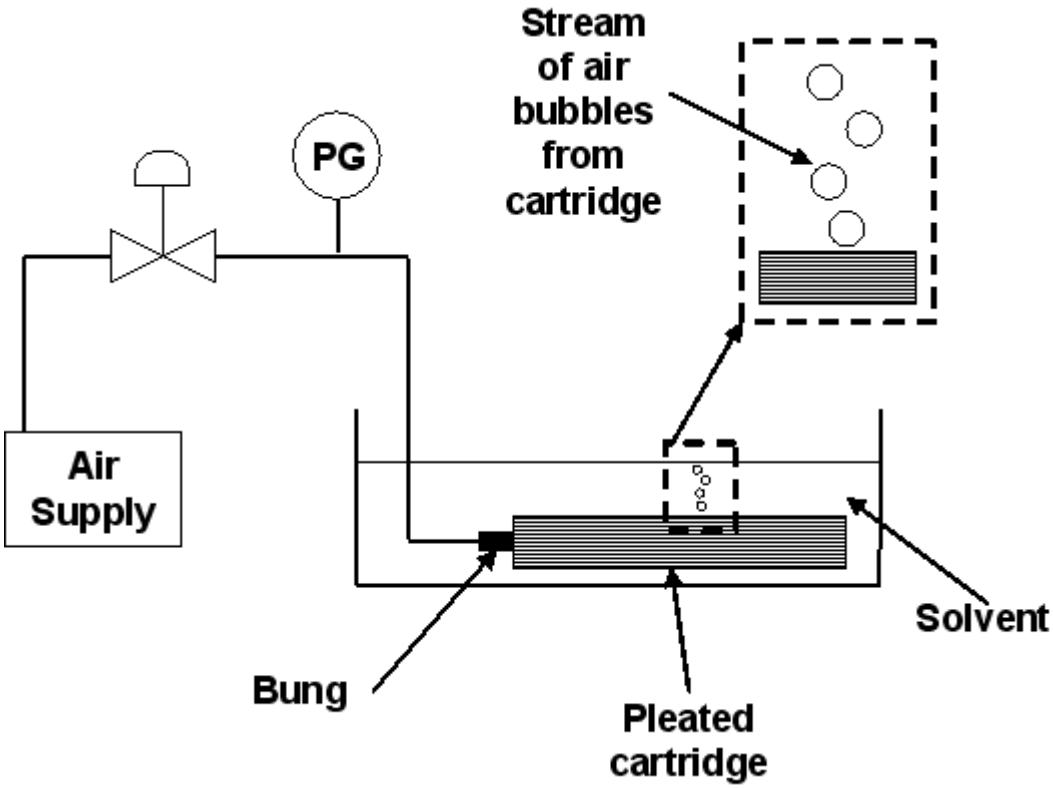

Figure 2-11: Experimental set-up for reverse bubble testing of membrane cartridges. Solvent used was a 60:40 mix (by volume) of IPA and water. Evidence of a leak is shown by the presence of a steady stream of bubbles originating from the cartridge.

2.3.2 Scale-Down Pleated Membrane Cartridges

For this study a novel design of scale-down cartridge was developed and fabricated. The new cartridge design maintained the same key pleat characteristics: height of pleat, type of pleat, pleat packing density, but reduced the active membrane area for liquid permeation. This reduction was achieved by incorporating a limited number of sections of pleated membrane, Supor® EAV (Pall Europe Ltd, Portsmouth, UK), into a pack of hydrophobic PTFE material. The standard polypropylene drainage support layer was located above and below all of the pleated sections whether hydrophilic or hydrophobic. Hydraulic integrity was achieved by heat sealing of the two elements. The hydrophobic material sections were impermeable to water-based feedstocks, thus regions of the pleated pack remained inactive and only the inserted EAV section was available for flow.

The heat sealed sections of the Supor® membrane into a hydrophobic pack is shown in Figure 2-12(a-d). Figure 2-12(a) shows detail of the configuration of a cartridge with just 1.5 pleats of Supor® membrane incorporated into the membrane pack. Figure 2-12(b) shows how this pleat is located within the cartridge. Figure 2-12(c) shows a cartridge containing one section of active membrane containing 4.5 active pleats of membrane, with Figure 2-12(d) representing a cartridge with four sections of active membrane, with each section containing 4.5 active pleats of membrane. In all cases where multiple inserts were used, then these were inserted so as to maintain an even radial distribution (Figure 2-13). A summary of the range of different pleat sections and pleat numbers used are given in Figure 2-13 and Table 2-2 respectively. The scale-down cartridges were fabricated in 1" and 10" configurations so as to investigate any impact of the cartridge length upon performance.

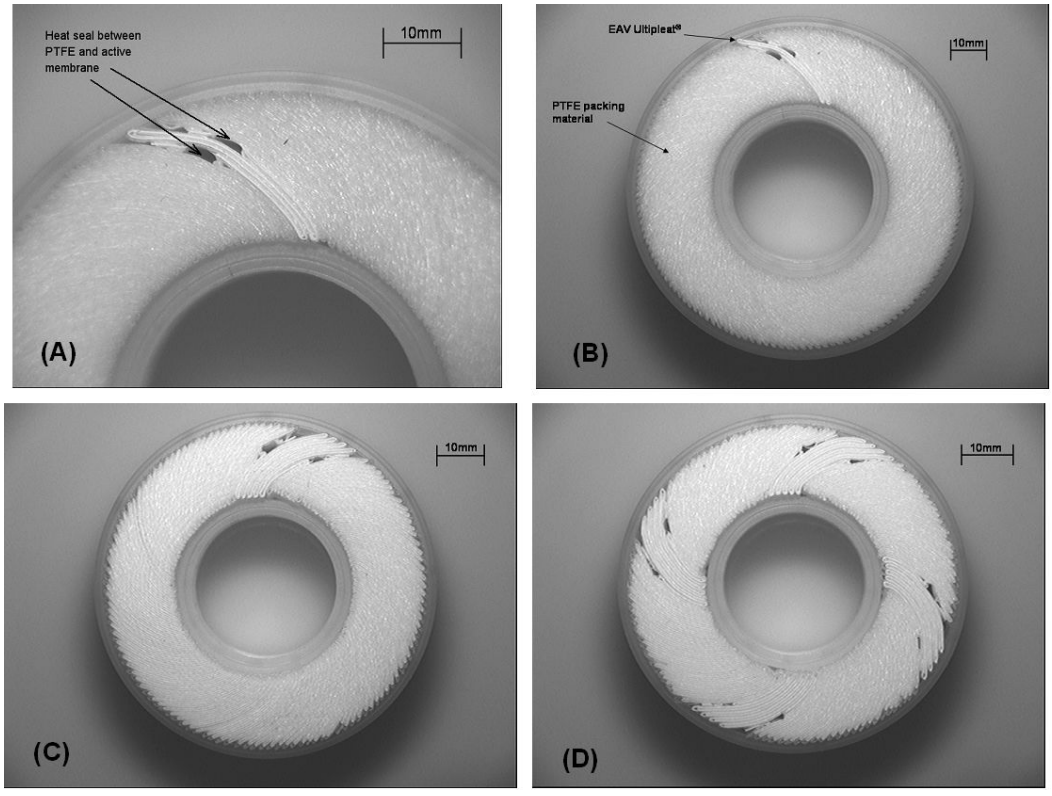

Figure 2-12: Cross sections through the various specially fabricated 1" scale-down pleated devices showing the range of pleat configurations of Supor® EAV membrane used within this study: (a) Magnification showing heat sealing of the pleat to the PTFE material. (b) 1 membrane section with 1.5 active pleats heat sealed to PTFE packing material. (c) 1 section with 4.5 pleats. (d) 4 sections each containing 4.5 pleats.

A greater number of pleats were incorporated into some cartridges so as to provide a means of investigating the effect that membrane variability and position of active pleat had upon the ability of the scale-down cartridges to predict the performance of a large-scale cartridge. The scale-down cartridge containing the least number of active membrane pleats (1.5) had a membrane area corresponding to that of a 50 mm flat sheet disc. All cartridges were leak tested to assure cartridge integrity, as described in Section 2.3.1.2.

The range of scale-down pleated devices are shown in Figure 2-13. Each variant of the pleated device has been labelled with a different subscript to identify it. The key properties of the pleated devices along are given in Table 2-2.

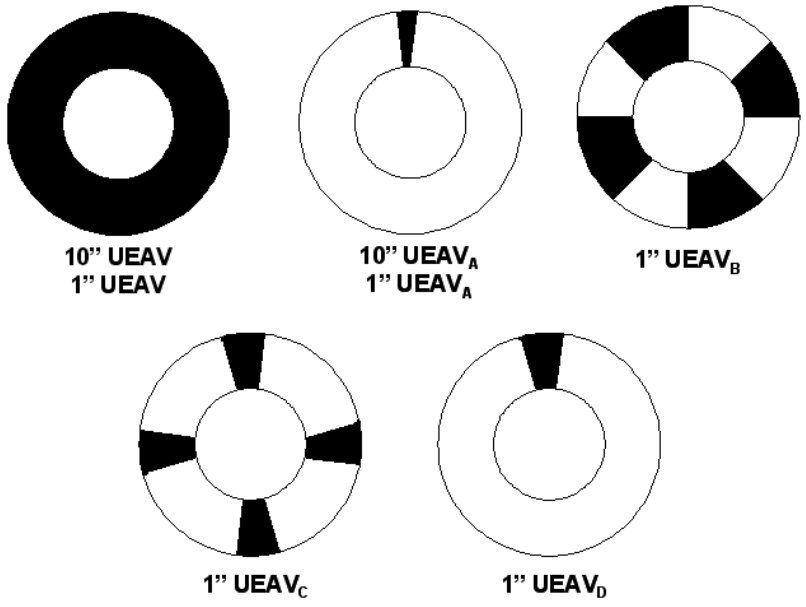

Figure 2-13: Schematic representation of the cross-section of the specially fabricated 1" USD cartridge configurations used in the study. Figure shows the number and distribution of active pleat sections (shaded black) that each cartridge contained. The pleat numbers and membrane areas for each configuration are given in Table 2-2.

Table 2-2: Characteristics of Supor® EAV 0.22 μm rated membrane cartridges used in study.Figure 2-13 shows the distribution of the pleat sections within the 1" cartridges.

Cartridge type	Number of active pleat sections	Number of hydrophobic sections	Total number of pleats within active pleat sections	Membrane area (m^2)
10" UEAV	1	0	-	1.06
1" UEAV	1	0	-	0.106
10" $UEAV_A$	1	1	1.5	1.51×10^{-2}
1" $UEAV_B$	4	4	11.5	4.64×10^{-2}
1" $UEAV_C$	4	4	4.5	1.81×10^{-2}
1" $UEAV_D$	1	1	4.5	4.54×10^{-3}
1" $UEAV_B$	1	1	1.5	1.51×10^{-3}
25mm flat sheet disc	-	-	-	3.8×10^{-4}

2.4 Quantification of Clean Water Flux

2.4.1 Experiments Using Cartridges

Clean water flux measurements were used to quantify the differences in performance of the various cartridges and calculate membrane resistances. Each cartridge was contained within a membrane filter housing (Pall Advanta®, Pall Europe Ltd, Portsmouth, UK). The design of this housing is shown in Figure 2-1. Feed enters at the base of the housing. The permeate stream also leaves at the base of the housing. Figure 2-14 shows the experimental set-up used for water flux measurement. The cartridge housing was connected to a pumping rig modified for normal flow operation (Maxim, Pall Europe Ltd, Portsmouth, UK). The pumping rig consisted of a diaphragm positive displacement pump (Quattro Flow, M & S Armaturen GmbH, Kürnbach, Germany) and a electromagnetic flowmeter on the permeate line (SO-55, Bürkert, Brimscombe, UK). The same rig was also used with the specially fabricated 1" cartridges, described in Section 2.3.1, except that in these cases a smaller housing was used to contain each cartridge.

The cartridge housing was filled with water prior to operation so that all air pockets were removed. Digital manometers (P2082, Digitron, Torquay, UK) were connected to the base and to the permeate exit of the housing. Before each experiment all membrane cartridges were flushed with water at a flow rate of 10 $Lmin^{-1}$ for a period of at least ten minutes. This ensured that all of the voids of the cartridge unit were filled with water, and that the cartridge was fully wetted. During permeate flux measurement the feed flowrate was altered and the corresponding feed and permeate pressures recorded. Except for the 1" $EAV_{10, 0.65}$ configuration all permeate flux measurements were made in triplicate using a fresh membrane cartridge. All flux measurements were within 1% of the mean for the 10" cartridge.

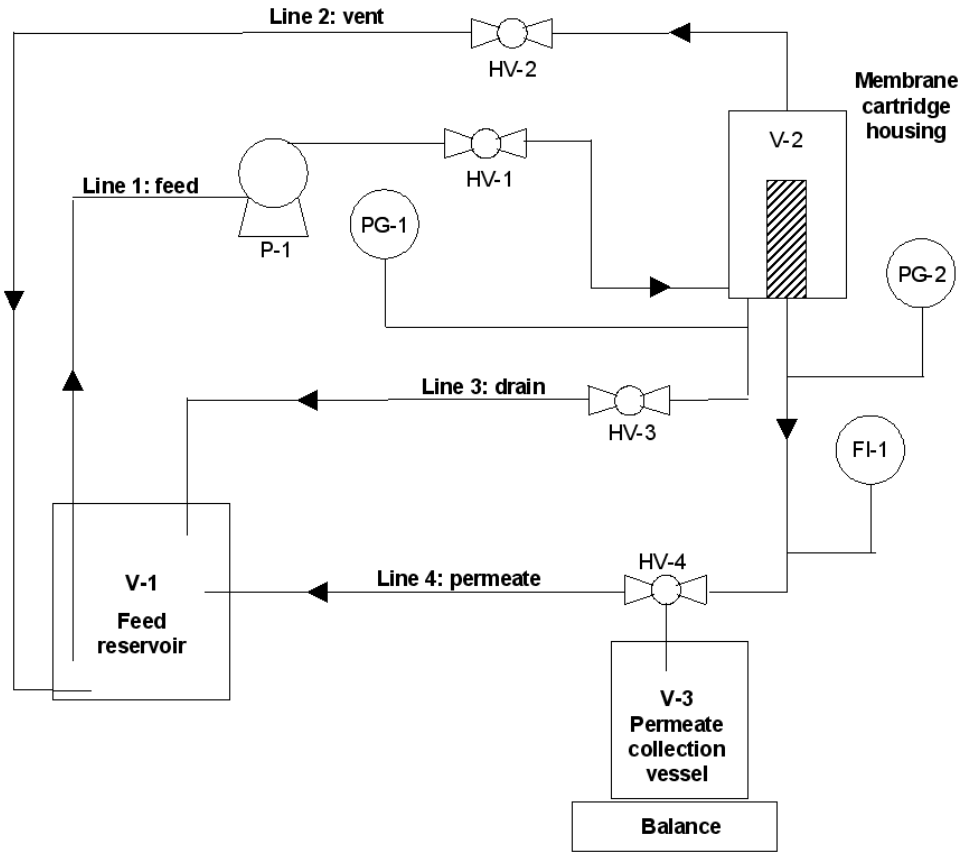

Figure 2-14: Piping and instrumentation diagram illustrating the experimental rig utilised for investigation of the different cartridge configurations of Supor® EAV 0.22 µm rated membrane. V = vessel, P = pump, HV = hand valve, PG = pressure gauge, FI = Flow indicator.

So as to establish accurately the transmembrane pressure difference the pressure drop across the empty housing was also evaluated as a function of feed flowrate. This housing pressure drop was subsequently subtracted from the pressure drop measured when a cartridge was present. In most cases the housing pressure drop was less than 15% of the combined housing plus cartridge measurement.

2.4.1.1 Validation of Clean Water Flux

A special rig has been fabricated at Pall Walton Road, to measure the transmembrane pressure difference without the need for accounting for the housing pressure drop. A standard housing base has been modified so that tubing enters the housing and is situated next to the feed and permeate surface of the membrane. This is shown in Figure 2-15.

A flowsheet for the experimental rig is shown in Figure 2-16. The outlet of the tubing connected to a pressure indicator, PI-1, which showed the differential pressure across the cartridge. The feed was pumped to the cartridge housing using a rotor pump (Merlin, Mono Pumps Ltd, Manchester, UK). A flow indicator (Schaevitz®, Measurement Specialities, Hampton, USA) on the outlet showed the permeate flowrate. The flowrate was varied and the corresponding differential pressure measured.

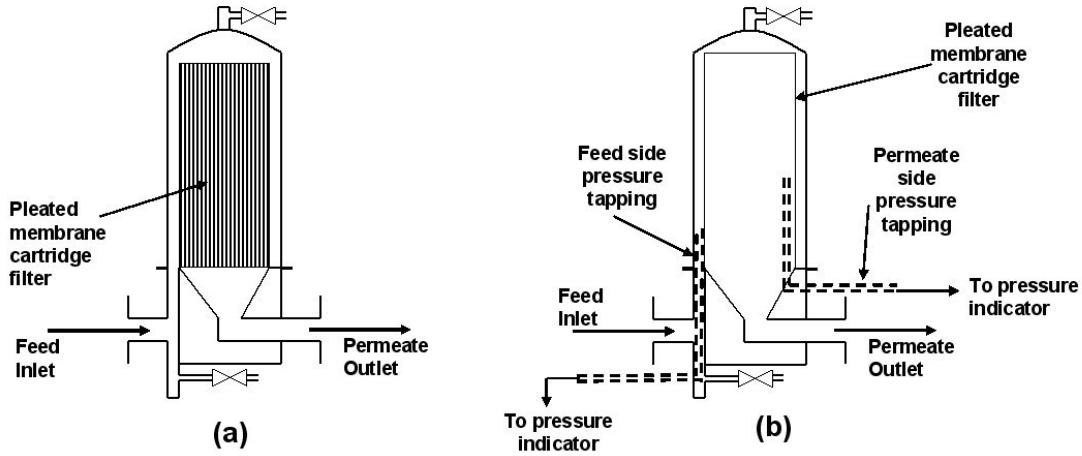

Figure 2-15: Illustration of a standard stainless steel housing (a) and a stainless steel housing modified such that steel pressure tappings (represented by broken line) are inserted into the housing on the feed and permeate side of the cartridge. The outlet from the pressure tappings go to a pressure indicator.

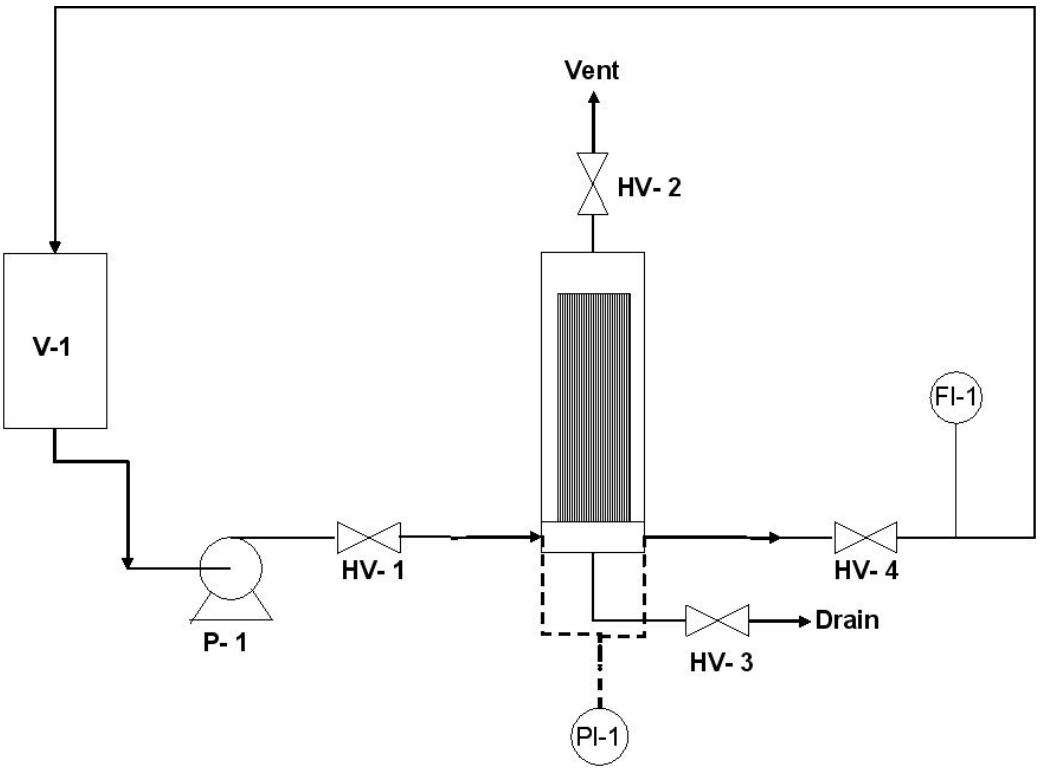

Figure 2-16: Flowsheet for Flow dP rig maintained at Pall Walton Road. V = vessel, P = pump, HV = hand valve, PI = pressure indicator, FI = Flow indicator.

2.4.2 Experiments Using Flat Sheet Discs

Filtration experiments with flat sheet discs were conducted using 0.22 μm rated Supor® EAV filters (25 mm FTKEAV, Pall Europe Ltd, Portsmouth, UK). Figure 2-17 shows the experimental set-up used. Each membrane disc was placed into a membrane holder (Amicon Stirred Cell 8010, Millipore, Watford, UK) and the holder was connected downstream of a vessel containing the feed to be filtered. Upstream of the feed vessel a positive pressure (<0.7 bar(g)) was applied using a nitrogen gas supply. A digital manometer (P2082, Digitron, Torquay, UK) was connected upstream of the feed vessel with the permeate open to atmosphere. Permeate was collected in a beaker on an electronic balance (PB3002-S, Mettler-Toledo GmbH, Urdorf, Switzerland). The balance was connected to a computer (Latitude D600, Dell, UK) via an RS232 interface. Readings of the permeate mass were collected every second to an accuracy of ±0.02 g. All permeate flux measurements were made in triplicate using fresh membrane. All flux measurements were within 6% of the mean.

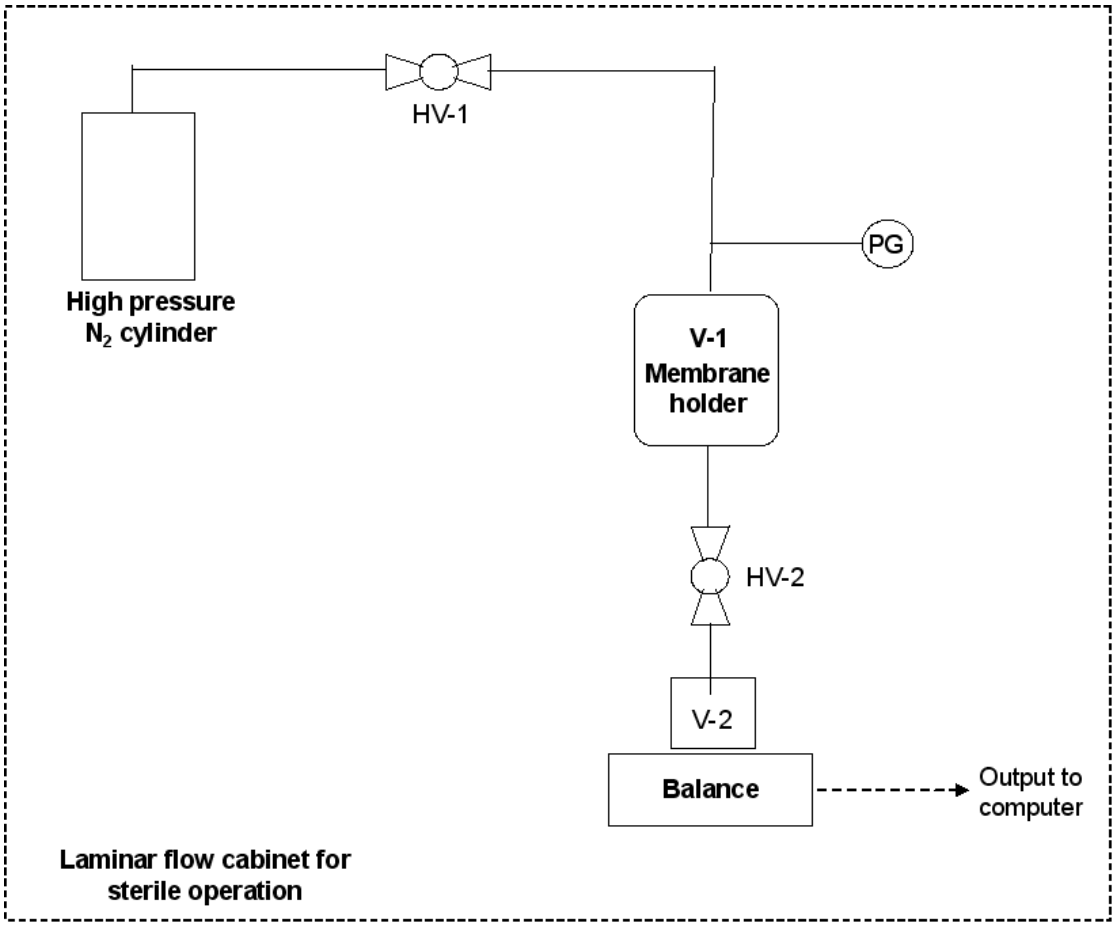

Figure 2-17: Representation of the experimental set-up for small-scale flat sheet discs of 25 mm diameter.

2.5 Visualisation and Quantification of Particle Deposition

2.5.1 Filtration With Yeast Suspensions

Yeast suspensions were used to explore and quantify the deposition of particles within the pleated membrane structure. Yeast solutions were prepared by suspending fresh bakers yeast (DCL Yeast Limited, Surrey) into 0.03 M sodium phosphate buffer (pH 7.5) to obtain a wet cell weight concentration of 7.7 gL^{-1}. A homogenous yeast suspension was achieved using a high speed mixer (Silverson Machines Ltd, Chesham, UK). To this solution Bovine Serum Albumin (BSA) (Sigma-Aldrich Company Ltd, Gillingham, UK) was added to a concentration of

1 gl^{-1}. Experiments were performed using the experimental rig shown in Figure 2-14.

The filtration was conducted at a constant feed flowrate until the cartridge became fouled and the feed pressure reached a maximum of 0.8 bar(g). At this stage the feed pump was switched off until the pressure reduced. Once it had dropped below 0.2 bar(g), the feed pump was activated until the pressure once again rose to 0.8 bar(g). This sequence was repeated for 30 minutes (~ 40 cycles), by which point the cartridge was considered to be completely fouled.

2.5.2 Quantification of Yeast Deposition

Following yeast filtration the cartridges were allowed to dry for three days in a drying cabinet at 50 ºC. In order to visualise yeast deposition within the pleats and the location of cake built up, the cartridge was cut open and the membrane removed. Care was taken to minimise the loss of dried yeast during this operation. The pleats were gently opened up and photographed using a digital camera (E501, Olympus, UK). This was repeated for three separate cartridges for each cartridge configuration apart from for a 10" $EAV_{10,\ 1}$ cartridge. More detailed grey-scale images were generated using a controlled lighting environment for one set of images for each of the cartridge (GelDoc-it Imaging System, UVP, Upland, USA). These images were then analysed using 'Image J', an image analysis package freely available within the public domain (Abramoff et al., 2004) to quantify the thickness of the cake build up and to characterise the pattern of deposition within the pleat. The variation in the grey level at various points within the image was recorded. Grey-scale variation data was plotted using a running average method with a sampling proportion of 0.1. Images from at least three separate experiments were analysed in this way.

2.5.3 Quantification of Clean Membrane Areas

The dried membrane used in Section 2.5.2 was re-photographed using a digital SLR camera (E501, Olympus, UK) and these image loaded into Image J (Abramoff et al., 2004) analysis software. For each image a horizontal line was drawn across the height of the pleat, and the scale was set to the length of the line. The image was converted from colour to an 8-bit grey scale and the contrast was enhanced by 2%. The image was cropped to remove any edges of the membrane. The threshold of the image (which defines the point at which colours within the image are either black or white) was adjusted to cover the fouled areas. The image was converted to a binary image, where white areas represented clean membrane. A particle analysis routine within the software application was used to quantify the area of the binary image that contained white particles.

2.6 Filtration of Protein Feedstocks

2.6.1 Experiments Using Cartridges

A pepsin feedstock was prepared by dissolving pepsin (Fisher Scientific, Loughborough, UK) in 30 mM sodium phosphate buffer (pH 7.4) (Sigma-Aldrich Company Ltd, Gillingham, UK). A concentration of 10 gL^{-1} of pepsin was used for all experiments.

A constant flow regime was used whilst filtering the pepsin feedstock. All cartridges contained 0.22 μm rated membrane, Supor® UEAV (Pall Europe Ltd, Portsmouth, UK). The cartridges were contained within a stainless steel housing (as shown in Figure 2-1) with the flowrate set using a pump. The experimental rig used was described previously in Section 2.4.1. Various pump sizes were used depending upon the cartridge to be tested. For experiments using a 10" UEAV cartridge a pilot-scale peristaltic pump was used (605Di, Watson-Marlow Ltd, Cornwall, UK). All other scales of cartridges used a lab-scale peristaltic pump (505Du, Watson-Marlow Ltd, Cornwall, UK). The ratio of the pump flowrate to active membrane area was maintained to ensure that the throughput

rates were similar for all the scales of cartridges used. During operation the feed pressure was measured using a digital manometer (P2082, Digitron, Torquay, UK). Permeate was collected in a vessel placed on a top pan balance; E2000 (August-Sauter GMBH, Albstadt, Germany), for pilot-scale studies, or a PB3002-S (Mettler-Toledo GmbH, Urdorf, Switzerland) for lab-scale studies. The lab balance was connected to a computer (Latitude D600, Dell, UK), via a RS232 interface. Readings of the permeate mass were collected every second and to an accuracy of ±0.02 g for lab-scale studies whilst mass measurements were taken manually with the pilot scale balance over a range of time intervals and to an accuracy of ±5 g.

Before any filtration run began feed solution was pumped into the housing until it exited from the vent. The vent was then closed off and filtration begun. The feed pressure was monitored over the course of the operation until it reached 0.8 bar(g). At this point the pump was de-activated and the feed pressure subsided. Once the feed pressure had dropped to 0.2 bar(g) the pump was activated. This sequence was repeated with periodic decreases in the pumping flowrate. The filtration was halted after the pumping flowrate had dropped below 85% of the starting value. Samples were taken from the feed and permeate to quantify protein concentration for all of the cartridges examined.

2.6.2 Experiments Using Flat Sheet Discs

2.6.2.1 Filtration of BSA Feedstock

A 10 gL^{-1} BSA solution was prepared by dissolving BSA (Sigma-Aldrich Company Ltd, Gillingham, UK) into a sodium phosphate solution (pH 7.4) (Sigma-Aldrich Company Ltd, Gillingham, UK). Long filtration times were achieved by using 4 L of the BSA solution as a feed. The filtration used the equipment set-up shown in Figure 2-18. A 47 mm disc of Supor® EAV membrane was inserted into the membrane disc holder (FTK200, Pall Europe Ltd, Portsmouth, UK). The BSA solution was added to V-1. HV-1 was opened, and the pressure set to 0.21 bar(g). HV-2 and HV-3 were opened to start the

filtration of the feedstock. Over the course of the filtration run, the permeate flowrate was measured by removing the permeate line from V-2 and inserting into a measuring cylinder, where the accumulation of permeate was measured after one minute.

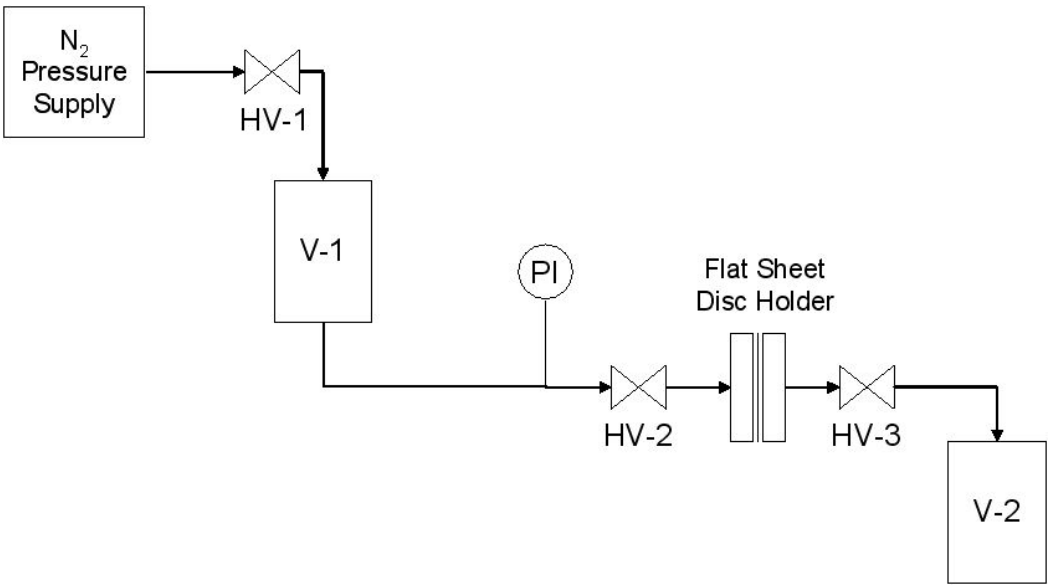

Figure 2-18: Flowsheet of experimental set-up for filtration of BSA feedstock. HV = hand valve, V = vessel, PI = pressure indicator.

2.6.2.2 Filtration of Pepsin Feedstock

Filtration experiments with flat sheet discs were conducted using 0.22 micron rated Supor® EAV filters (25 mm FTKEAV, Pall Europe Ltd, Portsmouth, UK). The experimental methodology was the same as for the clean water experiments described in section 2.4.2, however upstream of the feed vessel a positive pressure (0.8 bar(g)) was applied using a nitrogen gas supply. This feed pressure was selected as it represented the maximum pressure seen during the constant flow cartridge filtration experiments outlined in Section 2.6.1. Samples were taken from the feed and permeate to quantify the protein concentration.

2.6.3 Total Protein Concentration Assay

A Lowry assay method (Lowry et al., 1951) (with Onishi and Barr modification (Ohnishi et al., 1978)) was used to assess the concentration of pepsin in the samples taken during the filtration experiments. Using this method 0.2 mL of sample was added to 2.2 mL of Biuret reagent (Sigma-Aldrich Company Ltd, Gillingham, UK). After mixing the solution was allowed to stand for 10 minutes. 0.1 mL of Folin and Ciocalteau's phenol (Sigma-Aldrich Company Ltd, Gillingham, UK) was then added. After mixing the solution was allowed to stand for 30 minutes. A solution to blank a spectrophotometer (Aquarius, Cecil Instruments, Cambridge, UK) at 750 nm was prepared in the same way as the sample, but by replacing the sample with reverse osmosis water. The absorbance of the sample was measured at 750 nm. Absorbance measurements were within 0.08% of the mean. All readings were taken within 30 minutes of the first sample being measured. A standard curve prepared using known quantities of pepsin (Figure 2-19) was used to convert the absorbance readings from samples into protein concentrations.

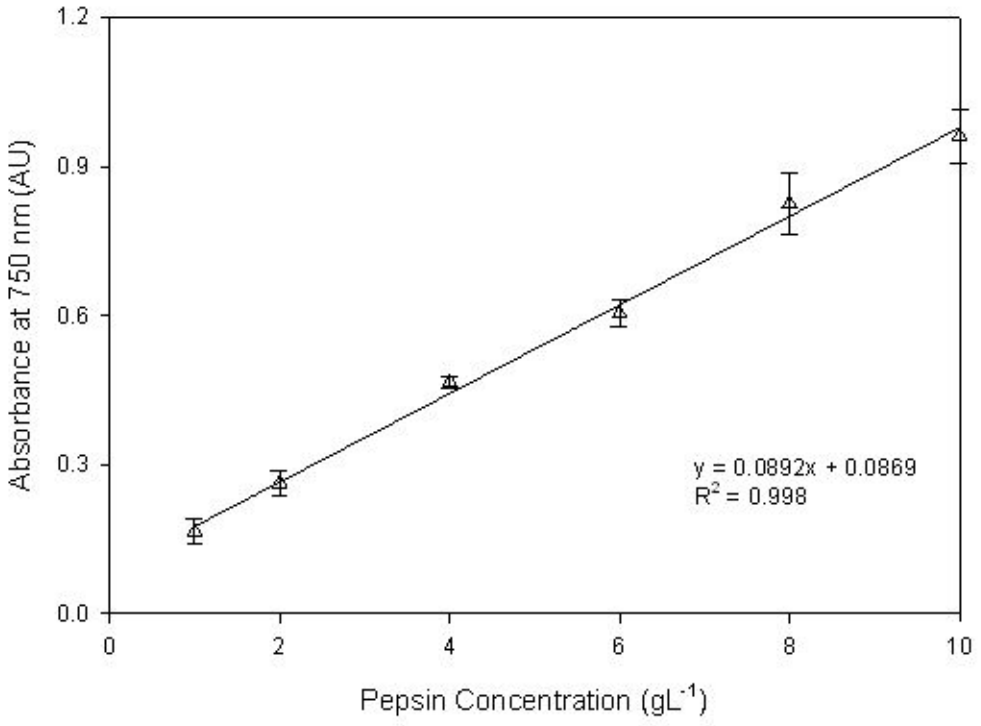

Figure 2-19: Standard curve for Lowry Assay used for quantification of pepsin concentration within the range $1gL^{-1}$ to $10gL^{-1}$. Error bars show one standard deviation around the mean (n=3). Solid line filled by linear regression was fitted to the data points ($R^2 > 0.99$).

2.6.4 Particle Size Analysis

Samples from filtration runs were analysed using dynamic light scattering (Zetasizer Nano, Malvern Instruments Ltd, Malvern, UK.). Before the analysis of each sample, RO water was first measured to ensure that the measurement cuvette was clean and did not contain dust particles. 100 µL of the sample to be measured was added to the empty measurement cuvette, which was inserted into the Zetasizer so that the sample could be analysed. After each sample was analysed the cuvette was cleaned using a specialist solution (Hellmanex® II, Hellma GmbH & Co., Müllheim, Germany.

3. Characterisation of Pleated Membrane Cartridge Performance

3.1. Introduction and Aims

The aim of this thesis, as set out in Section 1.8, is to develop and characterise scale down and ultra scale-down devices and methodologies that better predict the performance of large-scale pleated membrane filters.

The large-scale unit selected as the basis for this study is a 10" $UEAV_{24,1}$ cartridge, which contains a pleated 0.2 μm rated membrane. This filter is used within industry primarily for bioburden reduction; an operation that is used extensively within a typical bioprocess (Figure 1-1). Before the accuracy of the performance prediction from new scale-down or USD methodologies can be assessed, the basic performance of the 10" $UEAV_{24,\ 1}$ cartridge must be fully characterised when fitted in a standard cartridge housing (described in Section 2.1) for a range of feedstocks. As this type of filter is used extensively within a bioprocess flow sheet, then there is a large range of feedstocks that it can potentially process (Table 1-6). One example is relatively clean fluids such as buffers, and these feedstocks can be mimicked with water. However, the filters are also used with more complicated feedstocks containing proteins, which have been seen to foul 0.2 μm rated membranes (Girones et al., 2006; Kelly et al., 1995; Kelly et al., 1997) (Section 1.3.2).

There has been previous work reported in the literature to develop models that describe the fouling nature of proteinaceous feedstock with sterile filters (Kelly et al., 1995; Kelly et al., 1997) . It is unusual that such feedstocks should be capable of fouling the membranes, as the nominal pore size of 0.2 μm is significantly higher than the native size of proteins. It is thought, however, that aggregation of the protein is one of the mechanisms that leads to the fouling of the membrane (Kelly et al., 1993). Development of a realistic feed will allow for

studies to be conducted on the large and small scale devices for comparison of performance. From an experimental standpoint, it would also be beneficial to generate a feedstock for which multiple batches of consistent material can be generated easily with a minimum of pre-processing.

The aim of this chapter is therefore to characterise the basic filtration performance of a large-scale pleated cartridge in a standard cartridge housing for a range of feedstocks. The specific objectives of this chapter are:

- To investigate whether cartridge and housing hydrodynamic effects should be accounted for when performance data is generated using a scale-down version of a cartridge filter or an ultra scale-down approach.

- To establish a protein solution suitable for use as a realistic test feedstock, which can be used subsequently to characterise the filtration performance of the large-scale pleated cartridge.

- To characterise the basic filtration performance for a large-scale pleated cartridge filter within a standard housing, using a selection of fouling and non-fouling feedstocks.

This work seeks to develop small-scale techniques that account for pleating effects to provide accurate performance predictions. Once the basic performance of the cartridge has been characterised then a basis will have been set against which the predictions of other small-scale techniques can be assessed. This approach is highlighted in Figure 3-1.

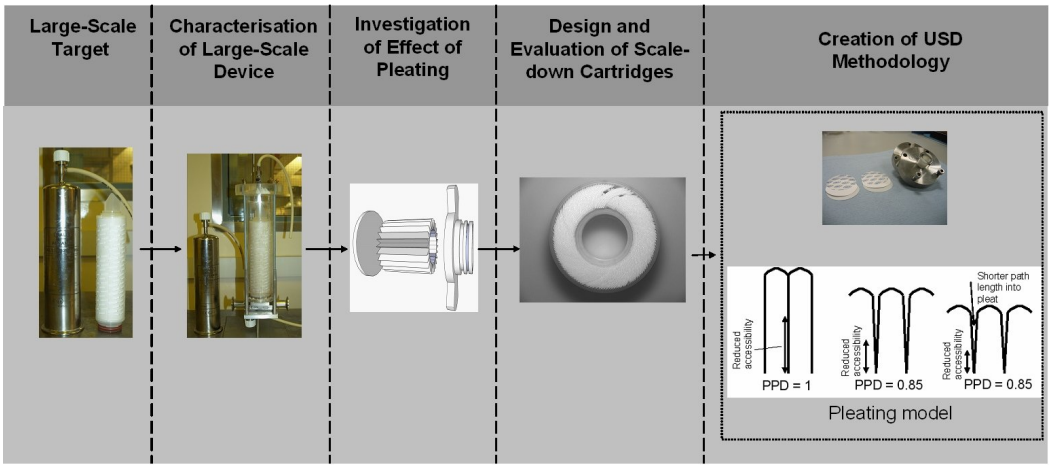

Figure 3-1: Overview of the structure of the thesis showing strategy towards the development of a USD methodology that accounts for pleating effects. This chapter seeks to characterise the basic filtration performance of a large-scale pleated membrane cartridge, against which the performance predictions generated using a USD methodology can be compared against other small-scale techniques.

3.2. Cartridge and Housing Hydrodynamics

3.2.1. Quantification of Housing Pressure Drop

Due to the design and fabrication of the cartridge housing, and the location of the digital manometers, as shown in Figure 2-3, a housing pressure drop is imposed upon the hydraulic system. This pressure drop must be accounted for if accurate measurements of transmembrane pressure drop are to be made when a cartridge is inserted into the housing. Consequently, the housing pressure drop was first characterised without a cartridge present. The measured pressure difference for standard 10” and 1” housings are given in Figure 3-2 as a function of applied feed (clean water) flowrate. It is evident that significant variation was experienced when measuring the pressure drop. From the size of the error bars, the measured variation was less for the 10” housing. A higher pressure drop was measured for the 1” housing due to the lower hold-up volume within the housing relative to the 10” housing. For the 1” housing an initial region of constant pressure drop was observed. However the housing pressure drop became a function of feed flowrate at flowrates above 4 $Lmin^{-1}$. For the 10” housing, no significant change in pressure drop, beyond changes due to measurement error,

was seen for the range of feed flowrates used. The pressure drop was constant at 3.7 mbar as indicated by the dashed line in Figure 3-2.

Given the variation in housing pressure drop, especially for the 1" housing, the pressure drops shown in Figure 3-2 were subsequently used throughout this thesis to correct water flux data. A typical example of water flux data correction for a 10" $UEAV_{24,\ 1}$ cartridge is shown in Figure 3-3.

In Figure 3-3 a small effect was seen when the flux data for a 10" $UEAV_{24,\ 1}$ filter cartridge was corrected for the housing pressure drop. This is due to the low transmembrane pressure differences measured for the applied feed flowrates. For the range of flowrates used the housing pressure drop represented 7.5 – 37% of the total transmembrane pressure difference.

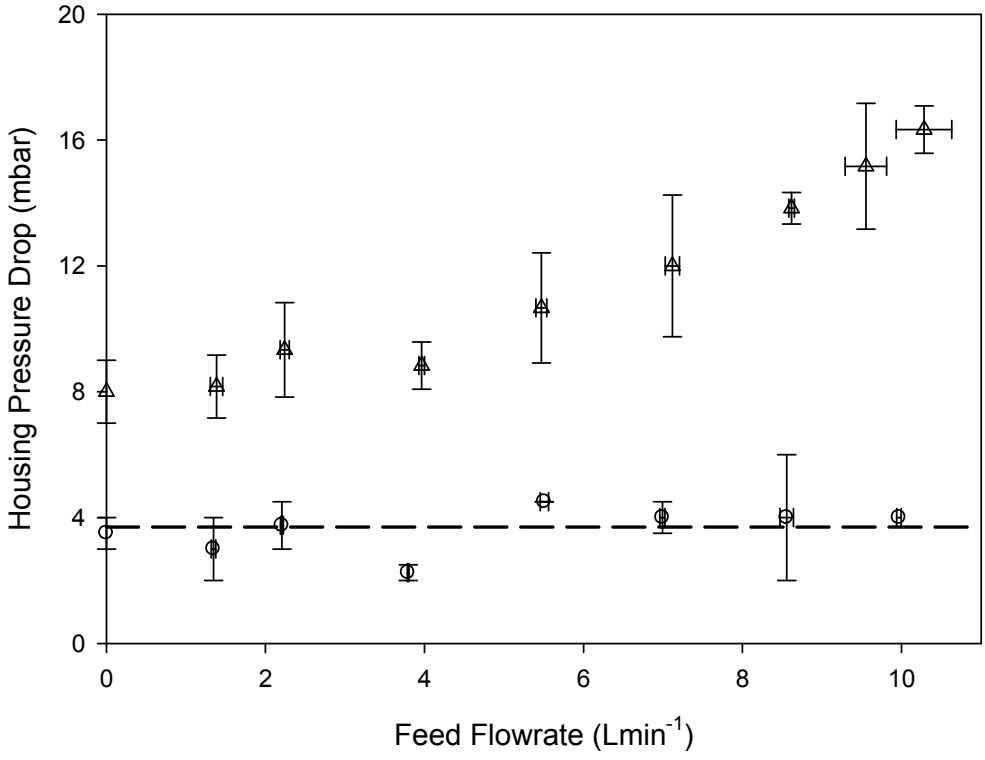

Figure 3-2: Measured pressure drops for a 10" cartridge housing (○) and a 1" cartridge housing (△).Error bars represent one standard deviation about the mean (n=3). Dashed line intersects the y-axis at 3.7 and represents the mean pressure drop for the 10" housing over the range of permeate flow rates used. Experiments were conducted as described in Section 2.3.1 but without a cartridge inside of the housing.

The 10" $UEAV_{24,\ 1}$ corrected water flux data in Figure 3-3 was compared to data recorded using a separate 'flow dP' rig as described in Section 2.3.1.1. The results are shown in Figure 3-4. The Pall 'flow dP' rig is modified so that fixed tubing connected to digital manometers, record the pressure at the feed and permeate side of the membrane cartridge, thus avoiding the housing pressure drop (see Figure 2-14). Figure 3-4 shows the two datasets to be in good agreement. This confirms that it is possible to correct the 10" TMP data for the housing pressure drop, thus ensuring the maximum accuracy of the data. The calculated membrane resistance was 3.48×10^{10} m^{-1} and 3.43×10^{10} m^{-1} for the Pall 'flow dP' and UCL rigs respectively. For comparison, the calculated membrane resistance for the dataset without the housing correction is 3.79×10^{10} m^{-1}.

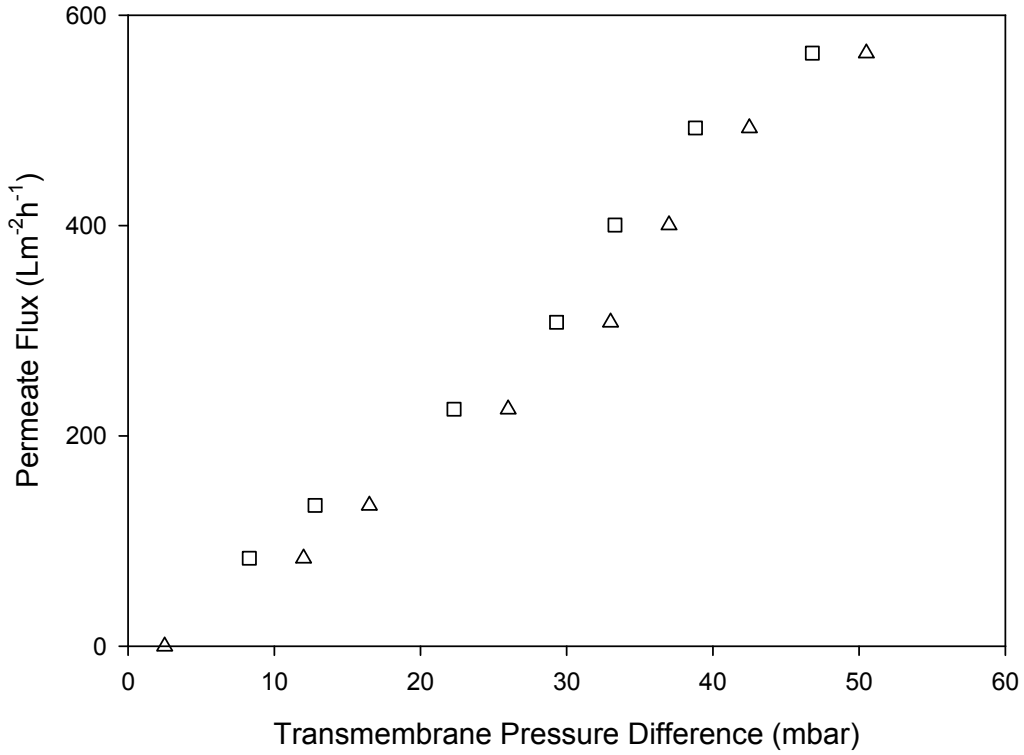

Figure 3-3: Permeate flux through a 10" $UEAV_{24,\ 1}$ cartridge for measured transmembrane pressure differences that were corrected (□) and not corrected (△) for the housing pressure drop. Experiments conducted with clean water as described in Section 2.3.1. Feed flowrates ranged from 0-10.6 $Lmin^{-1}$.

A typical example of water flux data correction for a 1" UEAV cartridge is shown in Figure 3-5. It can be seen in Figure 3-5 that despite the relatively large variation in housing drop reported in Figure 3-2, the correction to the water flux data was small. This is due to the higher feed pressure caused by the flow restriction that exists when a filter cartridge is present in the housing. The housing pressure drop, when compared to the filter cartridge pressure drop, is relatively small and accounts for less than 8% of the measured transmembrane pressure difference.

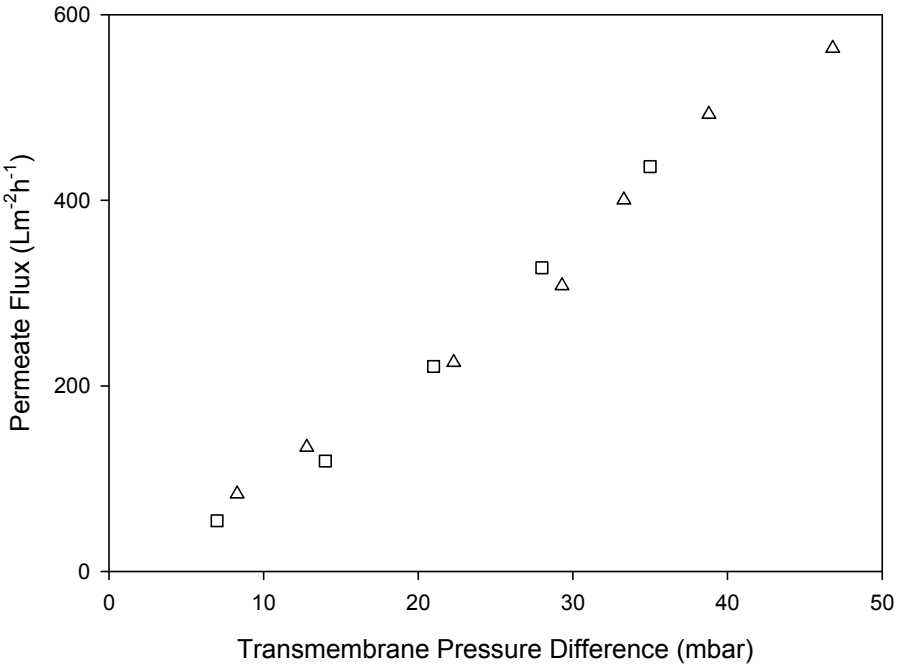

Figure 3-4: Permeate flux through a 10" $UEAV_{24,1}$ cartridge for measurements made at UCL, and corrected for the housing pressure drop (□) and measurements made at Pall Walton Road using the 'flow dP' rig (△). Measurements made at UCL as described in Section 2.3.1 Measurements at Pall Walton Road as described in Section 2.3.1.1.

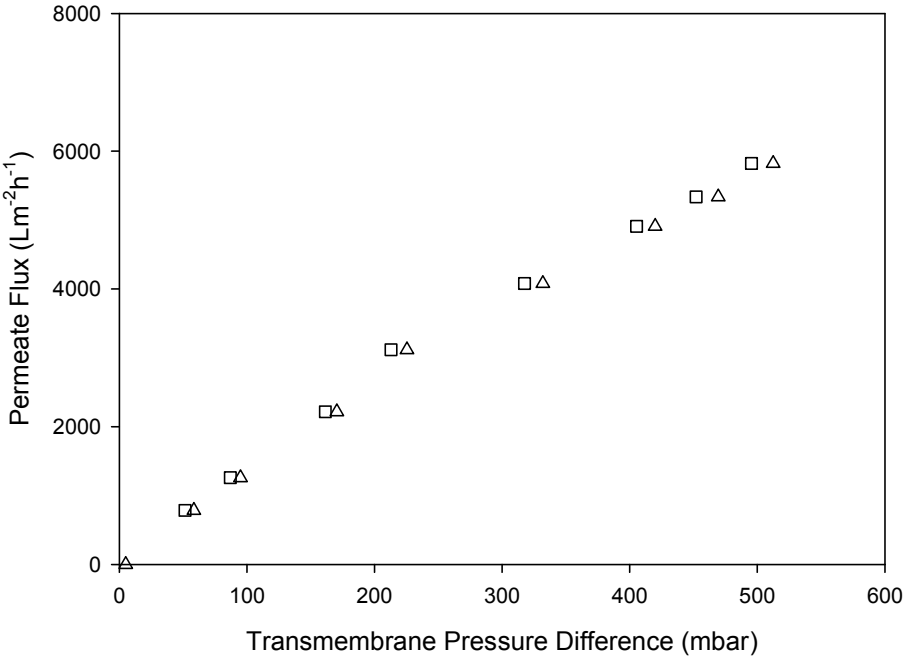

Figure 3-5: Permeate flux through a 1" $UEAV_{24,\ 1}$ cartridge for measured transmembrane pressure differences that were corrected (□) and not corrected (△) for the housing pressure drop. Experiments conducted with clean water as described in Section 2.3.1. Feed flow rates ranged from 0-10.6 $Lmin^{-1}$.

3.2.2. Axial Mixing Within Cartridge Housing

Having measured the pressure drop exerted on the experimental system by the cartridge housing, the liquid hydrodynamics within the 10" housing were investigated. A transparent housing with the same internal dimensions as a standard stainless steel housing was constructed as described in Section 2.1. This allowed for direct observation of fluid flow inside the housing during each experimental run. As described in Section 2.1 potassium permanganate was used to visualise the path of the feed into and around the housing from the inlet.

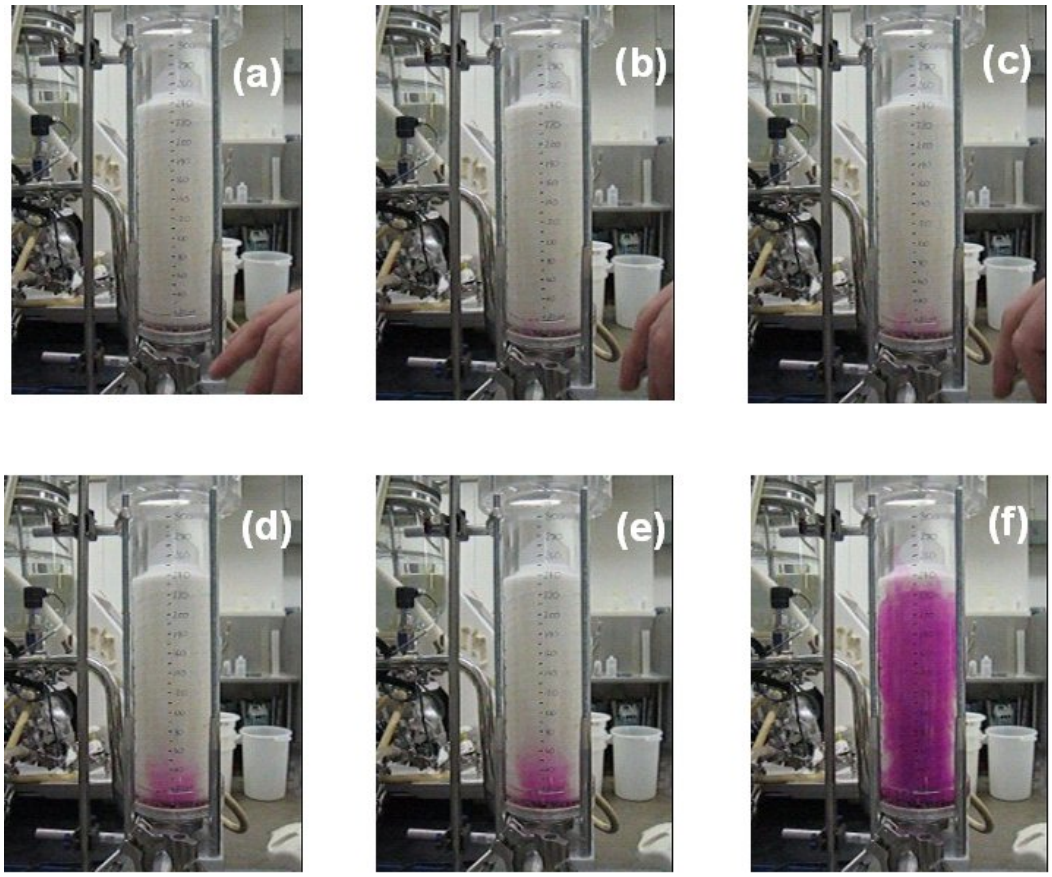

Figure 3-6: Time-lapse images showing the infiltration of dyed feed solution into the 10" cartridge housing when operated at a feed flowrate of 1.0 $Lmin^{-1}$. Images captured every 0.23 seconds from (a) t = 0 s, through (b) t = 0.23 s, (c) t = 0.46 s, (d) t = 0.92 s, (e) t = 1.15 s, (f) t = 8.23 s. Marked scale on side of housing used to plot the progression of the dyed feed up the length of the cartridge. Housing viewed from the side with the feed inlet. Experiments conducted as described in Section 2.2.1.

Figure 3-6 shows the infiltration of dye into the housing for a feed flowrate of 1.0 $Lmin^{-1}$ corresponding to a clean water flux of approximately 57 $Lm^{-1}h^{-1}$ at a TMP of 5 mbar. A marked scale on the side of the housing was used to record the progress of the dye from the feed inlet, situated at the base of the cartridge, to the top of the cartridge. The progression of the dyed feed solution was observed from the side of the feed inlet. It took 8 seconds from when the dye entered the housing for it to reach the top of the cartridge.

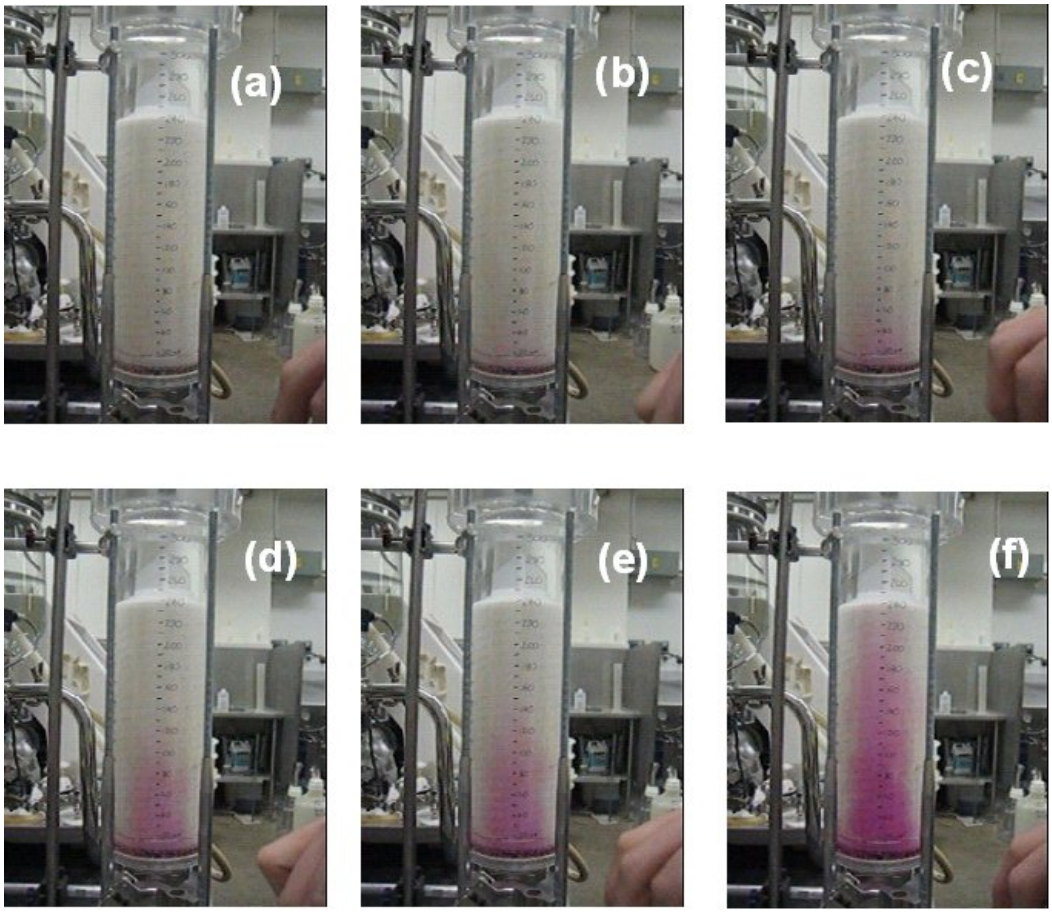

Figure 3-7: Time-lapse images showing the infiltration of dyed feed solution into the 10" cartridge housing when operated at a feed flowrate of 3.9 $Lmin^{-1}$. Images captured every 0.23 seconds from (a) t = 0 s, through (b) t = 0.23 s, (c) t = 0.46 s, (d) t = 0.92 s, (e) t = 1.15 s, (f) t = 2.20 s. Marked scale on side of housing used to plot the progression of they dye up the length of the cartridge. Housing viewed from the side with the feed inlet. Experiments conducted as described in Section 2.2.1.

Figure 3-7 shows the infiltration of dye for a higher feed flowrate of 3.9 $Lmin^{-1}$, corresponding to a clean water flux of approximately 220 $Lm^{-1}h^{-1}$ at a TMP of 19 mbar. Here it can be seen that the higher flowrate lead to greater infiltration up the height of the cartridge. This was due to the higher momentum in the axial direction caused by the higher linear velocity of the dyed feed at the inlet. A slight increase in radial dispersion was also observed for the higher feed flowrate.

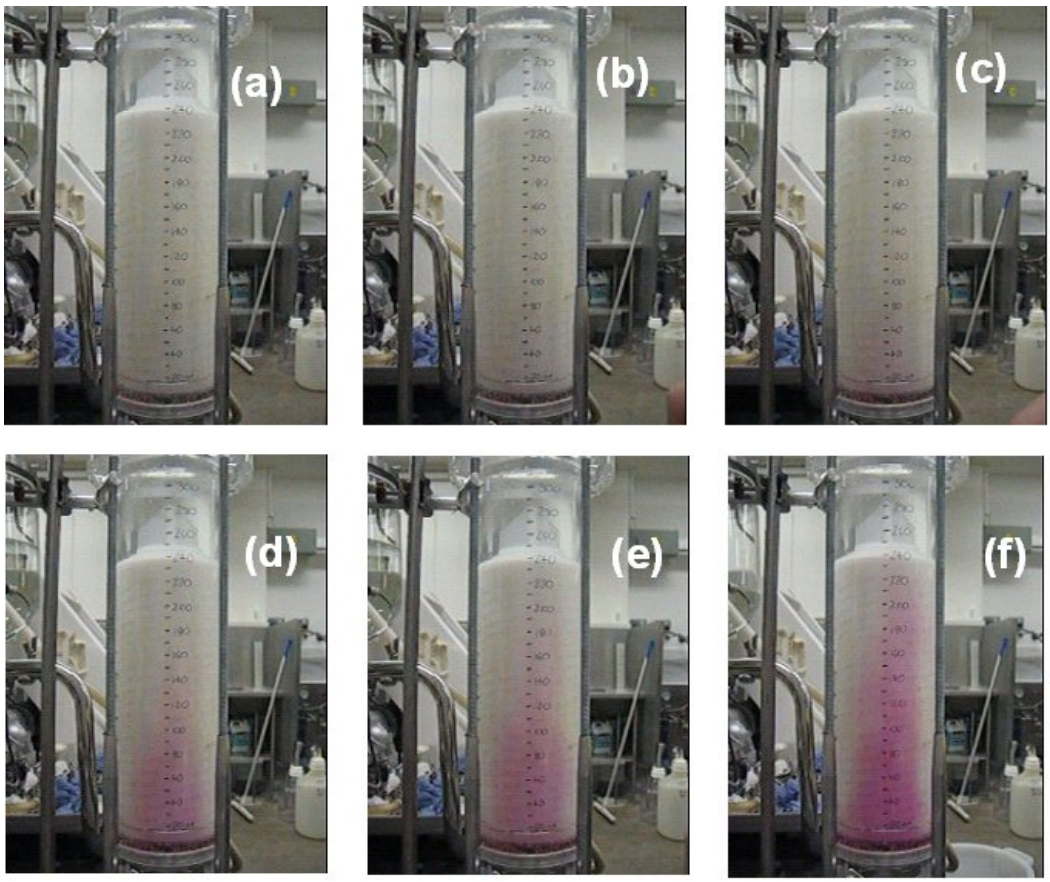

Figure 3-8: Time-lapse images showing the infiltration of dyed feed solution into the 10" cartridge housing when operated at a feed flowrate of 7.1 $Lmin^{-1}$. Images captured every 0.23 seconds from (a) t = 0 s, through (b) t = 0.23 s, (c) t = 0.46 s, (d) t = 0.92 s, (e) t = 1.15 s, (f) t = 1.36 s. Marked scale on side of housing used to plot the progression of they dye up the length of the cartridge. Housing viewed from the side with the feed inlet. Experiments conducted as described in Section 2.2.1.

Figure 3-8 shows that the degree of infiltration was seen to increase further for the highest feed flowrate tested of 7.1 $Lmin^{-1}$ corresponding to a clean water flux of approximately 400 $Lm^{-1}h^{-1}$ at a TMP of 34 mbar. Once again the increase in feed flowrate lead to an increase in axial momentum. It was again observed that radial dispersion did not increase significantly with the increase in feed flowrate.

Using the measuring scale on the side of the housing it was possible to plot the progression of the front of the dyed feed solution for each of the feed flowrates used in Figure 3-6 to Figure 3-8. The rate of infiltration as a function of feed flow rate is shown in Figure 3-9.

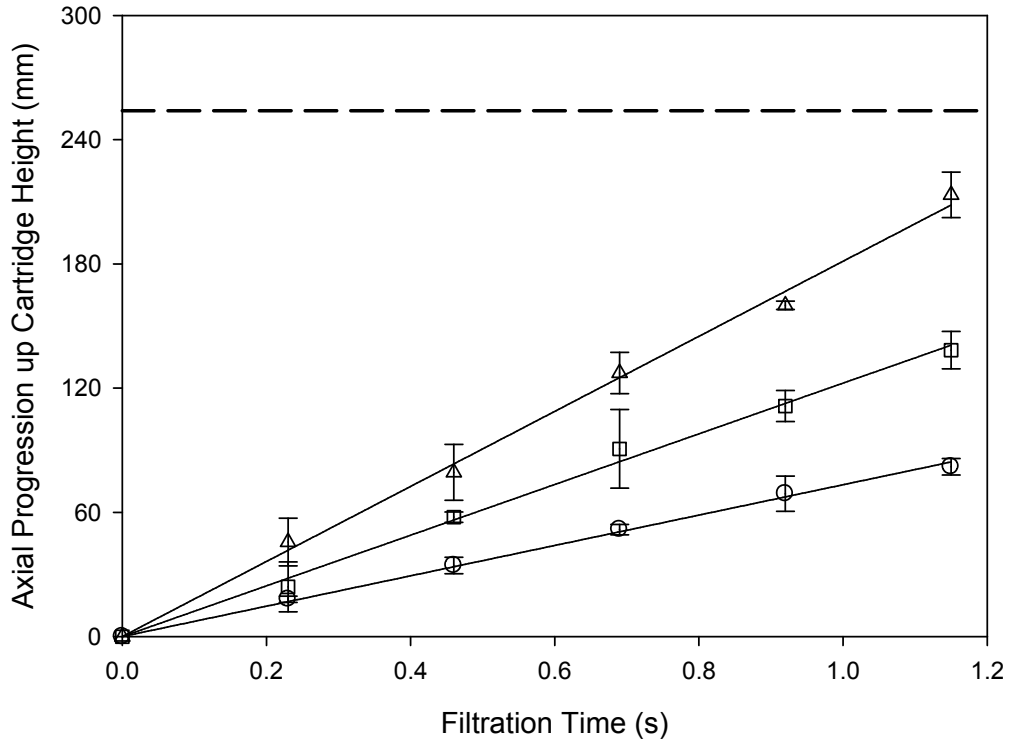

Figure 3-9: Progression of dyed feed front over time as a function of feed flowrate: (○) 1.0 $Lmin^{-1}$, (□) 3.9 $Lmin^{-1}$ and (△) 7.1 $Lmin^{-1}$. Error bars represent one standard deviation around the mean (n = 3). Solid lines fitted by linear regression (R^2>0.99). The dashed line indicates the top of the cartridge at a height of 10" (25.4 cm). Experiments were conducted as described in Section 2.2.1.

Figure 3-9 shows that, for each feed flowrate used, the progression of dye in the axial direction followed a linear relationship, which would be expected, as the feed flowrate (and thus feed velocity) remained constant. The dye front was almost seen to reach the top of the cartridge by the time that the recording was stopped (time = 8.2s) indicating rapid progression in all cases.

Progression of the dye front appears to be a function of the feed flowrate. To investigate further the time taken for the dye front to reach the top of the feed side of the cartridge was recorded for a wide range of feed flowrates as shown in Figure 3-10.

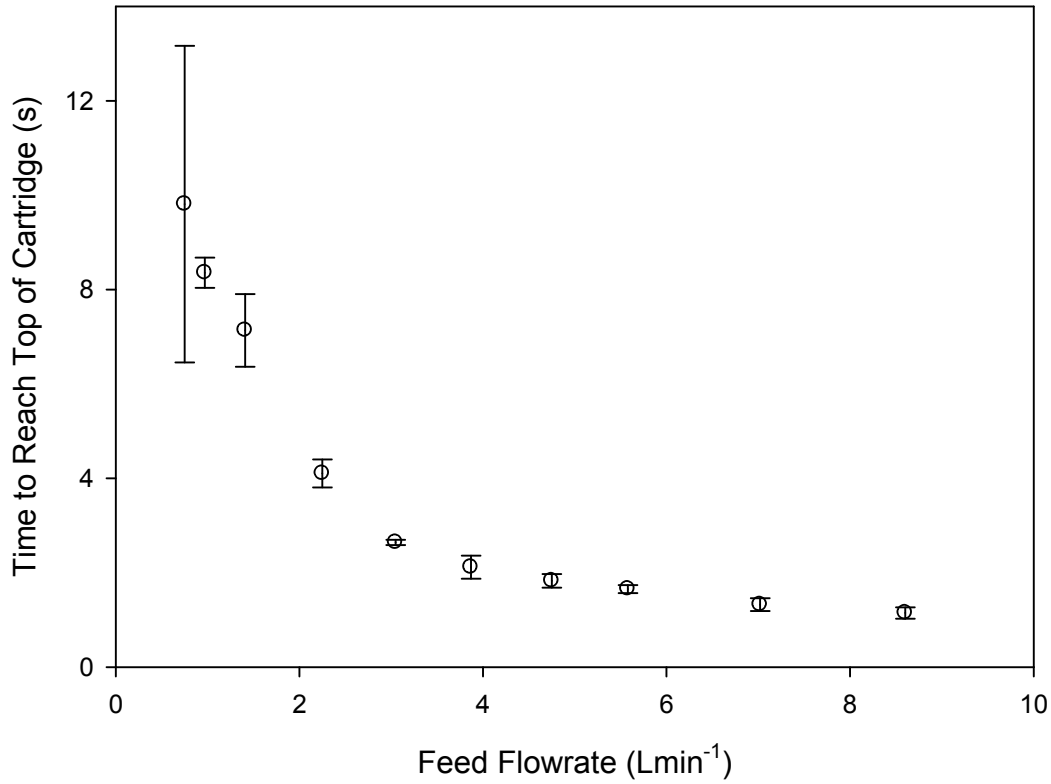

Figure 3-10: Time taken for dyed feed front to reach the top of the cartridge (h_C) on the feed side of the membrane as a function of feed flowrate. Error bars represent one standard deviation about the mean (n=3). Experiments performed as described in Section 2.2.1.

Figure 3-10 shows that as the feed flowrate increased there is an almost exponential decline in the time for the dye to reach the top of the cartridge. Higher measurement variation was seen in the measurement taken at lower flowrates. Whilst the time taken to reach the marked position was relatively high for low feed flowrate, the maximum time (~10 s) was still quick when placed in the context of a filtration operation (>15 min). Above a feed flowrate of 4 $Lmin^{-1}$ the time taken for fluid to reach the top of the cartridge was negligible. In a bioprocess it is likely that the cartridges would be operated at feed flowrates greater than 4 $Lmin^{-1}$ (Haslam, 2007), thus any effects seen below this rate are likely not to be significant.

3.2.3. Radial Mixing Within Cartridge Housing

Initial investigation of the images captured in Figure 3-6 – Figure 3-8 suggested that the rate of liquid dispersion in the radial direction may be lower than that in the axial direction. Thus the camera used to record the progression of the dye front into the housing was re-positioned to face the permeate side of the housing, at a position 180° from the feed inlet (Figure 2-4). Three measurement marks were made at the bottom, middle and top of the cartridge (h_C = 30 mm, 130 mm and 220 mm from the base respectively). Just as for the axial dispersion measurements, the time taken to reach these marks was recorded for the same range of feed flowrates.

The results for the measurement mark located at the bottom of the cartridge (h_C = 30 mm) are given in Figure 3-11. The line shows a non-linear decline similar to that observed for the axial mixing in Figure 3-10. However, for feed flowrates less than 4 $Lmin^{-1}$, the time to reach the measurement mark was greater than for the axial dispersion, even though the bottom permeate side measurement mark was closer to the feed inlet. Above a feed flowrate of 4 $Lmin^{-1}$ the time taken for the dye to reach the measurement mark was negligible. A degree of variation in the measured time was seen for the lower feed flowrates, as indicated by the error bars.

Similar trends are seen for radial dispersion measurements at the mid-point of the cartridge, h_C = 130 mm, (Figure 3-12) and the top of the cartridge, h_C = 220 mm, (Figure 3-13). As was found for the bottom measurement mark, greater variation was seen in the time measurements made at low feed flowrates. This was particularly the case at the middle of the cartridge. Also for the top and middle of the cartridges, the time measurement did not reduce to the same level as had previously been seen for the bottom of the cartridge.

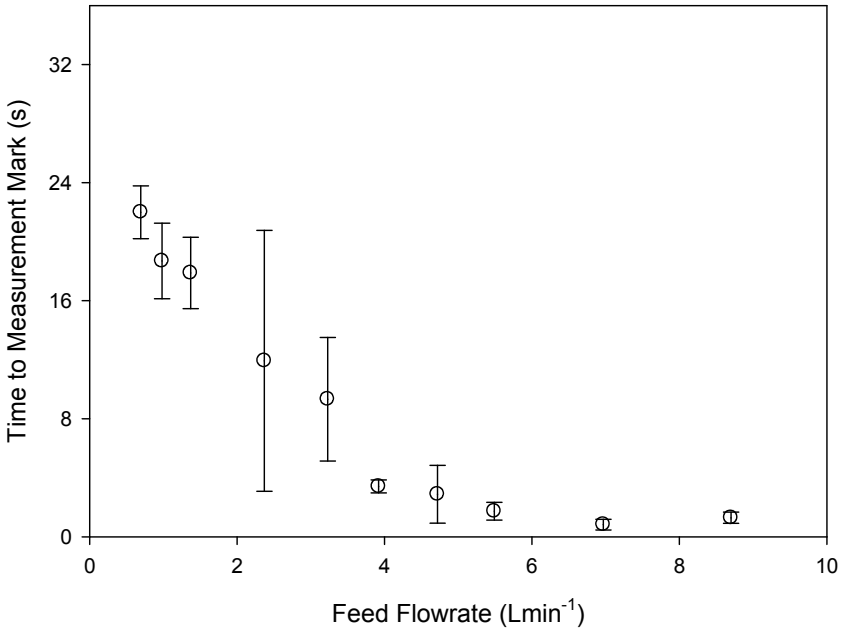

Figure 3-11: Plot of time taken for dyed feed front to reach the bottom measurement (h_C = 30 mm) mark on the permeate side of housing as a function of feed flowrate. Error bars represent one standard deviation around the mean (n=3). Experiments conducted as described in Section 2.2.2.

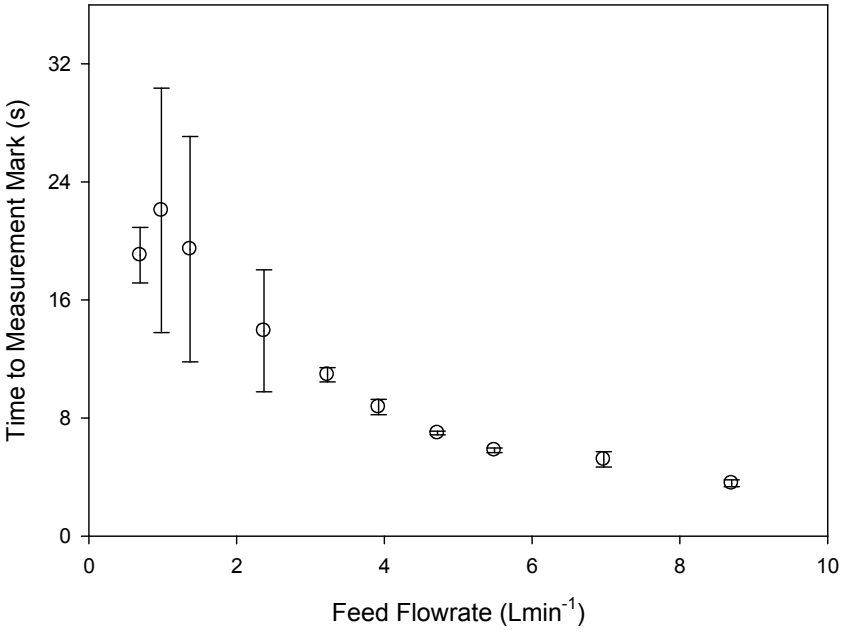

Figure 3-12: Plot of time taken for dyed feed front to reach the bottom measurement (h_C = 130 mm) mark on permeate side of housing as a function of feed flowrate. Error bars represent one standard deviation around the mean (n=3). Experiments conducted as described in Section 2.2.2.

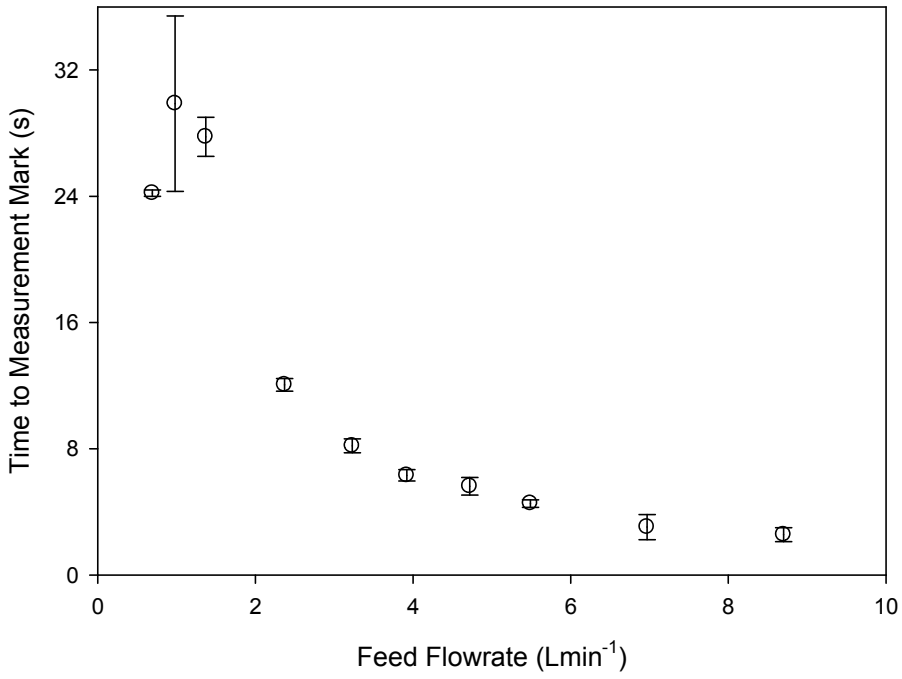

Figure 3-13: Plot of time taken for dyed feed front to reach bottom measurement (h_C = 220 mm) mark on the permeate side of the housing as a function of feed flowrate. Error bars represent one standard deviation around the mean (n=3). Experiments conducted as described in Section 2.2.2.

To compare more closely the axial and radial dispersion, the datasets for the two measurement marks at the top of the cartridge (with one on the feed side and the other on the permeate side) have been combined in Figure 3-14. It can be seen from the figure that it takes longer for dispersion to take place on the permeate side, than it does on the feed side. This difference in dispersion reduces at higher flowrates as greater axial and radial momentum enters the system at the feed inlet.

Whilst there appears to be a measurable housing effect in terms of variation in axial and radial hydrodynamics, in the context of a filtration operation the effect is likely to be insignificant.

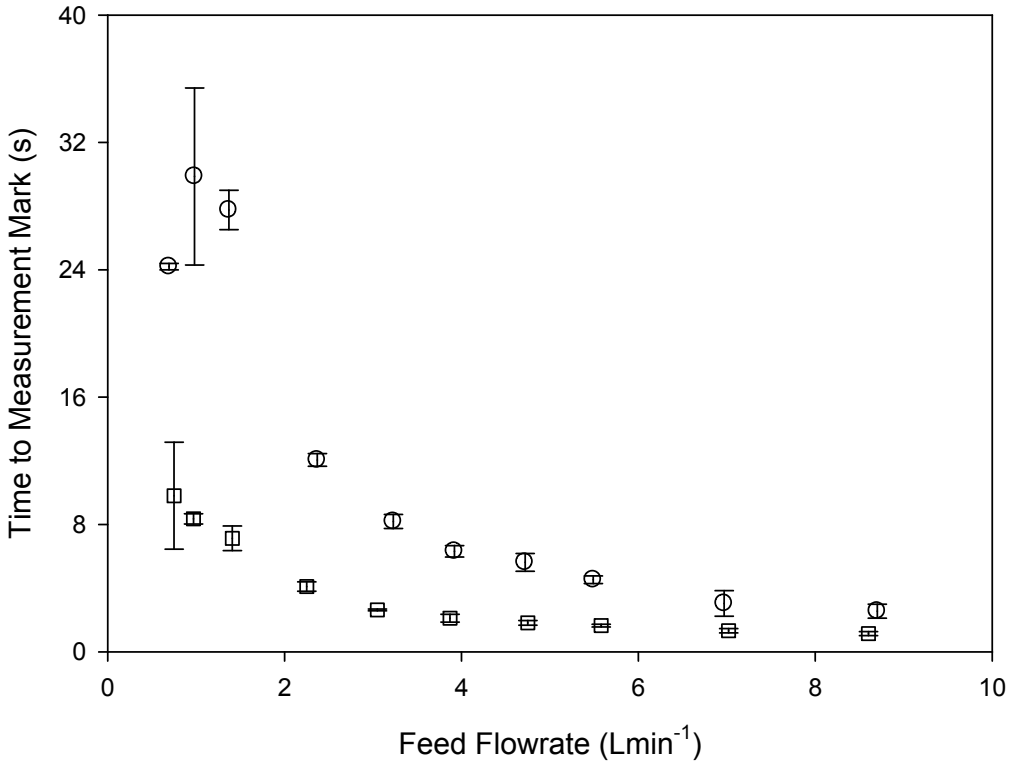

Figure 3-14: Combined plot of data contained in Figure 3.10 and 3-13. Error bars represent one standard deviation about the mean (n = 3). Both datasets were taken at the top of the cartridge, but with one on the feed side (□) and the other on the permeate side (○).

3.3. Development of a Realistic Fouling Feedstock

In Section 1.3.1 it was noted that a common feedstock that a sterile or bioburden reduction filter will face is a protein solution. In Section 1.3.2 the filterability of a range of protein solutions was discussed; in general the protein solutions were seen to foul a microfiltration membrane and the filterability varied depending upon the protein contained within the solution. As part of this work the assessment of the performance of a 0.22 μm rated membrane filter with a realistic feedstock is required for a range of size-scales. A protein solution would make an ideal test feedstock, however, as the filterability varies depending upon the protein selected then an initial study is required to select a suitable protein for use in this work, particularly as experiments will be conducted on the large-scale.

Based upon ease of availability and cost, bovine serum albumin (BSA) and pepsin were selected as initial candidates. The filterability of solutions of each of the proteins was assessed using flat sheet membrane. The selected protein will be used to characterise the performance of the large-scale 10" pleated cartridge later in Section 3.4.2.

3.3.1. Filterability of BSA Solution using a 0.2 µm rated Membrane Filter

A 1 gL^{-1} solution of BSA in 0.03 M phosphate buffer (pH = 7.4) was selected for initial investigation. BSA has been used extensively within the filtration studies outlined in Section 1.3.2, thus providing literature data for comparison (Girones et al., 2006; Kelly et al., 1995; Kelly et al., 1997). Furthermore, BSA is a species that is readily available.

Initial studies quantified permeate flux versus time relationships as a function of storage time of the BSA solution as shown in Figure 3-15 for a solution stored at 20°C between filtration runs. For fresh BSA solution (t = 1 hr) a 20% decline was seen in the permeate flow over the course of the filtration run. The decline in permeate flow was largely linear after an initial drop of 10% at the start of the filtration run.

After 24 hr of storage the filterability of the solution had declined significantly. A drop in permeate flux to below 20% of the initial flowrate was seen after 10 minutes of operation. From this point the permeate flow was seen to decline to less than 5% of the initial flow. The rate of decline in permeate flow increased further after a total storage time of 48 hr. When the solution was filtered a drop in permeate flow to below 20% of the initial rate was seen after 5 minutes of operation. Again, from this point further decline was seen to a point where the permeate flow was less than 5% of the initial rate.

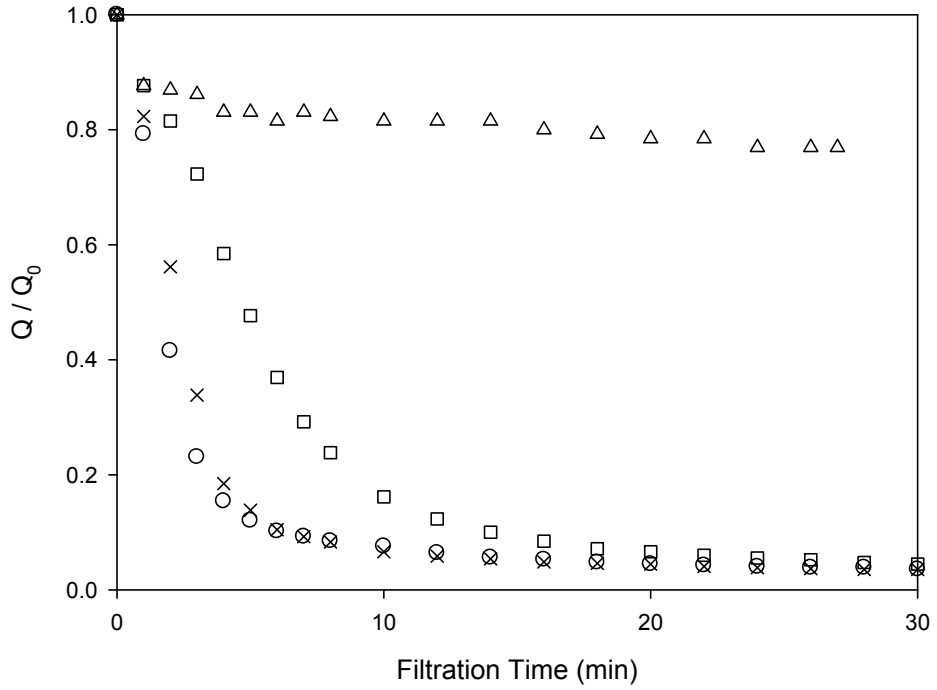

Figure 3-15: Impact of storage time (at 20 °C) upon the filterability of 1 gL^{-1} BSA solution in 0.03 M phosphate buffer (pH = 7.4). Q = Permeate flow rate ($mLmin^{-1}$). Q_0 = 130 $mLmin^{-1}$. Filtration experiments conducted at the following times after preparation: 1 hr (△), 24 hr (□), 48 hr (×), 72 hr (○). Experiments conducted with a single preparation of the BSA solution, which was filtered through 47 mm discs of Supor® EAV membrane as described in Section 2.6.2.1.

After storage for a further period of 24 hr (total storage time = 72 hr) no further change in the rate of decline in permeate flow was measured. It was seen that the non-linear flux decline was the same as after 48 hr of storage.

Another preparation of BSA solution was stored at a temperature of 4°C between filtration runs. The results for these experiments are shown in Figure 3-16. Just as for when stored at 20°C the filterability of the BSA solution declined during storage, however the rate of decrease in permeate flow was significantly slower than when the solution was stored at 4°C.

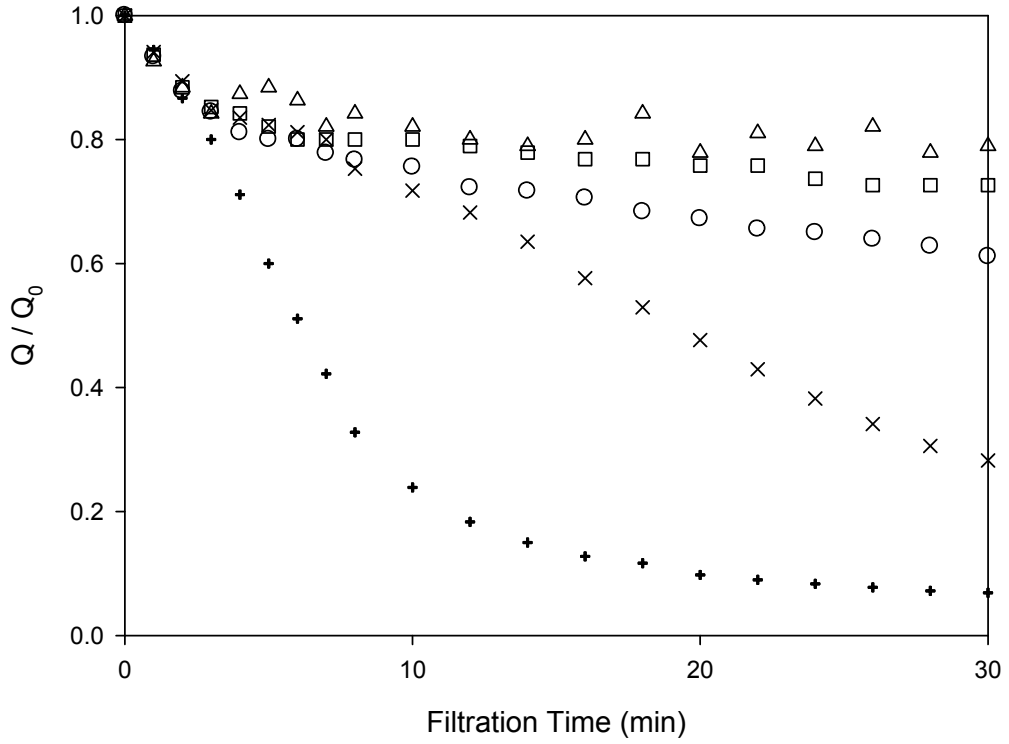

Figure 3-16: Impact of storage time (at 4°C) upon the filterability of 1 gL^{-1} BSA Solution in 0.03 M phosphate buffer (pH = 7.4). Q = Permeate flow rate ($mLmin^{-1}$). Q_0 = 90 $mLmin^{-1}$. Filtration experiments conducted at the following times after preparation: 1 hr (△), 48 hr (□), 120 hr (○), 216 hr (×), 552 hr (+). Experiments conducted with a single preparation of the BSA solution, which was filtered through 47 mm discs of Supor EAV membrane as described in Section 2.6.2.1.

After 1 hour of storage a 15% reduction in permeate flowrate was measured after filtration for 30 min. After 48 hr of storage the rate of decline remained slow although after 30 min of operation a drop in permeate flow of 25% was measured. The rate of decline in permeate flow continued to increase after total storage times of 120 and 216 hr, until after 552 hr the rate of decline in permeate flow increased to a level whereby the permeate flow declined to below 20% of the initial flow after 10 min of operation.

The datasets in Figure 3-15 and Figure 3-16, are summarised in Table 3-1 in terms of the time (t_{20}) taken for the permeate flow to drop to less than 20% of the starting flow rate (Q/Q_0 = 0.2). This value is presented for a range of storage

temperatures and storage times. It can be seen that the value of t_{20} after storage at 20°C for 72 hr is less than for the chilled solution stored at 4°C for 552 hr, indicating that the filterability of the BSA solution is worse after storing at room temperature. Values of t_{20} taken from other studies in the literature are also given in Table 3-1. In the case of storage at 20 °C, the value of t_{20} measured in this study was lower than that reported in the literature. However for storage at 4 °C, the value of t_{20} measured here was seen to higher than the values reported in the literature. It should be noted that for three different types of membranes were used for the literature studies and this may be cause in the differences noted.

These experiments have shown a BSA solution to foul a 0.22 μm rated membrane. However, the volume of feedstock required to conduct the experiment was high (2 L for low fouling conditions). Pepsin has been discussed in the literature as showing a greater propensity to foul microfiltration membranes (see Section 1.3.2.3), and thus may require a lower feedstock volume to gain representative data with a range of filtration devices.

Table 3-1: Measured values of t_{20} for the datasets given in Figure 3-15 and Figure 3-16. Literature values also presented for comparability of the values derived in this study.

Membrane Type		BSA Concentration (gL^{-1})	Max Storage Time (hr)	Storage Temperature (°C)	t_{20} (min)	Data Source
Material	Pore Size (µm)					
PES	0.2	1	1	20	-	Figure 3-15
PES	0.2	1	24	20	9	Figure 3-15
PES	0.2	1	48	20	4	Figure 3-15
PES	0.2	1	72	20	4	Figure 3-15
PES	0.2	1	1	4	-	Figure 3-16
PES	0.2	1	48	4	-	Figure 3-16
PES	0.2	1	120	4	-	Figure 3-16
PES	0.2	1	216	4	-	Figure 3-16
PES	0.2	1	552	4	10	Figure 3-16
PVDF	0.22	2	24	22	30	(Kelly et al., 1997)
PES	0.16	4	24	4	4	(Kelly et al., 1994)
PVDF	0.22	1	48	4	70	(Kelly et al., 1995)
Silicon Nitride	1.2	1	2	8	10	(Girones et al., 2006)

3.3.2. Filterability of Pepsin Solution using a 0.2 µm rated Membrane Filter

The filterability of three separate preparations of 10 gL^{-1} pepsin in 0.03 M phosphate buffer (pH 7.4) is shown in Figure 3-17. In Section 3.3.1 throughput was reported as Q/Q_0 due to the high permeate flow rates measured initially. In this section, throughput is reported as cumulative volume, as the flow rates were too small to measure accurately using this method. The three preparations varied in the processing that they received before filtration. As would be expected, the fresh preparation (filtered after 1 hr storage) yielded the best filtration performance. The preparation that was exposed to mixing for one hour showed a reduced filterability, which was likely caused by aggregation of the pepsin due to shear (Wang, 2005). The solution stored for three days at 20°C showed the worst filterability, in turn likely to be due to aggregation as a consequence of temperature and time effects.

The mechanism behind the fouling of the membrane has been partially investigated here through the analysis of samples taken from the feed stream and permeate stream during a filtration run. These samples were analysed using light scattering as described in Section 2.6.4 to identify the size of particles contained within the sample. The results of the analysis for the fresh preparation of pepsin solution (storage time = 1 hr) is given in Figure 3-18. The results of the analysis for the aged preparation of pepsin solution (storage time = 3 days) is given in Figure 3-19. It is important to note that the data shown in the two figures is qualitative and not quantitative. Also, the technique is sensitive to the range of particles, such that the presence of large particles in the sample will dominate the measured signal, hiding the presence of smaller particle species (Malvern Instruments, 2004).

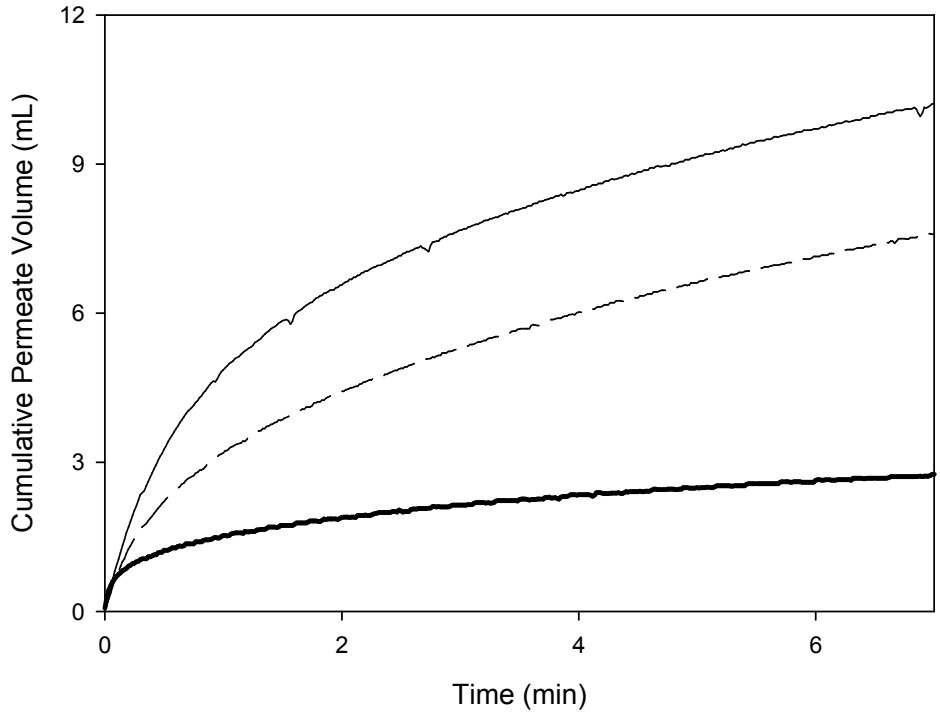

Figure 3-17: Filterability of three separate preparations of a feedstock consisting of 10 gL^{-1} pepsin in a 0.03 M phosphate buffer (pH = 7.4). One preparation was filtered within one hour of preparation (—), one underwent mixing for one hour (– –) and one was left in storage at a temperature of 20°C for three days (▬). All preparations were filtered at 0.14 bar(g) using 25 mm discs of Supor EAV membrane as described in Section 2.6.2.2.

The analysis of the samples taken during the filtration of the fresh preparation of the pepsin feedstock (Figure 3-18) showed that the feed sample was dominated by large aggregate species with a size range between 1-3 μm that would be large enough to block the pores of the 0.22 μm rated membrane. There was also a smaller peak between the size range of 20-40 nm. The permeate sample showed a similar taller peak at this size range, with an additional peak at the range of 1-9 nm. It is assumed that this peak was not observed in the feed sample as it was obscured by the larger particles present. The permeate sample did not show the presence of any particles in the 1-3 μm range as they had been removed by the membrane.

The analysis of the feed sample taken from the filtration of the aged pepsin solution stored for three days (Figure 3-19) showed similar trends to those seen for the filtration of the fresh preparation of the feedstock.

The controlling mechanism behind the fouling of the membranes cannot be identified from these results. It is possible that the largest particles are blocking the pores outright, following a complete blocking model (Table 1-4). However it is also possible that the smaller species in the range of 20-40 nm are collecting in the pores of the membrane leading to constriction of the pore according to the standard pore blocking model (Table 1-4). It has been previously suggested during another study that a two step mechanism is in action that consists of initial blocking of the pores by protein aggregates, followed by attachment of native protein to the growing deposit (Kelly et al., 1997).

The effect of feed pressure on the filtration of the pepsin feedstock is shown in Figure 3-20. It can be seen that the fouling nature of the feedstock is similar for both feed pressures used. However, throughput is dependent upon feed pressure, when an increase in feed pressure lead to higher throughput.

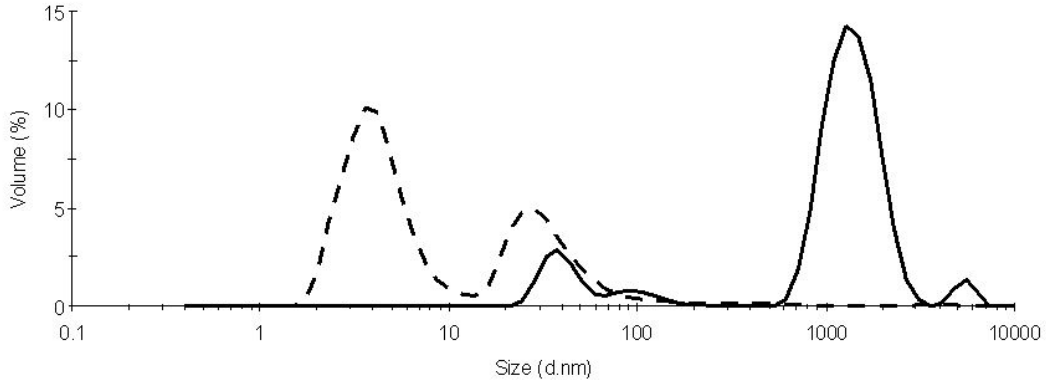

Figure 3-18: Size distribution of particles contained with samples taken during the filtration (Figure 3-17) of fresh (storage time = 1 hr) feedstock of 10 gL^{-1} pepsin in 0.03 M phosphate buffer (pH = 7.4) with a 0.22 µm rated Supor® EAV membrane. Samples taken were from the feed stream (—) and permeate stream (– –) after 7 min. Measurements made using light scattering as described in Section 2.6.4.

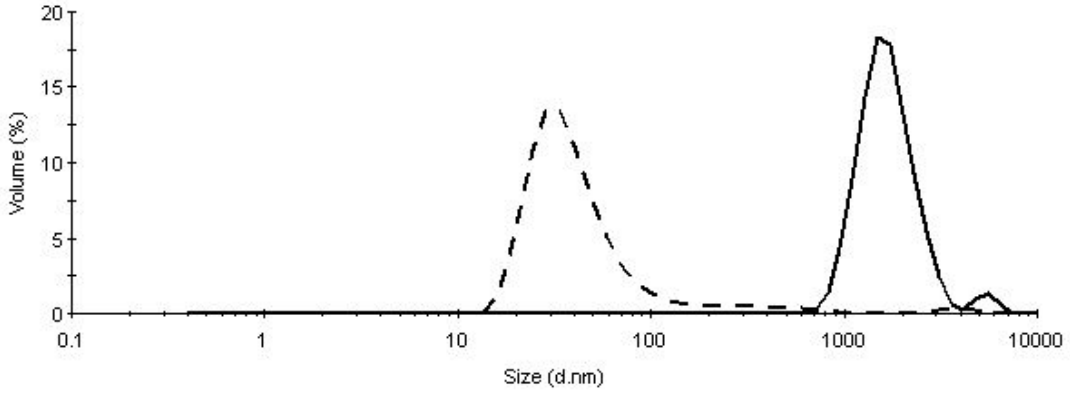

Figure 3-19: Size distribution of particles contained with samples taken during the filtration (Figure 3-17) of aged (storage time = 3 days) feedstock of 10 gL^{-1} pepsin in 0.03 M phosphate buffer (pH = 7.4) with a 0.22 µm rated Supor® EAV membrane. Samples taken were from the feed stream (—) and permeate stream (– –) after 7 min. Measurements made using light scattering as described in Section 2.6.4.

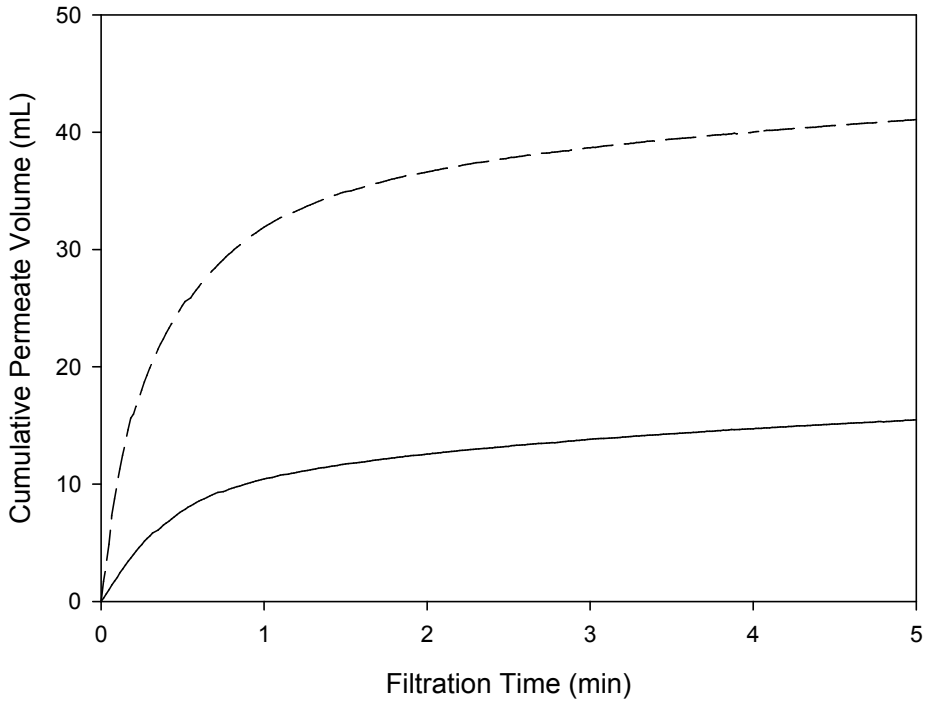

Figure 3-20: Filtration of feedstock consisting of 10 gL^{-1} pepsin in 0.03M phosphate buffer (pH = 7.4) with Supor® EAV membrane. Experiments conducted at two different feed pressures: 0.14 bar(g) (—) and 0.83 bar(g) (– –). Experiments conducted as described in Section 2.6.2.2.

Table 3-2: Estimated feed volume requirements for filtration of protein solutions using a 10" $UEAV_{24,1}$ cartridge calculated from filtration data for the various feedstocks stored at 20°C.

	BSA (fresh)	**BSA (stale)**	**Pepsin (fresh)**	**Pepsin (stale)**
Estimated Feed Volume (L)[I]	2700	250	40	10

[I] Calculated using the V_{max} method described in Section 1.7 applied to data contained in Figures 3.2 and 3.5.

A summary of the estimates of the volume of a BSA or pepsin feed required to determine V_{max} type data with a 10" $UEAV_{24,1}$ cartridge is given in Table 3-2. It can be seen that the feed volume required was much higher for BSA feedstocks. As the aim for the large-scale study is to work with less than 100 L, and ideally with less than 1 L, for each experiment then the pepsin feedstock should be used. Furthermore, to enable the material to be quickly generated for multiple batches, the fresh preparation should be used.

3.4. Basic Filtration Performance for 10" Pleated Membrane Cartridge Filters

Having investigated the design features of pleated cartridge housings that can impact upon accurate measurement of the performance of pleated cartridge filters with liquid feedstocks, the pressure drop across housing was seen to be of significance for the 10" scale cartridge, where the measured transmembrane pressure differences are relatively low for the operational flowrates used.

These findings will be used to generate a dataset for a 10" $UEAV_{24,1}$ cartridge, which is used in this thesis as the standard large-scale device against which all other scales are compared. Base data will be presented for both non-fouling (water) and two fouling feedstocks (protein solution and a yeast solution).

3.4.1. Water Flux Performance for 10" Pleated Cartridge Filter

The 10" $UEAV_{24,\ 1}$ cartridge was first characterised with water. The variation of water flux with a change in transmembrane pressure difference for three separate cartridges is given in Figure 3-21. The measured transmembrane pressure differences were relatively low, up to 50 mbar, due to the limitations of the pumping equipment used. However good agreement was seen between the three independent datasets.

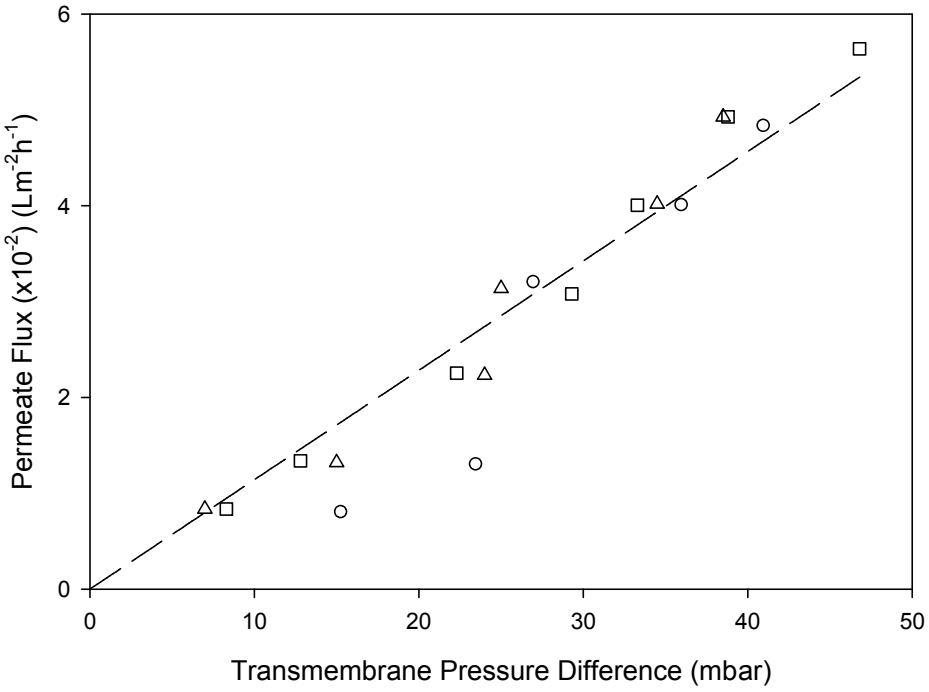

Figure 3-21: Clean water flux through a 0.2 µm rated 10" Supor® $UEAV_{24,\ 1}$ cartridge. Results for three separate cartridges presented. Dashed line (— —) fitted by linear regression (R^2>0.92) represents the mean (n=3). Measurements made at ambient temperature (20°C) as described in Section 2.4.1. TMP measurements were corrected for housing pressure drop as described in Section 3.2.1.

3.4.2. Volume Throughput for Protein Solution Filtration

Earlier in this chapter (Section 3.3) the filterability of a range of different protein solutions was assessed using flat sheet membrane. Based upon an estimate of the volume required to operate at the large-scale, a 10 gL^{-1} pepsin solution was selected to work with as the feed volume required was lower than for BSA.

The filtration data using a 10" $UEAV_{24,\ 1}$ cartridge of three separate preparations of the pepsin solution is shown in Figure 3-22. A new cartridge was used to filter each fresh preparation of the pepsin feedstock. The volume of pepsin required to perform the filtration of pepsin was significantly greater than the 40 L that was predicted in Section 3.3.2 (Table 3-2). Thus the performance prediction generated on the flat sheet membrane was poor (this will be discussed further in Section 5.3). From the figure it can be seen that volume throughput of the permeate was constant during the start of the filtration operation, whilst a rise in the feed pressure was measured. After approximately 15 minutes a second operational region was observed whereby the volume throughput no longer remained at a constant rate. During this region the equipment used to pump the feed into the filtration rig had to be switched off to allow the feed pressure to drop. After the feed pressure had dropped below 0.2 bar the pumping was activated until the feed pressure again rose to 0.8 bar. This cycle was repeated until an operational time of 55 minutes had been reached.

It can be seen in Figure 3-22 that variation in the filtration performance was seen in the throughput performance of the three cartridges used. This variation has been attributed to differences in the composition of the feedstock.

During each filtration experiment samples were taken from the feed and permeate streams. The procedure described in Section 2.6.3 was used to measure the concentration of pepsin in each sample. The average transmission rate measured for the three filtration experiments was 95%.

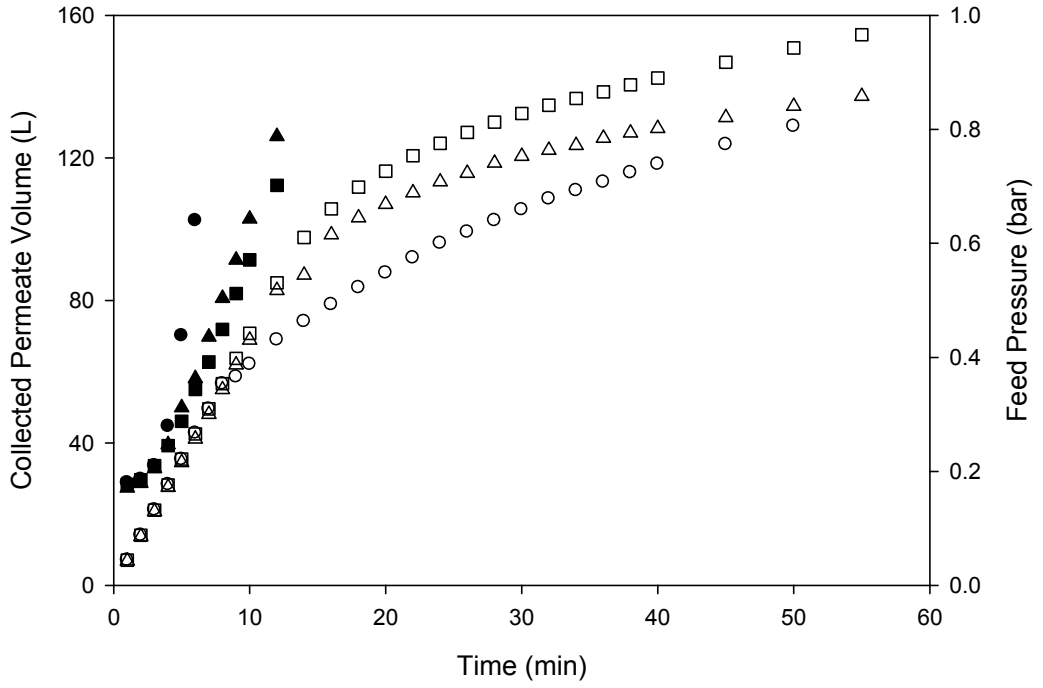

Figure 3-22: Filtration performance of 10" $UEAV_{24,1}$ cartridges for three separate preparations of 10 gL^{-1} pepsin solution in 0.03 M sodium phosphate buffer (pH 7.4). A new cartridge was used to filter each preparation of the pepsin solution. Filled symbols represent the measured feed pressure, whilst unfilled symbols represent the measured permeate volume. Experiments performed as described in Section 2.5.

3.4.3. Volume Throughput for Yeast Solution Filtration

The performance of the 10" $UEAV_{24,1}$ cartridge has also been characterised for a 7.7 gL^{-1} yeast solution containing 1 gL^{-1} BSA in a 0.03 M sodium phosphate buffer (pH = 7.4). The filtration of two separate preparations of the feedstock is given in Figure 3-23. A new filter cartridge was used for each filtration experiment. The volume throughput data given in Figure 3-23 shows a similar trend as that seen in Figure 3-22 for the pepsin feedstock, whereby two distinct regions are evident. The variation between experiments was seen to be low, which is in contrast to the higher variation seen with the pepsin feedstock. Average transmission of BSA from the feed to permeate streams for the two experiments was 86%, indicating that the yeast cake upon the surface of the membrane of the membrane may be acting to retain BSA on the feed side.

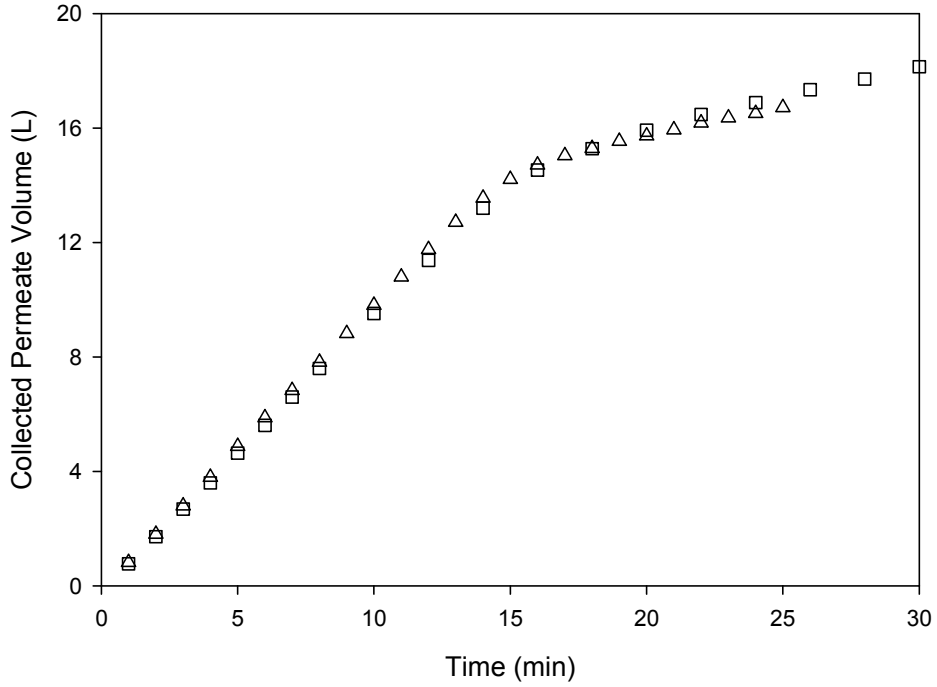

Figure 3-23: Filtration performance of 10" $UEAV_{24,\ 1}$ cartridges for three separate preparations of 7.7 gL^{-1} yeast and $1gL^{-1}$ BSA solution in 0.03 M sodium phosphate buffer (pH 7.4). A new cartridge was used to filter each preparation of the yeast solution. Experiments performed as described in Section 2.5.1.

3.5. Discussion and Summary

The aim of this chapter was to characterise the basic filtration performance of a large-scale pleated cartridge in a standard cartridge housing for a range of feedstocks. This aim was achieved through a number of objectives that were fulfilled. The main conclusions are:

- Whilst there is some variation in the measured transmembrane pressure difference (Figure 3-3) and both axial (Figure 3-10) and radial (Figure 3-14) mixing in the cartridge housing at lower flow rates, the magnitude of the effects are considered small relative to the operation of a real filtration process. Consequently, hydrodynamic effects related to the cartridge housing can most probably be neglected in the design of any scale-down cartridge device. The effect seen in Figure 3-10 and Figure 3-14 may be

more pronounced when using feeds with greater viscosity. In the case of bioprocesses it is unlikely that non fouling feeds filtered by the cartridge filters would differ widely from that of water.

- The impact of storage conditions (time and temperature) upon the filterability of a model BSA system were investigated. The filterability of BSA solution was seen to decrease over the course of storage, such that after 72 hrs of storage the permeate flow would drop to below 20% of the initial permeate flow after 5 minutes of operation. The rate of decline in filterability was slowed by reducing the storage temperature, although the decline could not be prevented.

- A 10 gL^{-1} pepsin solution was seen to be a good candidate for use within the thesis as a realistic fouling feedstock, as the propensity for fouling was such that it was estimated that 40 L of a fresh preparation would foul a large-scale 10" $UEAV_{24,\ 1}$ cartridge. However, when the performance of the large-scale cartridge was characterised for the pepsin solution (Figure 3-22), then the performance prediction generated using the flat sheet membrane was seen to significantly underpredict the volume required (150 L). This confirms the utility of pepsin as a fouling feedstock and also the poor scale-up predictions from flat sheet disks (Chandler et al., 2004; Rajniak et al., 2008).

- The performance of the 10" $UEAV_{24,\ 1}$ cartridge was characterised for three feedstocks: water (non-fouling), pepsin solution (fouling), yeast and BSA solution (fouling). This provides the basic flux, volume throughput and transmission data against which the scale-down approaches studied in this thesis can be assessed.

In the next chapter, the design of the membrane pleats and their impact on filtration performance will be considered in more detail.

4 Influence of Pleat Geometry on Membrane Cartridge Performance[1]

4.1 Introduction and Aims

It was seen in Figure 1-1 that 0.2 μm rated and sterilising grade pleated microfiltration cartridges are widely used within the biopharmaceutical industry at many positions within a bioprocess sequence. Typical applications include filtration of buffers (Jornitz et al., 2007), final product stream clarification after depth filtration and sterile product filtration prior to formulation (Sundaram, 1998). In most applications the filter will be exposed to large volumes of process fluid containing high protein concentration but relatively low concentration of suspended solids (Jornitz et al., 2007). Due to the large process volumes it is common practice to strive for the highest membrane area per unit volume of cartridge to minimise the footprint of the overall unit. One option to achieve this is by pleating of the flat sheet membrane and packing a high density of pleats around a central core. As was discussed in Section 1.6, pleating has been associated with a drop in cartridge performance when compared with flat sheet membranes (Chandler et al., 2004; Rajniak et al., 2008).

In the previous chapter it was shown that hydrodynamic effects within the membrane housing had a negligible impact on membrane cartridge performance. Consequently this chapter will focus on the membrane pleat geometry since in the literature there has yet to be a study to determine the role that each pleat characteristic has upon the performance of the pleated cartridge.

[1] The majority of the results presented in this chapter have been published in: Brown, A.I., Levison P., Titchener-Hooker, N.J., Lye G.J.. 2009. Membrane pleating effects in 0.2μm rated microfiltration cartridges. Journal of Membrane Science. 341: 76-83.

The aim of this chapter is to investigate in more detail the influence of pleat design on filtration performance in order to define which characteristics of the pleat geometry must be preserved in any scale-down device. The specific objectives of this chapter are:

- To fabricate a range of cartridges that enable the first systematic investigation of the influence of pleat geometry upon cartridge performance.

- To assess particle access into the pleat structure to further elucidate potential fouling mechanisms and the effective membrane area used during filtration.

- To determine the impact of pleating upon the optimal use of pleats within cartridges that handle liquid feeds.

- To define the pleat characteristics that must be maintained in any scale-down cartridge device.

In this chapter the results of a systematic experimental investigation is presented, which considers the effect that membrane pleating has upon the clean water flux of a large scale cartridge and studies the change in clean water flux when transitioning from a flat sheet disc of membrane to a large scale cartridge. The insights gained, coupled with the findings from Chapter 3, will later be used to develop scale-down strategies that better mimic the performance of large-scale pleated cartridges. This strategy is illustrated in Figure 4-1.

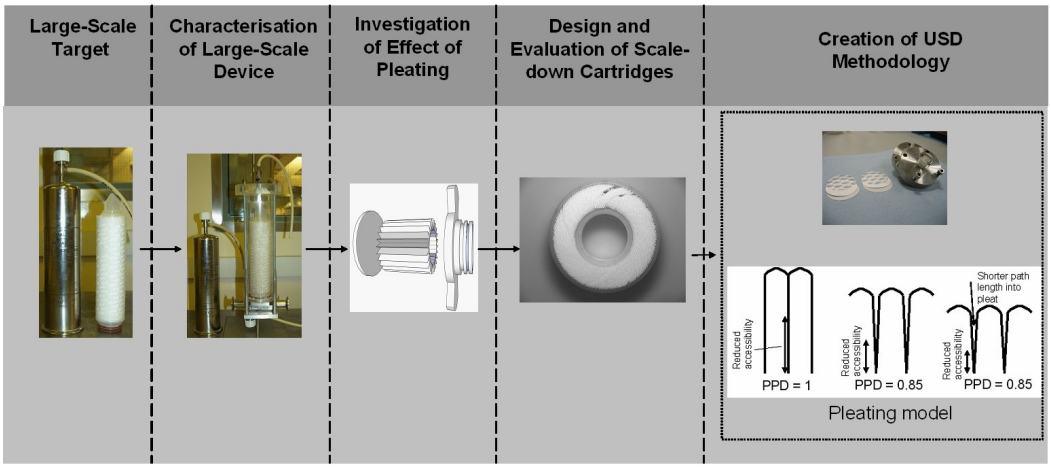

Figure 4-1: Overview of the structure of the thesis showing strategy towards the development of a USD methodology that accounts for pleating effects. This chapter seeks to investigate the effect that pleating has upon the performance of membrane cartridge filters.

4.2 Effect of Pleating on Clean Water Flux

The clean water flux performance for the large-scale target cartridge (10" $UEAV_{24,\ 1}$) has previously been evaluated in Figure 3-21. For comparative purposes the clean water flux of a flat sheet disc of the same membrane has also been measured. The mean flux for the two different configurations are given in Figure 4-2 as a function of applied TMP. The smaller area of the flat sheet disc lead to higher variation in the quantification of the flux (indicated by the large error bars) than for the 10" cartridge. This is in agreement with previous findings when working with small areas of membrane (Jackson et al., 2006). From Figure 4-2 it can be observed that at an equivalent TMP, the permeate flux was considerably lower for the 10" cartridge than for the flat sheet disc. The reduction in flux is about 53% on average. This compares well with a measured flux reduction of 53% for a PVDF sterilising grade membrane cartridge when compared to a flat sheet (Rajniak et al., 2008), though is lower than a flux reduction of 70% for a pleated glass fibre cartridge (Wakeman et al., 2005).

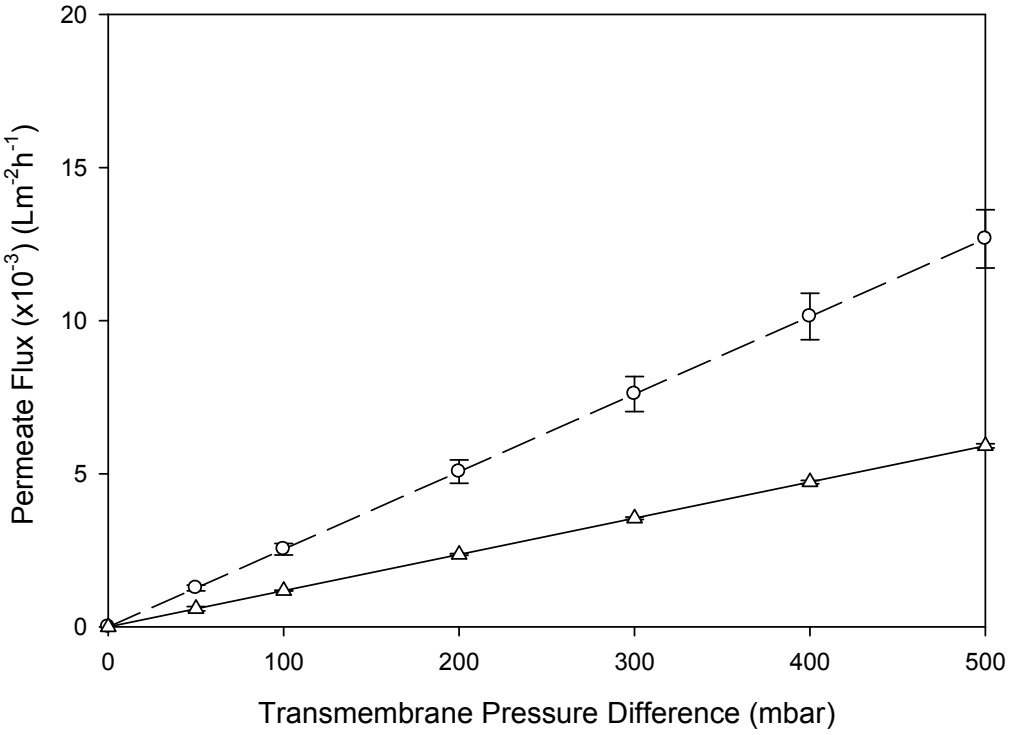

Figure 4-2 Measured clean water flux through 0.2 μm Supor® EAV membrane for different module configurations and scales. The small-scale (○) utilises 25 mm diameter flat sheet discs of membrane. The large scale (△) data given is the mean of the three datasets given in Figure 3-21 and also the data given in Figure A-1 (Appendix A). Measurements made at ambient temperature (20°C) as described in Section 2.4. Lines fitted by linear regression (R^2>0.92). Error bars represent one standard deviation about the mean (n = 3).

Average membrane resistances (R_m) for the flat sheet discs and the 10" pleated cartridge based on the data in Figure 4.3 were calculated using Equation 1-4 to be 1.60×10^{10} m^{-1} and 3.43×10^{10} m^{-1} respectively. In principle the membrane resistance due to the porosity of the membrane and the resistance to flow that the pores create (Reif, 2006) should be identical since both the cartridge and flat sheet are made from the same material. The primary factors that changed between the two configurations were: the flat sheet was pleated with a Ultipleat® configuration, h_P = 24 mm, and the pleats were packed into a cartridge to yield a pleated packing density (defined in Section 2.3.1) = 1.

4.3 Effect of Pleat Geometry on Clean Water Flux

In order to further investigate the influence of membrane pleating on the measured membrane resistance, a series of 1" pleated membrane cartridges were specially fabricated as described in Section 2.3.1. They were fabricated to enable systematic investigation of the type of pleat (Fan or Ultipleat®), the pleat height (h_P) and the pleat density as shown in Figures 2-7 – 2-10 . The properties of these are summarised in Table 4-1. As was described in Section 2.3.1.2, all cartridges were tested after manufacture to ensure that no leaks were present. The measured water flux profiles for various specially fabricated 1" cartridges with a Fan pleat and h_P = 15 mm and varying PPD are shown in Figure 4-3. It can clearly be seen that as the pleat structure becomes more open (reduced PPD) so water flux increased and TMP decreased. The 1" cartridge with a PPD of 0.65 shows a performance closest to that of the flat sheet membrane.

Table 4-1: Properties of the various membrane cartridges used within this study. All cartridges contained a Supor® EAV 0.2µm rated membrane. Cartridge configuration nomenclature as defined in Section 2.3.1.1. Pleat characteristics as defined in Figure 2-7 – 2-9.

Cartridge Configuration	Membrane area (m^2)	Pleat type	Pleat height, h_p (mm)	Pleat packing density (PPD)	Angle between pleats, θ (°)
10" $UEAV_{24, 1}$	1.1	Ultipleat®	24	1	~0
10" $EAV_{10, 1}$	0.72	Fan	10	1	~0
1" $EAV_{10, 1}$	0.079	Fan	10	1	~0
1" $EAV_{10, 0.85}$	0.067	Fan	10	0.85	~6
1" $EAV_{10, 0.65}$	0.052	Fan	10	0.65	~12
1" $EAV_{15, 1}$	0.090	Fan	15	1	~0
1" $EAV_{15, 0.85}$	0.076	Fan	15	0.85	~6
1" $EAV_{15, 0.65}$	0.059	Fan	15	0.65	~12

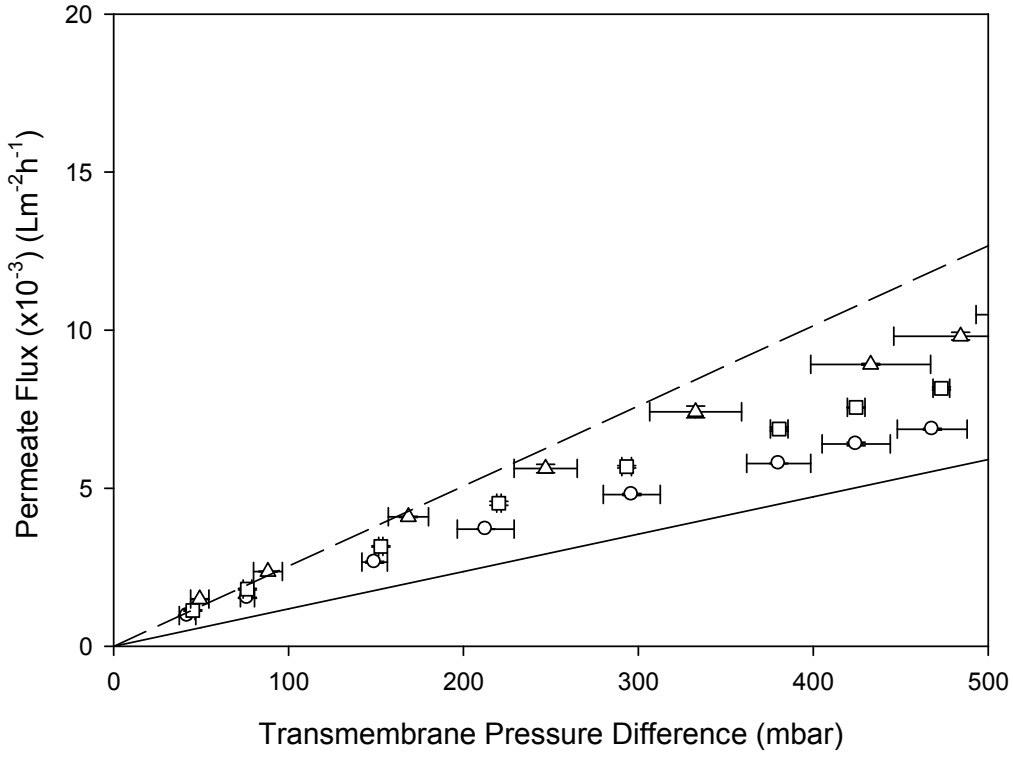

Figure 4-3: Measured clean water flux through 0.2 µm Supor® EAV membrane in pleated membrane cartridges with different pleat configurations: 1" Cartridges with h_P = 15 mm, PPD of 1 (○), 0.85 (□) and 0.65 (△) were used. Flat sheet data (---) and 10" cartridge data (—) shown for comparison. Measurements made at ambient temperature (20°C) as described in Section 2.4. Error bars represent one standard deviation about the mean (n = 3).

The measured water flux profiles for 1"cartridges with the same Fan pleat type but reduced pleat height (h_P = 10 mm) and varying PPD are shown in Figure 4-4. The results for these cartridges showed the same trend as for the 1" Fan pleat cartridges with h_P = 15 mm, however, for h_P = 10 mm the flux profiles shifted still closer to that of the flat sheet disc. By application of an ANOVA analysis (Hinkelmann et al., 2008) it was seen that for PPD = 0.65 the water flux profile is not significantly different (P = 0.7) to that of the flat sheet disc. Hence, at this level of pleat packing, height and type, there ceases to be a significant difference between performance of a pleated or a flat sheet membrane.

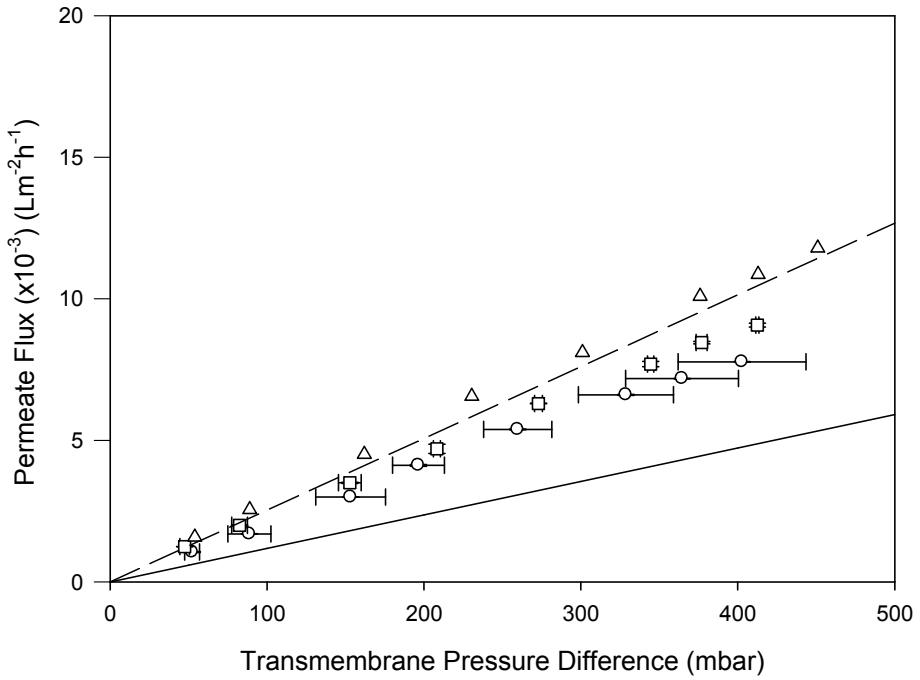

Figure 4-4: Measured clean water flux through 0.2 µm Supor® EAV membrane in pleated membrane cartridges with different pleat configurations: 1" Cartridges with h_P = 10 mm, PPD of 1 (○), 0.85 (□) and 0.65 (△) were used. Flat sheet data (---) and 10" cartridge data (—) shown for comparison. Measurements made at ambient temperature (20°C) as described in Section 2.4. Error bars represent one standard deviation about the mean (n = 3).

Table 4-2: Calculated membrane resistances for Supor® EAV 0.2 µm rated membrane fitted in each of the cartridges described in Table 4.1. Errors represent one standard deviation about the mean (n=3). Only one 1" $EAV_{10, 0.65}$ cartridge was available for the study.

Cartridge Configuration	**Membrane Resistance ($\times 10^{10}$) (m^{-1})**
10" $UEAV_{24, 1}$	3.43 ± 0.04
1" $EAV_{10, 1}$	2.01 ± 0.20
1" $EAV_{10, 0.85}$	1.78 ± 0.02
1" $EAV_{10, 0.65}$	1.50
1" $EAV_{15, 1}$	2.59 ± 0.12
1" $EAV_{15, 0.85}$	2.20 ± 0.02
1" $EAV_{15, 0.65}$	1.93 ± 0.14
Flat sheet	1.60 ±0.13

Average R_m values, calculated using Equation 1-4, for all the cartridge configurations used are shown in Table 4-2. In all cases changes in pleat height and PPD from the standard 10" $UEAV_{24,\ 1}$ configuration caused the measured R_m value to decrease. In general it was seen that R_m decreased as both PPD and h_P decreased. The 1" cartridge with h_P = 10mm and PPD = 0.65 had a resistance closest to that of the flat sheet membrane. The calculated membrane resistance is critically dependent upon the effective area of the membrane as defined in Equation 1-4. The increase in membrane resistance caused by the increasing h_P and PPD may cause the effective filtration area available for flow to be lower as has been hypothesised by other researchers (Wakeman et al., 2005). Such a hypothesis would be valid if the characteristics of the pleat affected fluid accessibility to the entire surface area of the installed membrane within a cartridge. This would also account for the measured variation in clean water fluxes. This possible mechanism of performance loss was therefore investigated further.

4.4 Probing Particle Penetration within Pleats

To further investigate the hypothesis of reduced membrane accessibility with increased PPD and h_P, a yeast (*S. cerevisiae*) suspension with a wet cell weight concentration of 7.7 gL^{-1} was used to probe the ability of micron-sized particles to penetrate into the pleat structure and to access the whole membrane surface area. A selection of 1" and 10" membrane cartridges, as described in Table 4-1, were used to filter the yeast solution until the permeate flux fell to a negligible level as described in Section 2.5. After each experiment the cartridges were allowed to dry and were then carefully cut open. The unfolded membrane was then examined to ascertain the extent to which cells had deposited at different points within the membrane pleats. Photographs illustrating typical deposition patterns in 10" and 1" cartridges are shown in Figure 4-5 and Figure 4-6.

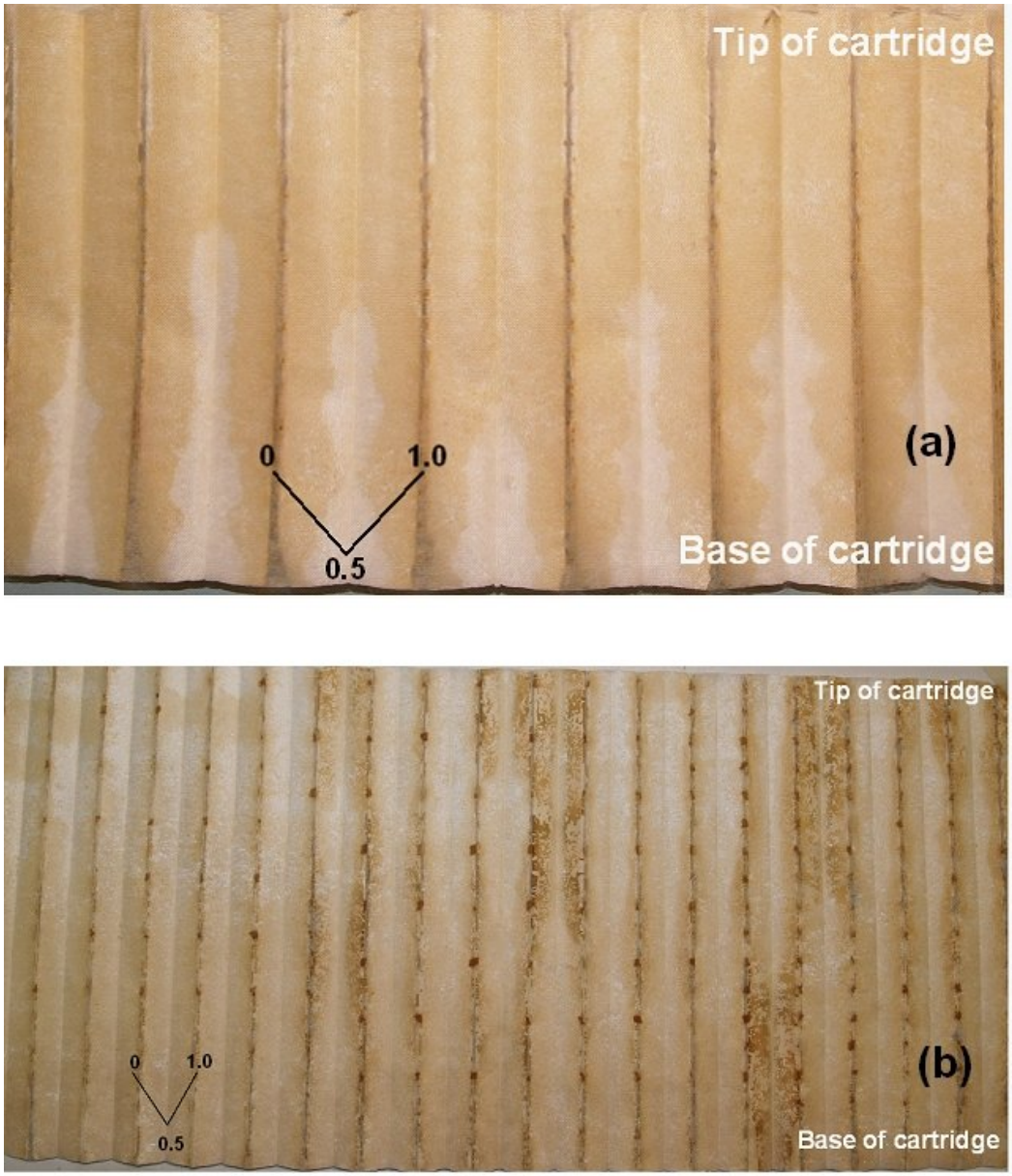

Figure 4-5: Typical photographs of fouled membrane surfaces from 10" module configurations of varying h_P showing yeast cell deposition. Inset shows the position within the pleat, where 0 and 1 indicate the apex of the pleat, 0.5 indicates the base of the pleat. (a) 10" $UEAV_{24,\,1}$ cartridge containing tightly packed pleats of h_P = 24 mm; areas of clean membrane are clearly visible corresponding to the inner surfaces of each pleat. (b) 10" $EAV_{10,\,1}$ cartridge containing Fan pleats of h_P = 10 mm; similar areas of clean membrane are also seen on the inner surface of each pleat. Membranes imaged as described in Section 2.5.

Membrane from 10" cartridges with h_P = 24 mm and an Ultipleat® pleat type (Figure 4-5(a)) and h_P = 10 mm and Fan pleat type (Figure 4-5(b)) showed areas of relatively clean membrane where yeast particles had been unable to penetrate into the pleat structure. These clean areas were predominantly located towards the base of each pleat and the total area of yeast-free membrane, as estimated visually, was smaller for the cartridge with h_P = 10 mm compared to h_P = 24 mm. Yeast cell deposition varied along the length of each membrane cartridge. Areas of clean membrane tended to be found at the base of the cartridge (h_P = 24 mm) and at the top of the cartridge with h_P = 10 mm. For both pleat heights there was a greater deposition of yeast within the pleats toward the middle of the cartridge. Heat sealing of the pleated membrane to the plastic endcaps during cartridge fabrication at the base and the top may lead to these longitudinal variations and contribute to the formation of tighter, more closed structures in the membrane cartridge at these points. This would in turn account for the decreased accessibility into the pleat structure by the yeast particles at the ends of the unit.

The 1" cartridge with h_P = 10 mm and PPD = 1 (Figure 4-6(a)) showed large areas where the membrane was free from particle deposition, predominantly at the base of the pleat. As the PPD decreased the deposition of yeast across all areas of the membrane was seen to increase based upon visual inspection. The cartridge with a PPD = 0.85 (Figure 4-6(b)) exhibited few areas of clean membrane, while at a PPD = 0.65 (Figure 4-6(c)) there was deposition of yeast across the entire membrane surface.

In summary the series of specially fabricated cartridges have helped identify the two main design characteristics of a pleat, h_P and PPD, which appear to impact upon the accessibility of suspended solids into the pleat structure. Quantification of the extent and distribution of yeast cell deposition on the membrane for each of the configurations shown in Figure 4-5 and Figure 4-6, was used later in the chapter to gain further insight into the influence of pleat design on performance.

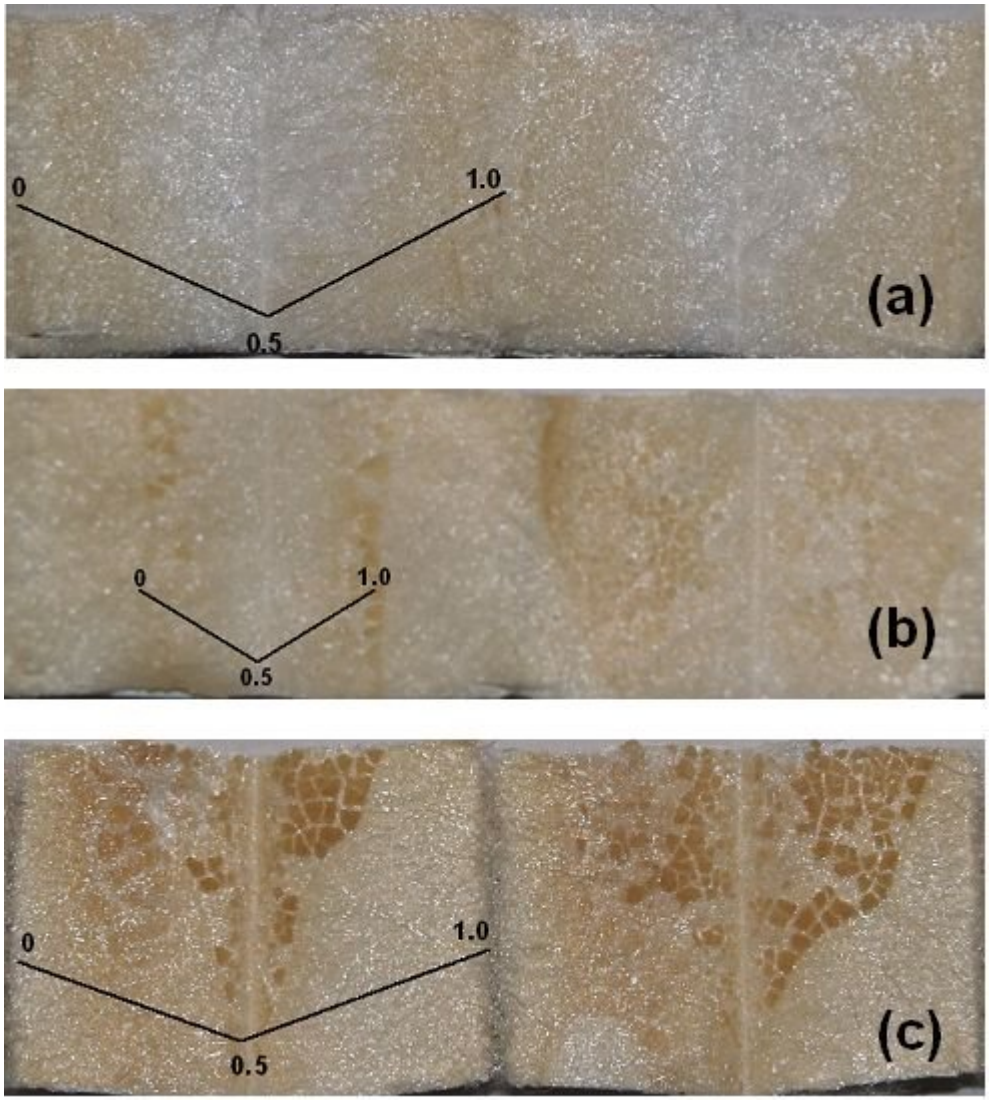

Figure 4-6: Typical photographs of fouled membrane surfaces from specially fabricated 1" module configurations of varying PPD (h_P = 10 mm) showing yeast cell deposition. (a) 1" $EAV_{10, 1}$ (b) 1" $EAV_{10, 0.85}$ (c) 1" $EAV_{10, 0.65}$. Images show that as the pleat structure opens up (decreasing PPD) there is a thicker layer of yeast upon the inner surface of each membrane pleat. Membranes imaged as described in Section 2.5. Cartridge configurations as defined in Table 4.1.

4.4.1 Variation in Suspension Deposition

To assess the degree of experimental variation in the deposition of the yeast suspension within the pleated cartridges, experiments have been repeated in at least duplicate for each of the cartridge configurations used in Figure 4-5 and Figure 4-6. Images of the membrane surface for each of the configurations are shown in Figure 4-7 to Figure 4-11 for all three experiments conducted.

The yeast cell deposition for the 10" $UEAV_{24,\ 1}$ cartridges are shown in Figure 4-7. The results of the three experiments showed similar fouling patterns with the largest areas of clean membrane seen toward the base of the cartridge and the least yeast deposition within the pleat. For the 10" $EAV_{10,\ 1}$ cartridge similar fouling patterns were also seen (Figure 4-8) with evidence of small areas of clean membrane found at the top of the cartridge. However, for the second experiment clean areas were also located towards the base of the cartridge. For both experiments the total area of clean membrane within the pleat structure was small when compared with the areas of clean membrane seen for the 10" $UEAV_{24,\ 1}$ cartridge.

The fouling deposition for three 1" $EAV_{10,\ 1}$ cartridges are shown in Figure 4-9. The first and third experiments showed similar fouling patterns with large areas of clean membrane evident towards the base of the pleat. The areas of clean membrane were smaller in size for the second experiment, but still located towards the base of the pleat. The three experiments conducted for the 1" $EAV_{10,\ 0.85}$ cartridges, i.e. with the more open pleat structure, showed consistent results as shown in Figure 4-10. Deposition of yeast was heavier and seen across the whole pleat with some evidence of heavier patches towards the apex of the pleat.

Finally, the observation of the membrane surface for the three 1" $EAV_{10,\ 0.65}$ cartridges (Figure 4-11) showed that for all three experiments large areas of heavy deposition was seen, with the deposits typically located towards the apex of the pleat. There was little evidence of clean membrane for each of the three experiments.

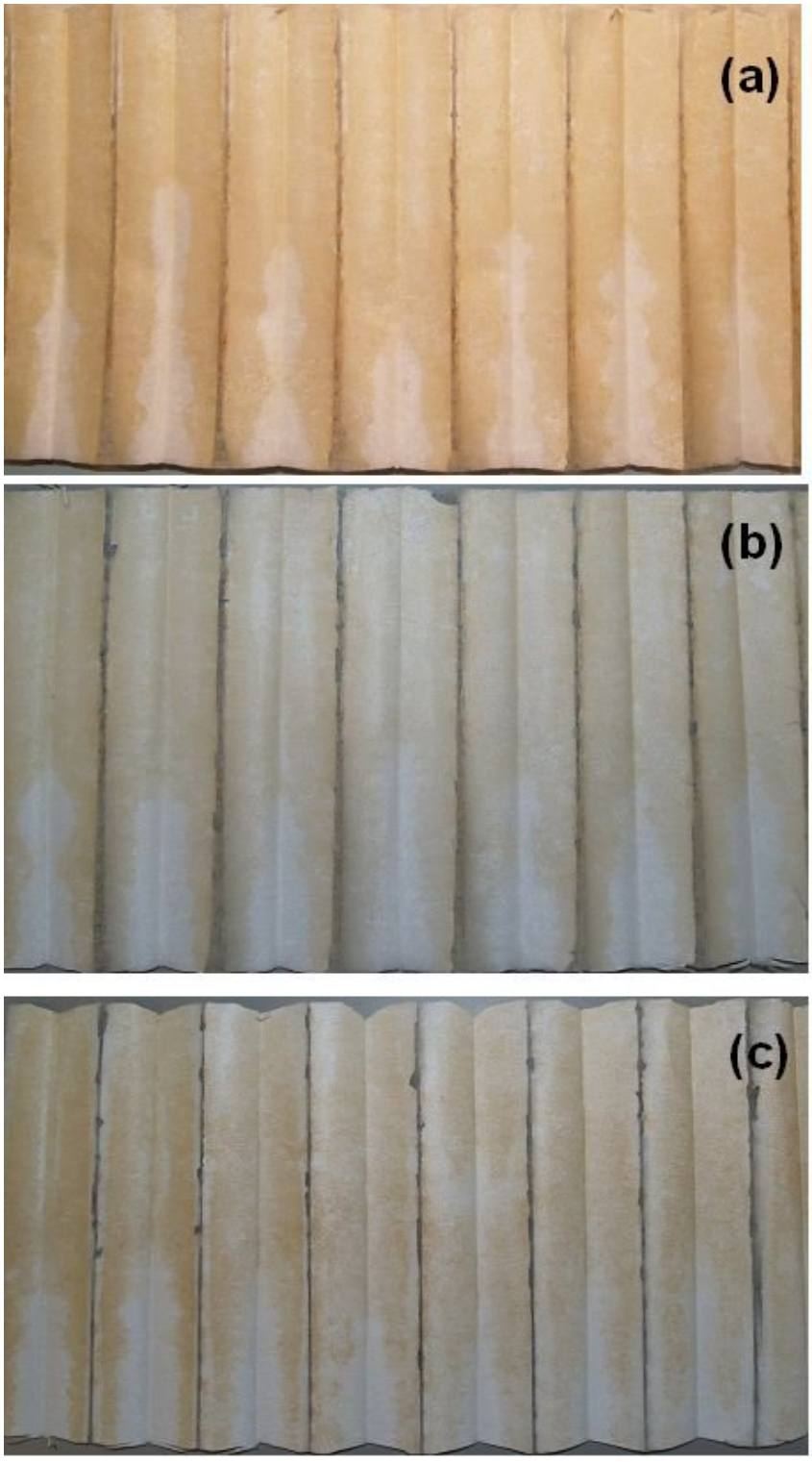

Figure 4-7: Photographs of fouled membrane surfaces from 10" $UEAV_{24,\ 1}$ cartridge containing tightly packed pleats. The images are taken from three separate cartridges, where (a) is the same image shown in Figure 4-5(a). Membranes imaged as described in Section 2.5.

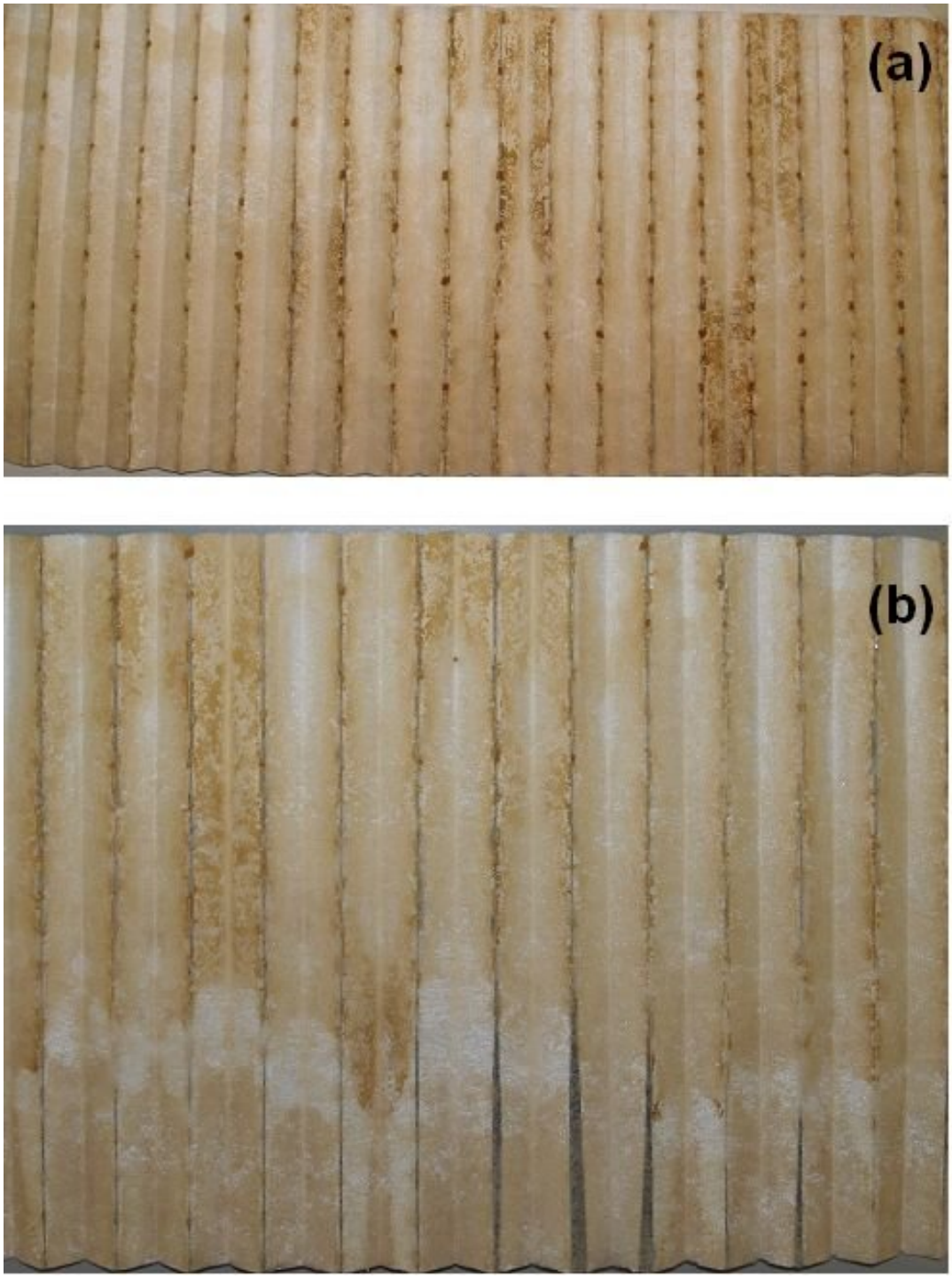

Figure 4-8: Photographs of fouled membrane surfaces from 10" $EAV_{10,\ 1}$ cartridge containing tightly packed pleats. The images are taken from two separate cartridges, where (a) is the same image shown in Figure 4-5(b). Membranes imaged as described in Section 2.5.

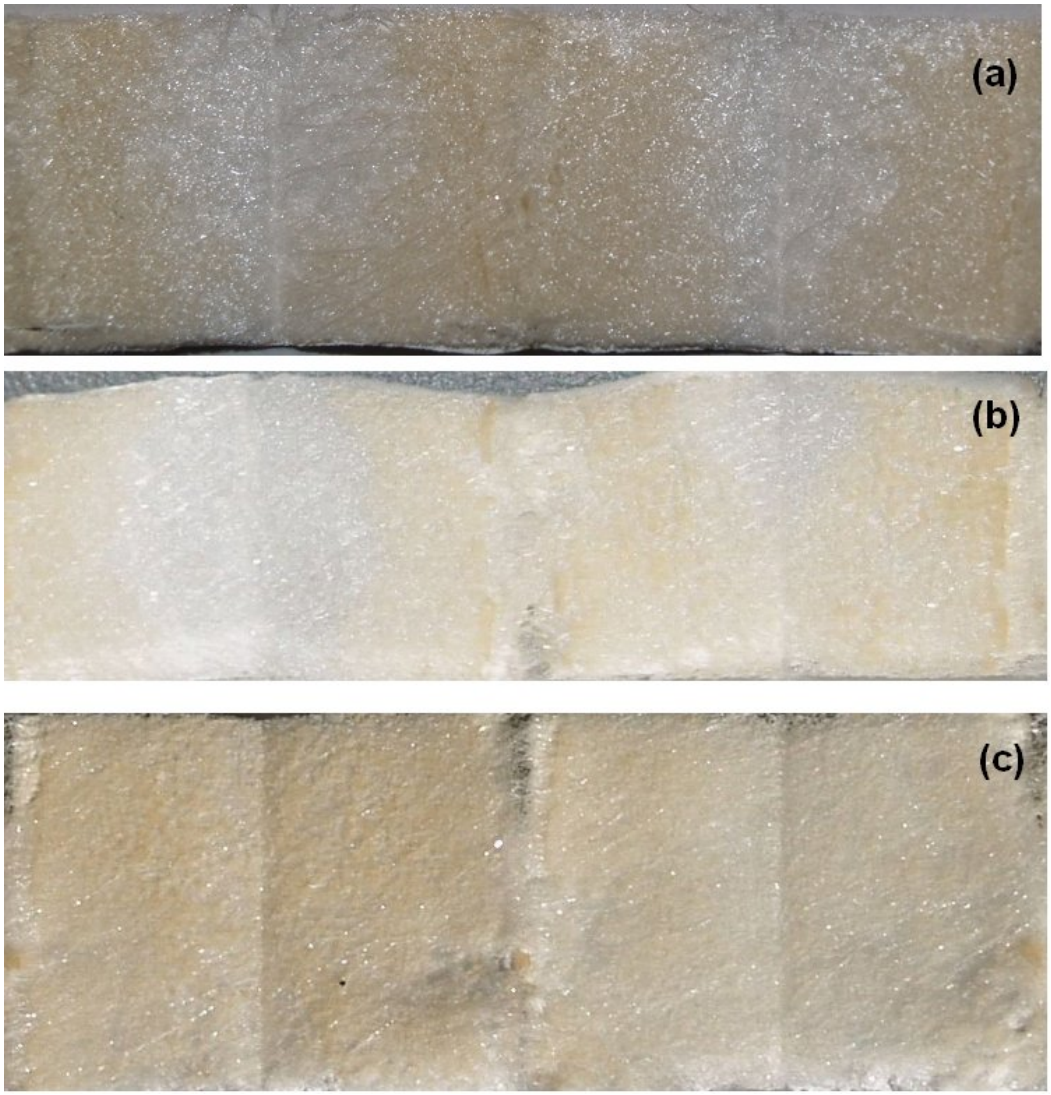

Figure 4-9: Photographs of fouled membrane surfaces from 1" $EAV_{10,\ 1}$ cartridge containing tightly packed pleats. The images are taken from three separate cartridges, where (a) is the same image shown in Figure 4-6(a). Membranes imaged as described in Section 2.5.

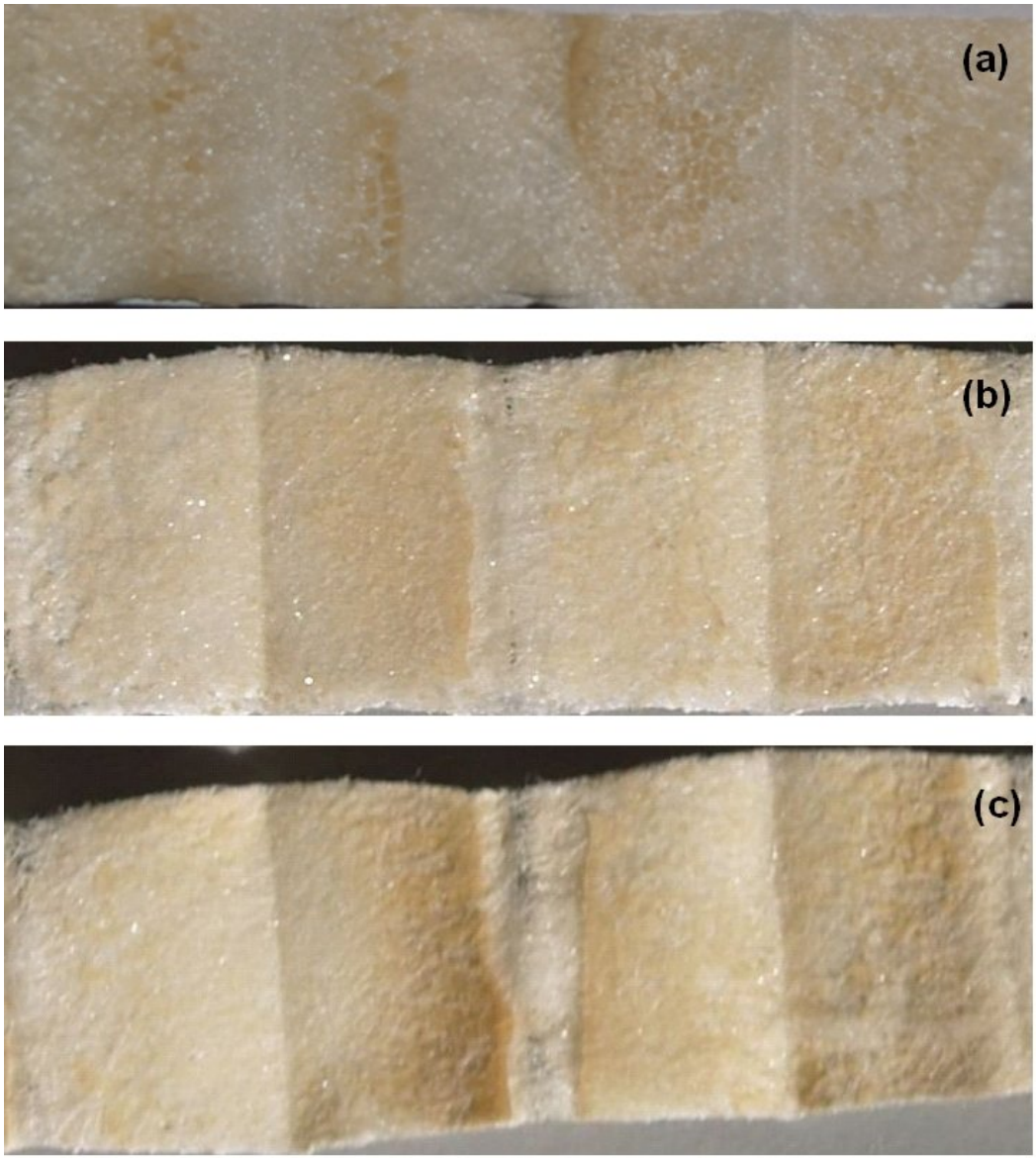

Figure 4-10: Photographs of fouled membrane surfaces from 1" $EAV_{10,\ 0.85}$ cartridge containing more open pleat structure. The images are taken from three separate cartridges, where (a) is the same image shown in Figure 4-6(b). Membranes imaged as described in Section 2.5.

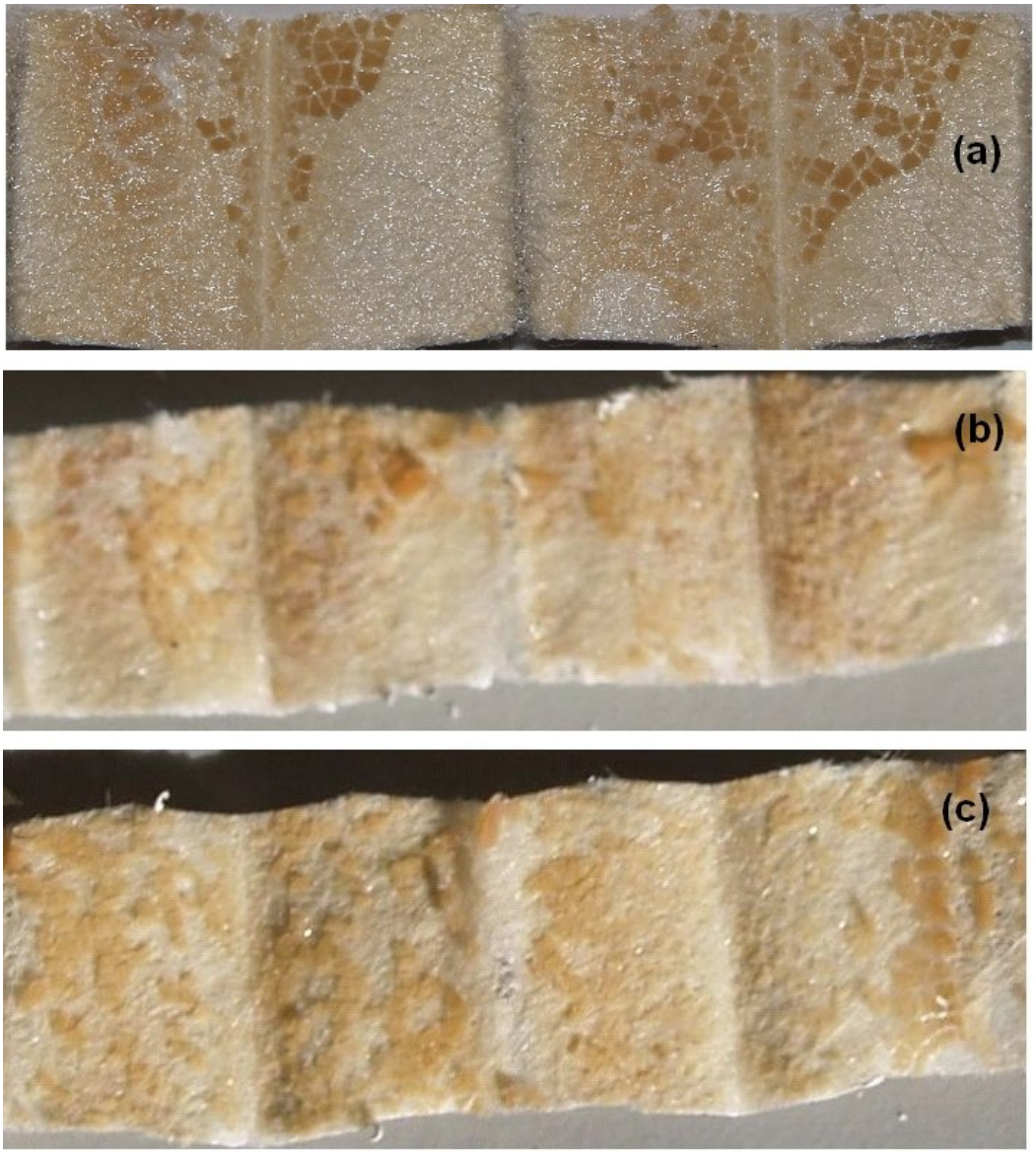

Figure 4-11: Photographs of fouled membrane surfaces from 1" $EAV_{10,\ 0.65}$ cartridge containing most open pleat structure of configurations used. The images are taken from three separate cartridges, where (a) is the same image shown in Figure 4-6(c). Membranes imaged as described in Section 2.5.

Based upon the results reported in this section where similar deposition patterns were observed when duplicate experiments were conducted for each cartridge configuration, the results reported in Section 4.4 and shown in Figure 4-5 and Figure 4-6 are considered representative of the deposition patterns seen, and will be used for further analysis of the degree of deposition seen for the different membrane configurations.

4.5 Quantification of Effective Membrane Area

To more accurately quantify the effective membrane area (based upon micron sized particle deposition) high quality grey scale images of membranes abstracted from each cartridge configuration were first generated (as described in Section 2.5). Image analysis was used to measure the intensity of the grey level from the apex to the base of each pleat. The results of this analysis are given in Figure 4-12 to 4-14. The clean membrane data was plotted using a global average across the pleat height from apex to apex. The grey scale intensity can be used as a measure of the degree of yeast cell deposition. In this case a lower number represents darker areas and heavier deposition. Here, a grey scale intensity ranging between: 140 - 130 is taken to represent clean membrane: 130 - 110 represents light yeast cell deposition: 110 - 90 represents heavy yeast cell deposition.

Figure 4-12 shows the analysis of a 10" cartridge with h_P = 24 mm, PPD = 1 and Ultipleat® pleat type. Three measurements were taken of the yeast deposition within a pleat at the top, middle and base of the cartridge. The membrane at the base of the cartridge revealed areas of light yeast cell deposition towards the apex of the pleat. Yeast cell deposition within each pleat then gradually reduced so that only clean membrane was measured towards the base of the pleat. The measurements of all deposits within pleats located at the middle and top of the cartridge both showed light levels of deposition within the whole pleat, with the measurement from the top of the cartridge showing the highest degree of yeast deposition.

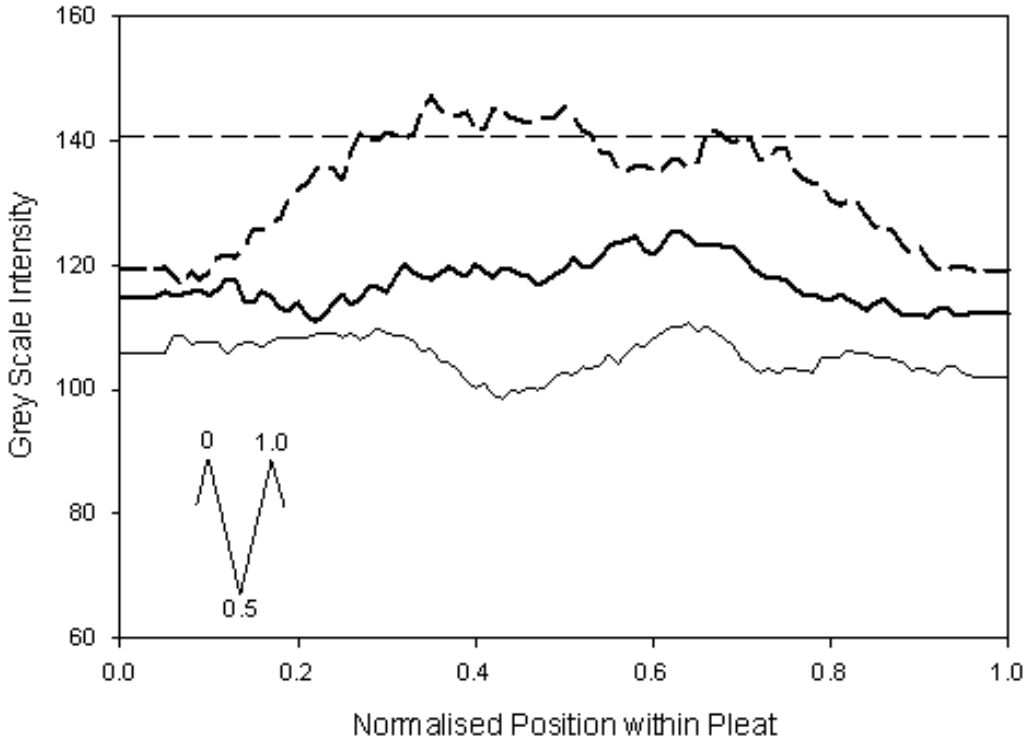

Figure 4-12: Quantification of yeast cell deposition and distribution within a representative individual pleat for a 10" $UEAV_{24,\ 1}$ cartridge. Image analysis was used to quantify the intensity across the height of the pleat from each apex (0 and 1.0) to the base (0.5) as shown in the inset. A low grey level indicates heavy fouling.. Pleats were analysed at the base (— —), middle (—), and top (—) of the cartridge. Dashed line (– –) represents average grey scale data from a clean membrane. Experiments and image analysis performed as described in Section 2.5.

Measurements were also taken from pleats located at the top, middle and base of the 10" cartridge with h_P = 10 mm, PPD = 1 and Fan pleat type (Figure 4-13). Cell deposition measurement at the base of the cartridge showed predominantly light deposition at the apex of the pleat with evidence of clean membrane areas towards the base of the pleat. Pleats at the top of the cartridge were also predominantly clean. A uniform level of light yeast deposit was seen in the middle of the cartridge. This was in agreement with the sample taken from the middle of the 10" cartridge with an Ultipleat® pleat type (Figure 4-12).

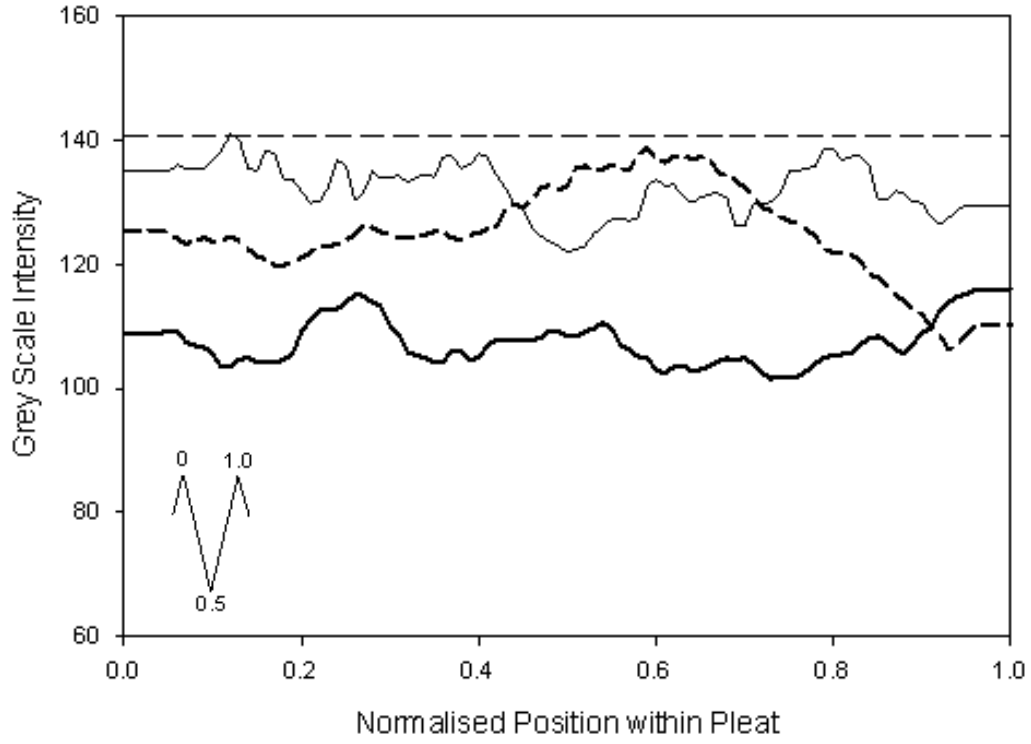

Figure 4-13: Quantification of yeast cell deposition and distribution within a representative individual pleat for a 10" $EAV_{10,\ 1}$ cartridge. Image analysis was used to quantify the intensity across the height of the pleat from each apex (0 and 1.0) to the base (0.5) as shown in the inset. A low grey level indicates heavy fouling. Pleats were analysed at the base (— —), middle (—), and top (—) of the cartridge. Dashed line (– –) represents average grey scale data from a clean membrane. Experiments and image analysis performed as described in Section 2.5.

The specially fabricated 1" cartridges also enabled investigation of yeast cell deposition as a function of PPD. Cartridges with a PPD of 1 showed areas of clean membrane at the base of the pleat with a low level of yeast deposits towards the apex. Figure 4-14 shows the effect that PPD has upon the deposition of yeast for measurements taken at the mid point of each cartridge length. At a PPD of 0.85 there was a uniform level of yeast deposits and at a slightly higher level than for a PPD of 1, across the entire membrane area within the pleat. Significantly higher levels of yeast deposits were measured for the cartridge with a PPD = 0.65, where position within the pleat appeared to have little effect upon the degree of yeast deposition.

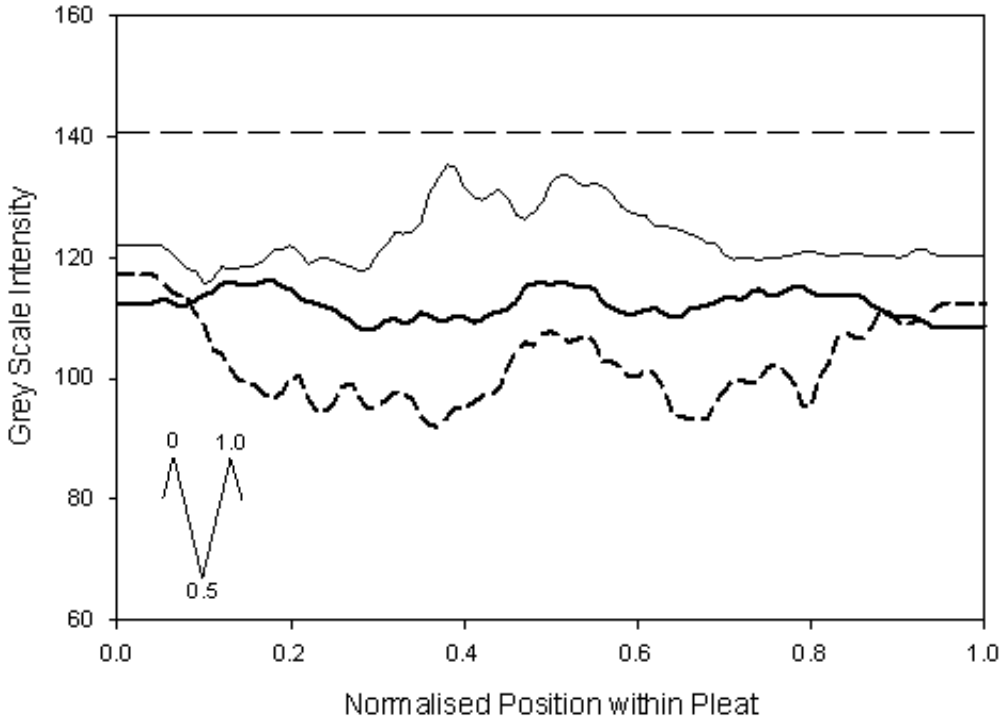

Figure 4-14: Quantification of yeast cell deposition and distribution within a representative individual pleat for various pleat sizes and configurations. Image analysis was used to quantify the intensity across the height of the pleat from each apex (0 and 1.0) to the base (0.5) as shown in the inset. A low grey level indicates heavy fouling. 1" $EAV_{10,\ 1}$ (—),1" $EAV_{10,\ 0.85}$ (▬), 1" $EAV_{10,\ 0.65}$ (▬ ▬). Dashed line (– –) represents average grey scale data from a clean membrane. Experiments and image analysis performed as described in Section 2.5.

Overall, both pleat height, h_P, and PPD, affected the deposition of yeast within the pleat. With these results it was seen that by manipulating the characteristics of the pleat, particularly reducing the PPD, the ability of yeast to enter the pleat and to then deposit upon its surface increased. With a h_P = 10 mm and PPD = 0.65, patches of a thick cake were evident. This suggests that the pleat was fully accessible for the yeast to deposit upon its surface.

Taken together these results show that though increasing the pleating density increases the membrane area within each cartridge, beyond a critical level this is at the expense of accessibility of both the process fluid (as indicated by a

decrease in the normalised clear water flux in Figure 4-2) and any suspended solids in the feed as indicated in Figure 4-12 to 4-14.

4.6 Optimal Use of Pleating in Membrane Cartridges

Pleat geometry has so far been shown to affect normalised performance characteristics of pleated membrane cartridges, such as flux-TMP profiles (Figure 4-2) and calculated R_m values (Table 4-2). However, it has not yet been seen what affect pleating has upon the real filtration performance of the cartridge. To investigate this further the calculated processing time required to filter 100 L of feed were calculated for three solutions of the same protein (MAb1 in 16 mM histidine, 266 mM Sucrose, 0.03% polysorbate 20, pH 6.0) but with different concentrations (10 $mgmL^{-1}$, 60 $mgmL^{-1}$ and 80 $mgmL^{-1}$) and different viscosities (3 cP, 6 cP and 11cP respectively) (Liu et al., 2005). The operational time was calculated for each of the 1" configurations defined in Table 4-1 by using the values of A_m and R_m given in Table 4-1and Table 4-2 respectively and using Equation 1-4. For this exercise, the protein solution was assumed to be non-fouling. The calculated values of the processing times are given in Table 4-3. The "optimum" condition represents that which leads to the minimum processing time.

It can be seen that for a given protein solution viscosity generally a reduction in PPD leads to an increase in processing time, meaning that the reduction in R_m with increased PPD does not compensate for the reduction in A_m in less tightly packed cartridges. It can also be seen that the lower pleat height lead to lower processing times, suggesting that higher pleat heights are not optimal as the increase in R_m is greater than the increase in A_m. As would be expected an increase in viscosity can be seen to increase the processing time for each cartridge configuration. However, increase in viscosity also increases the differences in processing time between the different cartridge configurations. However it should be noted that the differences seen in Table 4-3 are small.

Table 4-3: Processing time required to filter 100 L of three solutions of the same protein (MAb1 in 16 mM histidine, 266 mM Sucrose, 0.03% polysorbate 20, pH 6.0) but with different concentrations (10 $mgmL^{-1}$, 60 $mgmL^{-1}$ and 80 $mgmL^{-1}$) and different viscosities (3 cP, 6 cP and 11cP respectively) (Liu et al., 2005). A transmembrane pressure difference of 0.41 bar(g) also used. Values given are calculated from the membrane filter data in Table 4-1 and Table 4-2.

Cartridge Configuration	**Processing Time (min)**		
	μ = 3 cP	**μ = 6 cP**	**μ = 11 cP**
1" $EAV_{15, 1}$	35	70	129
1" $EAV_{15, 0.85}$	35	71	129
1" $EAV_{15, 0.65}$	40	80	146
1" $EAV_{10, 1}$	31	62	114
1" $EAV_{10, 0.85}$	32	65	119
1" $EAV_{10, 0.65}$	35	70	129

The predicted processing times of 100 L of protein solution (MAb1 in 16 mM histidine, 266 mM Sucrose, 0.03% polysorbate 20, pH 6.0) with μ = 6 cP (Liu et al., 2005), at three different values of TMP are given in Table 4-4. Again it can be seen that generally a higher PPD leads to a lower processing time, although for h_P = 15 mm there was a difference seen between the processing time for PPDs = 1 and 0.85. Also, lower processing times were again calculated for cartridges with smaller pleat heights, although the differences seen between the two pleat heights reduced as TMP increased. However, the differences measured between the different configurations were small.

Thus, the optimum pleating conditions for the filtration of clean fluids such as this protein solution, appears to favour fully packed cartridges with lower pleat heights. However, this optimum condition would only result in a small increase in performance over other cartridge configurations.

Table 4-4: Processing time required to filter 100 L of protein solution (60 $mgmL^{-1}$ MAb1 in 16 mM histidine, 266 mM Sucrose, 0.03% polysorbate 20, pH 6.0, μ = 6 cP) (Liu et al., 2005). Three different values of TMP used. Values given are calculated from the membrane filter data in Table 4-1 and Table 4-2.

Cartridge Configuration	Processing Time (min)		
	TMP = 0.21 bar(g)	TMP = 0.41 bar(g)	TMP = 0.62 bar(g)
1" $EAV_{15, 1}$	137	70	46
1" $EAV_{15, 0.85}$	138	71	47
1" $EAV_{15, 0.65}$	156	80	53
1" $EAV_{10, 1}$	121	62	41
1" $EAV_{10, 0.85}$	127	65	43
1" $EAV_{10, 0.65}$	137	70	47

This investigation has been for protein solution that has been assumed to be non-fouling. For other protein-containing feedstocks a fouling phenomena may also take place. The rate of fouling will be proportional to membrane area, thus for a pleated scale-down device high PPD and h_P will be favoured as representative of larger cartridge configurations.

4.7 Discussion and Summary

The aim of this chapter was to describe and to quantify the effect that pleat design has upon cartridge performance, leading to insights into the optimal use of pleats within cartridges. The main conclusions are:

- A range of novel cartridges were fabricated, which contained a range of PPD and h_P configurations. These cartridges were leak tested and found to be suitable for conducting the first systematic investigation into the effect of pleat geometry upon cartridge performance.

- A significant difference (53%) was measured between the clean water flux performance of the target large-scale pleated cartridge and non-pleated flat sheet disc (Figure 4-2).

- Using the newly fabricated cartridge it was seen that clean water flux performance varied as a function of PPD and h_P (Figure 4-3 and Figure 4-4). In turn R_m decreased as PPD and h_P decreased (Table 4-2).

- Access into the pleat was initially probed visually using a dilute yeast suspension. It was seen that at PPD values beyond 0.85 and at an h_P of 10 mm, areas of the cartridge were inaccessible to the yeast challenge (Figure 4-6 and Figure 4-14). This was concluded to be due to the affects of pleat crowding. As the PPD and h_P were reduced, accessibility of the particles to the inner surface of each pleat improved, until the whole membrane surface became covered with yeast.

- For non-fouling buffer feedstocks it was estimated that in terms of time to process a given volume of feedstock, then the optimum pleat configuration favoured high PPD and low h_P. However, this optimum arrangement gave a negligible improvement over other pleat configurations.

- These results suggest that in the design of any scale-down approach, maintenance of the pleat geometry (PPD, h_P) will be vital if the large-scale cartridge is to be accurately reproduced. If the pleat geometry cannot be maintained then an alternative approach that accounts for the effect of pleating is required.

In the next chapter, a new scale-down cartridge, which contains the same pleat characteristics as the large-scale target, will be designed and evaluated to assess whether an improved performance prediction can be achieved.

5 Scale-Down Approaches to Performance Prediction of Pleated Cartridge Filters[2]

5.1 Introduction and Aims

In Chapter 4 it was seen that the characteristics of membrane pleat geometry impact significantly upon the filtration performance of a pleated membrane cartridge. Consequently the performance prediction from a flat sheet membrane when compared to a large-scale-pleated cartridge was seen to be poor (Figure 4-2). A scale-down approach that incorporates the geometric characteristics of the pleat with a reduction in membrane area may offer a means of achieving an improved performance prediction with reduced requirements of feed material.

In Section 1.7.4 a study was discussed that showed a scale-down approach to improved small-scale performance prediction for a disk stack centrifuge. This was achieved by reducing the active separation area of a pilot scale centrifuge, thus rendering areas of the centrifuge in-accessible to the feed (Mannweiler et al., 1992; Maybury et al., 1998). A key feature of this approach required that the bowl diameter remained constant, and subsequently the grade efficiency curves closely matched the large-scale target, whilst a reduction in feed volume was also reported. A similar approach has been adopted in this work to achieve a small-scale pleated cartridge device that maintains the characteristics of the pleat as constant, i.e. the h_P, PPD and pleat type. A description of this new scale-down pleated cartridge device is given in Section 2.3.2.

The reduction in active area has been achieved through the incorporation of sections of a hydrophobic material into the pleated membrane pack. In this way the area available for separation is reduced, as the feed material will be unable to penetrate into the hydrophobic sections. The scale-down pleated cartridge

[2] The majority of the work presented in this chapter has been submitted for publication as: Brown, A.I., Titchener-Hooker, N.J., Lye, G.J. Scale-Down Prediction of Industrial Scale Pleated Membrane Cartridge Performance. Biotechnology and Bioengineering

devices were fabricated with a range of active pleat sections. Different configurations were built into the small-scale pleated device so as to assess whether the findings in Chapter 3, where an uneven flow distribution was seen within the housing, would impact upon the performance predictions of the scale-down cartridges. Thus, these new cartridges represent a new scale-down approach that can be utilised to generate performance predictions to the large-scale target. How this approach fits within the overall strategy of this work is given in Figure 5-1.

The aim of the chapter is to design and fabricate a range of scale-down pleated membrane cartridges and evaluate their performance prediction compared to the large-scale 10" $UEAV_{24,1}$ cartridge. They will be evaluated for a range of feedstocks as defined in Chapter 3. The specific objectives of the chapter are:

- Design and fabricate a range of scale-down pleated cartridges that have a reduced area of active membrane, but that retain the pleat geometry of the large-scale target.

- Evaluate the scale-down pleated cartridge devices with a non-fouling water feedstock, comparing calculated R_m values between the various size scales and configurations.

- Evaluate the scale-down cartridge device with a fouling feedstock comprising pepsin aggregates by comparing experimentally determined V_{max} / A_m ratios for the various scale-down devices and configurations.

- Investigate the effects of membrane variability and housing hydrodynamics upon the performance predictions of the scale-down pleated cartridge device.

- Investigate the utilisation of the P_{max} test as a means to reduce further the volume of feedstock required to conduct a scale-up study with the scale-down pleated cartridge device.

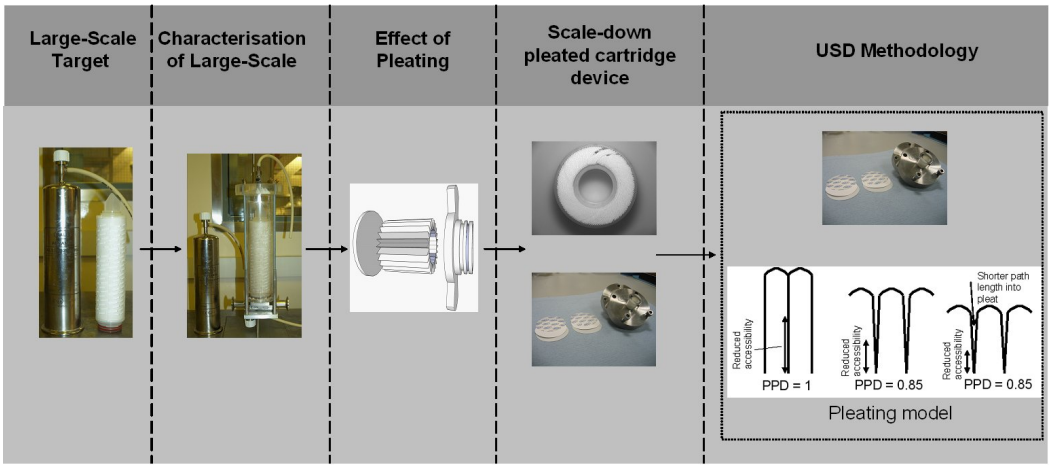

Figure 5-1: Overview of this thesis highlighting the strategy used to generate scale-down and USD methodologies aimed at providing a robust prediction of the performance of a large-scale pleated cartridge filter.

5.2 Pleated Cartridge Clean Water Flux Predictions

The design of the scale-down has been described earlier in Section 2.3.2. A range of scale-down pleated cartridges were fabricated and leak tested as described in Section 2.3.1.2. The nomenclature used for the various cartridge configurations is described in Figure 5-2.

The methodology for carrying out a scale-up prediction with the various scale-down pleated cartridges is summarised in Figure 5-3. The normalised performance data that is generated, such as clean water flux, product transmission and volume throughput, requires validation against the large-scale pleated cartridge counterpart so as to verify that the performance prediction is within an acceptable range (arbitrarily defined here as <10%). The type of large-scale cartridge used as the basis for comparison is the 10" $UEAV_{24,\ 1}$ that was characterised for a range of feedstocks in Chapter 3.

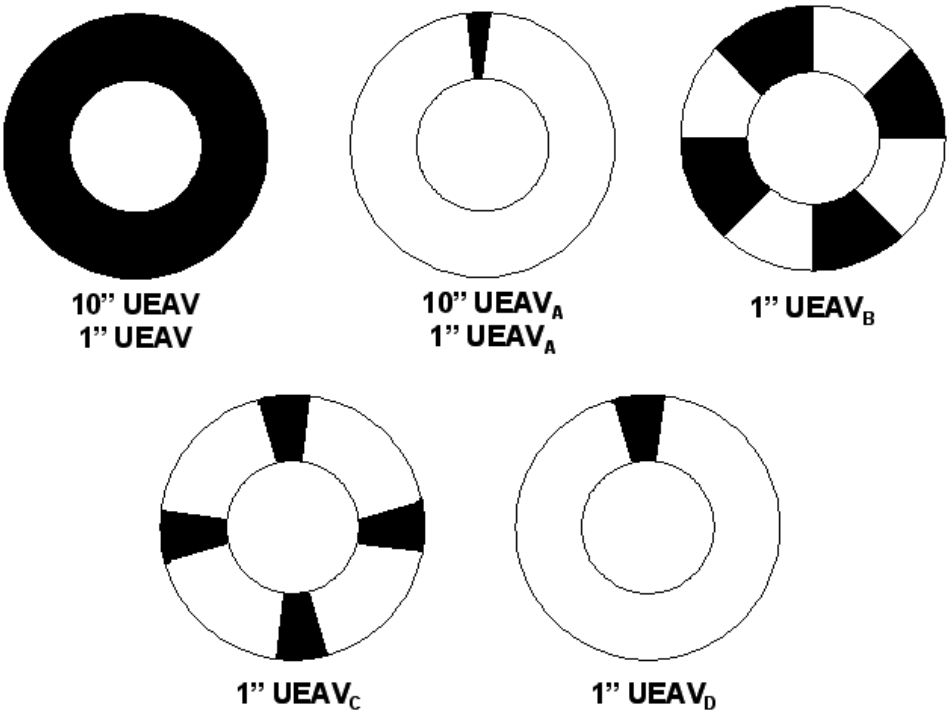

Figure 5-2: Schematic representation of the cross-section of 1" scale-down cartridge configurations used in this chapter, showing the number and distribution of active pleat sections (shaded black) that each type represents.

The evaluation of the performance of the scale-down pleated devices compared to the large-scale 10" cartridge was first carried out using clean water to represent a non-fouling feedstock. The clean water flux profiles for various cartridge and flat sheet configurations are given in Figure 5-4. It can be seen that there was a significant difference between the water flux profile of a flat sheet disc (solid line) compared to the large-scale 10" pleated cartridge (dashed line). This would lead to an overestimation of 53% if the flat sheet data were used to predict the performance of the large-scale cartridge. This is identical to the measured flux reduction described in Section 1.6 of 53% for a pleated PVDF sterilising grade membrane compared to a flat sheet (Rajniak et al., 2008), but lower than a flux reduction of 70% measured for a pleated glass fibre cartridge (Wakeman et al., 2005).

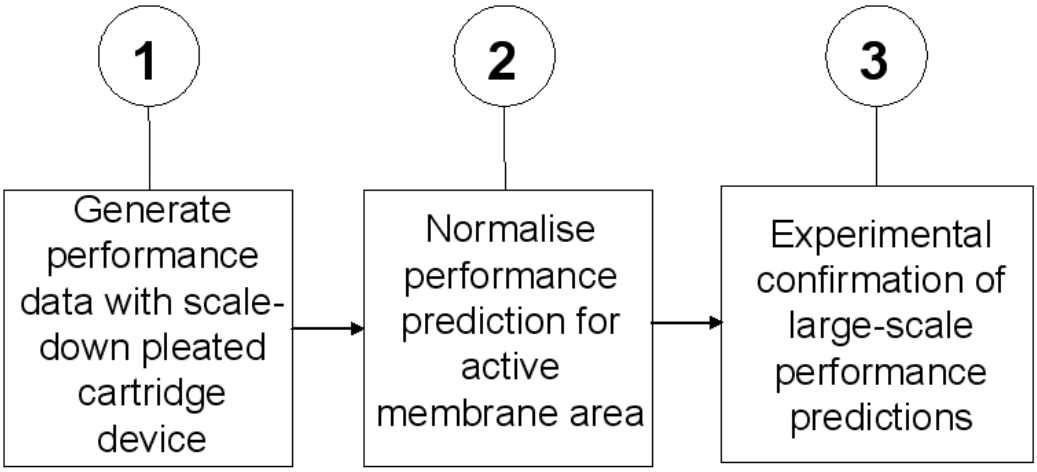

Figure 5-3: Flowsheet showing the methodology used to generate performance predictions (such as clean water flux, product transmission or volume throughput) from the scale-down pleated cartridge device, which can then be compared and verified against the performance of the large-scale pleated cartridge.

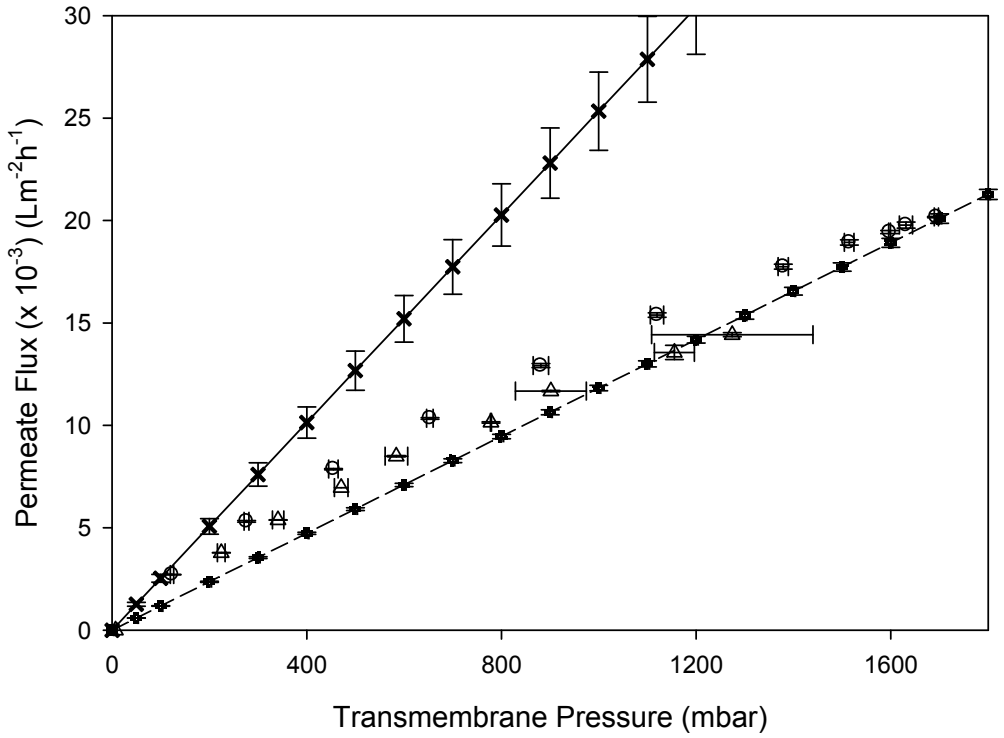

Figure 5-4: Water flux data for various Supor® cartridge and flat sheet membrane configurations. The large-scale 10" $UEAV_{24,1}$ cartridge (+) contained fully pleated membrane. The scale-down cartridges were 1" $UEAV_A$ (○) and 10" $UEAV_A$(△). Each scale-down cartridge contained 1.5 active pleats. Also used was a standard 25 mm flat sheet disc (×). Error bars represent one standard deviation about the mean (n = 3). Experiments performed as described in Section 2.4.

Figure 5-4 also shows the results for two of the scale-down cartridges fabricated for this study. The first, 10" $UEAV_A$ (Figure 5-2), contained 1.5 active pleats with a membrane area of 1.51×10^{-2} m^2. The second, 1" $UEAV_A$ (Figure 5-2), contained 1.5 active pleats with a membrane area of 1.51×10^{-3} m^2. In contrast to the flat sheet disc, the scale-down devices showed significantly better predictions of the 10" cartridge performance. At low transmembrane pressure a discrepancy between the performance of the 1" and 10" scale-down devices compared to the 10" large-scale cartridge can be seen. However this discrepancy becomes reduced at higher transmembrane pressures, > 1200 mbar, and over the whole operational range the performance of the scale-down cartridges more closely resembled that of the 10" $UEAV_{24,\ 1}$ cartridge than the flat sheet disk. Of the two scale-down devices, the 10" cartridge with 1.5 active pleats (10" $UEAV_A$) gave the better prediction of 10" $UEAV_{24,}$ 1 performance. However, this still operated with feed requirements comparable in volume to the 10" $UEAV_{24,\ 1}$ cartridge (> 1 L) that makes it unsuitable as a small-scale performance prediction tool. The 1" cartridge with 1.5 active pleats (1" $UEAV_A$) only required 180 mL of feed material and thus represents a good trade-off between quantitative performance prediction and greatly reduced feed requirements.

Table 5-1 shows the calculated membrane resistances (Hermia, 1982) from the flux profiles shown in Figure 5-4. The 53% flux variation between the flat-sheet disk and 10" $UEAV_{24,\ 1}$ cartridge resulted in a lower flat sheet membrane resistance as found previously in Section 4.2. The resistances calculated for the two small scale cartridges were close to that of the 10" $UEAV_{24,\ 1}$ cartridge. Variation from the R_m value for the 10" $UEAV_{24,}$ 1 cartridge was 2% and 8% for the 10" $UEAV_A$ and 1" $UEAV_A$ cartridges respectively. These percentage variations are within 10% of the large-scale cartridge and thus offer a good prediction of performance, especially when compared to the flat sheet disc.

Table 5-1: Summary of the key performance parameters generated in this chapter for a selection of cartridge configurations that contained Supor® EAV 0.22 µm rated membrane.

Cartridge type	R_M ($\times 10^{10}$) (m^{-1})	V_{max} / A_m (Lm^{-2})[I]	Protein transmission (%)[II]	Feed volume requirements (L)[III]
10" $UEAV_{24, 1}$	3.43	152	95	137
1" $UEAV_{24, 1}$	3.26	146	84	12.9
10" $UEAV_A$	3.38	-	-	1.8
1" $UEAV_A$	3.14	144	93	0.18
Flat Sheet	1.60	110	94	0.04

[I] Values taken from Figure 5-6
[II] Measured for pepsin solutions as described later in Section 5.3.
[III] Calculated based on collected permeate volume.

5.3 Volume Throughput Predictions for Protein Solution Filtration

Having shown that the scale-down devices gave a good prediction of large-scale cartridge performance (10" $UEAV_{24, 1}$) when a clean water feedstock was used, a more realistic pepsin feedstock was used to further evaluate the various configurations of scale-down cartridge. As was discussed in Section 1.3.2.3 and seen in Chapter 3.4.2, a solution of pepsin has previously been shown to foul 0.22 µm polyvinylidene fluoride (PVDF) membranes through a dual-mode mechanism consisting of initial pore blockage by protein aggregates, followed by

further attachment of protein to the aggregates (Kelly et al., 1997). The pepsin feedstock consisted of 10 gL^{-1} pepsin in a 0.03 M sodium phosphate buffer (pH = 7.4), prepared as described in Section 2.6. This solution was considered representative of a concentrated pure protein solution typically processed using sterile filters at the end of a biopharmaceutical process (Sundaram, 1998). It was reported in Section 3.3.2 that the feed contained aggregates of 1-4 μm in size that were capable of blocking the 0.2 μm rated membrane, and which lead to fouling.

Figure 5-5 shows the cumulative permeate volume normalised for membrane area (Table 5-1) measured over the course of the filtration operation. Close agreement is seen between the performance of the 1" $UEAV_A$ scale-down cartridge, containing 1.5 pleats of active membrane and the large-scale 10" $UEAV_{24,\ 1}$ cartridge over the course of the total filtration operation. Other configurations used included a fully pleated 1" $UEAV_{24,\ 1}$ cartridge and a flat sheet disc. The flat sheet and cartridge filtration runs were carried out over different operational times (10 min and 55 min respectively), so the operational time is presented in Figure 5-5 as normalised against the total operating time. The different operational mechanisms are evident between the flat sheet disc, which is run under a constant pressure regime, and the cartridges, which are run under a constant flow regime. The 1" $UEAV_A$ scale-down device showed considerably better agreement with the large-scale cartridge over the course of the operation, than did the flat sheet disc. This may be because the flat sheet experiments were conducted at constant pressure, whilst experiments performed with the 1" $UEAV_A$ cartridge were conducted at constant flow. However, the measured feed pressure during the cartridge experiments was not allowed to exceed the pressure that was set during the flat sheet experiments. Hence the driving forces should be similar. However, if the difference is a consequence of the different operating regimes, then it is important to note that the large-scale target will always be operated with a constant flow regime, and as such, the scale-down pleated cartridge matches the large-scale target in this respect.

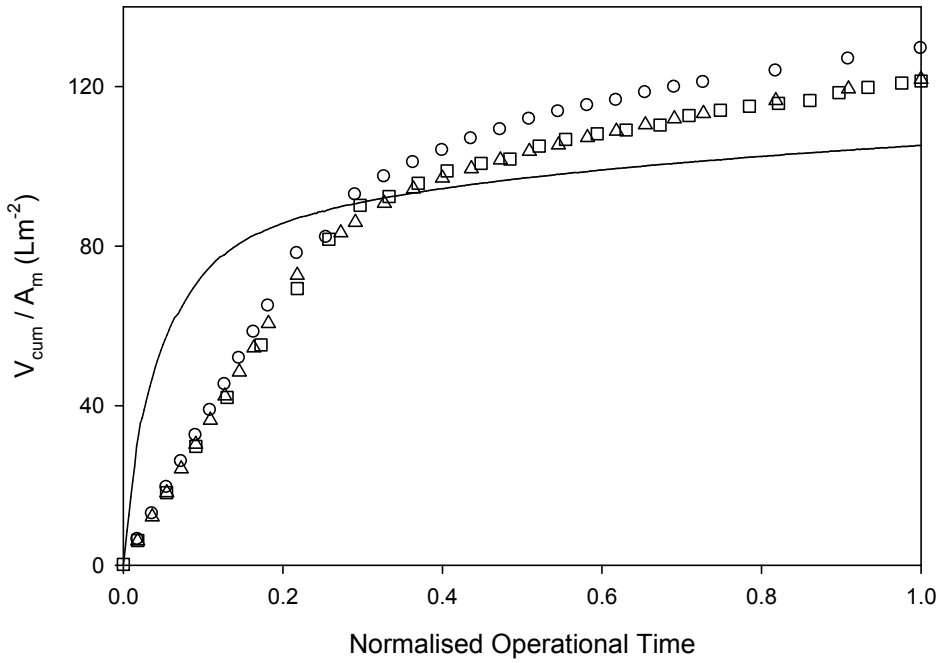

Figure 5-5: Representative volume throughput data for a range of cartridge and flat sheet membrane configurations for the filtration of a protein solution (10 gL^{-1} pepsin in 0.03 M sodium phosphate buffer, pH 7.4). Cumulative permeate volume normalised for membrane area and plotted against normalised operational time. Flat sheet data is represented by a solid line (—). Cartridges used were: 10" $UEAV_{24,\ 1}$ (○), 1" $UEAV_{24,\ 1}$ (△) and 1" $UEAV_A$ (□). Cartridges described in Section 2.3.2 and Figure 5-2. Experiments performed as described in Section 2.6.

All the curves shown in Figure 5-5 can be divided into two regions. The first region shows a linear increase in cumulative volume as the membrane pores became blocked, but the flowrate remained constant. During this period, when operating with a constant flow regime, the feed pressure increased. After a given maximum operating pressure, and as the pump was switched on and off, an operational region was evident where the permeate flowrate was low. This reduction in throughput was attributed to membrane fouling. Fouling by pore constriction (Hermia, 1982) was found to be the most likely mechanism to describe the reduction in throughput, as an excellent fit to the experimental data (R^2>0.99) was achieved for the results obtained from all the cartridges used. An example plot of the fouling mechanism to throughput data for a 10" $UEAV_{24,\ 1}$ cartridge is given in Figure 5-6.

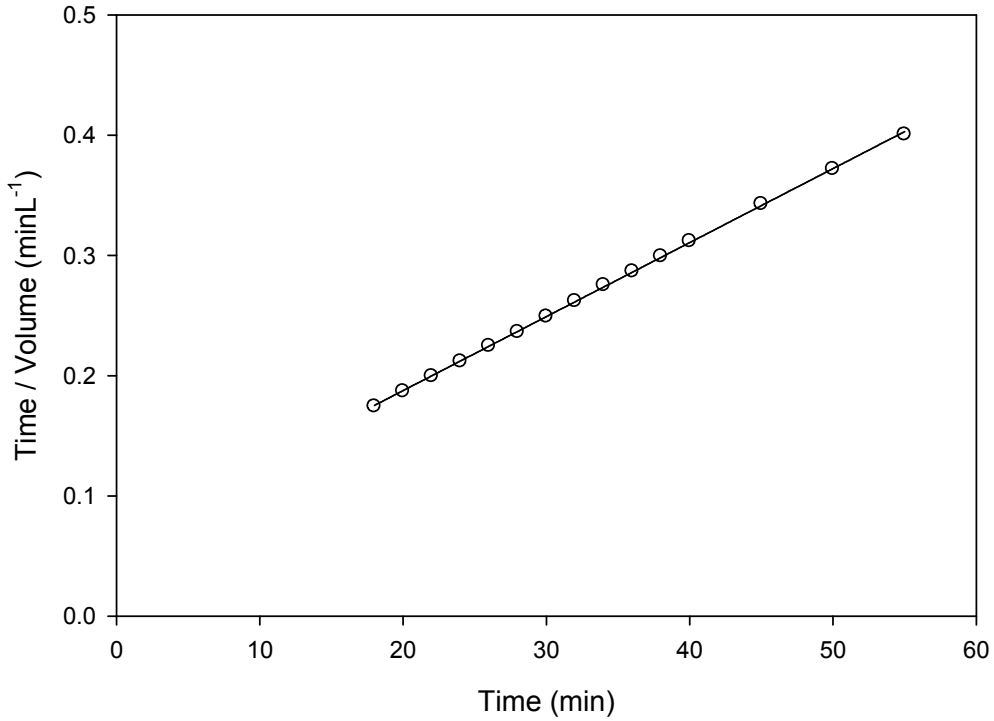

Figure 5-6: Plot of t / V against t for 10" $UEAV_{24,\ 1}$ throughput data reported in Figure 5-5. Gradient of the line can be used to calculate V_{max}. Excellent fit of line to datapoints achieved (R^2>0.99).

During the period controlled by pore constriction, the V_{max} values, defined as the maximum filtered volume before complete fouling occurs (Badmington et al., 1995), were calculated from the throughput data. The V_{max} value, described in Section 1.7, was used as an industrially relevant method to compare the filtration performance of various scales tested with the aim to seek the closest match to the performance of the 10" UEAV pleated cartridge. V_{max} is defined as the maximum filtered volume before complete fouling occurs, and was obtained by plotting t/V against t. The V_{max} value is defined by the inverse of the gradient from the subsequent line. Typical V_{max} values and the R^2 values from the lines used to generate the V_{max} are given in Table 5-2.

The calculated V_{max} values were subsequently normalised by dividing by the area of active membrane. This provided a method of directly comparing the performance predictions of differing scale down devices with different

membrane areas, and is also a method through which scale-up could be achieved. To facilitate linear scale-up prediction, the V_{max}/A_m ratios should be the same for all scales. The V_{max}/A_m values calculated for each of the three independent experimental data sets are given in Figure 5-7. It can be seen that the 1" $UEAV_A$ cartridge shows good agreement to the two cartridges used that contained a full pack of active membrane pleats (10" and 1" $UEAV_{24,\ 1}$). The flat sheet disc was seen to under-predict the performance of the 10" $UEAV_{24,\ 1}$ cartridge in all cases.

The mean of these V_{max}/A_m values are given in Figure 5-8 together with the error bars calculated from the triplicate measurements. It can be seen that the 1" $UEAV_A$ cartridge performance is within 10% of the 10" $UEAV_{24,\ 1}$ cartridge, compared with 41% for the flat sheet disc. The performance of the 1" $UEAV_{24,\ 1}$ cartridge was closer to that of the 10" $UEAV_{24,\ 1}$ cartridge (within 3.5%), but due to a reduced A_m (Table 5-1) the 1" $UEAV_A$ had a 1000-fold lower feed material requirement. Based on these results the 1" $UEAV_A$ represents the best scale-down approach for predicting large-scale cartridge throughput performance.

As well as being predictive of flux performance, the scale-down cartridge devices should also accurately replicate product transmission performance. Table 5-1 lists the associated protein transmission data. All scales of pleated membrane cartridge were seen to give similar protein transmission levels of >90% w/w with the exception of the 1" $UEAV_{24,\ 1}$ cartridge. The 1" $UEAV_A$ cartridge again gave a good prediction of protein transmission performance to the 10" $UEAV_{24,\ 1}$ cartridge as it did with volume throughput prediction, this is likely to be because the blocking of the pores and build up of any cake takes place at a similar rate due to the pleat geometry remaining the same.

Table 5-2: Typical V_{max} values from various cartridge configurations. R^2 values from the lines used to generate values of V_{max} also listed.

Cartridge Configuration	V_{max} (L)	R^2
10" $UEAV_{24, 1}$	161	>0.99
1" $UEAV_{24, 1}$	15	>0.99
1" $UEAV_A$	0.217	>0.99

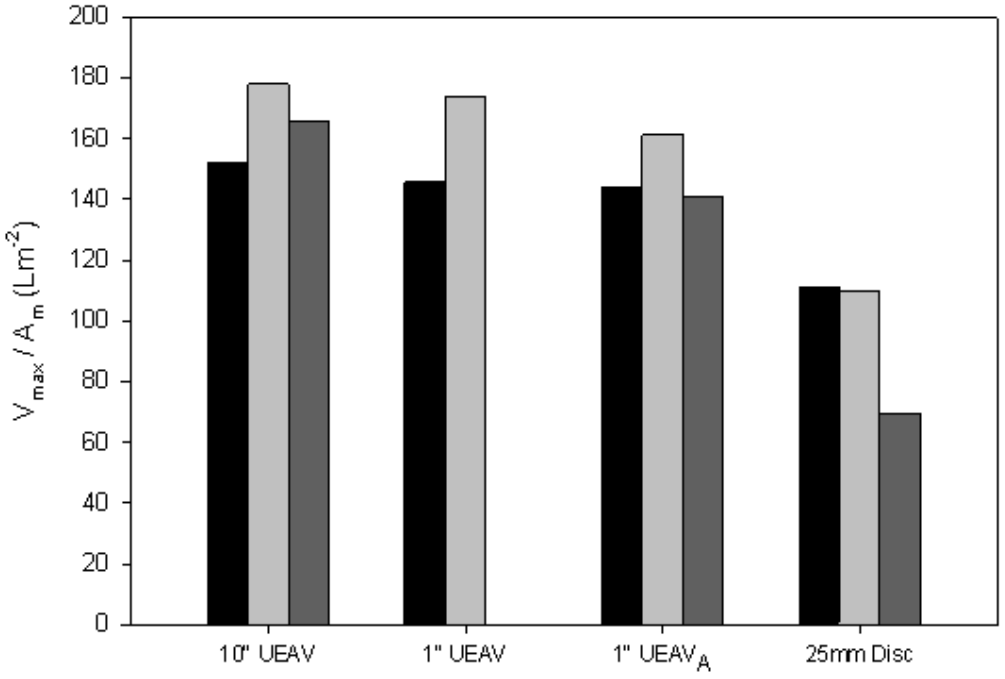

Figure 5-7: Comparison of experimentally determined V_{max} / A_m values, a scaling factor for processing of a protein solution (10 gL^{-1} pepsin in 0.03 M Sodium Phosphate buffer, pH = 7.4), for the different cartridge configurations and a flat sheet disc. Supor® EAV membrane used in all configurations. For accurate scaling, the value of V_{max} / A_m should be the same for all size scales. Each bar represents a separate independent experiment. Experiments performed as described in Section 2.6.

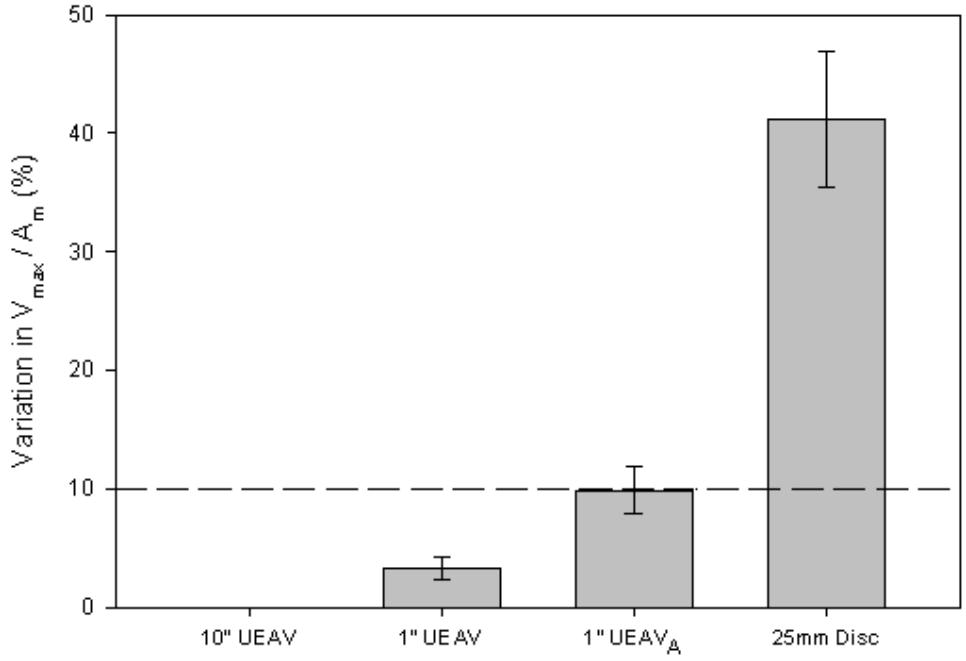

Figure 5-8: The percentage variation between the throughput performance (V_{max} / A_m) for each membrane configuration relative to the 10" $UEAV_{24, 1}$ cartridge. The dashed line indicates 10% variation, which is considered here to be acceptable for accurate scale-up predictions. Error bars show one standard deviation about the mean (n=3). Experiments performed as described in Section 2.6.

5.4 Effect of Membrane Variability and Housing Design Upon Scale-Down Device Performance

In Section 1.6, studies were described that have previously shown measurable differences in the performance of membrane taken from different locations within a manufactured roll (Chandler et al., 2004; Jackson et al., 2006). Thus it may be expected that reduced pleat levels lead to an increase in experimental error when quantifying permeate flux and protein transmission. In Chapter 3, a detailed study on the hydrodynamics of fluid flow and mixing within the membrane housing has suggested there may be some limited radial and axial variation in the liquid distribution within the housing. This might suggest that inclusion of more than just one active membrane section and for these active pleat sections to be evenly distributed around the central core of the cartridge

might further improve the accuracy of the throughput prediction. To investigate if this is indeed the case, a number of further scale-down cartridge devices were fabricated which contained a range of active number of pleats and number of pleat bunches (see Figure 5-2 and Section 2.3.2. for a description of the cartridges used). Performance variation of the scale-down devices from that of a large-scale 10" cartridge was calculated from experimental data for a clean water feed and a fouling pepsin feed (described above in Sections 3.4.1 and 3.4.2 respectively).

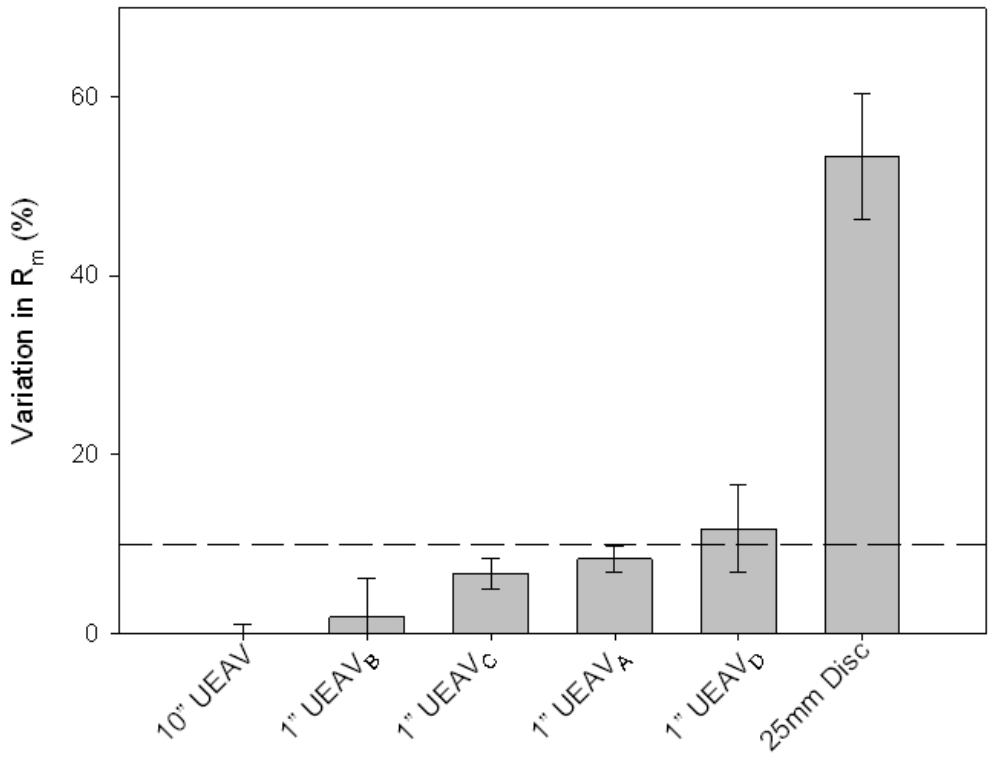

Figure 5-9: Effect of pleat number and pleat location upon scale-up performance of different scale-down pleated cartridge configurations compared to a standard 10" $UEAV_{24,\ 1}$ cartridge. Feed stock used was clean water. A description of the different configurations is given in Section 2.3.2 and Figure 5-2. Solid bars represent the mean of independent experiments (n=3) while error bars represent the standard deviation of calculated R_m values. Experiments performed as described in Section 2.6.

The variations in R_m calculated for the six cartridges investigated in clean water flux experiments are given in Figure 5-9. It can be seen that the percentage variation in calculated membrane resistance (R_m) in general decreased as more active pleats were incorporated into the pleat structure. This suggests that incorporating more membrane sections helps improve the accuracy of scale-up when working with a clean water feedstock. However, the accuracy of the scale-up prediction measured for the scale-down device with the lowest active membrane area (1" $UEAV_A$) was still acceptable in terms of scale-up performance, as it was less than 10% of that for the full scale 10" $UEAV_{24,\ 1}$ cartridge. Hence, the increases in performance prediction seen with an increase in active membrane area are not sufficiently large to counteract the increase in feed volumes required for operation.

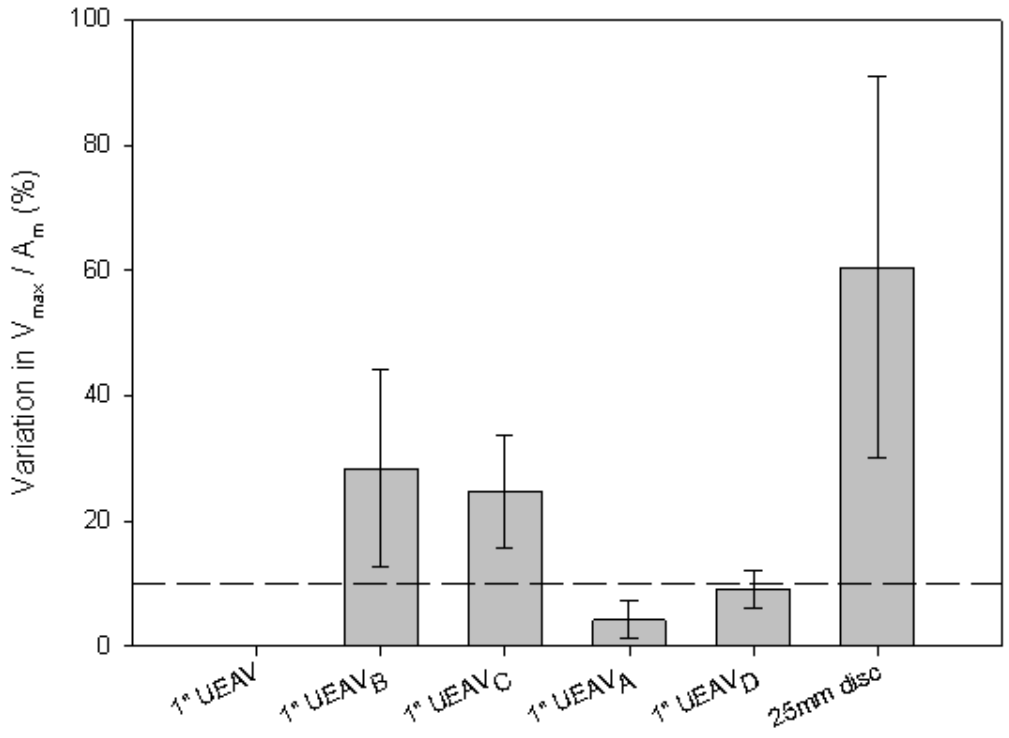

Figure 5-10: Effect of pleat number and pleat location upon scale-up performance of different scale-down cartridge configurations compared to a standard 1" $UEAV_{24,\ 1}$ cartridge. Feed stock used was $10gL^{-1}$ pepsin in 0.03 M Sodium Phosphate buffer, pH = 7.4. A description of the different configurations is given in Section 2.2.2 and Figure 5-2. Solid bars represent the mean of three independent experiments (n=3), except for the 25 mm disc where n = 5. Error bars represent the standard deviation of measured V_{max}/A_m values. Experiments performed as described in Section 2.5.

A similar outcome is shown in Figure 5-10 when the various scale-down cartridge designs were evaluated with a fouling pepsin feedstock. However, in the case of 1" $UEAV_B$ and 1" $UEAV_C$ variation form the large-scale target was seen to be greater. This may be due to hydrodynamic effects within the housing. It can be seen that the best performance for the scale-down devices was for the device that contained 1.5 active pleats. When this performance is coupled to the low feed volume requirements this scale-down device represents a superior option for scale-up over a flat sheet disc of membrane.

5.5 Impact of Woven Support Material Upon Performance of Flat Sheet Membrane

All previous flat sheet experiments have been conducted in the absence of the woven support material that a pleated cartridge contains above and below the membrane material (Section 2.3). It is possible that the large differences that have been measured in Section 5.2 between the pleated cartridge and the flat sheet disc may be due to the woven support material acting as a pre-filter, which removes fouling components that would otherwise foul the membrane. To test whether this was the case, a preparation of the pepsin feedstock was filtered with a 1" $UEAV_{24,\ 1}$ cartridge and two flat sheet discs as per the protocol in Section 2.5.2.2. Above one of the flat sheet discs was placed a 25 mm disc of the woven support material. The volume throughput measured for the two flat sheet discs is given in Figure 5-11. It can be seen that the addition of the woven support material above the membrane disc did lead to an increase in volume throughput, however this increase in performance was small.

Table 5-3: Calculated scale-up parameters for a range of flat sheet configurations. For experiment with the woven support, a 25 mm disc was cut from the same woven material used within a cartridge and placed directly on top (upstream) of the 25 mm disc of membrane within the membrane holder.

Configuration	**Scale**	**V_{max} / A_m Lm^{-2}**	**% variation in V_{max} / A_m compared to 1" $UEAV_{24,1}$**
1" $UEAV_{24,1}$	Large	56	NA
25 mm flat sheet disc with woven support above membrane disc	Small	10	82
25 mm flat sheet disc without woven support	Small	8	85

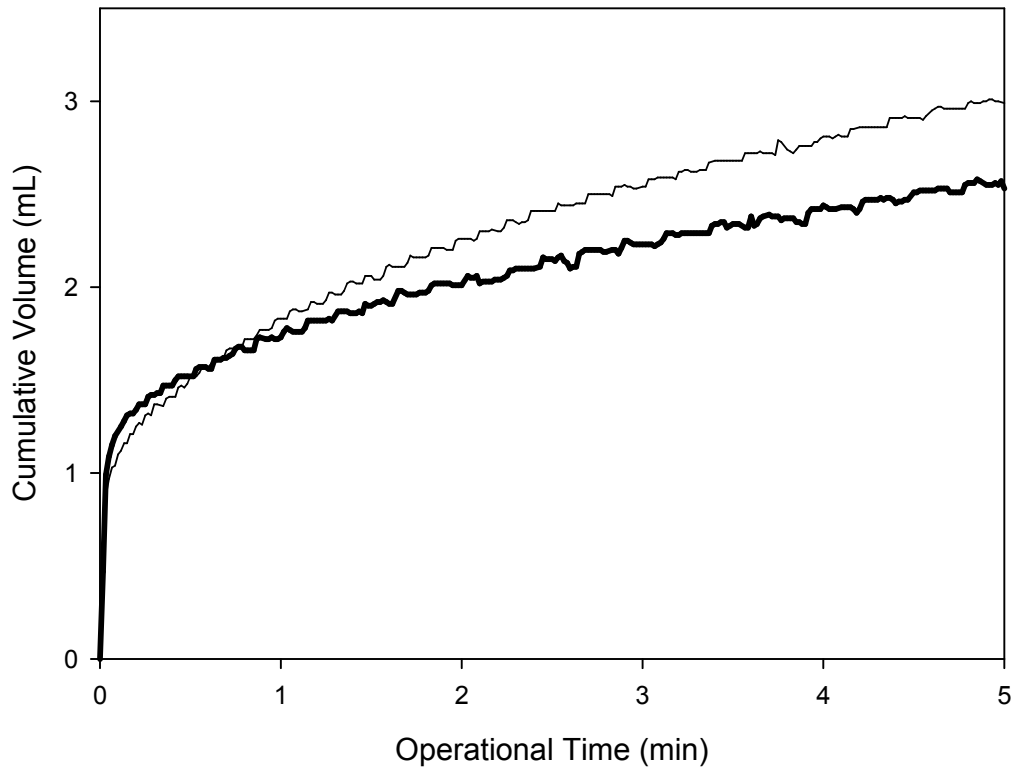

Figure 5-11: Filtration of 10 gL^{-1} pepsin in 0.03 M phosphate buffer (pH = 7.4) with 25 mm flat sheet discs of membrane. Experiments conducted with a 25 mm disc of woven support material on top of the membrane (—) and without (**▬**). Experiment conducted as per protocol in Section 2.5.2.2.

The calculated V_{max} / A_m values are given in Table 5-3 for the configurations used to filter the pepsin feedstock. It can be seen that the addition of the woven support material reduced the variation between the performance of the flat sheet disc and 1" UEAV cartridge by 3%. However, this is not considered a significant enough improvement to explain the differences measured in this section and Section 5.3.

5.6 Use of P_{max} Method to Calculate V_{max}

It has been noted in Section 5.3 that two distinct operational regions existed during the filtration of the pepsin feedstock by a pleated cartridge. This is illustrated in Figure 5-12. For a V_{max} test to be conducted, data must be collected from well within the region where volume throughput is variable and membrane performance is limited by the fouling that has occurred within the membrane pores. For the experiments performed with cartridges in Section 5.3, and reported in Figure 5-7, the feed pressure was recorded throughout the filtration operation. During the first period, when the volume throughput was at a constant rate, the feed pressure was seen to change, as shown in Figure 5-12. It can be seen that after an initial lag phase the feed pressure rapidly increased as the pores became blocked, until a maximum operating pressure of 0.8 bar(g) was achieved. At this point the pump was turned off to allow the feed pressure to decrease. After the pressure was less than 0.2 bar(g) the pump was turned on again and the cycle was repeated.

The P_{max} test, discussed in Section 1.7.3 has been used with depth filters to enable the measurement of increasing feed pressure to predict V_{max}. The same approach can be taken for the filters used in this study. Assuming a standard pore blocking fouling mechanism then based upon the theory outlined in Section 1.7.3 the linear form of the fouling mechanism is:

$$\frac{1}{P^{1/2}} = a - b \cdot V \tag{5.1}$$

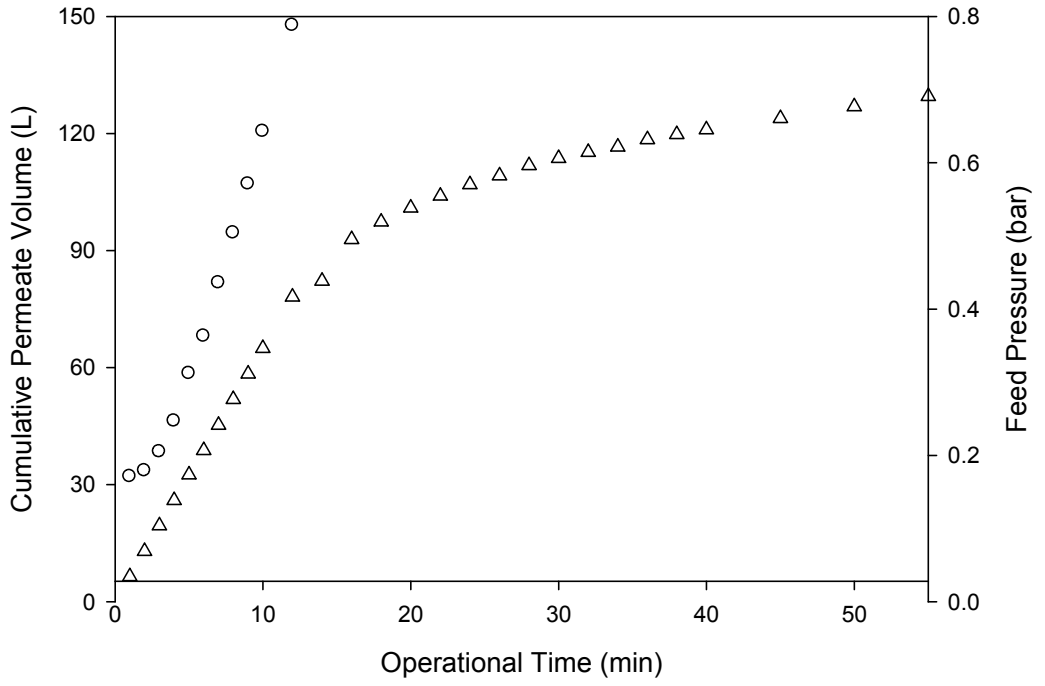

Figure 5-12: Measured outputs from filtration run. Change in pressure (○) and cumulative permeate volume (△) over the course of a filtration run with feedstock of 10 gL^{-1} pepsin in 0.03M sodium phosphate buffer (pH = 7.4). Filter cartridge used was 10" $UEAV_{24,\ 1}$. Experiments performed as described in Section 2.5.1.

Where: P is the feed pressure, V is the cumulative permeate volume collected. The constants 'a' and 'b' can be obtained from a plot of $P^{-0.5}$ against V, where a is the y-intercept and b is the gradient of the line.

An example of a plot of $P^{-0.5}$ against V is given in Figure 5-13 for the filtration of the pepsin feedstock by a 10" $UEAV_{24,\ 1}$ cartridge. The data was seen to fit well to the linear form of the fouling mechanism ($R^2 = 0.95$), as was the case for all of the cartridges tested. For Equation 5.1, as P goes to infinity, V approaches V_{max}, therefore:

$$V_{\max} = \frac{a}{-b} \tag{6.2}$$

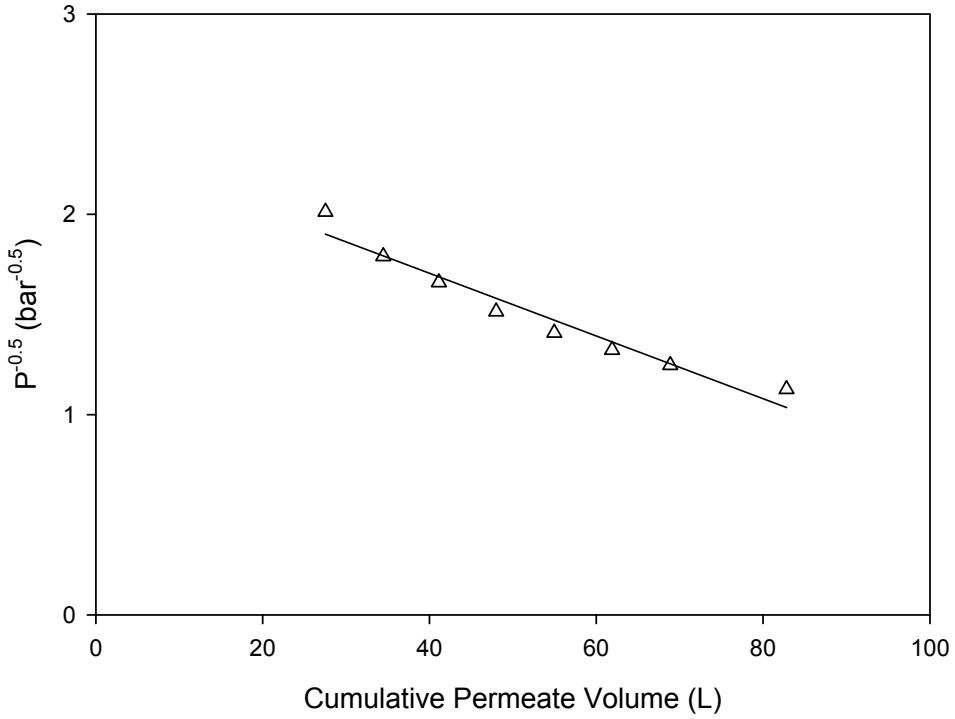

Figure 5-13: Plot of $P^{-0.5}$ against volume for filtration data reported in Figure 5-12. The y-intercept and gradient of the line can be used in Equation 5.2 to calculate V_{max}.

Thus from the plot in Figure 5-13 the V_{max} can be calculated once the y-intercept and gradient of the line are known.

The V_{max} / A_m ratios were calculated using the P_{max} method for a range of cartridge configurations. The values for three separate experiments are given in Figure 5-14. The 1" $UEAV_A$ scale-down pleated cartridge was seen to have calculated V_{max} / A_m values that closely matched the V_{max} / A_m value of the large-scale 10" $UEAV_{24,\ 1}$ cartridge. This was the case for all three experiments conducted. The V_{max} / A_m value for the third experiment conducted was less than for the other two experiments. This is likely due to variation in the preparation of the feedstock. It should be noted that the decrease in V_{max} / A_m was also seen for the large-scale 10" $UEAV_{24,\ 1}$ cartridge. The average variation in performance from the 10" $UEAV_{24,\ 1}$ cartridge for the 1" $UEAV_A$ cartridge was within ± 10%.

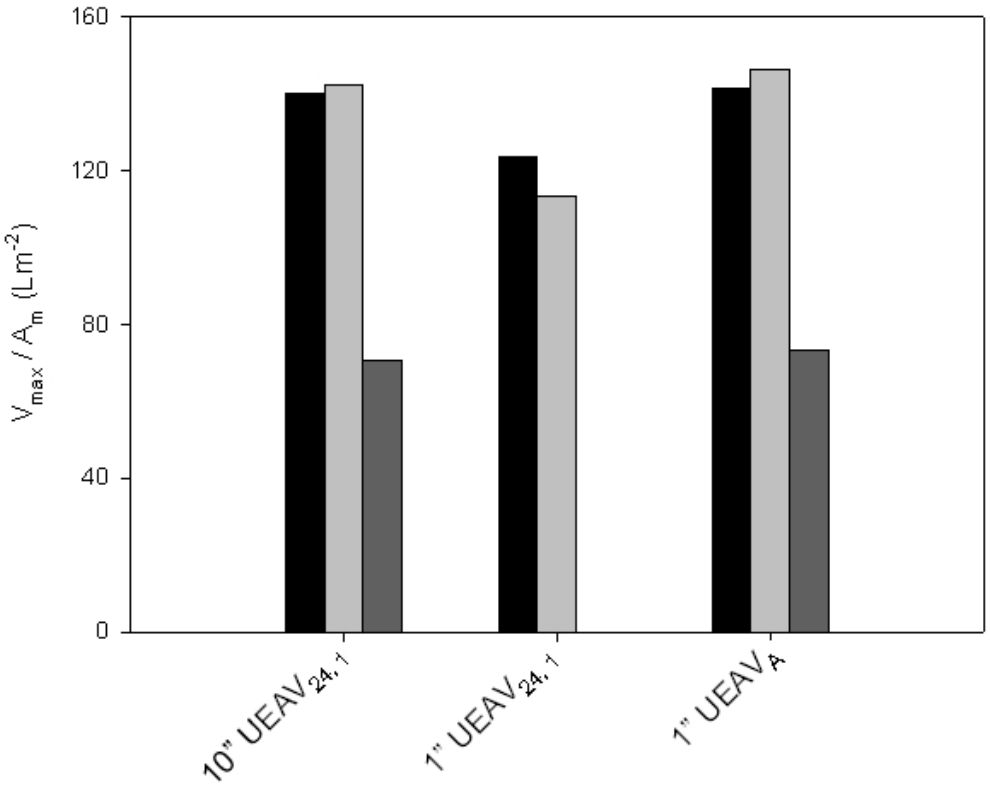

Figure 5-14: V_{max} / A_m ratios for the filtration of a 10 gL^{-1} Pepsin in 0.03M sodium phosphate buffer (pH = 7.4) feedstock by three cartridge configurations. Each colour of bar represents a separate experiment with a fresh preparation of the feedstock. Values of V_{max} / A_m generated using the P_{max} method as described in Section 5.6.

5.7 Comparison of P_{max} and V_{max} Methodologies

The various performance aspects of the P_{max} (Section 5.6) and V_{max} (Section 5.3) methods are summarised in Table 5-4. It can be seen that for each cartridge configuration the P_{max} method tends to underestimate the value of V_{max} compared with its experimental determination using the standard V_{max} method. This is not a significant problem as the predicted value of V_{max} from the P_{max} method lies well within the region where the membrane is fouled and performance is poor relative to the initial period. It is unlikely that a cartridge would actually be operated for long periods of time within this region.

The percentage variation in V_{max}/A_m between the 10" $UEAV_{24,\ 1}$ cartridge and the 1" $UEAV_A$ scale-down pleated device was lower for the P_{max} method, than for the V_{max} method, although in both instances the variation was well within the 10% threshold set as the limit to show adequate large-scale performance prediction.

In terms of the volume of feed required to obtain the performance prediction then the P_{max} method requires less feed to obtain an estimate of V_{max} than does the standard V_{max} method. For the 1" $UEAV_A$ cartridge this represented a 28% reduction in feed volume. However, at 131 mL the feed required is still higher than that required for the flat sheet disc (40 mL). Furthermore the feed volume requirement does not include housing or tubing dead volumes.

The R^2 values for the standard blocking mechanism that was fitted to the datasets were higher for the V_{max} test. However, the R^2 values for the P_{max} method were sufficiently high enough to justify using the standard blocking model.

In terms of matching the performance of the 10" $UEAV_{24,\ 1}$ cartridge whilst minimising the amount of feed required, the P_{max} method is suggested here to be better than the more established V_{max} method.

Table 5-4: Comparison of performance characteristics for the V_{max} and P_{max} methodologies. Data generated for a range of cartridge configurations.

Cartridge Configuration	**V_{max} Method**				**P_{max} Method**			
	V_{max} / A_m (Lm^{-2})	R^2	% variation	V_{feed} (L)	V_{max} / A_m (Lm^{-2})	R^2	% variation	V_{feed} (L)
10" $UEAV_{24,\ 1}$	152	>0.99	0	137	140	0.95	0	83
1" $UEAV_{24,\ 1}$	146	>0.99	4	13	123	0.95	12	8
1" $UEAV_A$	144	>0.99	5	0.183	141	0.94	-0.8	0.131

5.8 Discussion and Summary

The aim of this chapter was to test the scale-down pleated cartridge designed and fabricated in Section 2.3.2 with a range of feedstocks, so as to determine whether the performance prediction obtained matched that of the counterpart large-scale fully pleated cartridge. This aim was achieved through a number of objectives that were fulfilled. The main findings and conclusions are:

- The scale-down pleated device was initially evaluated with a clean water feedstock (Figure 5-4). When the value of R_m for the scale-down pleated device with the smallest active membrane area (1" $UEAV_A$) was compared to the R_m measured for a large-scale 10" $UEAV_{24,\ 1}$ cartridge, the percentage variation between the two measurements was 8%, which represented a significant improvement over the 53% difference measured between the 10" cartridge and a flat sheet membrane disc (Table 5-1).

- The scale-down pleated device was subsequently evaluated with a fouling pepsin aggregate feedstock (Figure 5-5). When the value of V_{max} / A_m for the scale-down pleated device with the smallest active membrane area (1" $UEAV_A$) was compared to the V_{max} / A_m measured for a large-scale 10" $UEAV_{24,\ 1}$ cartridge, the percentage variation between the two measurements was 10% (Figure 5-7), which represented a significant improvement over the 41% difference measured between the 10" cartridge and a flat sheet membrane disc. Product transmission levels were also seen to be very similar between the large-scale target and the 1" $UEAV_A$ scale-down cartridge (95% and 93% respectively as reported in Table 5-1. The accuracy of the scale-up device with predicting the performance of the large-scale target would require verification with other feedstocks.

- Membrane variation and housing effects were seen to have a small effect on the performance of the scale-down pleated device. However, the effect was not significant enough to affect the robustness of the scale-up

performance prediction of the 1" $UEAV_A$ scale-down pleated device. Membrane variation and housing effects were not seen to have a significant effect when a fouling feedstock was used.

- A new application of the P_{max} method was used to determine whether V_{max} could be calculated using reduced feed volume requirements. When the P_{max} and V_{max} methods of generating the parameter V_{max} were compared, then the P_{max} method was seen to give a closer prediction of the performance of a large-scale 10" $UEAV_{24,\ 1}$ cartridge (Table 5-4). This was achieved with a 28% reduction in the volume of feedstock used by the smallest scale-down pleated device. Whilst the standard pore blocking model was seen to give a better fit to the V_{max} data, the fit to the P_{max} data was still sufficiently high enough ($R^2 > 0.94$) to not affect the validity of the results (Table 5-4).

While the performance predictions of the scale-down pleated membrane cartridges have been shown to be good, this approach still requires some 130 mL of feed material for V_{max} / A_m quantification. This value also does not include the hold-up volume within the housing of ~300 mL. In order to try and reduce the feed volume requirements further, Chapter 6 describes an ultra scale-down approach, which will aim to correct the experimental data obtained from flat sheet membrane so as to improve the performance prediction relative to large-scale pleated cartridges. The potential advantage of this method is that experiments could be conducted using small areas of membrane that require a lower feed volume. The scale-down pleated device evaluated in this chapter will be compared to the USD approach in the final discussion contained with the conclusion chapter of this thesis, so as to assess the relative merits of the various small-scale utilised during this work.

6 Ultra Scale-Down (USD) Approach to Prediction of Pleated Cartridge Performance

6.1 Introduction and Aims

The pleated scale-down device fabricated and tested in Chapter 5 demonstrated good prediction of the performance of a large-scale pleated cartridge to within 10% of both flux and transmission. However, the feed volume required (~180 mL) remained higher than that required for the initial membrane evaluation using flat sheet discs (~4 mL). This was primarily due to the hold-up and dead volumes within the 1" cartridge housing and associated pipework, and the constant flow filtration method used. However, it has been seen in Section 4.2, and then in Section 5.2 and 5.3 that the flat sheet discs can make poor predictions of the performance of a large-scale pleated cartridge. Thus, in order to capitalise on the lower feed volumes requirements achievable with the flat sheet membrane the performance prediction needs to be improved. An ultra scale-down approach was discussed in Section 1.7.5. The USD approach seeks to provide a more accurate scale-down performance by focussing on the generation of key performance parameters that dominate during the large-scale operation (Titchener-Hooker et al., 2008). Importantly, the USD approach does not seek to miniaturise the large-scale target, but uses modelling to bring the two scales into alignment (Tustian et al., 2007). The USD approach may offer a means of achieving an improvement in prediction of performance by combining models which account for pleating effects to the raw experimental data gathered using the flat sheet discs.

It has been previously shown in Section 4.3 that the effective area in pleated membrane cartridges available for filtration decreases due to pleat crowding and was seen to be a function of pleat height and pleat packing density. Incorporation of knowledge on the effect of pleating on the available membrane area into the USD flat sheet scale-up methodology, could help improve the robustness of the

flat sheet system for prediction of the performance of large-scale pleated cartridges.

This chapter covers the final step in the approach defined in Section 1.8. As illustrated in Figure 6-1, this chapter builds upon work carried out to characterise the effect of pleating in Section 4.3. A new methodology to improve USD predictions of pleated membrane cartridge performance is presented. The methodology can then be compared with the scale-down pleated cartridge device tested in Chapter 5.

The aim of this chapter is to develop and test a USD approach that improves predictions from small-scale flat sheet experiments by correcting for the pleating effects. The specific objectives of the chapter are:

- To investigate and model pleat crowding effects as a function of pleat height and pleat packing density.

- To develop USD methodology to improve scale-up predictions from a flat sheet disc by adjusting for the effects of pleating.

- To assess whether the USD methodology improves the performance prediction generated from a flat sheet membrane applied to large-scale pleated cartridge filters.

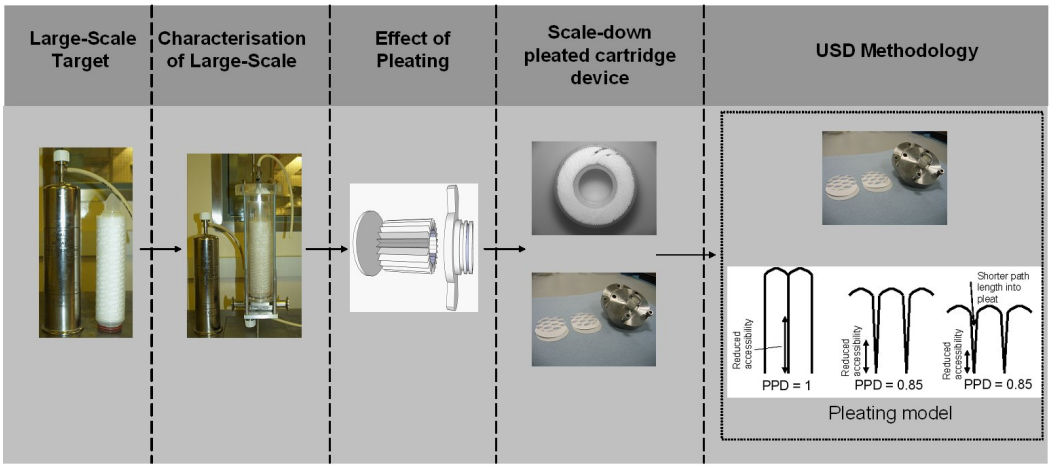

Figure 6-1: Overview of thesis showing the strategy towards the development of scale-down and ultra scale-down methodologies. This chapter seeks to design and evaluate a novel scale-down pleated cartridge, which retains the geometrical characteristics of the large-scale target, whilst reducing the active area of membrane inside the cartridge.

6.2 Quantification of Pleat Crowding Effects

Pleat crowding has previously been discussed in Section 4.3. In general an increase in h_P and PPD lead to decreased accessibility of solutes into the pleat due to the close proximity the membrane surface in each individual pleat (Section 4.3). This effect is illustrated in Figure 6-2. Pleat crowding has rarely been considered in the literature as a function of the pleat characteristics, and this is particularly the case for liquid feeds.

The standard approach to generate performance data for a non-fouling feedstock, such as clean water, is to assume that the membrane area is fully utilised as described in Section 3.4.1. It is then possible to determine values of membrane resistance. Figure 6-3 shows the systematic variation for a range of cartridges with varying pleat characteristics. It can be seen that the large-scale pleated cartridges exhibited a higher membrane resistance than the flat sheet disc. As pleat packing density decreased the membrane resistance decreased, and the same trend was seen for decreases in pleat height. Examples of cartridges with similar membrane resistance to the flat sheet membrane were seen however, such as for the pleated cartridge with a star pleat configuration. The 1" cartridge with PPD of 0.65 matched the flat sheet R_m value most closely. Due to difficulties in

the fabrication of the pleated cartridges, it was not possible to fabricate cartridges with reduced PPD for the Ultipleat® type.

It has previously been shown in Chapter 4 that the effective membrane area (A_{eff}) within each cartridge may not be equal to the actual installed membrane area (A_m) as a result of the pleat crowding effect. Therefore an alternate approach would be to maintain the membrane resistance as constant and alter the value of A_m to reflect the change in the effective membrane area.

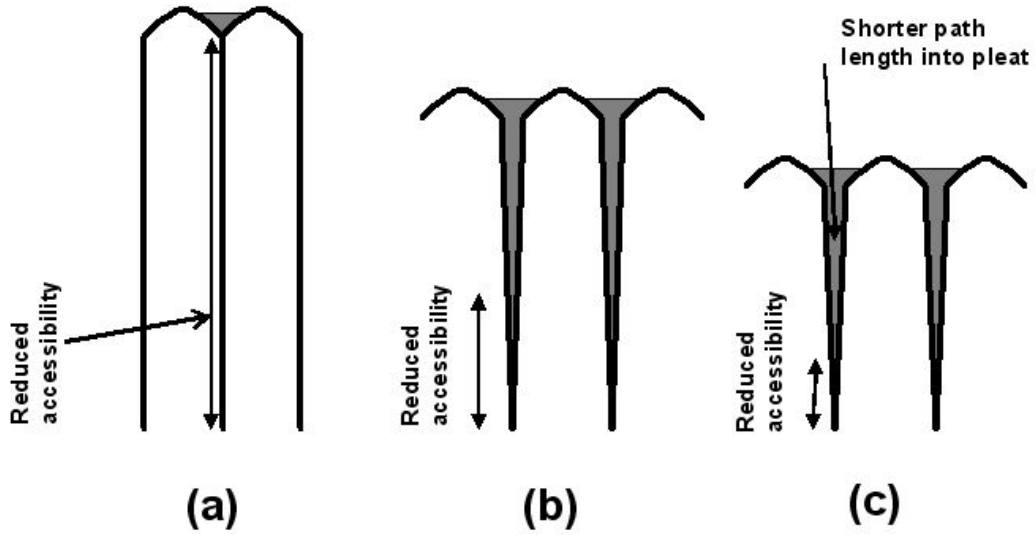

Figure 6-2: Illustration of the effect of pleat packing density (PPD) and pleat height (h_P) upon pleat crowding and solute accessibility into the pleat. Images shown represent a fan pleat design with: (a) h_P = 24 mm PPD = 1, (b) h_P = 15 mm PPD = 0.85, (c) h_P = 10 mm PPD = 0.85. Images shown are not to scale.

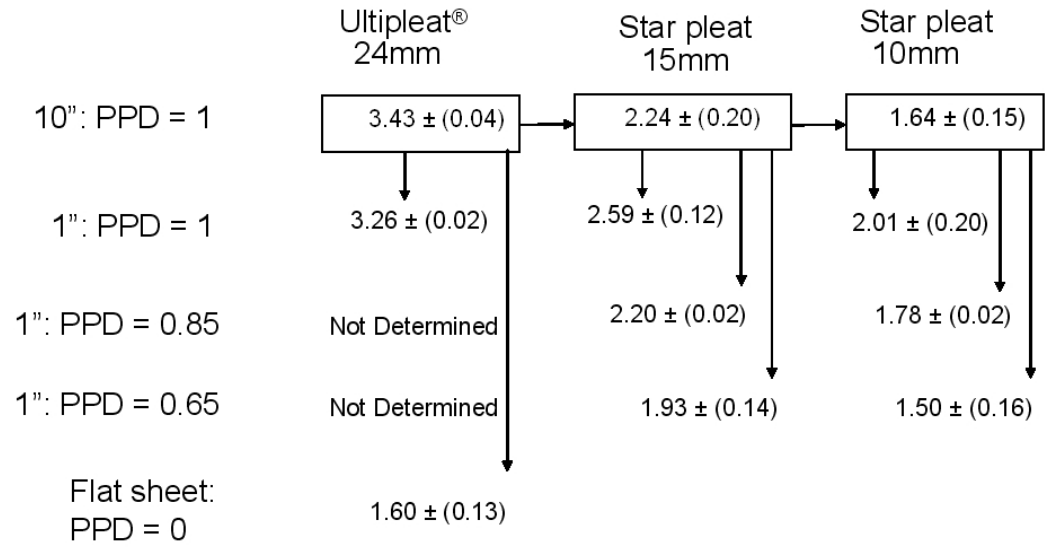

Figure 6-3: The effects of pleat crowding on measured membrane resistance (R_M, $\times 10^{10}$ m^{-1}). The matrix shows the variation in R_m calculated from clean water flux data. Experimental protocols performed as described in Section 2.3.1. Membrane resistances arranged, so as to show the change in R_m as a function of pleat type, h_P and PPD. Resistances calculated using Equation 6.1 by assuming that all membrane area is utilised (A_{eff} = A_m). Where possible the data is presented as one standard deviation about the mean (n=3).

6.3 K- Factor Development

In order to account for the difference in effective and actual membrane areas an ultra scale-down factor will be used here, the K-Factor, which will be a function of the pleat geometry. The definition of the K-factor is described as follows.

The effective membrane area, A_{eff}, can be calculated from the experimental permeate flow data, which was originally used to calculate the R_m values in Figure 6-3, by using Equation 6-1:

$$A_{eff} = \frac{Q \cdot \mu \cdot R_m}{\Delta P} \tag{6-1}$$

Where: Q is the permeate flow rate, μ is the viscosity, R_m is the membrane resistance, ΔP is the transmembrane pressure difference, and A_{eff} is the effective membrane area. The K-Factor is then used to relate A_{eff} to the actual membrane

area, A_m, to assess the degree of utilisation of membrane area as described below:

$$K = \frac{A_{eff}}{A_m} \tag{6-2}$$

The calculated K- factor values, derived from the data contained within Figure 6-3 are presented in Figure 6-4. It can be seen that the K-factor, and thus the effective utilisation of the installed membrane area, varies with changes in h_P and PPD. Reducing the heights of the pleat and pleat packing density eventually leads to a pleated cartridge (1" $EAV_{10,\ 0.65}$) with a K- factor close to 1. At this point the membrane area is being fully utilised and there is little or no difference between the actual and effective membrane resistances.

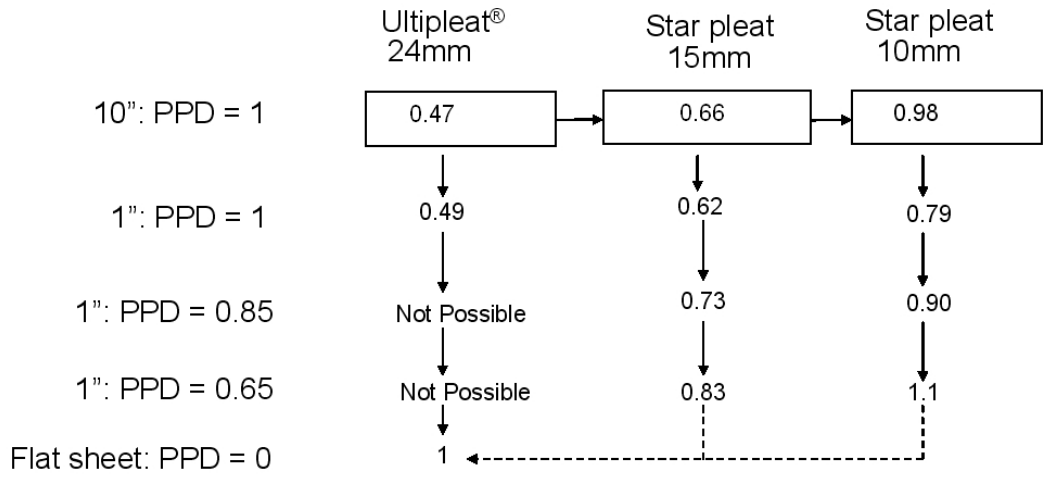

Figure 6-4: The effect of pleat crowding on calculated K-factors for various membrane pleat configurations. K- Factors calculated using Equation 6.2 based on clean water flux data given in Figure 6-3.

To further explore the effect of each of the pleat characteristics, on effective utilisation of the installed membrane area, the K-factor has been plotted as a function of h_P (Figure 6-5) and PPD (Figure 6-6). In Figure 6-5 the three datasets plotted appear to converge at h_P = 23 mm with a K-factor of 0.5. It can also be seen that as h_P increases, the K- factor follows a non-linear decline. Figure 6-6 shows that a non-linear relationship is also seen when the calculated K-factor is plotted as a function of PPD. In general it can be seen that K- factor declines as the PPD increases. The decrease in K-factor as a function of PPD was seen to be greater for h_P = 15 mm than it was for h_P = 10 mm.

Since the K-factor showed a non-linear decline with both h_P and PPD, the datasets were fitted with an equation with the general form given below.

$$y = A - Be^{(C \cdot x)} \tag{6-3}$$

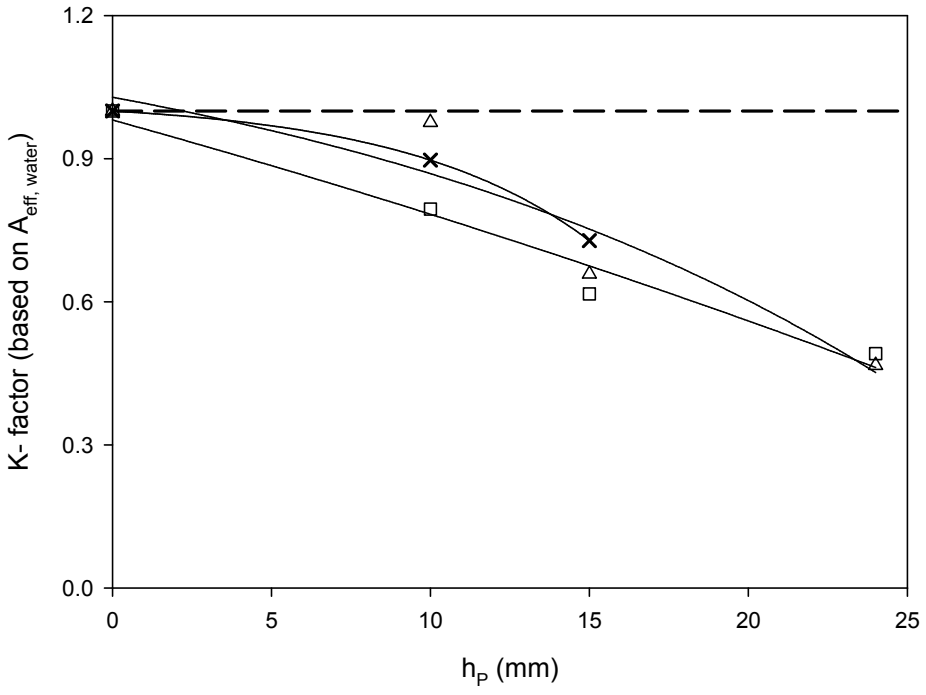

Figure 6-5: Variation of K- factor as a function of h_P. Data plotted is for: 10" cartridges with PPD = 1 (△), 1" cartridges with PPD = 1 (□) and 1" cartridges with PPD = 0.85 (○). The broken line shows a K- factor of 1, where all the membrane is fully utilised. Calculated K-Factor values taken from Figure 6-4. Solid lines fitted according to Equation 6-3.

Where: y is the K-factor, x is h_P or PPD, whilst A, B and C are fitted parameters. Equation 6-3 was fitted to the datasets using the built in function within Sigmaplot (Systat Software Inc., California, USA) that used a Marquardt-Levenberg algorithm to predict values for the fitted parameters. The algorithm was used to minimise the sum of the squared differences between the values of the predicted and observed dependent variable (K-factor). The fitted parameters and R^2 values for all of the datasets used are given in Table 6-1.

The fitted lines for the datasets where h_P was varied is shown in Figure 6-5. It can be seen that Equation 6.3 gives a reasonable fit to the dataset with R^2 values ranging from 0.89 to 1. These are acceptable given the limited number of cartridge configurations fabricated and hence K-factors determined. The experimental correlations could be used to calculate K-factors for any h_P, providing pleat packing density remained constant.

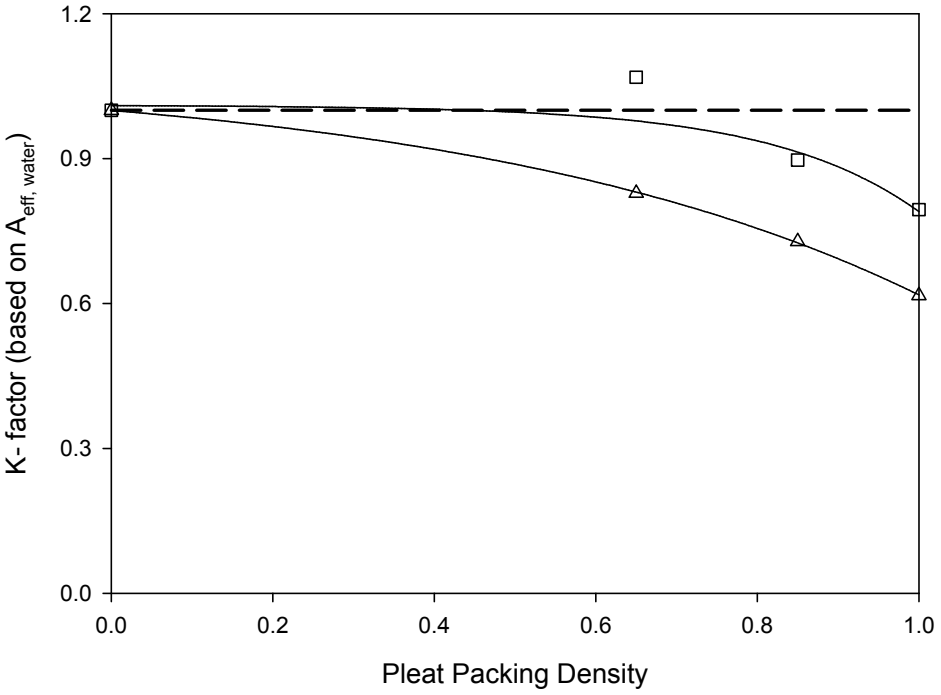

Figure 6-6: Variation of K-factor as a function of PPD. Data plotted is for a 1" cartridge with h_P = 10 mm (□) and 1" cartridge with h_P = 15 mm (△).The broken line shows a K-factor of 1, where all the membrane is fully utilised. Calculated K-factor values taken from Figure 6-4. Solid lines fitted according to Equation 6-3.

Table 6-1: Values of the fitted parameters generated for Equation 6-3 for various cartridge configurations. R^2 values are given to show the closeness of the fit between the equation and the data. Yeast solution comprised of 7.7 gL^{-1} yeast, 1 gL^{-1} BSA in 0.03 M sodium phosphate buffer (pH 7.5)

Pleat Characteristic	**Cartridge Configuration**	**Test Fluid**	**Fitted Model Parameters**			**R^2**
			A	**B**	**C**	
h_P	10", PPD = 1	Water	1.27	0.24	0.05	0.89
h_P	1", PPD = 1	Water	2.48	1.5	0.012	0.97
h_P	1", PPD = 0.85	Water	1.02	0.02	0.17	1
PPD	1", h_P = 10mm	Water	1.03	0.0004	6.36	0.84
PPD	1", h_P = 15mm	Water	1.08	0.08	1.78	> 0.99
PPD	1", h_P = 10mm	Yeast	1.01	0.01	3.79	> 0.99

Similarly, Equation 6.3 also produced a reasonable fit to the datasets where PPD was varied. These were shown previously in Figure 6-6. R^2 values ranged from 0.84 to >0.99, which are again acceptable given the limited dataset. These experimental correlations could be used to calculate K- factors for any PPD, providing h_P remained constant.

The reasonable fit of Equation 6-3 to the datasets used indicates that the model selected to describe the change in K-factor with a change in PPD or h_p may be valid. However, the model fits are based upon limited experimental data. It was not possible to run further experiments as it was only possible to fabricate a limited number of cartridge/pleat configurations. Thus the model requires verifying with another alternative feedstock that is independent of the current set of experiments. Once verified the model can be used to generate improved scale-up data from a flat sheet disc to compare against data for a large-scale pleated cartridge. This will be covered in Section 6.4.

6.4 Verification of K-Factor Experimental Model

The K-factor model described in Section 6.3 is based on a reduction in effective membrane area due to pleat crowding effects. So as to try and experimentally verify the reduction in membrane area seen in Figure 6-5 and Figure 6-6, membrane experiments were performed as presented in Section 4.4 where yeast was used as a probe to highlight areas of unused membrane.

Colour images of the membrane taken from the pleated cartridges used in Section 4.4 were captured and converted to an 8-bit grey scale image. The grey scale images were converted into a binary image using the protocol outlined in Section 2.4.3. The various images used in this process are shown in Figure 6-7, Figure 6-8, and Figure 6-9 for a 1" $EAV_{10,\ 1}$, 1" $EAV_{10,\ 0.85}$ and 1" $EAV_{10,\ 0.65}$ pleated cartridges respectively. Areas of white within the binary image represent membrane area without yeast deposits. It can be seen from Figure 6-7 to Figure 6-9 that the area of membrane without yeast deposits reduces as PPD decreases. This can be linked to the reduction in PPD leading to a more open pleat structure, which in turn allows greater accessibility for particles to enter the pleat and deposit upon the membrane surface.

Particle analysis was performed upon the binary images shown in Figure 6-7 – 6-9, using the protocol defined in Section 2.4.3. This analysis, quantified the number of pixels of each colour contained within the binary images. In turn this allowed for quantification of the membrane area that contained yeast deposits. This is assumed to represent the effective membrane area ($A_{eff,\ IA}$) available for filtration. A summary of the results of the particle analysis are given in Table 6-2 from which it can be seen that A_{eff} decreased as a function PPD. In turn Equation 6-2 was used to calculate K-factors, as the total area of the image represented A_m. Calculated values of K-factor are also given in Table 6-2. As was seen to be the case for the water experiments Section 6.3, K-factor decreased as a function of PPD, due to the decrease in A_{eff} caused by the increase in PPD.

A plot of K-factor as a function of PPD for the yeast suspension data is given in Figure 6-10. The data shows the same non-linear decline model found when evaluating the K-factors generated from clean water flow data. Equation 6.3 was fitted to the data points and the fit parameters are given in Table 6-1. The equation was seen to fit the data well and gave a curve with $R^2 > 0.99$.

The threshold, which defines the point at which an image pixel represents either clean membrane or a yeast deposit, was set manually with reference back to the original colour image. The error bars show the impact that a 10% variation in the threshold value had upon the calculated K-factor. Whilst the error bars are relatively large, there is still a significant difference between the data points (Student's t-test yields $P<0.05$).

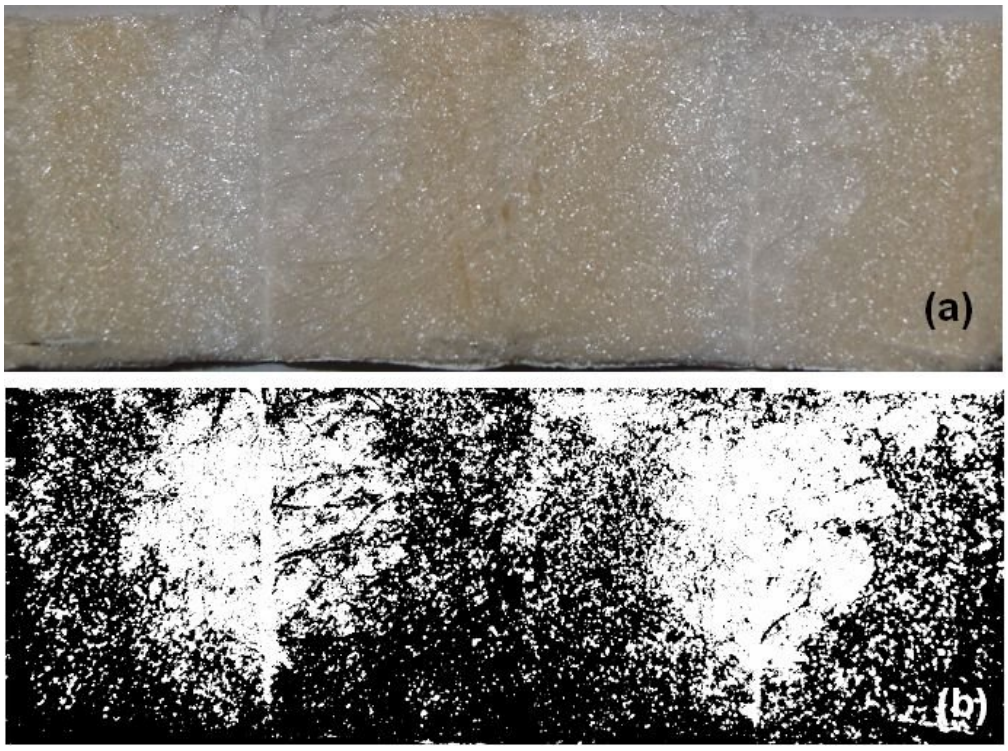

Figure 6-7: Images used to experimentally determine K-factors for a 1" $EAV_{10,1}$ cartridge based on deposition of yeast particles. Images are: (a) colour photograph of yeast cell deposition, (b) binary representation. Experiments were performed as described in Section 2.4.1. The generation of the binary images was carried out as per the experimental protocol outlined in Section 2.4.3.

The data points contained in Figure 6-10 have been combined with the data points contained in Figure 6-6 to compare the different approaches taken to generate K-factor. The results are shown in Figure 6-11. Whilst not exact, the trends in K- factor decline are similar for the datasets generated from water and yeast suspension experiments. This confirms that the models generated from the water system were reasonable and applicable. The models can now be used to improve the scale-up predictions from a flat sheet disc to a large-scale pleated cartridge using an ultra scale-down approach.

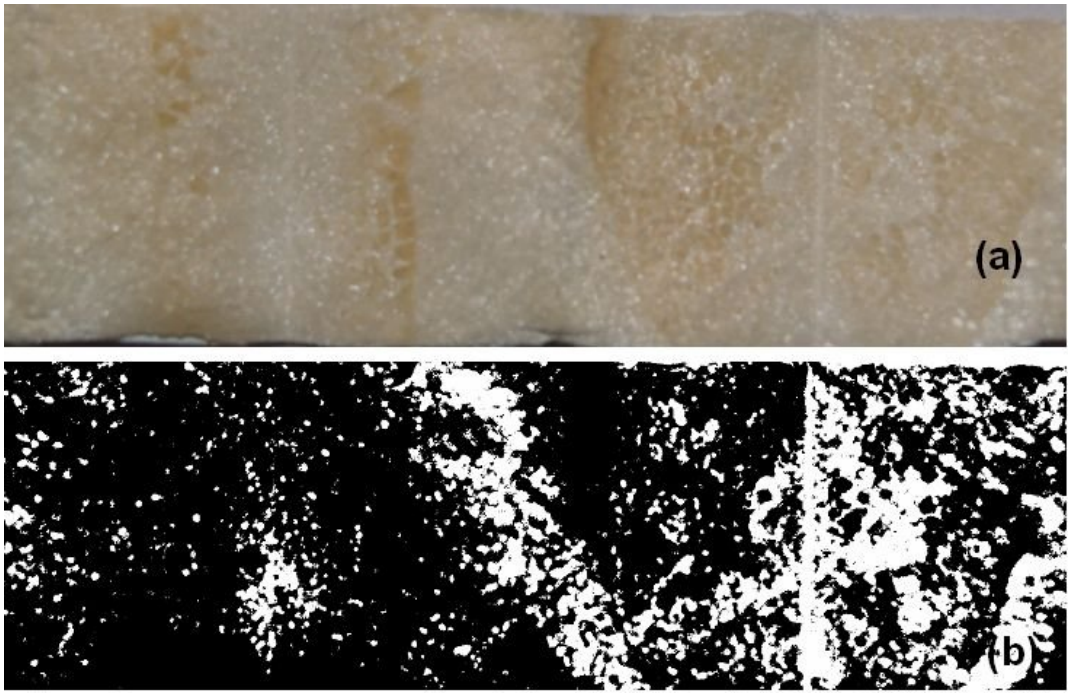

Figure 6-8: Images used to experimentally determine K-factors for a 1" $EAV_{10,\ 0.85}$ cartridge based on deposition of yeast particles. Images are: (a) colour photograph of yeast cell deposition, (b) binary representation. Experiments were performed as described in Section 2.4.1. The generation of the binary images was carried out as per the experimental protocol outlined in Section 2.4.3.

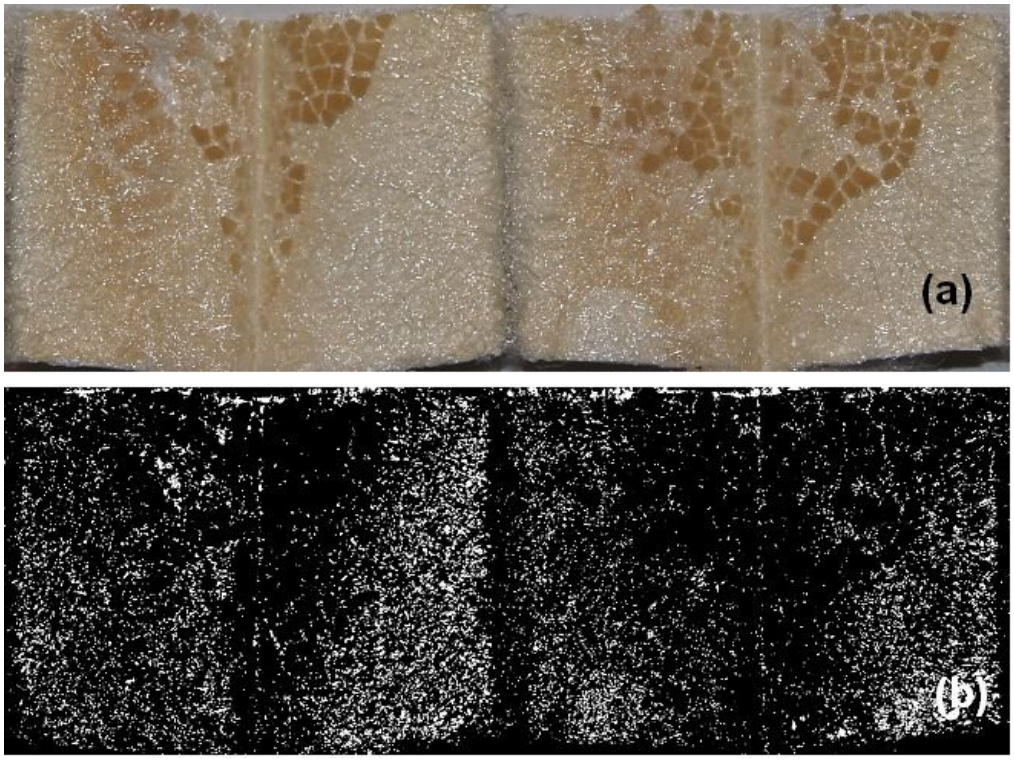

Figure 6-9: Images used to experimentally determine K-factors for a 1" $EAV_{10,\ 0.65}$ cartridge based on deposition of yeast particles. Images are: (a) colour photograph of yeast cell deposition, (b) binary representation. Experiments were performed as described in Section 2.4.1. The generation of the binary images was carried out as per the experimental protocol outlined in Section 2.4.3.

Table 6-2: Results of particle analysis performed upon membrane samples given in Figure 6-7 – 6.9. Particle analysis performed as described in Section 2.4.3. K-factor calculated by dividing the sample area with yeast deposits ($A_{eff,\ IA}$) by the total area of the sample (A_m). Values presented are averaged based upon generation of binary images as described in Section 2.4.3 with a 10% variation in the binary threshold value.

Cartridge configuration	Total area of sample ($\times 10^5$) ($pixels^2$)	Sample area with yeast deposits ($\times 10^5$) ($pixels^2$)	Sample area without yeast deposits ($\times 10^5$) ($pixels^2$)	K-factor (%)
1" $EAV_{10,\ 1}$	12.6	6.6	6.0	52
1" $EAV_{10,\ 0.85}$	12.5	9.1	3.4	73
1" $EAV_{10,\ 0.65}$	11.5	10	1.15	88

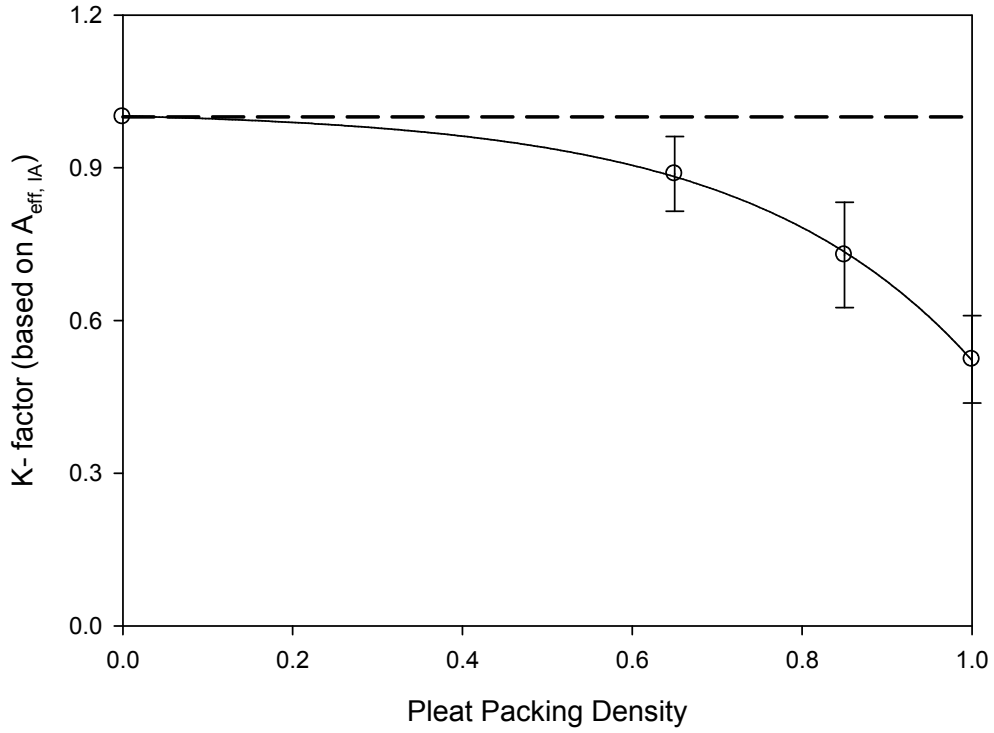

Figure 6-10: Variation of K-factor values based on image analysis with PPD. Data generated from yeast suspension experiments performed as described in Section 2.4.1. Quantification of the clean membrane area as described in Section 2.4.3. Error bars represent a 10% variation in the binary threshold value, set when converting from 8-bit grey scale to binary images. The solid line is a fit of Equation 6.3 to the dataset (the fitted parameters for the model are given in Table 6-1). The dashed line represents a K- factor of 1, where all the membrane area is effectively utilised.

So as to compare the degree of similarity seen in K-factor generated from either water flux experiments or image analysis the data points in Figure 6-11 were replotted as a parity plot, which is shown in Figure 6-12. It can be seen from this plot that there is a reasonable agreement between K-factor generated based upon $A_{eff, IA}$ and $A_{eff, water}$ obtained from cartridges containing a pleat height of 15 mm. The K-factors based upon $A_{eff, water}$ for cartridges with h_P = 10 mm were not seen to provide as good an agreement with those based upon $A_{eff, IA}$.

Whilst not being seen for the same pleat height, the agreement between the K-factor values obtained from the two separate approaches suggests that for a given cartridge configuration an estimate of A_{eff} based on a quick and cheap

clean water flux experiment may be adequate for obtaining a quantitative and accurate value of the K-factor.

The incorporation of this K-factor concept into a USD methodology aimed at improving the performance predictions of flat sheet membrane against the pleated cartridge counterpart will be presented in the next section. This new USD methodology will be tested against large-scale pleated cartridges used earlier in this thesis so as to assess whether an accurate scale-up can be achieved.

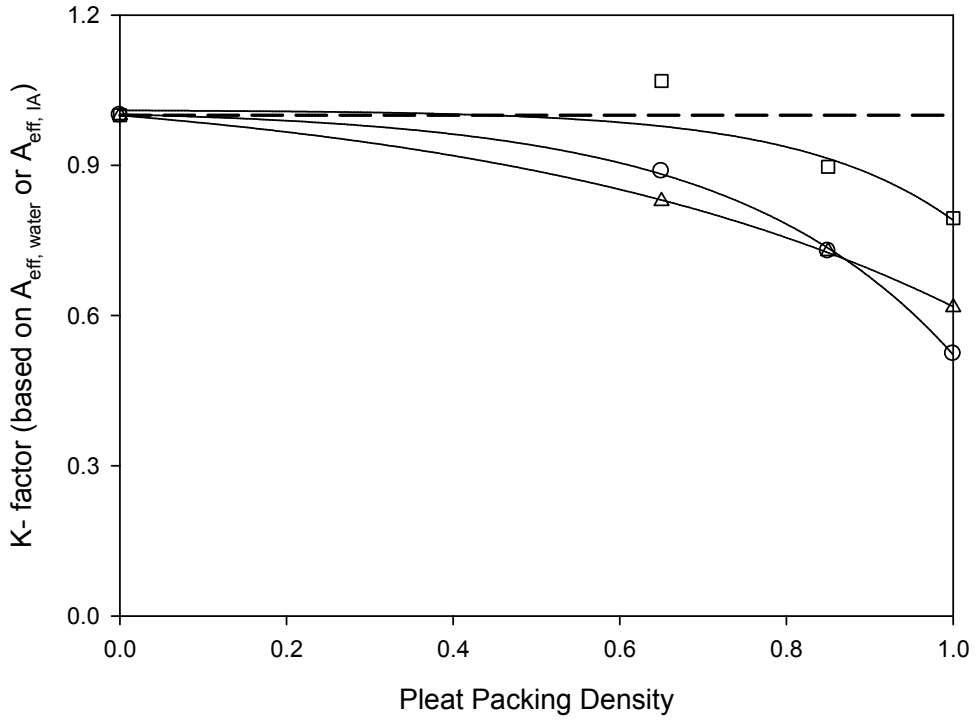

Figure 6-11: Datasets and fits of Equation 6.3 for the variation in K-factor as a function of PPD for 1" cartridges with h_P = 15 mm (△) and h_P = 10 mm (□,○). Data generated from clean water flow experiments (△,□) and from the quantification of yeast deposits (○). Experimental protocol for water flux experiments as described in Section 2.3.1. Experiments with yeast performed as described in Sections 2.4.1 and 2.4.3. The dashed line represents a K-factor of 1, where all the membrane area is effectively utilised.

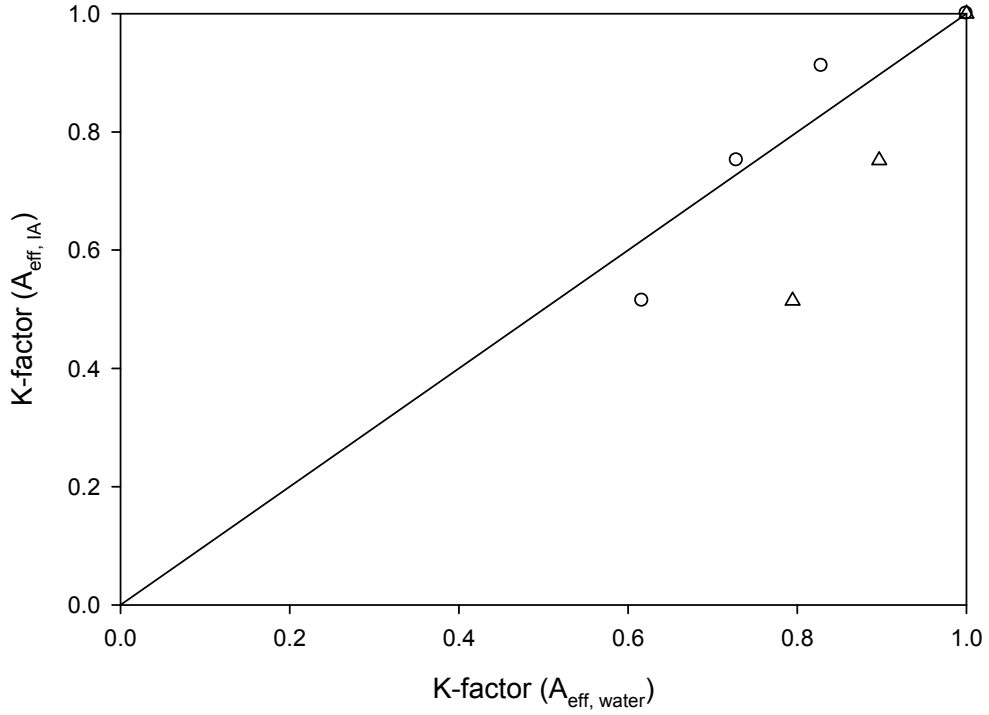

Figure 6-12: Parity plot of K-factor values obtained using either water flux measurements ($A_{eff, water}$) or image analysis after yeast suspension filtration ($A_{eff, IA}$). K-factor derived water flow experiments using cartridges with h_P = 10 mm (△) and h_P = 15 mm (○).

6.5 Definition and Testing of a K-Factor Based USD Methodology

Figure 6-13 illustrates the proposed USD methodology to improve the scale-up predictions from a flat sheet disc. The process is based on a quick and easy estimate of flux and product transmission with a minimum quantity of material using a flat sheet disk, followed by adjustment of the throughput performance using the K-factor approach, so as to quantitatively predict performance of a pleated membrane cartridge. A K-factor is selected that most closely matches the configuration of the large-scale cartridge in terms of h_P and PPD.

To test the proposed USD methodology a yeast suspension (7.7 gL^{-1}) containing BSA (1 gL^{-1}) in a 0.03M sodium phosphate buffer (pH = 7.4) was filtered

through a range of flat sheet and cartridge configurations. This is the same feedstock that was used to characterise the performance of the 10" $UEAV_{24,\ 1}$ cartridge in Section 3.4.3. An example of the throughput data obtained is given in Figure 6-14. The same V_{max} methodology, based upon a standard pore blockage model, as was used in Chapter 5 was again used to predict the maximum volume (V_{max}) that could be filtered by the membrane filters before blocking. A good fit (R^2>0.98) to the standard pore blockage model was seen during the period in which the volume throughput was no longer constant (after 16 min) due to fouling of the membrane. This was also the case for all of the configurations used. The values of V_{max} and R^2 for all the configurations tested are given in Table 6-3.

The performance prediction from a flat sheet membrane to the large-scale pleated cartridge is normally based upon product transmission and volume throughput. The product transmission for the configurations studied is given in Table 6-3. The small-scale flat sheet disc was seen to give a good prediction to the large-scale pleated cartridges with variations of 5% and 6% seen for the 10" $EAV_{10,\ 1}$ and 10" $UEAV_{24,1}$ cartridges respectively.

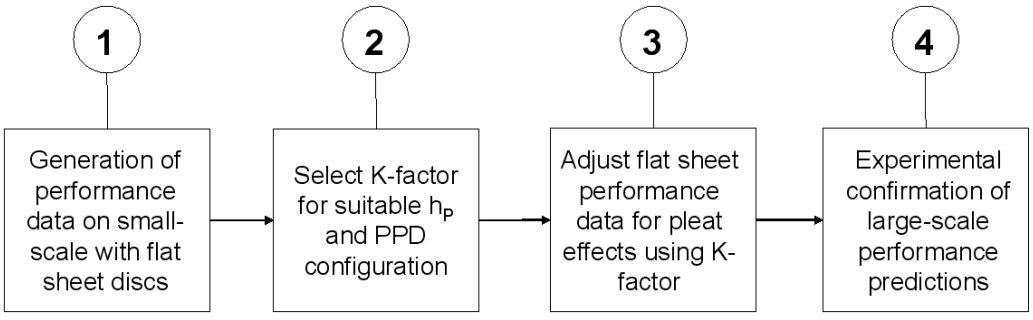

Figure 6-13: Illustration of the proposed USD K-factor methodology for improved scale-up prediction from a flat sheet disc to a pleated membrane cartridge.

In a typical throughput scale-up scenario, the calculated parameter V_{max}/A_m would be used to predict the large-scale performance from the small-scale performance prediction. Values of V_{max} / A_m parameters for the configurations used are given in Table 6-4. For the scale-up to be accurate, the value of the V_{max}/A_m for the flat sheet disc (57 Lm^{-2}) should closely match that of the large-scale counterpart. For scale-up prediction without the use of the K-factor approach, this is not seen to be the case for either of the large-scale configurations used in this study. The difference between the small-scale and the large-scale cartridge was 49% and 39% for the 10" $UEAV_{24,1}$ and 10"$EAV_{10,1}$ cartridges respectively.

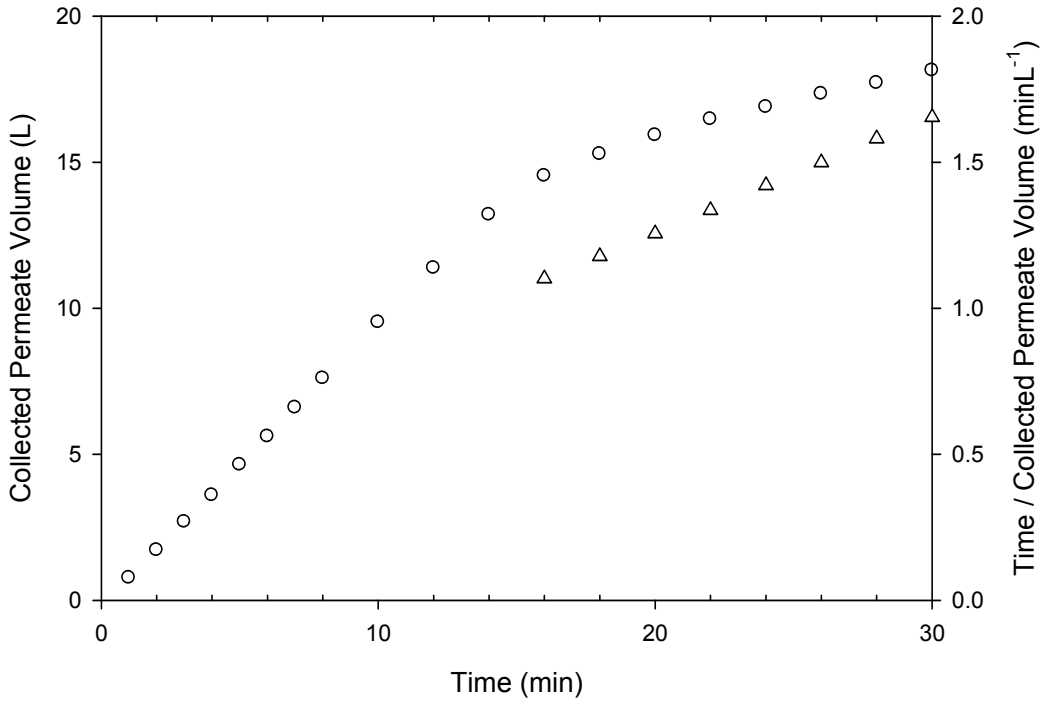

Figure 6-14: Volume throughput data for 10" $UEAV_{24,1}$ pleated cartridge, when filtering 7.7 gL^{-1} yeast solution containing 1 gL^{-1} BSA in a 0.03M phosphate buffer solution (pH=7.4). Data plotted is collected permeate volume (○) and time / collected permeate volume (△). Experiment conducted as described in Section 2.4.1.

Table 6-3: Calculated V_{max} values from experimental data. High R^2 values show good fit between the standard blocking model and the experimental data.

Cartridge configuration	Standard performance data				USD method parameters			
	V_{max} (L)	R^2	Product Transmission (%)	A_M (m^2)	K-factor (water)[1]	$A_{eff, water}$ (m^2)	K-factor (yeast)[2]	$A_{eff, IA}$ (m^2)
10" $UEAV_{24, 1}$	28	0.98	87	1.06	0.49	-	0.52	-
10" $EAV_{10, 1}$	28	0.99	88	0.68	0.79	-	0.52	-
25mm flat sheet disc	1.8×10^{-2}	>0.99	91	$3.8\times10^{--4}$	1	$3.8\times10^{—4}$	1	$3.8\times10^{--4}$

[1] K-factors taken from Figure 6-4. K-factor selected based upon closest match to configuration of h_P and PPD measured for the 1" cartridges used.
[2] K-factors taken from Figure 6-10. K-factor based upon closest match to configuration of h_P and PPD. Note that only K-factors derived for a h_P of 10 mm was available for this method.

Table 6-4: Comparison of performance prediction from a flat sheet disc to 10" pleated cartridges using the K- factor methodology outlined in Figure 6-13.

Cartridge configuration	Actual V_{max} /A (Lm^{-2})	Flat sheet predicted V_{max} / A (Lm^{-2})			% Difference between predicted and actual V_{max} / A (%)		
		A_M	$A_{eff, IA}$	$A_{eff, water}$	A_M	$A_{eff, IA}$	$A_{eff, water}$
10" $UEAV_{24,1}$	30	57	30	28	47	-2	-9
10" $EAV_{10,1}$	35	57	30	43	39	-17	23

So as to investigate whether use of the K-factor could improve the accuracy of the scale-up prediction, the methodology defined in Figure 6-13 was applied to the throughput performance data given in Table 6-3. K-factors derived from both the water flow and image analysis techniques presented in Section 6.3 and 6.4 respectively were used independently to assess their relative merits in improving the performance prediction of the flat sheet membrane. The selection of K-factor was based upon the closest match in terms of h_P and PPD to the large-scale cartridge that was the subject of the performance comparison. The K-factors used and the corresponding value of A_{eff} are given in Table 6-3 for all the configurations used.

The USD predictions based on the flat sheet disc experimental data were obtained by multiplying the value of V_{max} / A_m by the K-factor selected for each of the large-scale configurations. This generated a scale-up factor based upon A_{eff} and not A_m, and is a better reflection of the available membrane area within the pleated cartridge. The modified scale-up parameters are given in Table 6-4 based either on using $A_{eff, IA}$ or $A_{eff, water}$. Generally, an improvement in scale-up prediction was seen when the K-factor were used to adjust the experimentally derived performance data obtained from the flat sheet disc experiments. The K-factors generated using the image analysis technique in Section 6.4 ($A_{eff, IA}$), were seen to give the greatest improvement in the performance prediction. However, when the K-factor obtained from water flow experiments ($A_{eff, water}$) was used then improvements in performance prediction were still seen relative to the uncorrected performance prediction from the flat sheet. This was particularly seen to be the case for performance prediction of the 10" $UEAV_{24,1}$ cartridge which was seen to be within 10% of the large-scale performance.

It can be generally stated that, based upon the limited number of experiments conducted in this study, the performance prediction based upon a K-factor derived from $A_{eff, IA}$ gives is better than that generated by $A_{eff, water,}$ which in turn gives a better performance prediction than for uncorrected experimental data collected from flat sheet membrane.

6.6 Discussion and Summary

Based upon the improved performance predictions presented in Section 6.5, the USD methodology shows good promise as a means of improving the scale-up prediction made using flat sheet membrane, particularly when using a K-factor based upon $A_{eff, IA}$.

The improved performance predictions are based upon a limited number of experiments, and thus further validation of the technique would be required to establish the robustness of the technique. Furthermore, $A_{eff, IA}$ was based upon image analysis performed upon a cartridge with a h_P of 10 mm. As such it is not necessarily intuitive to use the effective area generated from cartridges with h_P = 10 mm to predict the performance of a large-scale cartridge such as 10" $UEAV_{24, 1}$ which has h_P = 24 mm.

As described in Section 6.1, the aim of this chapter was to develop and test a USD approach that improves the scale-up from a flat sheet by correcting for the pleating effects. This aim was partially achieved through a number of objectives that were fulfilled. The main conclusions are as follows:

- Pleat crowding was seen to reduce solute accessibility into the pleat, which in turn was seen to be a non-linear function of h_P and PPD. As both h_P and PPD increased, accessibility decreased leading to a reduction in effective membrane area, A_{eff} (Section 6.2).

- An USD methodology as shown in Figure 6-13, was developed and tested. The USD methodology used A_{eff} calculated from water flow experiments ($A_{eff, water}$) (Section 6.3) or image analysis ($A_{err, IA}$) (Section 6.4) to generate a scale-up parameter, K-factor, which in turn can be used to correct experimental data generated on the small-scale using flat sheet membrane (Section 6.5).

- The USD methodology was used to predict the performance of large scale pleated cartridges (Section 6.5). In some instances performance predictions were within -2% and -17% of a 10" $UEAV_{24,\ 1}$ and 10" $EAV_{10,\ 1}$ cartridge respectively. This represented a significant improvement over using flat sheet experimental data without any correction.

- Based upon a limited number of initial experiments the USD approach appears to work well for K-factors calculated from $A_{eff,\ IA}$ and to a lesser extent for $A_{eff,\ water}$. However, further experimental study is required to validate these results.

In the next chapter the commercial and validation aspects of the scale-down pleated cartridge evaluated in Chapter 5 will be considered, which is a requirement for the award of an Engineering Doctorate (EngD).

7 Challenges to the Commercialisation and Validation of the Scale-Down Cartridge[‡]

7.1 Introduction and Aims

The scale-down pleated device designed and evaluated in Chapter 5 currently exists as a prototype (Section 2.3.2) that has shown good scaleable performance with fouling (Section 5.2) and non-fouling (Section 5.3) feedstock. Despite these promising initial findings many challenges remain to conversion of the prototype device into a robust commercial product.

The aim of this chapter is to discuss the key challenges to commercialisation of the scale-down pleated device and the steps required in technical, commercial and validatory areas to overcome them. The specific objectives of the chapter are:

- To describe a means by which the hold-up volume of the cartridge can be minimised (as noted in Section 5.8 through the optimisation of the housing and the experimental rig).

- To define the quality assurance and testing procedures that would be required to bring the scale-down pleated device to market as a product.

- To define the key commercial benefits of the scale-down pleated device over the currently used flat sheet discs, and present an economic case to support the strategy to maximise exploitation of these benefits.

[‡] This chapter is included in partial requirement for the award of the UCL Engineering Doctorate in Bioprocessing.

7.2 Technical Issues Involved with Product Development

In Section 5.8 it was concluded that further technical work was required to test the general applicability of the scale-down pleated device with more feedstocks. However, there are other technical challenges that exist and require further product development work. Foremost is the requirement involved in the optimisation of a housing to hold the scale-down pleated device, and the pumping rig into which the device will be inserted. If these are not optimised then the scale-down pleated device will not be feasible as a small-scale device for utilisation with low volumes of a customer's feedstock.

7.2.1 Development of an Optimised Housing

Throughout this study the scale-down pleated device has been contained within a standard 1" stainless steel housing. This does not represent an optimised solution for the scale-down device as the hold-up volume within the housing is large (~300 mL). This increases the amount of a customer's feedstock that would be required for each experiment, which is undesirable. Alternatively, a molded plastic housing could be used with the scale-down cartridge permanently fused around the pleated membrane. By using a molded plastic housing, the dead volume of the housing could be filled in with a plastic insert so that only the volume around the active pleated section was exposed to the feed (Figure 7-1). Such measures would likely reduce the dead volume by a factor of 20 down to just 5-10 mL.

Construction of the housing from plastic would have the added advantage that the device would be single-use (Bardo, 2008) and allow the user to simply connect the device into an existing experimental rig. Upon completion of the experiment the scale-down device would be easily disconnected from the rig and disposed of by incineration. There would be no need for the user to come into contact with the pleated cartridge and the material that may have built up upon the surface of the cartridge leading to enhanced operator safety. The single-use nature of the product would also reduce cleaning costs and allow for the device

to be treated with gamma radiation to achieve sterility instead of through steam sterilisation. This strategy aligns well with the current use of disposable filter cartridges within the industry (Galka, 2007).

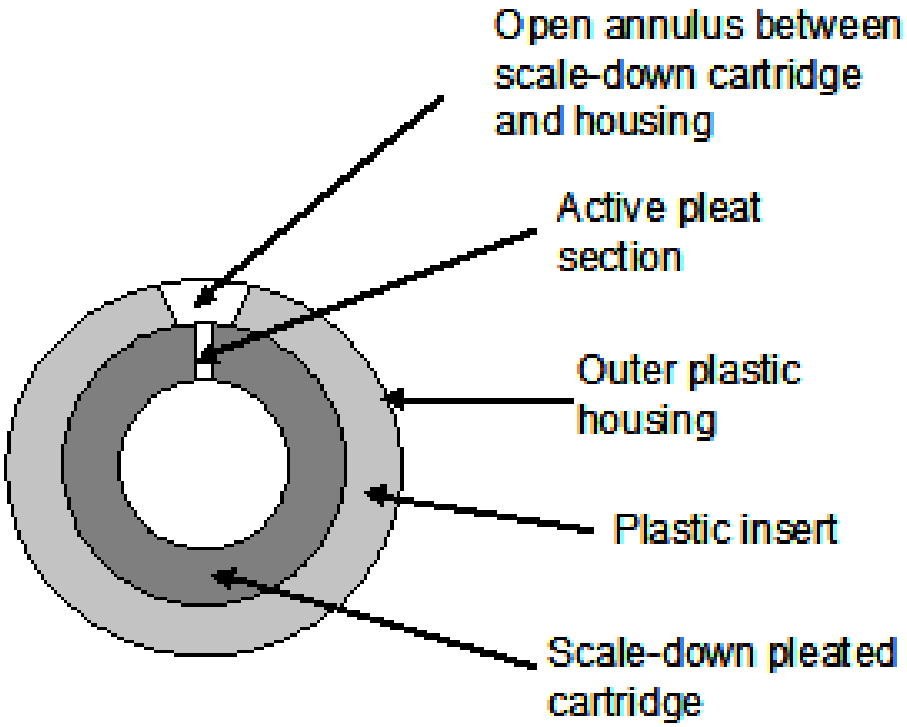

Figure 7-1: Illustration of cross-section of scale-down cartridge housed within a plastic housing containing a plastic insert to fill a section of the annulus between the outer casing of the scale-down pleated cartridge and the inner surface of the plastic housing.

7.2.2 Integration Within an Experimental Design Regime

The scale-down pleated device operates with the same constant flow regime as the large-scale pleated membrane cartridge filters (Section 5.3). As a result, a pump is required to supply the correct flowrate to the pleated cartridge. An experimental set-up can easily be produced into which the cartridge can be fitted. However, as the objective is to reduce hold-up volume, then an optimised pumping rig set-up is required to obtain the full benefits of scale-down experimentation. Such a set-up would require a pump able to supply a range of flow rates, a flow indicator upon the permeate line, all with a minimum hold up in tubing but without excessively large pressure drops. Two pressure indicators are required to provide the necessary transmembrane pressure and, based upon the results in Section 3.2.1, it would be advantageous if they were able to read the pressure from inside the housing, close to the surface of the scale-down filter cartridge. Such a rig, would provide a simple, optimised set-up into which the scale-down pleated cartridges could quickly be connected into. This would in turn give accurate prediction for large-scale performance using the minimum liquid volume.

7.3 Validation of Quality of Scale-Down Cartridge

7.3.1 Need for Validation

Validation in the bioprocess industry is the act of establishing documented evidence which provides a high degree of assurance that a specific process will consistently produce a bioproduct to pre-determined specifications and quality attributes (MHRA, 2007). Validation is necessary as the bioproduct will ultimately be used within humans and as such if not tightly controlled could generate serious side-effects including the potential to cause death (MHRA, 2007). Furthermore, the bioproduct itself is inherently complex as is the process that is required to produce it. The intended use of the scale-down pleated device, however, is not to form part of the process to generate the bioproduct. Instead it is a device intended to be used in the design, optimisation and scale-up of new

bioprocesses, as well as troubleshooting of existing processes, so as to remove the need for extensive pilot-scale process development. Thus the output from scale-down process development could be used to support the design and operation qualification of a process, and as such the device must provide performance predictions of the large-scale equipment that are robust and consistent. Hence, validation of these performance predictions to ensure that they are robust would be required. It is not envisaged that the scale-down cartridge would impact upon installation qualification or performance qualification as installation qualification is focussed on the validating the correct installation of critical components of the system (ISPE, 2001), whilst performance qualification is focussed on integrating equipment with correct procedures and systems (ISPE, 2001).

A summary of the key performance requirements for scale-down pleated devices are as follows:

- Consistent manufacture without leaks and consistent values for bubble test or forward flow test.
- Successful completion of specified filtration duty requirement, e.g. complete removal of microbial material for sterile filters, or 10 log reduction in virus levels for viral filters.
- Make no chemical change to the process stream before or after filtration, also avoiding the leaching of new components into the process stream.
- Provide accurate scale-up to the large-scale pleated cartridge.

The fourth point is especially important if companies are conducting the majority of their process characterisation and process validation using scale-down models, before qualification using full-scale lots (Thompson et al., 2007).

7.3.2 Troubleshooting of Failures in Performance Functions

In order to understand the ways in which failures in performance functions can take place and, more importantly, put in place activities to avoid them, a Failure Modes and Effects Analysis (FMEA) can be conducted by a team within the filter production company. A FMEA is a process for identifying likely defects before they occur, using a rating scale (Thomsett, 2005). The aim of the study is to identify areas at an early stage of product development where preventative measures will be useful in a process.

Whilst a FMEA study would normally be conducted by an experienced team, an example study for a scale-down pleated device containing a sterile rated membrane is given in Table 7-1 to illustrate the methodology. Function failures are arbitrarily rated on a 1-10 scale in terms of severity, occurrence and detection. The ratings are collected together in the Risk Priority Number (RPN) term. Failure modes with high ratings require investigation to ensure that there are activities in place to avoid the failures.

In Table 7-1 it can be seen that there are several failures with high risk priority numbers, making them important issues to deal with during a validation study. These failures have a high RPN primarily because they introduce new features into the manufacturing process. Recommended activities to reduce the impact of failures that show an RPN>100 will be discussed further. In Section 7.3.3.

Table 7-1: Example failure modes and effects analysis for the performance qualification of a scale-down pleated device containing sterile rated membrane.

Function	**Failure Mode**	**Effects**	**S[I]**	**Cause**	**O[II]**	**Current Controls**	**D[III]**	**RPN[IV]**
Sterile Filtration	Filter cartridge contains leak	Microbial material allowed to pass	8	Membrane not fully sealed into the cartridge	7	Leak test all cartridges	3	168
				Membrane pore size too large	2	Leak test all cartridges	3	48
				Exposure to high pressure	3	Rate cartridges for maximum operational pressure. Operate within rating.	5	120
				Process stream affects membrane structure	2	Test process stream with cartridge, followed by leak test.	3	48
				Degradation of membrane porous structure due to steam sterilisation	2	Forward flow testing before and after steam sterilisation	3	48
Filter Inert to Process Fluid	Leachates enter process stream from filter cartridge	Foreign materials enter a process stream with no means of removal	7	Filter cartridge materials of construction sensitive to stream	2	Selection of cartridge filters tested for leachables. Source of materials of construction tightly controlled.	5	70
				Composition of stream changes	2	Test variation in process stream conditions with filter cartridges.	4	70
Performance prediction	False large-scale performance prediction	Wrongly sized large-scale equipment	6	Leak in membrane	7	Leak test all cartridges	3	126
				Variation in active membrane area	5	None	10	300

Notes: [I] S = Severity rating. [II] O = Occurrence rating. [III] D = Detection rating. [IV] RPN = Risk priority numbers = S × O × D

7.3.3 Recommended Activities

7.3.3.1 Reduce Risk of Cartridge Leaking

There is the potential for an increased risk of leaks in the scale-down cartridge format for a number of reasons. Multiple side seals have been introduced where previously there was only one. The side seals used also involve a new material, the hydrophobic material of the inactive cartridge areas. Finally, the scale-down pleated device is a 1" cartridge, which does not have a fully validated manufacturing procedure to support the production of the cartridges.

To help overcome these issues, the following are recommended to be carried out in a validation plan:

- Leak test (see Section 1.5.3) heat seals present within the 1" scale-down pleated devices at a range of heat seal temperatures, with an aim to correlate cartridge hydraulic integrity against heat seal temperature. Thus, the heat seal temperature that gives the greatest hydraulic integrity would be identified.

- Carry out leak test with a range of cartridges containing different active membrane types, such as virus removal membranes. The aim here is to ensure that all membrane types envisaged for use in the scale-down cartridge can be sealed against the hydrophobic packing material.

- Develop a robust manufacturing procedure with well-defined procedures and operating ranges for production of the cartridges in a 1" format.

All of these options would require the generation of large numbers of scale-down cartridges to ensure that a low failure rate is achieved.

7.3.3.2 Reduce Risk of Failure Due to High Pressure

Whilst the scale-down pleated devices would be rated for a maximum operating pressure, the sensitivity of a failure to exposure above this maximum operating pressure can be pre-determined. Thus, a study would be required to test the strength of the membrane and heat seals to operation at a range of pressures close to and above the maximum specified operating pressure. A leak test could then be used to identify failures in the cartridges, which could be further linked to selection of membrane materials and the temperature used to achieve the heat seal. This study would require repetition for all membrane types to be installed within the scale-down cartridge.

7.3.3.3 Reduce Variation in Active Membrane Area

As the scale-down pleated device is a small-scale device containing a low active membrane area, the sensitivity of the device to changes in membrane area is high, particularly as all performance predictions are scaled-up based on the installed membrane area. However, well defined manufacturing procedures where by the exact length of pleated membrane are repeatedly used, and the trimming of the membrane area is precise would reduce the occurrence of variation in the membrane area. Once again, robust testing of the manufacturing process would be required whereby several hundreds of cartridges would be required without the addition of end caps (see Section 1.4) so that the cross-section of the pleated cartridge could be seen and the membrane area calculated.

Thus, whilst numerous areas exist whereby the quality of the scale-down cartridge and the scale-down approach could fail, there are many steps that can be implemented to reduce the occurrence of the failure. These steps can be documented in a master file to provide assurance to the customer and, where required, the regulator of the robustness and consistency of the devices and the scale-down approach.

7.4 Commercialisation Strategy

The market for pleated cartridge filters is populated by a large number of companies (Allegrezza et al., 2008), such that a new product would require significant improvements and benefits to the customer in order to further capture market share. This section outline a strategy to achieve this break into the market for the scale-down pleated device.

7.4.1 Benefits of the Device

It was discussed in Section 1.7.5.1 that the scale-down approach allows for process development to be carried out at an earlier stage in product development (see Figure 7-2), as it allows for the generation of process related data using small volumes of a feedstock that is likely to be scarce at this stage. This provides more time for process development related activities and removes the need for carrying out process design at the pilot-scale where it is more time-consuming and expensive. Such an approach would make a valuable proposition to a biopharmaceutical company. For the filter manufacturer, the scale-down approach allows for interaction with a potential customer at an earlier stage, when it is likely that the customer would be more receptive to new filter technologies. Also, the process development activities provide an opportunity to capture the later large-scale custom of the company should the drug under development be successful in clinical trials.

The scale-down approach also offers advantages for the biopharmaceutical companies who already have a process in place, as the scale-down pleated devices offers an opportunity to conduct process improvements, or trouble-shooting of the process using a small-scale device that closely matches the performance of the large-scale, whilst requiring significantly less feedstock.

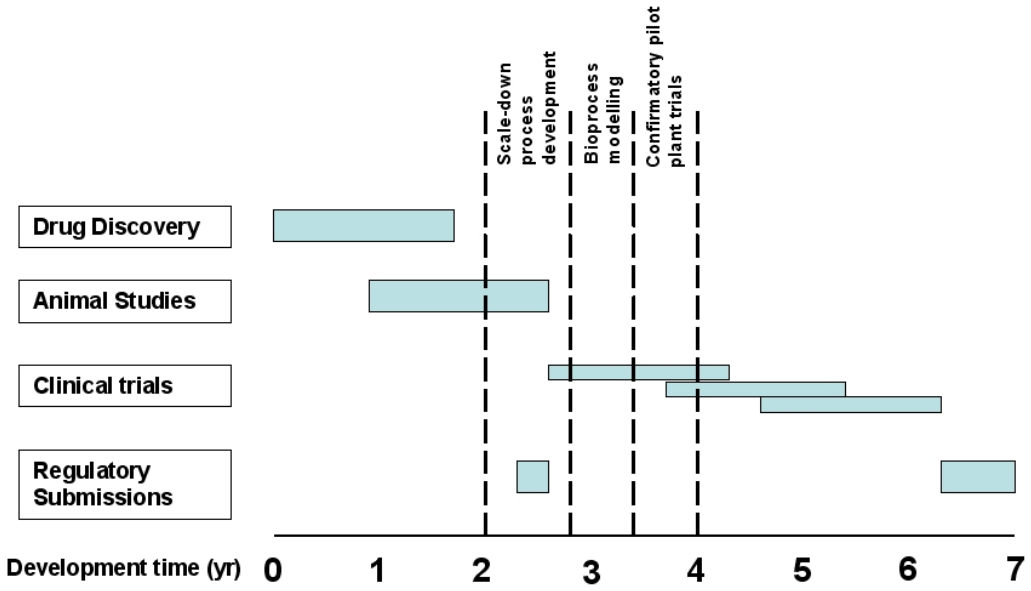

Figure 7-2: Typical timeline for biopharmaceutical drug development. Scale-down studies allow for process development to take place at an early stage during drug product development. This is compared with current practice, which would involve pilot plant trials using existing equipment from year 3 to year 4.

The benefits to both the filter company selling the scale-down pleated device and potential customers are summarised in Table 7-2. Specific performance advantages are such that at present the scale-down pleated device is about 45% better at predicting the performance of the large-scale 10" cartridge, than is the flat sheet disc (Figure 5-9). At the very least this will remain the same in the future, as there is room for improvement in the method of scaling from flat sheet discs. However, the scale-down pleated device is likely to improve in its performance relative to the 10" cartridge over time as greater consistency is achieved in installing the same area of active membrane area inside of each cartridge and in reduction of hold-up volume. The only foreseeable method to improve the performance of the flat sheet disc relative to a 10" cartridge is the USD approach outlined in Chapter 6 of this thesis. However, as discussed in the Section 6.6, there is considerable development work required to make the method robust in its prediction of performance. Thus, the scale-down device should enjoy a number of years of competitive market advantage, which should be exploited at the earliest opportunity to gain maximum financial benefit..

Table 7-2: Benefits of the scale-down approach to the filter manufacturer and their potential customers.

Benefits to the Filter Manufacturer	Benefits to the Customer
Improved confidence in prediction of performance of cartridge filters with the customer feedstock.	Improved scale-up to large-scale, optimising the use of the large-scale cartridge.
Competitive advantage against rival manufacturers who rely upon flat sheet discs and over-predictions of performance to sell to customers.	Ability to conduct meaningful process development studies at an early stage of drug development.
Enhanced tool for troubleshooting customer feedstock without requiring a fully pleated cartridge.	Reduce the scale of pilot-plant studies, such that only conformational batches are required.
	Troubleshoot existing processes without a requirement to use large-volumes of feedstock.

7.4.2 Commercial Exploitation of Benefits

It is considered unlikely that the scale-down pleated device cold be sold in sufficient volumes that it would generate enough revenue as a standalone product. This is due to the requirement for the device to be sold at a low enough price to make it acceptable as a small-scale process development tool. However, as discussed in the Section 7.4.1, the scale-down pleated device can be used to facilitate the capture of the large-scale pleated cartridge market, where cartridges are disposable and thus replaced on a regular basis. The strategy to capture more of the market would be to exploit the improved performance prediction of the scale-down pleated device to offer a more accurate and robust scale-up prediction to the large-scale cartridge. It is likely that the predicted size of the large-scale cartridge will be lower as the scale-down pleated device does not require over-designing of the large-scale process to account for the reduced confidence in scale-up prediction. This would present an attractive proposition to

potential customers to reduce their costs. An analysis of the economics of this strategy for a flat sheet disc and the scale-down pleated device are given below.

7.4.2.1 Economic Case for Flat Sheet Disc

The flat sheet disc represents the base case scenario, as it is the device currently in use in the biopharmaceutical industry. Key data from an economic case carried out to predict the cost of large-scale cartridges required annually is given in Table 7-3. It can be seen that whilst the cost of the study is relatively low, the cost of the over-prediction of the membrane area required for the large-scale process is high.

Table 7-3: Key data from the economic case for use of flat sheet disc for large-scale membrane process design. Assumptions for the study are given in Appendix B.

Cost of study	£500 per study
Variation from actual large-scale performance	55%[I]
Scale-up factor	50%[II]
Total over-prediction of large-scale performance	105%
Cost of over-prediction	£1050 per cartridge
Total cost of over-prediction[III]	£12,600 per year
Total revenue from cartridges[III]	£24,600 per year

[I] Based on Figure 5-10
[II] Assumed factor based upon uncertainty of prediction
[III] Assuming use of 12 cartridges per year.

7.4.2.2 Economic Case for Scale-Down Pleated Device

The same economic case as for the flat sheet disc (Section 7.4.2.1) has been applied to the scale-down pleated device described in Section 2.3.2. Key data from the case is given in Table 7-4. In this scenario it can be seen that the cost of the study is higher due to the increased cost of the scale-down device and an increase in the cost of the feed used. However, the scale-down pleated device significantly lowers the cost of over-prediction due to a more accurate scale-up. In this scenario a saving of over £10,000 would be achieved on a yearly basis, by the customer.

Table 7-4: Key data from the economic case for use of scale-down pleated device disc for large-scale membrane process design. Assumptions for the study given in Appendix B.

Cost of study	£2100 per study
Variation from actual large-scale performance	10%[I]
Scale-up factor	10%[I]
Total over-prediction of large-scale performance	20%
Cost of over-prediction	£200 per cartridge
Total cost of over-prediction[III]	£2400 per year
Total revenue from cartridges[III]	£14,400 per year

[I] Based on Figure 5-10
[II] Assumed factor based upon uncertainty of prediction
[III] Assuming use of 12 cartridges per year.

7.4.2.3 Discussion of the Economic Cases

By using the scale-down pleated device and based upon the experimental results described in Section 5.4, and also the data provided in Appendix B, a cost reduction of some £10,200 is achieved for the customer. This makes a valuable proposition for the customer to adopt the filter cartridges on the large-scale, thus allowing the filter manufacturer to capture a greater share of the market. Ironically, however, the reduction in customer filter costs will affect the revenues of the filter manufacturer. Thus, to make-up for the loss in revenue the filter manufacturer must capture another new customer of the same size for every two customers that have had their costs reduced. As a minimum, this is achievable and it is likely that with the potential cost reductions available to a customer the actual increase in adoption will be considerably more. The economic cases do not account for the opportunities to sell higher value cartridges to the customer during the early stages of process development. This would likely increase revenue further, if customers could be convinced of the advantages of adopting these new technologies by the scale-down study.

7.5 Discussion and Summary

The aim of this chapter was to present a discussion of the key challenges to commercialisation of the scale-down pleated device and the steps required in technical, commercial and validatory areas to overcome them. This aim was achieved through the proposition of solutions to a number of objectives that were outlined in Section 7.1.

- By using a molded plastic housing into which the scale-down pleated device is permanently fused it should be possible to reduce the hold-up volume in the housing from 300 mL to 10 mL (Section 7.2.1). Tubing should be minimised within the pumping rig so as to further minimise hold-up volume.

- A quality assurance study would be required to show that any risk to the quality of the scale-down pleating device is very low, and that the area of membrane in the scale-down pleated device can be reproducibly manufactured (Section 7.3.3). Otherwise these two effects would have considerable impact upon the robustness of the device, and its application in the marketplace.

The key benefits that the scale-down pleated device has over a flat sheet disc, is the similarity in performance with a large-scale pleated cartridge (Figure 5-10). Thus a more robust and accurate scale-up can be achieved, vastly reducing large-scale over-prediction. This could reduce over-prediction by over 80%. The scale-down approach also allows for process development to take place at an early stage, offering the filter manufacturer the opportunity to engage with potential customers at an earlier stage in their process development activities, when they are likely to be more open to new membrane technologies.

8 Summary and Conclusions

8.1 Overall Discussion and Conclusions

The production of therapeutic drugs using bioprocesses based upon recombinant expression systems is now a well established technique within industry and generates products that address conditions that previously had no treatment or were poorly treated (Titchener-Hooker et al., 2008). These drugs are typically complex proteins and require a large number of operations to achieve a purity level suitable for administration to patients (Kalyanpur, 2000). Within a typical bioprocess platform, as illustrated in Figure 1-1, it can be seen that pleated microfiltration cartridges are used extensively in many different areas. These microfiltration cartridges perform different roles depending upon whether the filter is rated for sterile filtration or just for bioburden reduction filtration (Campbell, 2005). The method by which the membrane filtration cartridges are manufactured was described in Figure 1-4. Flat sheet membrane is first corrugated, before packs of corrugated membrane are wrapped around a perforated core. For filters that face liquid feedstock, the typical manufacturing approach is to maximise the membrane area within the cartridge, which is achieved by packing a large number of pleats into the unit (high PPD), increasing the height of the pleat (h_P) and in some cases by folding it over.

Although the microfiltration cartridges contain pleated membrane, flat sheet membrane formats are currently used to conduct small-scale process development experiments that seek to predict the performance of the large-scale, pleated counterpart. These bioprocess development activities typically occur when the feedstock is limited in availability and is also expensive to produce (Zhang et al., 2007). However, a number of studies have reported that there are significant differences between the performance prediction of the flat sheet membrane when compared to the large-scale pleated cartridge (Chandler et al., 2004; Rajniak et al., 2008). This leads to inaccuracy in the scale-up prediction with cartridges over-sized so as to account for uncertainty in the small scale

trials. In turn this increases the cost of the large-scale process, as the cartridge filters are used extensively within the process and also are typically only used once before disposal (Bardo, 2008).

The reasons why there is such a difference between the performance of the flat sheet membrane and the pleated cartridge is not at present clearly understood. Previous studies have taken a simulation approach to model the characteristics of the pleat and the effect that this can have upon permeate flux (Waghode et al., 2007; Wakeman et al., 2005). However, these studies are not validated by experimentation, and do not produce a means by which performance predictions of the pleated membrane cartridge can be made on the small-scale. As such, a robust and accurate small-scale method by which the performance of large-scale pleated cartridges can be predicted, still remains to be identified. More accurate small-scale studies would also reduce the size of pilot-scale confirmation studies, increasing bioprocess development efficiencies further. Consequently, as described originally in Section 1.8, the aim of this thesis is to develop scale-down and ultra scale-down approaches to the rapid design and optimisation of microfiltration processes using pleated membrane cartridges. An overview of the approach taken to achieve this aim is shown in Figure 8-1, along with a summary of the key findings from this work.

For the purpose of this study the 10" $UEAV_{24,\ 1}$ 0.2 µm rated pleated cartridge filter was selected as the large-scale target due to its widespread use in industry. Initial studies sought to characterise the performance of the large-scale target within a standard cartridge housing (Chapter 3). Pressure drop and hydrodynamic housing effects were investigated (Section 3.2), to assess whether they should be accounted for when measuring the performance of the large-scale cartridge. However, the magnitude of the effects was considered small relative to the operation of a real filtration process. Consequently, it is concluded that the hydrodynamic effects related to the cartridge housing can most probably be neglected in the design of any scale-down cartridge device.

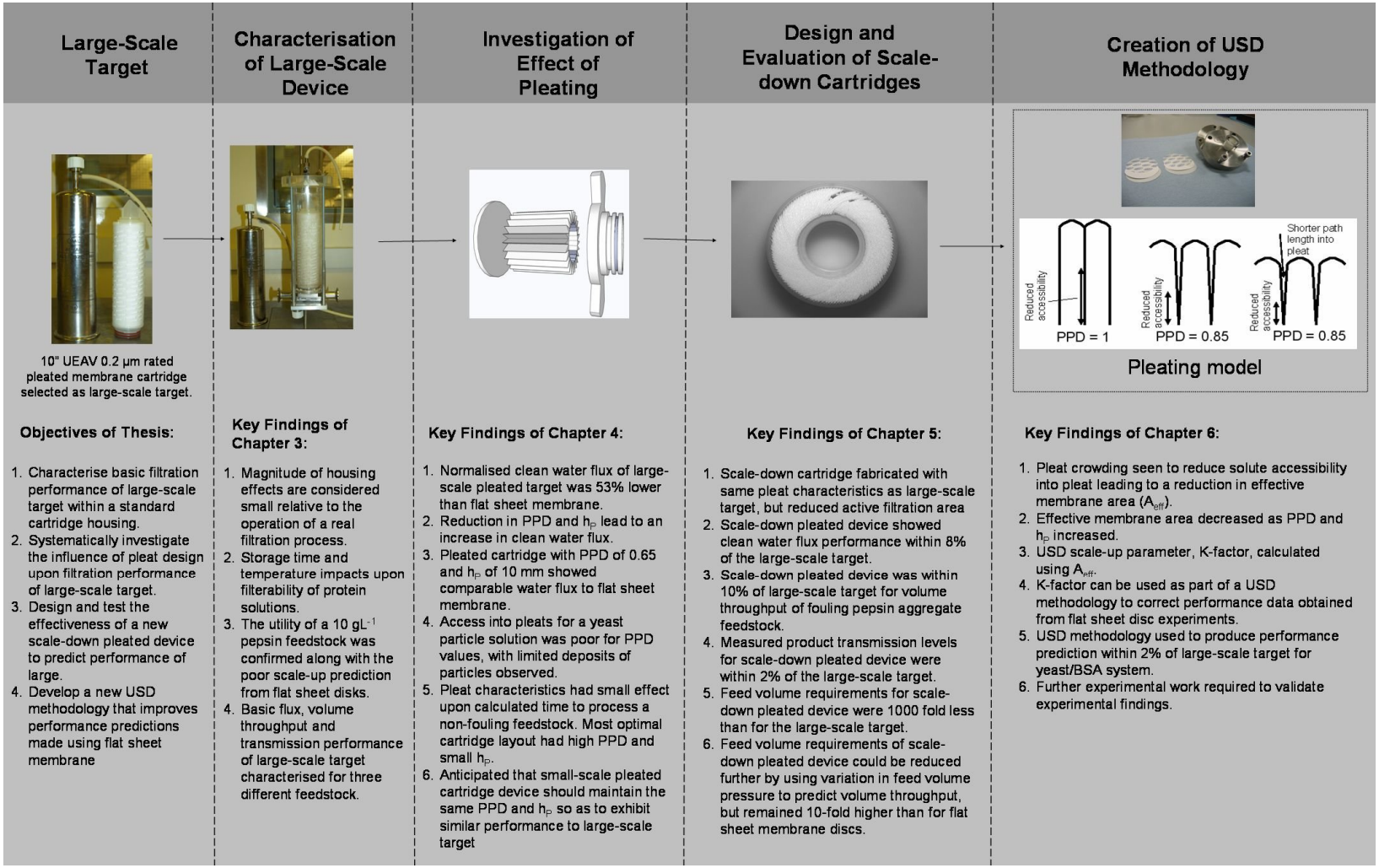

Figure 8-1: Overview showing approach taken for the creation of scale-down and USD methods for prediction of large-scale pleated membrane cartridge performance. The main findings of this work are summarised within for each of the chapters.

As protein solutions have typically been seen to foul microfiltration membranes during filtration (Kelly et al., 1997), an investigation was conducted (Section 3.3) to investigate this effect with the 0.2 μm rated EAV membrane that was used within the large-scale target. It was seen that both storage time and temperature had an impact the filterability of two protein solutions: 1 gL^{-1} solution of BSA in 0.03 M phosphate buffer (pH 7.4) (Figure 3-15 – 3-16); and 10 gL^{-1} pepsin in 0.03 M phosphate buffer (pH 7.4) (Figure 3-17). As such, it is concluded that for this study, fresh preparations of the protein solution should be used for filtration experiments so as to ensure that consistent feedstock properties were used throughout. Pepsin was chosen as a representative feedstock as the fouling potential was higher than BSA reducing the volume of feedstock required to conduct filtration studies on the large-scale. The performance of the large-scale target was characterised (Section 3.4) for three feedstocks: water (non-fouling), pepsin solution (fouling), yeast and BSA solution (fouling). This provided the basic flux, volume throughput and transmission data against which the small-scale approaches studied were compared.

The effect that pleating had upon the performance of the large-scale target was systematically investigated next, so as to understand which pleat characteristics might require further consideration when designing new small-scale approaches. Unlike the previous studies described in Section 1.6 this was achieved on an experimental basis using novel cartridges specifically fabricated with varying pleat characteristics. These differing characteristics were: pleat packing density (PPD), pleat height (h_P), and pleat type. The range of cartridges used is described in Table 2-1. The measured normalised clean water flux of the large-scale target was 53% lower than that measured for a flat sheet disc (Figure 4-2), which compared well to the difference reported by other researchers (Rajniak et al., 2008). It was seen that by reducing both PPD and h_P, the measured clean water flux increased (Figure 4-3 and 4-4) and that a cartridge with a PPD of 0.5 and h_P of 10 mm gave comparable clean water flux to that of the flat sheet membrane. Thus, it is concluded that pleating does impact upon the performance of the large-scale cartridge, and that the effect varies as a function of PPD and h_P.

To investigate the impact of pleating further, a yeast suspension was used as a probe to investigate particle access into the pleat. After filtration of this feedstock, inspection of the surface of the membrane showed, that, for cartridges with PPD beyond 0.85 (Figure 4-6) there were areas of limited or no evidence of particle deposition. Further analysis of the surface of the membrane revealed that the position of the areas without deposits were situated primarily towards the base of the pleat (Figure 4-14). It is concluded that pleat crowding, caused by high PPD, lead to areas within the pleat structure that were inaccessible to the yeast cell challenge. Furthermore, it is concluded that any small-scale technique must account for the effects of pleating by either incorporating the same pleat characteristics or modelling for the effects of pleating.

In Section 1.7.4, an approach taken by other researchers was described, in which they sought to scale-down the performance of a centrifuge by rendering areas of the centrifuge inaccessible to the process fluid. This approach lead to a reduction in the separation area and hold-up volume, which in turn lead to a reduction in feed volume requirements. However, as the key characteristic for separation (bowl diameter) of the centrifuge remained the same, the performance predictions obtained at the smaller scale were comparable to the large-scale centrifuge. A similar philosophy was taken in this work whereby areas of the pleated cartridge were rendered inactive for filtration by introducing hydrophobic material into the pleated membrane pack. This lead to a reduction in the active filtration area, whilst the characteristics of the pleat (PPD, h_P and pleat type) remained the same as for the large-scale target. The smallest scale-down pleated device contained 1.5 pleats of membrane (Figure 2-8) have an active membrane area of 1.51×10^{-3} cm^2. The performance prediction from these scale-down cartridges was assessed with two of the feedstocks used to characterise the large-scale target in Section 3.4: clean water; and a 10 gL^{-1} Pepsin solution in 0.03 M phosphate buffer (pH 7.4). The clean water flux of the small-scale pleated device was within 8% of the large-scale target, as seen in Figure 5-4. This represented a significant improvement over the 53% variation measured between flat sheet membrane and the large-scale target. For the pepsin solution, the performance of the small-scale pleated device was within 10% of the large-scale target as shown

in Figure 5-7. Again, this represented a significant improvement over the 41% variation measured between the flat sheet membrane and the large-scale target. Measured product transmission levels were within 2% from the measured level of the large-scale target. These performance predictions were obtained with a feedstock requirement 1000-fold less than the large-scale target (Table 5-1), however the feedstock requirement remained 10-fold higher than for the flat sheet membrane.

Further reductions in the feed volume requirement were achieved by applying a method typically used for predicting the performance of depth filters (Wang et al., 2006; Yavorsky et al., 2003) (P_{max} method), where the measured changes in feed pressure is used to calculate the maximum volume throughput of the cartridge (Section 5-6). This technique also generated performance predictions within 1% of the large-scale target, although the feed volume requirement still remained larger than for the flat sheet membrane.

Based upon these new findings it is concluded that the small-scale pleated device fabricated here represents an excellent scale-down technique for the generation of accurate performance predictions for pleated microfiltration cartridge filters. Thus, the scale-down device has applications in the design of new processes for the production of biopharmaceuticals, as an alternative to the current practice involving flat sheet membrane. The improvement in the predictive performance reduces the need to over-estimate large-scale membrane area requirements, which in turn should reduce the cost of the large-scale process and increase confidence in process development activities. The current scale-down pleated cartridge operates with feed volumes less than 200 mL, with the P_{max} method seen to use the least volume of feedstock. This reduction in volume would enable process studies to be performed earlier and to a certain extent more rapidly. However, further feed volume reductions would be difficult to achieve whilst maintaining the same pleat characteristics within the scale-down pleated cartridge as exists within the large-scale device.

To reduce the feed volume requirements even further, an approach whereby small-scale performance predictions based on flat sheet membrane data are corrected using key performance parameters was described in Section 1.7.5. This ultra scale-down (USD) approach was previously seen to improve the performance predictions achieved on the lab scale for centrifugation operations. This technique uses a small-scale technique that is not dependent upon maintaining the same configuration as the large-scale (Titchener-Hooker et al., 2008). Adoption of this philosophy was considered in Chapter 6 of this thesis, whereby experimental data generated using flat sheet membrane would be corrected for the effects of pleating seen in Chapter 4, thus improving the performance prediction from flat sheet membrane, whilst maintaining the low feed volume requirements.

Based on the results generated in Figure 4-3, 4-4 and 4-6 a new parameter, effective membrane area (A_{eff}) was calculated. As both PPD and h_P increased, accessibility to the membrane within the pleats decreased leading to a reduction in A_{eff} (Figure 6-4). Relating A_{eff} to the actual membrane area (A_M) lead to the generation of a scaling parameter, K-factor. Thus a USD methodology was developed, described in Figure 6-13 that allowed for the correction of experimental performance data generated from flat sheet membrane by using a K-factor based upon the pleat characteristics of the large-scale target.

The USD methodology was used to predict the performance of the large-scale target for a system containing 7.7 gL^{-1} yeast suspended in 0.03 M phosphate buffer solution (pH 7.4), which also contained 1 gL^{-1} BSA. In one instance this performance prediction was within 2% of the large-scale target (Table 6-4), representing a significant improvement over the un-corrected flat sheet membrane, which showed a 47% variation from the large-scale target. However, the accuracy of the performance prediction depended upon the means by which the K-factor was obtained. Two methods were used; one using the results of clean water flux experiments (Section 6.3) and the other using image analysis of particle deposition upon the surface of the membrane (Section 6.4). The K-factor obtained by the image analysis method gave a better correction to the

performance data. Thus, based upon the limited number of experiments conducted in this final aspect of this work it is concluded that the USD approach works well for the K-factors calculated using the image analysis method.

A number of scale-down approaches have been presented in this thesis. In Chapter 4, the current practice of using flat sheet membranes was seen to give discrepancies in performance prediction when compared to large-scale pleated membrane cartridges. In Chapter 5 a new scale-down pleated cartridge was presented and tested as a potential new scale-down approach. Finally in Chapter 6 a USD methodology was described and tested to improve the scale-up prediction from flat sheet membrane. Table 8-1 compares various aspects of these different small-scale techniques. The scale-down pleated device currently gives a good performance prediction for a range of feedstocks. However, as has been previously noted, the feed volume requirements are such that the device could not be integrated with other USD techniques which typically operate with 10-fold less volume of feedstock (Titchener-Hooker et al., 2008). The USD methodology was seen to also give a good performance for K-factor generated using $A_{eff,\ IA}$. However, this was based only upon the results from experiments using just one feedstock, and as such the accuracy of the USD method requires further experimental verification with different feedstocks. Furthermore, the K-factor used was based upon the results from a cartridge with a different h_P to the large-scale target. As such further development work is required to generate k-factor for a wider range of h_P and PPD, ideally leading to the definition of a single model that defines K-factor as a function of PPD and h_P. Until these developments have been achieved then it remains difficult to recommend the technique as a robust small-scale approach. Consequently, it is concluded that based upon the findings of this work, the small-scale pleated device represents best current practice method for obtaining performance predictions of large-scale pleated membrane cartridge filters on the small-scale.

Table 8-1: Summary of key performance factors for the small-scale approaches studied within this thesis.

Scale-up Approach	Feed Volume Requirements	Accuracy of Scale-up Prediction	Integration With Other USD Methods	Development Status
Performance prediction generated using flat sheet membrane	Very Low (<20ml)	Poor for throughput. Variation of 53% and 41% seen for water and pepsin feedstocks respectively.	Good	Current standard practice within industry for wide range of membrane materials.
Performance prediction generated using scale-down pleated cartridge device	Low (<150ml)	Experimentally shown to be very good; 8% and 10% for water and pepsin feedstocks respectively.	Poor due to high feedstock requirement.	Would require validating accuracy of performance prediction with other membrane types before being accepted by industry.
Performance prediction based on USD methodology	Very Low (<20ml)	Good for K-factor based on $A_{eff,\,IA}$. Requires further experimental verification with other feedstocks..	Good	Requires further development and verification studies

So as to meet the requirements of the Engineering Doctorate award, commercial and validation aspects were considered for the scale-down pleated device that was designed and evaluated in Chapter 5. In Section 7.1 it was concluded that further development work would be required to minimise the hold-up volume of the system that the scale-down cartridge device would be part of. In section 8.2 it was concluded that a quality assurance study would be required as part of the commercialisation process to ensure that the scale-down cartridges can be reproducibly manufactured such that there is minimal risk of the cartridge leaking and that any variation in batch to batch performance is low.

8.2 Future Work

This work has shown the application of new small-scale techniques to accurately predict the performance of large-scale pleated cartridge. Any future studies should build upon this work to make the small-scale techniques more robust and applicable for use on a wider scale.

In Chapter 4 novel cartridges were fabricated with different PPD and h_P. Due to limitations in manufacturing, it was only possible to produce cartridges with pleat heights of 10 mm or 15 mm. New tooling would be required to produce other pleat heights, but having these cartridges may help to better understand the effect that pleat height has upon the performance of pleated cartridges. Also, again due to manufacturing issues, no cartridges were fabricated with a PPD less than 0.65. It would be a valuable exercise to fabricate similar cartridges with PPD less than 0.65 so as to verify whether the non-linear decline displayed in Figure 6-11 is accurate.

In Chapters 4 and 6 the probing of particle accessibility into a pleat and effective area was achieved through the examination of yeast particle upon the surface of the membrane. However, the size of yeast particles is large and another tracer material, such as a protein modified with a luminescence tag may offer an alternative probe more representative of target biopharmaceutical proteins. This

could yield a more accurate picture of protein deposition in the pleats and the effective membrane area. Also, in Figures 4-6 and 6-7 – 6-9 only a limited number of pleats were used to determine the level of deposition. As a proof of concept, this approach is reasonable, however a more accurate approach would be to fully map the deposition across the whole membrane surface held within the cartridge.

Very little is presently understood at the microlevel about the hydrodynamics of flow of a fluid and particles within a pleat. The simulations run to date look at building factors which correct for the mismatch between flat sheet and pleated performance (Nassehi et al., 2005; Nassehi et al., 2006). More complete computational fluid dynamic models may offer a means by which a greater understanding of the flow within a pleat can be understood in terms of the driving forces that transport the particle from the bulk fluid to the membrane surface. This in turn could give insight into how and why particles deposit upon the surface of the membrane with a non-linear degree of deposition for high pleat packing densities and increased pleat heights. Particle size and concentration may play an important role in this non-linear deposition and incorporating these properties may provide a means by which pleating models can be further improved. CFD studies could also give greater insight into the optimal design of pleated cartridges for filtration of liquid feedstock.

The scale-down device presented in Chapter 5 has been tested with multiple feedstocks and was seen to give good performance predictions to the large-scale target. However, further work is required to verify whether the accuracy of the performance prediction can be maintained when the technique is applied to different membrane materials, such as: sterile filters (0.1 μm pore size) or viral filters (40 or 60 nm pore size). If successful, this would provide compelling evidence for the adoption of the scale-down pleated devices as a standard technique within industry.

The USD methodology described in Chapter 6 offered a means by which a more accurate prediction could be made using flat sheet membrane. However, the most

accurate predictions were made using $A_{eff, IA}$ which was derived from particle deposition patterns upon pleated membrane with h_P of 10 mm. These K-factors were subsequently used to correct for predictions to large-scale cartridges with h_P of 24 mm. It is not necessarily intuitive to use the effective area generated from cartridges with h_P = 10 mm to predict the performance of a large-scale cartridge containing a different h_P, thus further work is required to clarify this issue.

The accuracy of the USD methodology was only tested with one experimental system (yeast/BSA), testing of the methodology with further ranges feedstock systems would be required to validate the technique. Such a, system could be the pepsin feedstock used in Chapter 5. However, for this feedstock it should be noted that the flat sheet was seen to under-predict the performance of the large-scale target, as opposed to over-predict for the yeast/BSA system, and water system. This remains an issue, as in order for the USD method to be robust, knowledge of the large-scale is still required. Thus, further work is required to understand why the flat sheet membrane under-predicts some feedstocks, and not others.

The USD methodology at the moment depends upon selection of the K-factor from a limited number of PPD and h_P configurations. Generating these values is a time consuming process that requires large volumes of feedstock. Improving the accuracy of A_{eff} derived from water experiments would be an easier method for enlarging the matrix, however, if this cannot be achieved then work will need to continue with a particle suspension or a tracer system.

Experimental models have been presented that correlate the experimental data that has been obtained, but a more useful model would be one which combines both the effect of PPD and h_P into a single model that can be used to generate K-factor for a range of PPD and h_P. Such a model would be useful for the correction of performance predictions from flat sheet membrane, but may also provide a means by which the design of pleated cartridges can be optimised.

Ultimately it would be advantageous to use a robust pleating model with experimental data obtained from microwell flat sheet experiments, as these experiments allow for parallel and high throughput experimentation (Jackson et al., 2006). However, at the microwell scale, variation in the membrane porosity can become a dominant feature, such that membrane variation would have to be accounted for when carrying out the scale-up. Typical approaches have been to carry out a range of microwell experiments that use samples of flat sheet membrane from a number of locations with the roll of membrane. This may be an approach that will have to adopted if a pleating model was to be incorporated with microwell experiments.

As bioprocesses are typically a train of batch operations, it is convenient to think of them as discrete unit operations, however it is only by considering the development of the process as a whole that the entire process can be optimised, and that the interactions between unit operations can be understood (Pampel et al., 2008). Successful integration with other small-scale techniques would require a low feedstock requirement. A robust USD method for the prediction of pleated cartridge filters could be integrated with other USD techniques, with the aim being to achieve a full design of bioprocess using less than a litre of feedstock. To achieve this, further work may be required to develop ultra scale-down techniques for chromatography and cross-flow filtration.

References

Abramoff, M. D., Magelhaes, P. J., Ram, S. J. 2004. Image processing with ImageJ. Biophotonics International 11: 36-42.

Ahrer, K., Buchacher, A., Iberer, G., Jungbauer, A. 2006. Effects of ultra-/diafiltration conditions on present aggregates in human immunoglobulin G preparations. Journal of Membrane Science 274: 108-115.

Allegrezza, A., Ireland, T., Kools, W., Phillips, M., Raghunath, B., Wilkins, R., Xenopoulos, A. 2008. Membranes in the biopharmaceutical industry. In: Peinemann, K.-V. and Nunes, S. P., editor. Membranes for life sciences. Weinheim: Wiley-VCH. pp. 91-154.

Anderson, S. W., Collins, M., Manfred, M. 2009. Expanding disposable depth-filter applications. Genetic Engineering News 29:

Aranha-Creado, H., Brandwein, H. 1999. Application of bacteriophages as surrogates for mammalian viruses: A case for use in filter validation based on precedents and current practices in medical and environmental virology. Pda Journal of Pharmaceutical Science and Technology 53: 75-82.

Aranha-Creado, H., Peterson, J., Huang, P. Y. 1998. Clearance of murine leukaemia virus from monoclonal antibody solutions by a hydrophilic PVDF microporous membrane filter. Biologicals 26: 167-172.

Asenjo, J. A., Andrews, B. A. 2008. Challenges and trends in bioseparations. Journal of Chemical Technology and Biotechnology 83: 117-120.

ASTM. 2005. Standard test method for determining bacterial retention of membrane filters utilized for liquid filtration. ASTM F 838-05

Badmington, F., Wilkins, R., Payne, M., Honig, E. S. 1995. Vmax testing for practical microfiltration train scale-up in biopharmaceutical processing. Pharmaceutical Technology 8: 64-76.

Baleo, J. N., Subrenat, A., Le Cloirec, P. 2000. Numerical simulation of flows in air treatment devices using activated carbon cloths filters. Chemical Engineering Science 55: 1807-1816.

Bardo, B. 2008. Filter housings in the biopharmaceutical industry. In: Jornitz, M. W. and Meltzer, T. H., editor. Filtration and purification in the biopharmaceutical industry. New York: Informa Healthcare. pp. 193-230.

Baruah, G. L., Belfort, G. 2003a. A predictive aggregate transport model for microfiltration of combined macromolecular solutions and poly-disperse suspensions: Model development. Biotechnology Progress 19: 1524-1532.

Baruah, G. L., Belfort, G. 2004. Optimized recovery of monoclonal antibodies from transgenic goat milk by microfiltration. Biotechnology and Bioengineering 87: 274-285.

Baruah, G. L., Couto, D., Belfort, G. 2003b. A predictive aggregate transport model for microfiltration of combined macromolecular solutions and poly-disperse suspensions: Testing model with transgenic goat milk. Biotechnology Progress 19: 1533-1540.

Baruah, G. L., Nayak, A., Winkelman, E., Belfort, G. 2006. Purification of monoclonal antibodies derived from transgenic goat milk by ultrafiltration. Biotechnology and Bioengineering 93: 747-754.

Baruah, G. L., Venkiteshwaran, A., Belfort, G. 2005. Global model for optimizing crossflow microfiltration and ultrafiltration processes: A new predictive and design tool. Biotechnology Progress 21: 1013-1025.

Belfort, G., Davis, R. H., Zydney, A. L. 1994. The behavior of suspensions and macromolecular solutions in cross-flow microfiltration. Journal of Membrane Science 96: 1-58.

Berrill, A., Ho, S. V., Bracewell, D. G. 2008. Ultra scale-down to define and improve the relationship between flocculation and disc-stack centrifugation. Biotechnology Progress 24: 426-431.

Bessiere, Y., Abidine, N., Bacchin, P. 2005. Low fouling conditions in dead-end filtration: Evidence for a critical filtered volume and interpretation using critical osmotic pressure. Journal of Membrane Science 264: 37-47.

Bolton, G., LaCasse, D., Kuriyel, R. 2006a. Combined models of membrane fouling: Development and application to microfiltration and ultrafiltration of biological fluids. Journal of Membrane Science 277: 75-84.

Bolton, G. R., Boesch, A. W., Lazzara, M. J. 2006b. The effects of flow rate on membrane capacity: Development and application of adsorptive membrane fouling models. Journal of Membrane Science 279: 625-634.

Boulding, N., Yim, S. S. S., Keshavarz-Moore, E., Ayazi Shamlou, P. 2002. Ultra scaledown to predict filtering centrifugation of secreted antibody fragments from fungal broth. Biotechnology and Bioengineering 79: 381-388.

Bowen, R. 1993. Understanding flux patterns in membrane processing of protein solutions and suspensions. Trends in Biotechnology 11: 451-460.

Bowen, W. R., Calvo, J. I., Hernandez, A. 1995. Steps of membrane blocking in flux decline during protein microfiltration. Journal of Membrane Science 101: 153-165.

Bowen, W. R., Gan, Q. 1992. Properties of microfiltration membranes - The effects of adsorption and shear on the recovery of an enzyme. Biotechnology and Bioengineering 40: 491-497.

Bowen, W. R., Mongruel, A., Williams, P. M. 1996. Prediction of the rate of cross-flow membrane ultrafiltration: A colloidal interaction approach. Chemical Engineering Science 51: 4321-4333.

Bowen, W. R., Williams, P. M., Wilson, J. 2003. Quantifying extra interaction forces in charged colloidal dispersions from frontal ultrafiltration experiments. Colloids and Surfaces A-Physicochemical and Engineering Aspects 231: 67-83.

Bradford, M. M. 1976. A rapid and sensitive method for the quantitation of microgram quantities of protein utilizing the principle of protein-dye binding. Analytical Biochemistry 72: 248-255.

Buckland, B. 2005. The process development challenge for a new vaccine. Nature Medicine Supplement 11: S16-S19.

Caesar, T., Schroth, T. 2002. The influence of pleat geometry on the pressure drop in deep-pleated cassette filters. Filtration and Separation 39: 49-54.

Campbell, J. 2005. Validation of a filtration step. In: Rathore, A. S. and Sofer, G., editor. Process validation in manufacturing of biopharmaceuticals: Guidelines, current practices and industrial case studies. New York: Informa Healthcare. pp. 205-276.

Chan, R., Chen, V. 2004. Characterization of protein fouling on membranes: opportunities and challenges. Journal of Membrane Science 242: 169-188.

Chandler, M., Zydney, A. 2004. High throughput screening for membrane process development. Journal of Membrane Science 237: 181-188.

Chen, C. W., Huang, S. H., Chiang, C. M., Hsiao, T. C., Chen, C. C. 2008. Filter quality of pleated filter cartridges. Annals of Occupational Hygiene 52: 207-212.

Chen, D. R., Pui, D. Y. H., Liu, B. Y. H. 1995. Optimization of pleated filter designs using a finite-element numerical-model. Aerosol Science and Technology 23: 579-590.

Chen, J. C., Elimelech, M., Kim, A. S. 2005. Monte carlo simulation of colloidal membrane filtration: Model development with application to characterization of colloid phase transition. Journal of Membrane Science 255: 291-305.

Cohen, S. N., Chang, A. C. Y., Boyer, H. W., Helling, R. B. 1973. Construction of biologically functional bacterial plasmids *in vitro*. Proceedings of the National Academy of Sciences of the United States of America 70: 3240-3244.

Darcy, H. 1856. Les Fontaines Publiques de la Ville de Dijon. Paris: Dalmont.

Dileo, A. J., Vacante, D. A., Deane, E. F. 1993. Size-exclusion removal of model mammalian viruses using a unique membrane system. 1. Membrane qualification. Biologicals 21: 275-286.

Dowd, C. J. 2009. Multi-round virus filter integrity test sensitivity. Biotechnology and Bioengineering 103: 574-581.

Duclos-Orsello, C., Li, W., Ho, C. C. 2006. A three mechanism model to describe fouling of microfiltration membranes. Journal of Membrane Science 280: 856-866.

Dunnill, P., Hoare, M., Titchener-Hooker, N. J. 2003. A method and apparatus for producing a biomaterial product. GB 2364052 B.

Field, R. W., Wu, D., Howell, J. A., Gupta, B. B. 1995. Critical flux concept for microfiltration fouling. Journal of Membrane Science 100: 259-272.

Foley, G. 2006. A review of factors affecting the filter cake properties in dead-end microfiltration of microbial suspensions. Journal of Membrane Science 274: 38-46.

Galka, N. 2007. Life sciences: Trends in biopharmaceutical filtration and clarification. Filtration and Separation 44: 18-21.

Giglia, S., Yavorsky, D. 2007. Scaling from discs to pleated devices. Pda Journal of Pharmaceutical Science and Technology 61: 314-323.

Girones, M., Lammertink, R. G. H., Wessling, M. 2006. Protein aggregate deposition and fouling reduction strategies with high-flux silicon nitride microsieves. Journal of Membrane Science 273: 68-76.

Gitis, V., Adin, A., Nasser, A., Gun, J., Lev, O. 2002. Fluorescent dye labeled bacteriophages - a new tracer for the investigation of viral transport in porous media: 1. Introduction and characterization. Water Research 36: 4227-4234.

Gollan, A, Parekh, B. S. 1985. Hydrodynamic aspects of semi-dense pleat designs in pleated cartridges. Filtration and Separation 22: 326-329.

Griffiths, M. H., Andrew, P. W., Ball, P. R., Hall, G. M. 2000. Rapid methods for testing the efficacy of sterilization-grade filter membranes. Applied and Environmental Microbiology 66: 3432-3437.

Guell, C., Davis, R. H. 1996. Membrane fouling during microfiltration of protein mixtures. Journal of Membrane Science 119: 269-284.

Haslam, C., (Pall Corporation). Personal Communication. 2007

Hermia, J. 1982. Constant pressure blocking filtration laws - Application to power-law non-newtonian fluids. Transactions of the Institution of Chemical Engineers 60: 183-187.

Hinkelmann, K., Kempthorne, O. 2008. Design and analysis of experiments: Introduction to experimental design. 2nd edn . New York: Wiley.

Ho, C. C., Zydney, A. L. 2000. A combined pore blockage and cake filtration model for protein fouling during microfiltration. Journal of Colloid and Interface Science 232: 389-399.

Ho, C. C., Zydney, A. L. 2001. Protein fouling of asymmetric and composite microfiltration membranes. Industrial & Engineering Chemistry Research 40: 1412-1421.

Hutchinson, N., Bingham, N., Murrell, N., Farid, S., Hoare, M. 2008. Shear stress analysis of mammalian cell suspensions for prediction of industrial centrifugation and its verification. Biotechnology and Bioengineering 95: 483-491.

Ireland, T., Lutz, H., Siwak, M., Bolton, G. 2004. Viral filtration of plasma-derived human IgG: A case study using Viresolve NFP. Biopharm International 17: 38-44.

ISPE. 2001. Pharmaceutical engineering guides for new and renovated facilities: Commisioning and qualification. 1st edn . Tampa: ISPE.

Jackson, N. B., Liddell, J. M., Lye, G. J. 2006. An automated microscale technique for the quantitative and parallel analysis of microfiltration operations. Journal of Membrane Science 276: 31-41.

Jaffrin, M. Y. 2008. Dynamic shear-enhanced membrane filtration: A review of rotating disks, rotating membranes and vibrating systems. Journal of Membrane Science 324: 7-25.

Jornitz, M. W. 2006. Filter construction and design. Advances in Biochemical Engineering Biotechnology 98: 105-123.

Jornitz, M. W., Meltzer, T. H. 2007. Media and buffer filtration implications. In: Jornitz, M. W. and Meltzer, T. H., editor. Filtration and purification in the biopharmaceutical industry. London: Informa HealthCare. pp. 439-457.

Kalyanpur, M. 2000. Downstream processing in the biotechnology industry: An overview. In: Desai, M. A., editor. Downstream processing of proteins: Methods and protocols. Totowa: Humana Press Inc. pp. 1-10.

Kee, G-S., Pujar, N. S., Titchener-Hooker, N. J. 2008. Study of detergent-mediated liberation of hepatitus B virus-like particles from *S. cerevisiae* homogenate: Identifying a framework for the design of future-generation lipoprotein vaccine processes. Biotechnology Progress 24: 623-631.

Kelly, S. T., Opong, W. S., Zydney, A. L. 1993. The influence of protein aggregates on the fouling of microfiltration membranes during stirred cell filtration. Journal of Membrane Science 80: 175-187.

Kelly, S. T., Zydney, A. L. 1994. Effects of intermolecular thiol-disulfide interchange reactions on bsa fouling during microfiltration. Biotechnology and Bioengineering 44: 972-982.

Kelly, S. T., Zydney, A. L. 1995. Mechanisms for BSA fouling during microfiltration. Journal of Membrane Science 107: 115-127.

Kelly, S. T., Zydney, A. L. 1997. Protein fouling during microfiltration: Comparative behavior of different model proteins. Biotechnology and Bioengineering 55: 91-100.

Kim, K. J., Chen, V., Fane, A. G. 1993. Some factors determining protein aggregation during ultrafiltration. Biotechnology and Bioengineering 42: 260-265.

Levy, M. S., Collins, I. J., Yim, S. S., Ward, J. M., Titchener-Hooker, N. J., Ayazi Shamlou, P., Dunnill, P. 1999. Effect of shear on plasmid DNA in solution. Bioprocess Engineering 20: 7-13.

Liu, J., Nguyen, M. D. H., Andya, J. D., Shire, S. S. 2005. Reversible self-association increases the viscosity of a concentrated monoclonal antibody in aqueous solution. Journal of Pharmaceutical Sciences 94: 1928-1940.

Liu, W. R., Langer, R., Klibanov, A. M. 1991. Moisture-induced aggregation of lyophilized Proteins in the solid-state. Biotechnology and Bioengineering 37: 177-184.

Lowry, O. H., Rosebrough, N. J., Farr, A. L., Randall, R. J. 1951. Protein measurement with the folin phenol reagent. The Journal of Biological Chemistry 193: 265-275.

Lucke, T., Fissan, H. 1996. The prediction of filtration performance of high efficiency gas filter elements. Chemical Engineering Science 51: 1199-1208.

Madsen, R. E. 2006. Filter validation. Advances in Biochemical Engineering Biotechnology 98: 125-141.

Malvern Instruments. 2004. Zetasizer nano series user manual. Malvern: Malvern Instruments Ltd.

Mannweiler, K., Hoare, M. 1992. The scale-down of an industrial disc stack centrifuge. Bioprocess Engineering 8: 19-25.

Manttari, M., Pihlajamaki, A., Nystrom, M. 2006. Effect of pH on hydrophilicity and charge and their effect on the filtration efficiency of NF membranes at different pH. Journal of Membrane Science 280: 311-320.

Maybury, J. P., Mannweiler, K., Titchener-Hooker, N. J., Hoare, M., Dunnill, P. 1998. The performance of a scaled down industrial disc stack centrifuge with a reduced feed material requirement. Bioprocess Engineering 18: 191-199.

Meireles, M., Aimar, P., Sanchez, V. 1991. Albumin Denaturation During Ultrafiltration - Effects of Operating-Conditions and Consequences on Membrane Fouling. Biotechnology and Bioengineering 38: 528-534.

Meltzer, T. H., Jornitz, M. W. 1998. Filtration in the biopharmaceutical industry. New York: Marcel Dekker, Inc.

MHRA. 2007. Rules and guidance for pharmaceutical manufacturers and distributors. 7th edn . London: Pharmaceutical Press.

Mourouzidis-Mourouzis, S. A., Karabelas, A. J. 2006. Whey protein fouling of microfiltration ceramic membranes - Pressure effects. Journal of Membrane Science 282: 124-132.

Mulder, M. 1997. Basic principles of membrane technology. 2nd edn . Dordrecht: Kluwer Academic Publishers.

Nakamura, K., Matsumoto, K. 2006. Protein adsorption properties on a microfiltration membrane: A comparison between static and dynamic adsorption methods. Journal of Membrane Science 285: 126-136.

Nassehi, V., Hanspal, N. S., Waghode, A., Ruziwa, W. R., Wakeman, R. J. 2005. Finite-element modelling of combined free/porous flow regimes: Simulation of flow through pleated cartridge filters. Chemical Engineering Science 60: 995-1006.

Nassehi, V., Waghode, A. N., Hanspal, N. S., Wakeman, R. J. 2006. Mathematical modelling of flow through pleated cartridge filters. Progress in Industrial Mathematics at Ecmi 2004 8: 298-302.

Neal, G., Keshavarz-Moore, E., Ayazi Shamlou, P. 2003. Ultra scale-down approach for the prediction of full-scale recovery of ovine polycolonal immunoglobulins used in the manufacture of snake venom-specific fab fragment. Biotechnology and Bioengineering 81: 149-157.

Nealon, A. J. 2006. Microwell methods for fast process development. Eng. D. Thesis, University of London.

Ohnishi, S. T., Barr, J. K. 1978. A simplified method of quantitating proteins using the biuret and phenol reagents. Analytical Biochemistry 86: 193-200.

Okamoto, Y., Ohmori, K., Glatz, C. E. 2001. Harvest time effects on membrane cake resistance of Escherichia Coli broth. Journal of Membrane Science 190: 93-106.

Oshima, K. H., Evans-Strickfaden, T. T., Highsmith, A. K. 1998. Comparison of filtration properties of hepatitis B virus, hepatitis C virus and simian virus 40 using a polyvinylidene fluoride membrane filter. Vox Sanguinis 75: 181-188.

Palacio, L., Ho, C. C., Pradanos, P., Hernandez, A., Zydney, A. L. 2003. Fouling with protein mixtures in microfiltration: BSA-lysozyme and BSA-pepsin. Journal of Membrane Science 222: 41-51.

Palacio, L., Ho, C. C., Zydney, A. L. 2002. Application of a pore-blockage - Cake-filtration model to protein fouling during microfiltration. Biotechnology and Bioengineering 79: 260-270.

Pall Life Sciences. 2004. USD 2293: Supor UEAV filter cartridges. www. Pall. com

Pampel, L. W., Boushaba, R., Titchener-Hooker, N. J. 2008. A methodical approach to ultra scale-down of process sequences: Application to casein removal from the milk of transgenic animals. Biotechnology Progress 24: 192-201.

Parnham, C. S., Davis, R. H. 1996. Protein recovery from bacterial cell debris using crossflow microfiltration with backpulsing. Journal of Membrane Science 118: 259-268.

Pavlou, A. K., Reichert, J. M. 2004. Recombinant protein therapeutics - success rates, market trends and values to 2010. Nature Biotechnology 22: 1513-1519.

Postlethwaite, J., Lamping, S. R., Leach, G. C., Hurwitz, M. F., Lye, G. J. 2004. Flux and transmission characteristics of a vibrating microfiltration system operated at high biomass loading. Journal of Membrane Science 228: 89-101.

Rajniak, P., Tsinontides, S. C., Pham, D., Hunke, S. D., Reynolds, R. T., Chern, R. T. 2008. Sterilizing filtration - principles and practice for successful scale-up to manufacturing. Journal of Membrane Science 325: 223-237.

Reif, O. W. 2006. Microfiltration membranes: Characteristics and manufacturing. Advances in Biochemical Engineering Biotechnology 98: 73-103.

Reynolds, T., Boychyn, M., Sanderson, T., Bulmer, M., More, J. 2003. Scale-down of continuous filtration for rapid bioprocess design: Recovery and dewatering of protein precipitate suspensions. Biotechnology and Bioengineering 83: 454-464.

Subrenat, A., Bellettre, J., Le Cloirec, P. 2003. 3-D numerical simulations of flows in a cylindrical pleated filter packed with activated carbon cloth. Chemical Engineering Science 58: 4965-4973.

Sundaram, S. 1998. Protein adsorption in microporous membrane filtration. In: Meltzer, T. H. and Jornitz, M. W., editor. Filtration in the biopharmaceutical industry. New York: Marcel Dekker Inc. pp. 533-575.

Tarrach, K., Köhler, K., Grimm, C. 2003. Managing initial recovery processes with multilayer depth filtration. Pharmaceutical Technology Europe 20: 71-77.

Thompson, R. E., Jones, S. D., Magil, S., Levine, H. L. 2007. Validation of recovery and purification processes. In: Agalloco, J. and Carleton, F. J., editor. Validation of pharmaceutical processes. New York: Informa Healthcare. pp. 455-472.

Thomsett, M. C. 2005. Getting started in six sigma. Hoboken: John Wiley and Sons, Inc.

Titchener-Hooker, N. J., Dunnill, P., Hoare, M. 2008. Micro biochemical engineering to accelerate the design of industrial-scale downstream processes for biopharmaceutical proteins. Biotechnology and Bioengineering 100: 473-487.

Tracey, E. M., Davis, R. H. 1994. Protein fouling of track-etched polycarbonate microfiltration membranes. Journal of Colloid and Interface Science 167: 104-116.

Tronville, P., Sala, R. 2003. Minimization of resistance in pleated-media air filter designs: Empirical and CFD approaches. HVAC & R Research 9: 95-106.

Tustian, A. D., Salte, H., Willoughby, N. A., Hassan, I., Rose, M. H., Baganz, F., Hoare, M., Titchener-Hooker, N. J. 2007. Adapted ultra scale-down approach for predicting the centrifugal separation behavior of high cell density cultures. Biotechnology Progress 23: 1404-1410.

van Reis, R., Leonard, L. C., Hsu, C. C., Builder, S. E. 1991. Industrial scale harvest of proteins from mammalian cell culture by tangential flow filtration. Biotechnology and Bioengineering 38: 413-422.

van Reis, R., Zydney, A. 2001. Membrane separations in biotechnology. Current Opinion in Biotechnology 12: 208-211.

van Reis, R., Zydney, A. 2007. Bioprocess membrane technology. Journal of Membrane Science 297: 16-50.

Waghode, A. N., Hanspal, N. S., Wakeman, R. J., Nassehi, V. 2007. Numerical analysis of medium compression and losses in filtration area in pleated membrane cartridge filters. Chemical Engineering Communications 194: 1053-1064.

Wakeman, R. J., Hanspal, N. S., Waghode, A. N., Nassehi, V. 2005. Analysis of pleat crowding and medium compression in pleated cartridge filters. Chemical Engineering Research and Design 83: 1246-1255.

Wang, A., Lewus, R., Rathore, A. 2006. Comparison of different options for harvest of a therapeutic protein product from high cell density yeast fermentation broth. Biotechnology and Bioengineering 94: 91-104.

Wang, W. 2005. Protein aggregation and its inhibition in biopharmaceutics. International Journal of Pharmaceutics 289: 1-30.

Waterhouse, S., Hall, G. M. 1995. The Validation of Sterilizing Grade Microfiltration Membranes with Pseudomonas-Diminuta. Journal of Membrane Science 104: 1-9.

Yavorsky, D., Blanck, R., Lambalot, C., Brunkow, R. 2003. The clarification of bioreactor cell cultures for biopharmaceuticals. Pharmaceutical Technology 27: 62-76.

Zaidi, S. K., Kumar, A. 2005. Experimental analysis of a gel layer in dead-end ultrafiltration of a silica suspension. Desalination 172: 107-117.

Zeman, L. J, Zydney, A. L. 1996. Microfiltration and ultrafiltration: Principles and applications. New York: Marcel Dekker, Inc.

Zeng, X., Ruckenstein, E. 1999. Membrane chromatography: Preparation and applications to prtoein separation. Biotechnology Progress 15: 1003-1019.

Zhang, H., Kong, S., Booth, A., Boushaba, R., Levy, M. S., Hoare, M. 2007. Prediction of shear damage of plasmid DNA in pump and centrifuge operations using an ultra scale-down device. Biotechnology Progress 23: 858-865.

Zydney, A. L. 2009. Membrane technology for purification of therapeutic proteins. Biotechnology and Bioengineering 103: 227-230.

Zydney, A. L., Ho, C. C. 2003. Effect of membrane morphology on system capacity during normal flow microfiltration. Biotechnology and Bioengineering 83: 537-543.

Appendix A: Additional Datasets for 10” UEAV Cartridge

Clean water flux data for the large-scale target (10” $UEAV_{24,\ 1}$) has been obtained from two other sources other than the experimental data generated at UCL. The first source was by using an experimental rig at Pall Portsmouth described in Section 2.4.1.1. The second source is data taken from the product specification sheet for the 10” Supor® UEAV cartridge (Pall Life Sciences, 2004). The advantage of the two alternative sources of data is that they were obtained at higher transmembrane pressure differences, which corresponds to higher fluxes. The two data sources for the 10” $UEAV_{24,1}$ cartridge are given in Figure A-1.

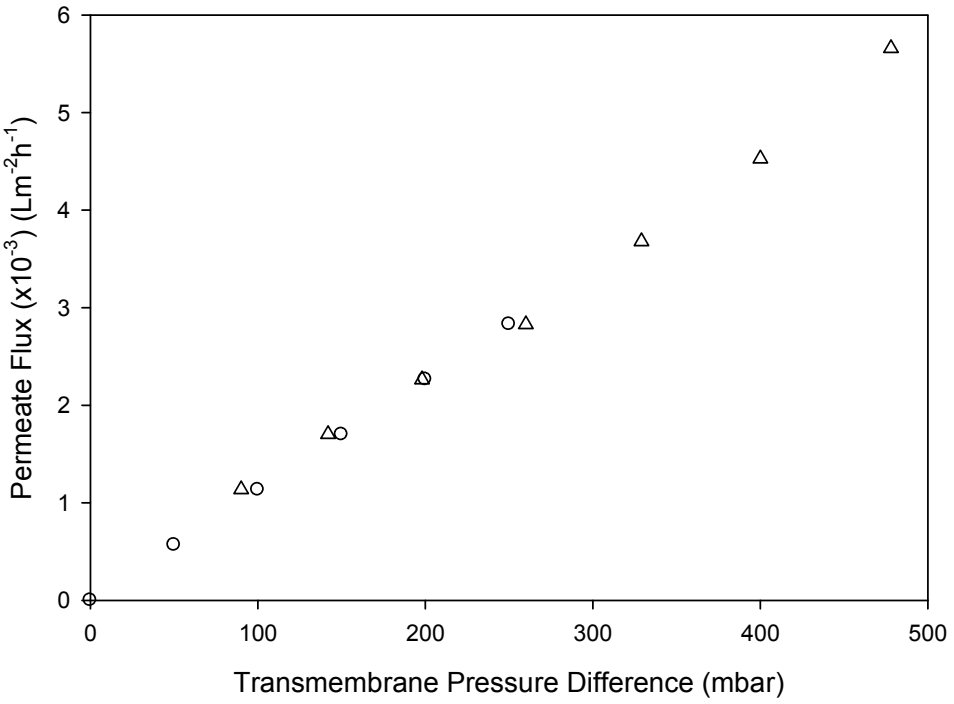

Figure A-1: Clean water flux data for 10” $UEAV_{24,1}$. Data obtained from two sources (△) generated using Pall dP rig using protocol described in Section 2.4.1.1. (○) Taken from 10” $UEAV_{24,\ 1}$ product specification sheet (Pall Life Sciences, 2004).

Appendix B: Assumptions and Calculations for Economic Cases

The assumptions and calculations for the economic cases presented in Section 7.4.2.1 and Section 7.4.2.2 are outlined below.

Assumptions		
Operating Costs	60	%
Cost of Feed	1000	£/L
# FS experiments	4	
Cost of 10" cartridge	£1,000	each
BASE CASE: Flat Sheet Disc		
Costs		
Flat Sheet Disc	25	£ per disc
# Experiments	4	
Total Cost FS	100	£
Feed Volume	0.025	L per experiment
Total Feed Volume	0.1	L
Feed Cost	100	£
Ancillary Equipment	350	£
Total Cost	**550**	**£ per study**
% Difference in Prediction	55	%
Uncertainity estimate	50	%
Total over-prediction	105	%
Cost of over prediction	**1050**	**£ Per 10" cartidge**
Number of runs per year	12	
Total cost of over-prediction	12600	£ per year
Revenue from Cartridges	£24,600.000	

Scale-down pleated cartridge

Costs		
USD Pleated Device	100	£ each (10% of 10" cartridge)
# Experiments	4	
Total Cost USD	400	
Feed Volume	0.3	L per experiment
Total Feed Volume	1.2	L
Feed Cost	1200	£
Ancillary Equipment	500	£
Total Cost	2100	**£ per study**
% Difference in Prediction	10	%
Uncertainity estimate	10	%
Total over-prediction	20	%
Cost of over prediction	200	**£ Per 10" cartidge**
Number of runs per year	12	
Total cost of over-prediciton	2400	£ per year
Saving to customer due to over-prediction	10200	£ per year
Revenue from USD Sales	400	Per study
Revenue from Cartridges	14400	